

---

# Utilisation of Column Profile Maps for the Design and Optimisation of Complex Distillation Processes

Ronald Abbas

A thesis submitted to the Faculty of Engineering and the  
Built Environment, University of the Witwatersrand, in  
fulfilment of the requirements for the degree of Doctor of  
Philosophy

Johannesburg, 2011

---



---

## Declaration

I declare that except where acknowledged, this thesis is my own un-aided work. It is being submitted for the degree of Doctor of Philosophy to the University of the Witwatersrand, Johannesburg. It has not been submitted before for any degree or examination in any other University.

.....

.....day of.....year.....

## Abstract

A novel technique for computing the minimum reflux for multi-component conventional columns as well as complex configurations has been developed. The technique is a short cut, geometrical, non-iterative method. It predicts how the minimum reflux solution and hence the profile orientation is related to the feed-component distribution for all possible operating conditions and any number of components. The technique makes use of Column Profile Maps and the eigenvectors of the Jacobian matrix of the separation vector evaluated at the feed condition. An integral part of the method is the development of the feasible regions in composition space that restrict our choice of the product specification. The Column Profile Map-Eigenvector technique has shown to produce results exactly equivalent to those as predicted by the Underwood method.

To demonstrate the Column Profile Map-Eigenvector technique to complex configurations the method is employed in the detailed design of the Petlyuk Column. Although the overall column minimum reflux calculation is not shown, the application of the Column Profile Map-Eigenvector technique is utilised to determine the complete feasible operating region. The feasible column parameter region derived from the CPM-E technique is shown to encompass five flow patterns for the Petlyuk column derived from the Column Profile Map techniques.

In order to exhibit the value of the Column Profile Map techniques developed by Tapp et al. (2004) to higher order systems, the design methods are applied to the fully thermally coupled Kaibel column under sharp split conditions. From the results of the topological analysis, it is shown that, for set product specifications, when dealing with ideal systems (constant relative volatilities), there is only one set of feasible operating parameters. The line of solutions for feasible profile intersection is then sectioned and the CPM-E technique is applied to the quaternary configuration that produces all feasible operating parameters.

---

The Column Profile Map technique has also been applied to the design of a variety of quaternary feeds for sets of columns consisting of a main column with various combinations of side rectifiers and strippers. The graphical nature of the technique allows one to easily assess feasible designs for systems with less than five components, but is shown to algebraically extend to higher order systems. The minimum vapour requirements of the various coupled side unit systems are compared using the Column Profile Map-Eigenvector technique.

## **Dedication**

This work is dedicated to my mother and father, Dilene and Siegfried. Thank you for your support, love and unwavering belief in me.

## Acknowledgements

I would like to express my gratitude to my supervisors, Professor Diane Hildebrandt and Professor David Glasser who have provided invaluable contribution to my research. Professor Glasser who has been a continuous source of inspiration, and has shown me that immeasurable wisdom is possible. Prof Hildebrandt has always provided a helping hand in all aspects, not only in my work. Your continuous perseverance and determination has been the anchor in the Distillation Research Group. It has been an absolute privilege working with two researchers of such amazing talent and extraordinary calibre.

I am grateful to Dr. Ivar Halvorsen from the Norwegian University of Science and Technology, whose insight into the Underwood methods application was invaluable and Professor Sigurd Skogestad for the opportunity to work with his research team in Norway.

My good friend and colleague Dr Simon Holland has been a pillar during my research. His approach to problems during our many heated debates and discussions has been a continuous motivation during the few years as a postgraduate.

The friends that have been with me during the good times and those times of struggle, I thank you for standing by me. The many years I have been at Wits would not have been regarded as amusing without the presence of Craig Griffiths (aka Pun Boy). His brilliant mind and logical thinking made for interesting topics of conversation during our endless cups of coffee. Daniel Beneke, a friend whom I had the honour of working closely with, has shown me the true value of hard work. I thank him for giving me a wider perspective on things. Nik Felbab, for his ability to make any situation just seem so much better. Mark Peters, for the many “driehoeks” and muffins we’ve had in the mornings before meetings and for giving me direction in my research when I first started my postgraduate degree.

Scott Gover, my very good friend, whom I want to thank for his support in all and any of my endeavours over the last 16 years.

I want to show appreciation to my family for always believing in me and showing me that there is always light at the end of the tunnel. I want to express my gratitude to my aunts, Dee and Gina, who give without expectation of reward. My time in London would not have been as productive without their nurturing support. Most importantly I wish to thank my mother and father. This work would not have been possible without their encouragement and constant reminders of the goal when it was a mere blur.

Finally, I would like to thank the National Research Foundation (NRF), the University of the Witwatersrand and the Centre of Materials and Process Synthesis (COMPS) for their financial support.

---

# Table of Contents

<b>Declaration</b>	<b>I</b>
<b>Abstract</b>	<b>II</b>
<b>Dedication</b>	<b>IV</b>
<b>Acknowledgements</b>	<b>V</b>
<b>List of Figures</b>	<b>XIV</b>
<b>List of Tables</b>	<b>XXV</b>
<b>Chapter 1 : Introduction</b>	<b>1</b>
1.1 Overall Introduction	1
1.2 Aim of thesis	2
1.3 Thesis overview	3
<b>Chapter 2 : Novel Minimum Reflux determination using Column Profile Maps</b>	<b>6</b>
2.1 Introduction	7
2.1.1 General Overview of minimum energy demand methodologies	9
2.1.1.1 Boundary Value Method	9
2.1.1.2 Zero Volume Criteria	10
2.1.1.3 Eigenvalue Criterion	11
2.1.1.4 Rectification Body Method	12
2.1.1.5 $V_{\min}$ Diagrams	13
2.1.1.6 Shortest Stripping Line	13

---

2.2	Background	14
2.2.1	Column Profile Maps	14
2.2.2	$\Delta$ and $X_{\Delta}$ material balance within a conventional column	17
2.2.3	Eigenvector Maps	19
2.3	Conditions for Minimum Reflux and Transformed Triangles	20
2.4	Co-linearity Line Rule	24
2.5	Degrees of Freedom and Design Variables	26
2.6	CPM-E Technique derivation and description	28
2.6.1	Eigenvector Application	28
2.6.2	CPM-E technique	30
2.7	Complete CPM-E Solutions	34
2.8	Preferred Splits and Double Feed pinches	41
2.9	Minimum Reflux Regions	44
2.9.1	Complete minimum reflux regions	44
2.9.2	Sloppy split minimum reflux regions	48
2.10	Application to higher order systems	50
2.11	Simulation and Methodology Comparison	55
2.12	$R_{\min}$ for Non-Sharp Split, Non-Ideal and Azeotropic Systems	57
2.12.1	Non-Sharp Solutions	57
2.12.2	Non-Ideal and Azeotropic Solutions	58
2.13	Discussion and Conclusion	60
<b>Chapter 3</b>	<b>: Complex Column Design - Sharp Split Petlyuk Column</b>	<b>63</b>
3.1	Introduction	64
3.2	Column Profile Maps	68
3.3	Properties of $\Delta_k$ , $X_{\Delta k}$ and $R_{\Delta k}$	71
3.4	CPM Design Methodology	72

3.5	Column Section Breakdown and Net Flow	73
3.6	Net Flow and Difference Point Material Balances in the Petlyuk Column	74
3.6.1	Net Flow and the Material Balance	74
3.6.2	Difference Points and the Material Balance	78
3.7	Composition Matching Criteria	80
3.8	Feasible Topology	82
3.8.1	Implications of Sharp Distillate Product Specifications	83
3.8.2	Implications of Sharp Side-Draw Product Specifications	85
3.8.3	Implications of Sharp Product Specifications for CS 3 and CS 5	85
3.8.4	Summary of the Topological Effects of Sharp-Split Specifications	85
3.9	General form of the Petlyuk Composition Profiles	86
3.10	Degrees of Freedom and Variable Selection	91
3.10.1	Degrees of Freedom	91
3.10.2	Variable Selection	93
3.11	Difference Point Placement for the Petlyuk Column	94
3.12	Variable Representation in $\Phi_V$ vs. $\Phi_L$ Space	100
3.12.1	Net Flow Regimes in $\Phi_V$ vs. $\Phi_L$ Space	101
3.12.2	Physical Limits on $\Phi_V$ and $\Phi_L$	103
3.12.3	Reflux Ratio in $\Phi_V$ vs. $\Phi_L$ Space	104
3.12.4	Constant $X_\Delta$ in $\Phi_V$ vs. $\Phi_L$ Space	105
3.13	Constructing Split Ratio Regions of Feasibility	106
3.13.1	Coupled Column Section Minimum Reflux and binary CPM-E technique	107
3.13.2	Limiting Conditions for Overlap of TT <sub>3</sub> 3 and TT <sub>3</sub> 5 and ternary CPM-E technique	111
3.13.3	Satisfying the Remaining Matching Criteria	114
3.13.4	Overall Column Feasibility in $\Phi_V$ vs. $\Phi_L$ Space	115
3.14	Overall Minimum Reflux	119

---

3.15	The Effect of Varying $R_{\Delta I}$ _____	123
3.15.1	CS 2 and CS 4 minimum reflux _____	123
3.15.2	Negative Flow Boundaries _____	124
3.15.3	Zero Net Flow Boundaries _____	124
3.15.4	PEB1 and PEB2 _____	124
3.15.5	Feasible $\Phi_L$ and $\Phi_V$ regions _____	125
3.16	Discussion _____	127
 <b>Chapter 4 : Complex Column Design - Sharp Split Kaibel Column</b> _____		<b>132</b>
4.1	Introduction _____	133
4.2	CPMs for Ternary and Quaternary Systems _____	136
4.2.1	Quaternary System Boundary definition _____	140
4.2.2	Properties of internal material _____	142
4.3	CPM Design Methodology _____	143
4.4	Column Section Breakdown _____	144
4.5	Net Flow and Mass Balances in the Kaibel Column _____	145
4.6	Difference Point and Mass Balances in the Kaibel Column _____	151
4.7	Kaibel Column Composition Matching Criteria _____	152
4.8	Sharp Splits and related Feasible Topology _____	154
4.8.1	Sharp Distillate and Bottoms Specifications _____	156
4.8.2	Sharp Side Draw Specifications _____	158
4.8.3	Implications of Sharp Product Specifications on CS 3 and CS 5. _____	158
4.8.4	TT <sub>4</sub> and Topological Effects of Sharp-Split Specifications. _____	159
4.9	Design parameters _____	159
4.10	$X_{\Delta}$ Placements for the Kaibel Column _____	160
4.10.1	$X_{\Delta}$ Placement for the Distillate and Bottoms column sections _____	160
4.10.2	$X_{\Delta}$ Placement for the Coupled Column Sections _____	161

4.11	Consequences of $X_A$ Placement on Net Flow _____	165
4.11.1	Implications on Net Flow _____	165
4.11.2	Zero Net Flow Implications on Column Section Profile _____	169
4.12	Variable Representation in Liquid vs. Vapour Split Ratio Space _____	170
4.12.1	Net Flow regimes in $\Phi_V$ vs. $\Phi_L$ Space _____	170
4.12.2	Limits in $\Phi_V$ vs. $\Phi_L$ Space _____	172
4.12.3	Reflux Ratio in $\Phi_V$ vs. $\Phi_L$ Space _____	174
4.13	Feasibility in the Split Ratio Region _____	176
4.13.1	Determining feasibility in $\Phi_L$ vs. $\Phi_V$ _____	176
4.13.2	Overall feasible topology _____	184
4.14	Differences between Single Dividing wall Columns and a Two-Column arrangement _____	187
4.15	Discussion and Conclusion _____	188
<b>Chapter 5</b>	<b>: Optimal operation of the Sharp Split Kaibel Column _____</b>	<b>192</b>
5.1	CPMs Quaternary Systems _____	193
5.2	Column Section Breakdown _____	197
5.3	Recapitulate of the Sharp Split Kaibel Column solution _____	198
5.4	Feasible region development _____	202
5.4.1	Coupled Column Minimum Reflux _____	202
5.4.1.1	$R_{\min}$ in the CSs adjacent to the side product _____	202
5.4.1.2	$R_{\min}$ in the CSs adjacent to the feed _____	206
5.4.1.3	Overall Kaibel Column Feasibility _____	210
5.5	The Effects of varying $R_{A1}$ _____	213
5.5.1	$R_{A2}$ and $R_{A4}$ effects _____	214
5.5.2	Negative Flow Boundaries effects _____	215
5.5.3	$R_{A3}$ and $R_{A5}$ effects _____	215
5.5.4	$\Delta_7 = 0$ effects _____	216

---

5.5.5	Feasible $\Phi_L$ and $\Phi_V$ regions corresponding to $\Delta_7 = 0$	216
5.6	Overall Minimum Reflux	217
5.7	Discussion and Conclusion	219
<b>Chapter 6</b>	<b>: Design and Analysis of multiple thermally coupled configurations using Column Profile Maps</b>	<b>221</b>
6.1	Introduction	222
6.2	Background: Column Profile Maps	224
6.3	Design procedure	228
6.3.1	Initialisation	228
6.3.2	Net flow patterns	230
6.3.3	Difference Point placement	232
6.3.4	Variable selection	234
6.3.5	Feasibility criteria	235
	Eigenvector criteria	235
	Special feed conditions	239
6.3.6	Thermally coupled column sections	242
6.3.7	Stepwise design algorithm	244
6.4	Finalising the design	245
6.4.1	Iso-reflux analysis	245
6.4.2	Identifying optimal designs	255
6.5	Discussion and Conclusions	259
<b>Chapter 7</b>	<b>: Conclusions and Future Work</b>	<b>261</b>
7.1	Thesis Conclusion	261
7.1.1	Petlyuk Column	262
7.1.2	Kaibel Column	263
7.1.3	Side Unit Configurations	265
7.2	Future work	266

---

<b>Publications and Presentations</b>	<b>270</b>
Posters and Presentations:	270
Publications and peer reviewed conference proceedings:	271
<b>References</b>	<b>273</b>
<b>Appendix A</b>	<b>286</b>
<b>Appendix B</b>	<b>287</b>
<b>Appendix C</b>	<b>288</b>
<b>Appendix D</b>	<b>292</b>
<b>Appendix E</b>	<b>294</b>
<b>Appendix F</b>	<b>296</b>
<b>Appendix G</b>	<b>300</b>
<b>Appendix H</b>	<b>304</b>
<b>Appendix I</b>	<b>312</b>

# List of Figures

## Chapter 2:

- Figure 2.1: Column section breakdown for the Conventional column. \_\_\_\_\_ 15
- Figure 2.2: Ternary Column Profile Map for  $X_d = [0.45 \ -0.25]$  and  $R_\Delta = 6$ . \_\_\_\_ 16
- Figure 2.3: Material balance around feed point. \_\_\_\_\_ 17
- Figure 2.4: Eigenvector map for an ideal system. The compositions  $x_1$  and  $x_2$  are in the range  $X_i = [-0.5, +1.5]$ . \_\_\_\_\_ 20
- Figure 2.5: Composition profiles and their associated transformed triangles in descending order of reflux. (a) Crossing Profiles with corresponding overlapping  $TT_3$ s. (b): Smaller reflux, but still over refluxed system. (c): System at minimum reflux conditions. \_\_\_\_\_ 23
- Figure 2.6: Multiple overlap of  $TT_3$  with decreasing reflux ratio. Line indicates the last possible intersection for a direct split.  $X_D = [1 \ 0]$ ,  $X_B = [0 \ 0.486]$ ,  $X_F = [1/3 \ 1/3]$ . \_\_\_\_\_ 25
- Figure 2.7: Reflux ratio selected below the minimum for a direct split.  $X_D = [1 \ 0]$ ,  $X_B = [0 \ 0.486]$ ,  $X_{Feed} = [1/3 \ 1/3]$ . \_\_\_\_\_ 25
- Figure 2.8: Different product specifications with the same feed composition produces the same CLL at minimum reflux (a)  $\alpha = [4 \ 1 \ 2]$ ,  $X_D = [0.9 \ 0]$ ,  $X_B = [0 \ 0.527]$ ,  $X_F = [1/3 \ 1/3]$ ,  $R_{min} = 1.63$ . (b)  $\alpha = [4 \ 1 \ 2]$ ,  $X_D = [0.8 \ 0]$ ,  $X_B = [0 \ 0.556]$ ,  $X_F = [1/3 \ 1/3]$ ,  $R_{min} = 1.04$ . \_\_\_\_\_ 25
- Figure 2.9: A point chosen along one of the eigenvector lines will have eigenvectors that point directly at the same singularities. \_\_\_\_\_ 30
- Figure 2.10: Eigenvector evaluated at the feed composition corresponds to CLL1. \_\_\_\_\_ 30
- Figure 2.11: Co-linear points evaluated at a liquid pinch point. \_\_\_\_\_ 32
- Figure 2.12: CLL stationary point with mixing and separation vector passing through the node of the transformed triangle for the minimum reflux solution. \_\_\_\_\_ 34

- Figure 2.13: Minimum reflux solution revealing the existence of CLL2 by shifting the distillate product towards the intermediate along the light intermediate axis for an equimolar feed. \_\_\_\_\_ 35
- Figure 2.14: CLL1 and CLL2 determined from eigenvectors evaluated at the feed composition. \_\_\_\_\_ 37
- Figure 2.15: Minimum reflux solution. (a) Minimum reflux  $TT_3$  solution along CLL1 (b) Associated minimum reflux profile termination on CLL1 and RS. (c) Profiles produced from CLL1 minimum reflux solution 38
- Figure 2.16: Minimum reflux solution. (a) Minimum reflux  $TT_3$  solution along CLL1 (b) Associated minimum reflux profile termination on CLL1 and RS. (c) Profiles produced from CLL1 minimum reflux solution 40
- Figure 2.17: Preferred Split for conventional column.  $X_D = [0.75 \ 0]$ ,  $X_B = [0 \ 0.6]$ ,  $X_F = [1/3 \ 1/3]$ ,  $R_{min} = 0.75$ . \_\_\_\_\_ 42
- Figure 2.18: Double Feed Pinch Solutions. (a) Double feed pinch solution for low heavy key impurity in distillate. (b) Double feed pinch solution for high heavy key impurity in distillate. \_\_\_\_\_ 43
- Figure 2.19: Bow-tie region for equimolar feed with associated preferred split. 47
- Figure 2.20: (a) Rectifying sections positive reflux regions associated to common CLL1. (b) Rectifying sections positive reflux regions associated to common CLL2. (c) Combined positive reflux regions. \_\_\_\_\_ 47
- Figure 2.21: (a) Feasible and infeasible regions associated to common CLL1. (b) Feasible and infeasible regions associated to common CLL2. (c) Combination of CLL1 and CLL2 regions of interest. \_\_\_\_\_ 48
- Figure 2.22: Sloppy Split minimum reflux regions. \_\_\_\_\_ 50
- Figure 2.23: A design for an equimolar quaternary mixture in a simple column for the component AB-CD split. At minimum reflux the planes of the transformed tetrahedrons intersect, created from the eigenvectors evaluated at the feed condition. \_\_\_\_\_ 52
- Figure 2.24: Three classes of a quaternary systems minimum reflux solutions. (a) Plane interaction. ( $\alpha = [6 \ 4 \ 2 \ 1]$ ,  $X_F = [1/4 \ 1/4 \ 1/4 \ 1/4]$ ,  $X_T = [0.5 \ 0.5 \ 0 \ 0]$ ,  $X_B = [0 \ 0 \ 0.5 \ 0.5]$ ,  $R_{min} = 1.21$ ). (b) Edge interaction ( $\alpha = [6 \ 4 \ 2 \ 1]$ ,  $X_F = [1/4 \ 1/4 \ 1/4 \ 1/4]$ ,  $X_T = [0.439 \ 0.436 \ 0.125 \ 0]$ ,  $X_B = [0 \ 0.004 \ 0.416 \ 0.58]$ ,

$R_{min} = 0.47$ ). (c) Point interaction depicting a double feed pinch solution ( $\alpha = [6 \ 4 \ 2 \ 1]$ ,  $X_F = [1/4 \ 1/4 \ 1/4 \ 1/4]$ ,  $X_T = [0.55 \ 0.33 \ 0.12 \ 0]$ ,  $X_B = [0 \ 0.18 \ 0.36 \ 0.46]$ ,  $R_{min} = 0.44$ ). \_\_\_\_\_ 54

Figure 2.25: Comparison of the CPM-E technique to an ASPEN Plus simulation using a Dodecane, Tridecane and Tetradecane system. Equimolar feed,  $\alpha_{equivalent} = [2.41 \ 1 \ 1.55]$  and  $X_T = [0.85 \ 0]$ ,  $X_B = [0.1 \ 0.48]$  Reflux = 2.72. \_\_\_\_\_ 55

Figure 2.26: (a)  $TT_3$  overlap for feasible non sharp minimum reflux. (b) Non sharp solution with SS profile termination on RS profile. \_\_\_\_\_ 59

### Chapter 3:

Figure 3.1: Column Profile Map for  $X_A = [0.3, -0.2]$  and  $R_A = 9$ . \_\_\_\_\_ 70

Figure 3.2: Difference point regions of Residue Curve Map \_\_\_\_\_ 71

Figure 3.3: Transformed regions of Column Profile Map \_\_\_\_\_ 71

Figure 3.4: Petlyuk column (main column with pre-fractionator) \_\_\_\_\_ 74

Figure 3.5: Column section breakdown for the Petlyuk column \_\_\_\_\_ 74

Figure 3.6: Mixing point between Column Section 3 and 5. \_\_\_\_\_ 74

Figure 3.7: Feasible net flow patterns at the point of feed addition. (a)  $\Delta_3 > 0$ ,  $\Delta_5 > 0$ , Feasible. (b)  $\Delta_3 < 0$ ,  $\Delta_5 < 0$ , Feasible. (c)  $\Delta_3 > 0$ ,  $\Delta_5 < 0$ , Feasible. (d)  $\Delta_3 < 0$ ,  $\Delta_5 > 0$ , Infeasible. \_\_\_\_\_ 75

Figure 3.8: Feasible net flow patterns at the mixing point of the rectifying section. (a)  $\Delta_2 > 0$ ,  $\Delta_3 > 0$ , Feasible. (b)  $\Delta_2 > 0$ ,  $\Delta_3 < 0$ , Feasible. (c)  $\Delta_2 < 0$ ,  $\Delta_3 > 0$ , Feasible. (d)  $\Delta_2 < 0$ ,  $\Delta_3 < 0$ , Infeasible. \_\_\_\_\_ 76

Figure 3.9: Feasible net flow patterns at the mixing point of the stripping section. (a)  $\Delta_4 < 0$ ,  $\Delta_5 < 0$ , Feasible. (b)  $\Delta_4 > 0$ ,  $\Delta_5 < 0$ , Feasible. (c)  $\Delta_4 < 0$ ,  $\Delta_5 > 0$ , Feasible. (d)  $\Delta_4 < 0$ ,  $\Delta_5 < 0$ , Infeasible. \_\_\_\_\_ 76

Figure 3.10: Feasible net flow patterns at the first side draw. (a)  $\Delta_2 > 0$ ,  $\Delta_4 > 0$ , Feasible. (b)  $\Delta_2 < 0$ ,  $\Delta_4 > 0$ , Feasible. (c)  $\Delta_2 < 0$ ,  $\Delta_4 < 0$ , Feasible. (d)  $\Delta_2 > 0$ ,  $\Delta_4 < 0$ , Infeasible. \_\_\_\_\_ 76

Figure 3.11: Various Flow patterns that arise due to feasible net flow combinations. (a) Flow Pattern 1. (b) Flow Pattern 2 (c) Flow Pattern 3. (d) Flow Pattern 4. (e) Flow Patter 5.	77
Figure 3.12: Component mixing point between column Section 3 and 5	79
Figure 3.13: Various compositions matching criterion. (a) Matching criteria 1 (b) Matching criteria 2. (c) Matching criteria 3. (d) Matching criteria 4	82
Figure 3.14 a-c: Rectifying profiles for difference points at varying distances from the light-intermediate axis. Implications of Sharp Bottoms Product Specifications	84
Figure 3.15: Stripping profiles for difference points at varying distances from the intermediate-heavy axis.	85
Figure 3.16a: Rectifying composition profiles	89
Figure 3.17a: Stripping composition profiles	89
Figure 3.18a: CS 2 composition profiles	90
Figure 3.19a: CS 4 composition profiles	90
Figure 3.20: CS 3 composition profiles	90
Figure 3.21a: CS 5 composition profiles	91
Figure 3.22a: Petlyuk composition profiles	91
Figure 3.23: Low intermediate purity difference point with liquid profile sampling high intermediate purity	96
Figure 3.24: Mixing and separation vector co-linearity	96
Figure 3.25a: CS 2 profile pinching outside MBT for $R_{A2} > 0$	97
Figure 3.26: Residue curve tangent lines at potential pinch points	99
Figure 3.27a: Material balance – net flow pattern 3	99
Figure 3.28: Net Flow Regimes in $\Phi_V$ vs. $\Phi_L$	102
Figure 3.29: Constant reflux lines in $\Phi_V$ vs. $\Phi_L$	105
Figure 3.30: Constant $X_\Delta$ lines in $\Phi_V$ vs. $\Phi_L$ space.	106
Figure 3.31: Transformed triangle boundary definitions	107
Figure 3.32: $TT_3$ for CS 1 and CS 2 at minimum $R_{\Delta 2}$	110
Figure 3.33: $TT_3$ for CS 4 and CS 6 at minimum $R_{\Delta 4}$	110
Figure 3.34: $TT_3$ for CS 1 and CS 2 for positive $R_{\Delta 2}$	110
Figure 3.35: $TT_3$ for CS 4 and CS 6 for negative $R_{\Delta 4}$	110

Figure 3.36: Minimum $R_{\Delta 2}$ and $R_{\Delta 4}$ in $\Phi_V$ vs. $\Phi_L$ space _____	111
Figure 3.37a: Liquid TT <sub>3</sub> 3 and TT <sub>3</sub> 5 shift at constant $\Phi_L$ varying $\Phi_V$ _____	118
Figure 3.38a: Liquid TT <sub>3</sub> 3 and TT <sub>3</sub> 5 shift at constant $\Phi_V$ varying $\Phi_L$ _____	118
Figure 3.39: Triangles bordering along CLL1 _____	118
Figure 3.40: Triangles bordering along CLL2 _____	118
Figure 3.41: PEB1 and PEB2 _____	119
Figure 3.42: Region of $\Phi_L$ and $\Phi_V$ space resulting in feasible Petlyuk solutions. _____	119
Figure 3.43: Double feed pinch column TT <sub>3</sub> s – saturated liquid feed _____	121
Figure 3.44: Matching criterion 1 satisfied but criterion 4 is not _____	121
Figure 3.45: Matching criterion 4 satisfied along CLL1 but criterion 1 is not. _____	122
Figure 3.46: Matching criterion 4 satisfied along CLL2 but criterion 1 is not. _____	122
Figure 3.47: Matching criterion 2 satisfied but criterion 4 is not _____	122
Figure 3.48: Matching criterion 4 satisfied along CLL1 but criterion 2 is not. _____	122
Figure 3.49: Matching criterion 4 satisfied along CLL2 but criterion 2 is not. _____	122
Figure 3.50: No overlap of feasible regions in split ratio space below min column reflux. _____	122
Figure 3.51: TT <sub>3</sub> for column at minimum reflux _____	123
Figure 3.52: Region of feasibility shrinks to line at minimum reflux _____	123
Figure 3.53: $R_{\Delta 2MIN}$ and $R_{\Delta 4MIN}$ at varying reflux _____	125
Figure 3.54: Negative flow boundaries varying reflux _____	125
Figure 3.55: PEB1 and PEB2 varying reflux _____	126
Figure 3.56: $\Delta_5$ and $\Delta_2$ zero net flow lines varying reflux _____	126
Figure 3.57: $\Delta_3$ and $\Delta_4$ zero net flow lines varying reflux _____	126
Figure 3.58: Feasible region varying reflux _____	126
Figure 3.59: Feasible solutions in region 2, 3 and 4 _____	126
Figure 3.60: Feasible TT <sub>3</sub> s for net flow pattern 2 _____	126
Figure 3.61: Feasible TT <sub>3</sub> s for net flow pattern 4 _____	127
Figure 3.62: Feasible solutions in region 1, 2, 3, 4 and 5 _____	127
Figure 3.63: Feasible TT <sub>3</sub> s for net flow pattern 1 _____	127
Figure 3.64: Feasible TT <sub>3</sub> s for net flow pattern 5 _____	127

## Chapter 4:

- Figure 4.1: Ternary Column Profile Map for  $X_{\Delta k} = [-0.3, 0.2]$  and  $R_{\Delta k} = 10$ . Note:  
 $x_1$  – Heavy Component,  $x_2$  – Light Component,  $x_3$  – Intermediate Component \_\_\_\_\_ 138
- Figure 4.2: Quaternary Column Profile Map for  $X_{\Delta k} = [0.3, -0.2, -0.3]$  and  $R_{\Delta k} = 9$ . \_\_\_\_\_ 139
- Figure 4.3: Fifteen regions of the RCM with differing topology. \_\_\_\_\_ 141
- Figure 4.4: (a) Quaternary right angled tetrahedron boundary definitions. (b) Quaternary equilateral tetrahedron boundary definitions \_\_\_\_\_ 142
- Figure 4.5: Kaibel column (main column with post-fractionator). \_\_\_\_\_ 145
- Figure 4.6: Column section breakdown for the Kaibel column \_\_\_\_\_ 145
- Figure 4.7: Kaibel column feed point material balance \_\_\_\_\_ 146
- Figure 4.8: Feasible net flow patterns at the point of feed addition. (a)  $\Delta_3 > 0$ ,  $\Delta_5 > 0$ , Feasible. (b)  $\Delta_3 < 0$ ,  $\Delta_5 < 0$ , Feasible. (c)  $\Delta_3 > 0$ ,  $\Delta_5 < 0$ , Feasible. (d)  $\Delta_3 < 0$ ,  $\Delta_5 > 0$ , Infeasible. \_\_\_\_\_ 147
- Figure 4.9: Feasible net flow patterns at the mixing point of the rectifying section. (a)  $\Delta_2 > 0$ ,  $\Delta_3 > 0$ , Feasible. (b)  $\Delta_2 > 0$ ,  $\Delta_3 < 0$ , Feasible. (c)  $\Delta_2 < 0$ ,  $\Delta_3 > 0$ , Feasible. (d)  $\Delta_2 < 0$ ,  $\Delta_3 < 0$ , Infeasible. \_\_\_\_\_ 147
- Figure 4.10: Feasible net flow patterns at the first side draw. (a)  $\Delta_2 > 0$ ,  $\Delta_7 > 0$ , Feasible. (b)  $\Delta_2 < 0$ ,  $\Delta_7 > 0$ , Feasible. (c)  $\Delta_2 < 0$ ,  $\Delta_7 < 0$ , Feasible. (d)  $\Delta_2 > 0$ ,  $\Delta_7 < 0$ , Infeasible. \_\_\_\_\_ 147
- Figure 4.11: Feasible net flow patterns at the second side draw. (a)  $\Delta_4 > 0$ ,  $\Delta_7 > 0$ , Feasible. (b)  $\Delta_4 < 0$ ,  $\Delta_7 > 0$ , Feasible. (c)  $\Delta_4 < 0$ ,  $\Delta_7 < 0$ , Feasible. (d)  $\Delta_4 > 0$ ,  $\Delta_7 < 0$ , Infeasible. \_\_\_\_\_ 148
- Figure 4.12: Feasible net flow patterns at the mixing point of the stripping section. (a)  $\Delta_4 < 0$ ,  $\Delta_5 < 0$ , Feasible. (b)  $\Delta_4 > 0$ ,  $\Delta_5 < 0$ , Feasible. (c)  $\Delta_4 < 0$ ,  $\Delta_5 > 0$ , Feasible. (d)  $\Delta_4 < 0$ ,  $\Delta_5 < 0$ , Infeasible. \_\_\_\_\_ 148
- Figure 4.13: Various Flow patterns that arise due to feasible net flow combinations. (a) Flow Pattern 1. (b) Flow Pattern 2 (c) Flow Pattern 3. (d) Flow Pattern 4. (e) Flow Patter 5. (f) Flow Pattern 6. \_\_\_\_\_ 150
- Figure 4.14: Kaibel column feed point component material balance. \_\_\_\_\_ 151

Figure 4.15: The Range of Matching Criterion. (a) Matching Criteria 1. (b) Matching Criteria 2. (c) Matching Criteria 3. (d) Matching Criteria 4. (e) Matching Criteria 5. _____	154
Figure 4.16 a-c: Rectifying profiles for difference points at varying distances from the L-LI axis. _____	157
Figure 4.17 a-c: Stripping profiles for difference points at varying distances from the HI-H axis. _____	158
Figure 4.18: Material balance for Kaibel Column. (a) Infeasible Material balance. (b) Feasible Material balance _____	164
Figure 4.19: General Component Material Balance on Light Intermediate Component across CS2 and CS7. _____	166
Figure 4.20: General Component Material Balance on Light Intermediate Component over CS7 and CS4. _____	166
Figure 4.21: Infeasible FP 4 with zero net flow in CS7. _____	167
Figure 4.22: Sharp Split reduction diagram illustrating all the FPs for the Kaibel Column. _____	168
Figure 4.23: Column Section 7, residue curve between light and heavy intermediate pure components. _____	169
Figure 4.24: Net Flow Regimes in $\Phi_V$ vs. $\Phi_L$ for the Kaibel Column. _____	173
Figure 4.25: Feasible operating line in $\Phi_V$ vs. $\Phi_L$ for the Sharp Split Kaibel Column. _____	177
Figure 4.26: TT <sub>4</sub> for CS1 and CS2 not satisfying matching criteria 1. _____	179
Figure 4.27: TT <sub>4</sub> for CS4 and CS6 not satisfying matching criteria 4. _____	179
Figure 4.28: TT <sub>4</sub> for CS3 and CS5 satisfying matching criteria 5. _____	179
Figure 4.29: TT <sub>4</sub> for CS1 and CS2 satisfying matching criteria 1. _____	179
Figure 4.30: TT <sub>4</sub> for CS4 and CS6 satisfying matching criteria 4. _____	180
Figure 4.31: TT <sub>4</sub> for CS3 and CS5 not satisfying matching criteria 5. _____	180
Figure 4.32: TT <sub>4</sub> for CS1 and CS2 with an increase in vapour and liquid split ratio. _____	181
Figure 4.33: TT <sub>4</sub> for CS4 and CS6 with an increase in vapour and liquid split ratio. _____	181

Figure 4.34: $TT_4$ for CS3 and CS5 with an increase in vapour and liquid split ratio. _____	182
Figure 4.35: $TT_4$ for CS1 and CS2 with a decrease in vapour and liquid split ratio. _____	182
Figure 4.36: $TT_4$ for CS4 and CS6 with a decrease in vapour and liquid split ratio. _____	182
Figure 4.37: $TT_4$ for CS3 and CS5 with a decrease in vapour and liquid split ratio. _____	182
Figure 4.38: $\Phi_L, \Phi_V$ space with feasible operating line shown as the solid line.	183
Figure 4.39: Rectifying composition profile. _____	184
Figure 4.40: $TT_4$ for Rectifying profile. _____	184
Figure 4.41: Column profile for CS3. _____	185
Figure 4.42: $TT_4$ for CS3 _____	185
Figure 4.43: Column profile for CS5. _____	185
Figure 4.44: $TT_4$ for CS5. _____	185
Figure 4.45: Column profile for CS2. _____	185
Figure 4.46: $TT_4$ for CS2. _____	185
Figure 4.47: Column profile for CS4. _____	186
Figure 4.48: $TT_4$ for CS4 _____	186
Figure 4.49: Stripping composition profile _____	186
Figure 4.50: $TT_4$ for Stripping profile _____	186
Figure 4.51: Kaibel Column composition profiles. _____	186
Figure 4.52: All seven $TT_4$ for Kaibel Column. _____	186
Figure 4.53: Feasible operating point for single divided wall column in $\Phi_V, \Phi_L$ space. _____	187

## Chapter 5:

Figure 5.1: Quaternary Column Profile Map for $X_{\Delta k} = [0.3, -0.2, -0.3]$ and $R_{\Delta k} = 9$ . _____	194
Figure 5.2: (a) Quaternary right angled tetrahedron boundary definitions. (b) Quaternary equilateral tetrahedron boundary definitions. _____	196
Figure 5.3: Column section breakdown for the Kaibel column. _____	197

Figure 5.4: Net Flow Pattern 3 with the associated flow direction. (a) Net flow of material through each CS. (b) Net flow of components through each CS. _____	199
Figure 5.5: Split ratio space with the CS 7 zero net flow as the only feasible sharp split Kaibel solution shown in red. _____	200
Figure 5.6: Constant reflux lines in the split ratio space for $R_{\Delta I} = 12$ . _____	201
Figure 5.7: $TT_4$ for CS 1 and CS 2 at $R_{\Delta 2-\min}$ . _____	203
Figure 5.8: $TT_4$ for CS 6 and CS 4 at $R_{\Delta 2-\min}$ . _____	204
Figure 5.9: Minimum reflux lines in CS 2 and CS 4. _____	205
Figure 5.10: Common eigenvectors that define the intersecting plane for $TT_{4-3}$ and $TT_{4-5}$ . _____	207
Figure 5.11: $TT_{4-3}$ and $TT_{4-5}$ intersection under minimum reflux conditions. _	208
Figure 5.12: Minimum reflux lines in CS 3 and CS 5. _____	210
Figure 5.13: Reduced $\Delta_7 = 0$ line (red) defined by the region of $\Phi_L$ and $\Phi_V$ space resulting in feasible Sharp Split Kaibel solutions. _____	212
Figure 5.14: $R_{\Delta 2-MIN}$ and $R_{\Delta 4-MIN}$ with varying CS 1 reflux. _____	214
Figure 5.15: Negative flow boundaries with varying CS 1 reflux. _____	214
Figure 5.16: $R_{\Delta-MIN}$ and $R_{\Delta 4-MIN}$ with varying CS 1 reflux. _____	215
Figure 5.17: CS 7 Zero Net Flow Boundary with varying CS 1 reflux. _____	215
Figure 5.18: CS 7 Zero Net Flow Boundary and feasible region with varying CS 1 reflux. _____	216
Figure 5.19: Minimum reflux conditions for the Kaibel Column. _____	218
Figure 5.20: Split ratio space as a function of the reflux in CS 1 indicating the solution towards the minimum reflux in CS 1 as well as the overall column. _____	219

## Chapter 6:

Figure 6.1: An example of a generalised column section _____	225
Figure 6.2: A quaternary Column Profile Map with $R_{\Delta} = 9$ and $X_{\Delta} = [0.2, -0.3, -0.2]$ and relative volatilities of 6, 4 and 2. The “shifted tetrahedron” in red indicates the movement of stationary points at finite reflux from the pure component vertices at infinite reflux. _____	226

- Figure 6.3: A liquid eigenvector map for relative volatilities of 3 and 1.5. \_\_\_\_ 228
- Figure 6.4: A column section breakdown of the four possible structures to separate a quaternary mixture with a main column and thermally coupled side stream units: (a) the DSS, (b) the DSR, (c) the HSSR, and (d) the Kaibel column. \_\_\_\_\_ 229
- Figure 6.5: A summary of the only possible net flow directions in the (a) DSR (b) DSS (c) HSSR and (d) Kaibel column. \_\_\_\_\_ 231
- Figure 6.6: Difference Point placement for (a) the DSS, (b) the DSR, (c) the HSSR, showing the relationship between the respective Difference Points and adjacent column sections. \_\_\_\_\_ 233
- Figure 6.7: A simple, one feed two product column with the associated column section breakdown. \_\_\_\_\_ 235
- Figure 6.8: A design for an equimolar quaternary mixture in a simple column for the AB-CD split at (a) minimum reflux, (b) above minimum reflux, (c) below minimum reflux and (d) planar intersection through eigenvectors evaluated at the feed condition. \_\_\_\_\_ 237
- Figure 6.9: Minimum reflux Transformed Triangle interaction depicting the co-linear common eigenvector. \_\_\_\_\_ 238
- Figure 6.10: Pinch point locations for various feed qualities \_\_\_\_\_ 240
- Figure 6.11: A generic thermally coupled (a) side rectifying and (b) side stripping with the corresponding net flow directions of each column section. 243
- Figure 6.12: An iso-reflux plot for the DSS at minimum reflux. \_\_\_\_\_ 246
- Figure 6.13: Transformed tetrahedrons at minimum reflux for the DSS. (a) Column sections 1 and 3. (b) Column sections 4 and 6. (c) Column sections 2 and 5. (d) Column sections 1 and 2. (e) Column sections 2 and 4. \_\_\_\_\_ 249
- Figure 6.14: An iso-reflux plot for the DSR at minimum reflux. \_\_\_\_\_ 250
- Figure 6.15: Transformed tetrahedrons at minimum reflux for the DSR. (a) Column sections 5 and 6. (b) Column sections 3 and 4. (c) Column sections 1 and 2. (d) Column sections 2 and 4. (e) Column sections 4 and 6. \_\_\_\_\_ 251

- Figure 6.16: An iso-reflux plot for the HSSR and Kaibel column at minimum reflux. \_\_\_\_\_ 252
- Figure 6.17: Transformed tetrahedrons at minimum reflux for the HSSR and Kaibel columns. (a) Column sections 1 and 3. (b) Column sections 2 and 4. (c) Column sections 5 and 6. (d) Column sections 1 and 2. (e) Column sections 4 and 6. \_\_\_\_\_ 254

## Chapter 7:

- Figure 7.1: Transformed triangles for a range of refluxes which depicts the tangency of the light-heavy boundary on the focus region boundary. \_\_\_\_\_ 267
- Figure 7.2: Reflux value representation on the Complex Boundary. \_\_\_\_\_ 268

## List of Tables

### Chapter 2:

Table 2.1: Solution values for examples discussed in Figure 2.15 and Figure 2.16. _____	39
Table 2.2: Comparison of the CPM-E techniques to valued methods. _____	56

### Chapter 3:

Table 3.1: Geometric Interpretation of Material Balance over CS 3 and 5 _____	79
Table 3.2: Profile and $TT_3$ Legend of Composition Diagrams _____	89
Table 3.3: Legend Figure 3.27a-e _____	100
Table 3.4: Summary of net flow regions illustrated in Figure 3.28 _____	102

### Chapter 4:

Table 4.1: Summary of net flow regions illustrated in Figure 4.24. _____	173
--------------------------------------------------------------------------	-----

### Chapter 5:

Table 5.1: Key of components for a general quaternary feed _____	199
------------------------------------------------------------------	-----

### Chapter 6:

Table 6.1 A summary of $X_d$ placement for various structures with sharp splits and an equimolar feed. Shaded cells indicate rectifying sections. _____	233
Table 6.2: Summary of pseudo feed streams to the generic side rectifying and stripping sections _____	244
Table 6.3: Reflux ratios at minimum reflux for all respective minimum structures _____	254
Table 6.4: Minimum vapour flows and thermodynamic efficiencies for all respective thermally coupled structures for volatilities of 6, 4, 2 and 1. _____	256

---

Table 6.5: Minimum vapour flows and thermodynamic efficiencies for all respective simple column sequences for volatilities of 6, 4, 2 and 1 258

## Nomenclature

$i$	[-]	<i>Component index</i>
$x_1$	[-]	<i>Light component composition</i>
$x_2$	[-]	<i>Heavy component composition</i>
$x_3$	[-]	<i>Intermediate component composition</i>
$X$	[-]	<i>liquid phase molar composition</i>
$Y^*(X)$	[-]	<i>equilibrium vapour phase molar composition</i>
$X_f$	[-]	<i>liquid phase feed composition</i>
$Z_f$	[-]	<i>Two-phase feed composition</i>
$CS$	[-]	<i>column section</i>
$i, j, k, p, q, r$	[-]	<i>column section index</i>
$R_{\Delta k}$	[-]	<i>Reflux ratio of column section k</i>
$L_k$	$[\frac{mol}{s}]$	<i>Column Section k internal liquid flow rate</i>
$L_{RS}$	$[\frac{mol}{s}]$	<i>Rectifying section internal liquid flow rate</i>
$L_{SS}$	$[\frac{mol}{s}]$	<i>Stripping section internal liquid flow rate</i>
$V_k$	$[\frac{mol}{s}]$	<i>Column Section k internal vapour flow rate</i>
$V_{RS}$	$[\frac{mol}{s}]$	<i>Rectifying section internal vapour flow rate</i>
$V_{SS}$	$[\frac{mol}{s}]$	<i>Stripping section internal vapour flow rate</i>
$\Delta_k$	$[\frac{mol}{s}]$	<i>Net flow of Column Section k: <math>\Delta_k = V_k - L_k</math></i>
$\Delta_{RS}$	$[\frac{mol}{s}]$	<i>Net flow of the Rectifying Section: <math>\Delta_{RS} = V_{RS} - L_{RS}</math></i>
$\Delta_{SS}$	$[\frac{mol}{s}]$	<i>Net flow of the Stripping Section: <math>\Delta_{SS} = V_{SS} - L_{SS}</math></i>
$n$	[-]	<i>stage number equivalent</i>
$X^T$	[-]	<i>liquid molar composition at the top of the CS</i>
$Y^T$	[-]	<i>vapour molar composition at the top of the CS</i>

$X^B$	[-]	<i>liquid molar composition at the bottom of CS</i>
$Y^B$	[-]	<i>vapour molar composition at the bottom of CS</i>
$X_D$	[-]	<i>liquid molar composition for the distillate product</i>
$Y_D$	[-]	<i>vapour molar composition for the distillate product</i>
$X_B$	[-]	<i>liquid molar composition for the bottoms product</i>
$Y_B$	[-]	<i>vapour molar composition for the bottoms product</i>
$X_S$	[-]	<i>liquid molar composition at a stationary point</i>
$Y_S$	[-]	<i>vapour molar composition at a stationary point</i>
$X_{\Delta k}$	[-]	<i>difference point of CS k</i>
$X_{\Delta k, i}$	[-]	<i>element i difference point of CS k</i>
$\tilde{s}$	[-]	<i>Mixing vector: [ <math>x_i - Y_i^*(x_i)</math> ]</i>
$\tilde{m}$	[-]	<i>Mixing vector: [ <math>X_{\Delta k, i} - X_i</math> ]</i>
$\alpha_i$	[-]	<i>Relative volatility for component i</i>
$\delta_k$	[-]	<i>Difference vector for CS k</i>
$D$	$[\frac{mol}{s}]$	<i>Distillate flow rate</i>
$B$	$[\frac{mol}{s}]$	<i>Bottoms flow rate</i>
$S$	$[\frac{mol}{s}]$	<i>Side-draw flow rate (Petlyuk column)</i>
$S_1$	$[\frac{mol}{s}]$	<i>First side-draw flow rate (Kaibel column)</i>
$S_2$	$[\frac{mol}{s}]$	<i>Second side-draw flow rate (Kaibel column)</i>
$\Phi_L$	[-]	<i>Liquid split ratio (<math>L_2/L_1</math>)</i>
$\Phi_{L1}$	[-]	<i>Liquid split ratio (<math>L_2/L_1</math>)</i>
$\Phi_{L2}$	[-]	<i>Liquid split ratio (<math>L_4/L_2</math>)</i>
$\Phi_L'$	[-]	<i>Liquid split ratio (<math>L_4/L_6</math>)</i>
$\Phi_V$	[-]	<i>Vapour split ratio (<math>V_2/V_1</math>)</i>
$\Phi_{V1}$	[-]	<i>Vapour split ratio (<math>V_2/V_1</math>)</i>
$\Phi_{V2}$	[-]	<i>Vapour split ratio (<math>V_2/V_1</math>)</i>
$\Phi_V'$	[-]	<i>Vapour split ratio (<math>V_4/V_6</math>)</i>

---

$Q_R$	$[\frac{J}{s}]$	<i>Reboiler Duty</i>
$Q_C$	$[\frac{J}{s}]$	<i>Condenser Duty</i>
$\Delta H_{vap}$	$[\frac{J}{mol}]$	<i>Difference in Enthalpy for vaporisation</i>
$\Delta S_{vap}$	$[\frac{J}{mol.K}]$	<i>Difference in Entropy for vaporisation</i>
$\Delta S_{mix}$	$[\frac{J}{mol.K}]$	<i>Difference in Entropy for mixing</i>
$\Delta S_{irr}$	$[\frac{J}{mol.K}]$	<i>Defined by equation D2</i>
$T_R$	$[K]$	<i>Reboiler temperature</i>
$T_C$	$[K]$	<i>Condenser temperature</i>
$TT / TT_3$	$[-]$	<i>Transformed Triangle (Ternary system)</i>
$TT_{3-k}$	$[-]$	<i>Transformed Triangle for CS k (Ternary system)</i>
$TT_4$	$[-]$	<i>Transformed Tetrahedron (Quaternary system)</i>
$TT_{4-k}$	$[-]$	<i><math>TT_4</math> for CS k (Quaternary system)</i>

# Chapter 1: Introduction

## 1.1 Overall Introduction

Distillation units are responsible for a significant part of the total energy consumption in the world's process industry (Halvorsen, 2001). It has been found that distillation columns may consume up to 40% of the energy (Shinskey, 1977) in a chemical plant. Consequently distillation has become a crucial area of concern for reducing energy requirements. With the escalating cost of energy and more so the stringent laws implemented restricting emissions due to the use of the energy, has provided a strong incentive for the development of more energy efficient distillation designs (Linhoff, 1979; Bharwada, 1982; Frey et al., 1984).

Two different classes of distillation sequences have been proposed in literature: conventional configurations (single feed, two products) and complex arrangements, more commonly known as thermally coupled configurations. These configurations include side-rectifiers, side-strippers, dividing wall columns, Petlyuk columns and Kaibel columns (Cahn et al., 1962; Petlyuk, 1965; Kaibel, 1987). It is well established that the employment of complex column configurations leads to significant savings of both capital and energy costs (Barrtfeld and Aguirre, 2003). Although complex configurations present better advantages, it is interesting to note that conventional distillation columns are more readily employed (Holland, 2005). The contributing factors regarding the under employment of the thermally coupled arrangements is, possibly due to a lack of understanding and knowledge of these columns.

The calculation of minimum reflux for any column is important as an initial step in the design of distillation columns (Shiras et al., 1950). The computation

accompanying minimum reflux may entail demanding and laborious calculations. These calculations may utilise process simulation programs, or alternatively simplifying assumptions are made (Koehler et al., 1995).

The ideas and methodologies for calculating minimum reflux for conventional columns can be extended to complex configurations (Carlberg and Westerberg, 1989). Up to now, no simple technique exists to model these complex configurations. The techniques proposed may have the draw-back that they are mathematically intensive and in some instances produce graphical representation of feasible designs that are cumbersome and difficult to understand. Therefore, a better technique will hence present the opportunity to better describe and consequently improve the understanding of these columns and envisage an improved realisation of the dynamics within these columns (Holland et al., 2004b).

## **1.2 Aim of thesis**

This thesis will illustrate the extended use of Column Profile Maps (CPMs) to find the minimum reflux solutions for conventional and complex configurations. We will attempt to improve the understanding of the internal workings, not only for conventional columns but more importantly of complex integrated distillation columns. This will diminish some of the uncertainties that have led to underemployment of these configurations.

The initial phase of the work introduces the Column Profile Map Eigenvector (CPM-E) technique which produces the non-iterative minimum reflux solutions and the regions of feasibility limiting the choices of product specifications in a conventional column. These ideas are then applied to the comprehensive design and analysis of the Petlyuk column. We will then demonstrate a direct extension of the Petlyuk column illustrating the potential of the CPM techniques to higher

order systems by designing and analysing the Kaibel column. The development of the feasible and optimal operating parameters is then acquired for the Kaibel Column. Finally, we investigate the value of the CPM-E technique to higher order systems by designing several thermally coupled multiple side unit configurations.

A summary of each chapter is discussed in the thesis overview below.

### 1.3 Thesis overview

Since each chapter has either been published or is in the process of being published, each chapter is prepared as a paper and can be read independently, hence there is repetition in the introduction to each chapter. This repetition specifically covers the derivation of the difference point equation as well as the associated column profile maps. Even though it does seem somewhat tedious, it does allow the reader a better understanding of the concepts discussed. Each chapter contains its own introduction and conclusion.

**Chapter 2** extends the application of Column Profile Maps to find the minimum reflux for multi-component systems for simple configurations. The method called Column Profile Map-Eigenvector (CPM-E) technique which is applicable to any number of components is applied to ternary and quaternary systems and makes use of eigenvector theory developed by Holland et al (2004a). This chapter demonstrates a novel method, in order to determine the minimum energy demand in any conventional column. However, the concepts of the method can be applied to almost any complex system such as the Petlyuk and Kaibel column. The CPM-E technique was originally developed to eliminate onerous and tedious calculations when finding the minimum energy demand for distillation configurations. The technique is non iterative and utilises simple mathematics which makes it an attractive alternative to other current methods. Dr. Ivar Halvorsen, of the Norwegian University of Science and Technology, offered great

insight and much guidance in this work, for which I am extremely grateful. The work has been presented at the peer reviewed Distillation and Absorption 2010 conference held in Eindhoven, Netherlands and an extended abstract will appear in the *IChemE Symposium* series. The extended abstract can be found in Appendix I.

**Chapter 3** deals with the first application of Column Profile Maps to a finite reflux complex system and shows the comprehensive design methodology for the Petlyuk column at sharp-split conditions. The first application of the CPM-E technique is used in this chapter to find the region of feasibility in the split ratio space and hence the minimum reflux conditions for the coupled sections of the Petlyuk column. The CPM as well as the application of the CPM-E technique methodology for Petlyuk design is very powerful and efficient. The procedure for generating the feasible/optimality region and minimum reflux allow for the determination of all feasible solutions and minimum reflux ratio, for all zeotropic systems. On selecting a reflux ratio and split ratio pair, individual column solutions can be generated without requiring iteration. The work has been published in *Industrial and Engineering Chemistry Research* (see Holland et al, 2010). Although my name appears as the second author on this paper, the work is largely Dr. Simon Holland's ideas. This chapter can also be found in Dr. Holland's thesis (Holland, 2005).

**Chapter 4** is an extension of the Petlyuk column analysis which deals with the sharp split Kaibel column design. The purpose of the work is to illustrate the application of the Column Profile Map techniques to higher order systems. The formulation of the operating line allows for the determination of all feasible solutions for all zeotropic systems. The methodology proposed allows for parameters such as feed stage placement, side-draw stage placement, total required stages, column section stage requirements as well as internal vapour and liquid ratios are an expected outcome of the CPM technique. Much of the guidance in this chapter was offered by Dr. Simon Holland, for which I am extremely thankful. Parts of the concepts of this chapter have been published in

*Computers and Chemical Engineering* (See Hildebrandt et al. (2010)) which deals with the general application of Column Profile Maps to complex distillation configurations. This publication was originally work presented at the FOCAPD 2009 conference held in Breckenridge, Colorado. As a result of the significant contribution the work made to knowledge, the concepts from the presentation were published. The extended abstract can be found in Appendix H.

**Chapter 5** is the second part of the Kaibel column solution and follows on directly from chapter four. This chapter presents the development of the parameterised region containing all feasible column solutions for a given feed composition. The solutions and ideas of over-refluxed Kaibel columns are extended to the minimum reflux solution. This chapter utilises the CPM-E method for a quaternary system. This chapter is as of yet unpublished.

**Chapter 6** explores several options of multi-component thermally coupled distillation configurations. The investigation utilises the CPM-E techniques focusing more specifically on a quaternary system and determines whether there is a superior structure under certain conditions in terms of energy demand and efficiency. Determination of a superior structure will allow the designer to negate irrelevant structures and designs under certain applicable conditions. This work was done together with Daniel Beneke and equal effort and insight into the paper was given from both parties. Daniel Beneke's thesis also contains this chapter and I am grateful for his insights and hard work in achieving our goal. Aspects of this chapter have been submitted to the *American Institute of Chemical Engineers Annual Meeting 2011*.

## Chapter 2: Novel Minimum Reflux determination using Column Profile Maps

*This work has been prepared in the form of a paper for future publication. Dr. Ivar Halvorsen, of Norwegian University of Science and Technology, offered great insight and much guidance in this work, for which I am extremely grateful. The work has been presented at the peer reviewed Distillation and Absorption 2010 conference held in Eindhoven, Netherlands.*

---

### **Abstract**

Column Profile Map Eigenvectors (CPM-E) technique is introduced to determine the minimum energy demand for multi-component feed in two-product distillation processes. The new method makes use of Column Profile Maps and the concept of "moving triangles" and develops co-linearity criteria based on the eigenvectors of the Jacobian of the separation vector evaluated at the feed composition. The technique is a short cut, geometrical, non-iterative method and can be used to predict how the minimum reflux solution is related to the feed-component distribution for all possible operating conditions. The CPM-E technique is a powerful tool that can be applied to complex column arrangements, such as Petlyuk or Kaibel Columns. The CPM-E approach is non-exclusive and can therefore be applied to any type of split, sharp or sloppy split, irrespective of the number of components. It will be shown that the CPM-E technique can be used to determine minimum reflux solutions quickly and effectively. From this, it is shown that three limiting product composition regions under minimum reflux conditions are present within a ternary system.

---

## 2.1 Introduction

Although distillation is a very energy intensive unit operation, it is the most used separation technique in the chemical industry. Distillation is employed for about 95% of liquid separations in chemical process industries, and the energy used for this accounts for an estimated 3% of the world's energy consumption (Hewitt et al., 1999; Parkinson., 2009). The use of distillation for separation processes in the long term is unlikely to change, because alternative unit operations are often either not technically feasible or commercially competitive (Koehler et al., 1995).

The continuous escalating cost of energy has forced industry to reduce its energy consumption. In addition to this, the effort to prevent climate change has caused stringent environmental regulations that have generated the need to adopt new and efficient unit operations. The energy demand in distillation can be reduced for instance by the thermal integration of distillation columns and sections within the distillation configuration, such as hybrid arrangements, as well as apposite incorporation of distillation systems with the overall process, and heat pumping techniques (Malinen and Tanskanen, 2009; Knapp and Doherty, 1990). From this, intensive investigations have been undertaken to develop new and more useful models to operate the distillation units as optimally as possible.

Work on minimum flows and minimum energy use in distillation is large and dates back to the 1940s. One of the first published papers for finding minimum reflux was the work of Brown and Holcomb (1940). The works of Underwood (1945, 1946a, 1946b, 1948) for the case of constant relative volatilities is of the earliest work most cited in distillation. It is well known that minimum energy requirements correspond to minimum reflux and/or boil-up ratios and an infinite number of equilibrium stages so that the column just performs for the desired separation. Most methods for determining minimum energy requirements are based on either methods for directly finding pinch points or rigorous column simulations.

Koehler et al. (1995) give a review of methods for determining minimum energy requirements for conventional columns as well as complex column configurations up to 1995. They show that many of the minimum energy demand techniques are related to the methods of Underwood. They also give an example of a minimum energy column that corresponds to non-pinched profiles. The equations of Underwood (1945, 1946a, 1946b and 1948) have been applied by many authors for the analysis of multi-component distillation. These include Shiras et al. (1950), King (1980), Franklin and Forsyth (1953), and Wachter et al. (1988). Minimum-energy expressions for Petlyuk type arrangements with three and more components have been presented by Fidkowski and Krolikowski (1986), Carlberg and Westerberg (1986a, 1986b), Halvorsen and Skogestad (2003b and 2003c). Work presented by Halvorsen and Skogestad (2003 a, b, c) introducing  $V_{\min}$  diagrams produce solutions for minimum energy requirements for the general multi-component case. Although the Underwood methodologies only apply almost exclusively to ideal systems, work from Vogelpohl (1974) and Hausen (1952) have applied the Underwood routes to binary azeotropic mixtures.

For non-ideal multi-component mixtures which includes azeotropic systems, methodologies for finding minimum reflux and boil-up ratios are more complicated in comparison to ideal systems. A great many works done by Doherty and co-workers (Levy et al., 1985; Pham et al., 1989; Fidkowski et al., 1991) who have proposed several techniques that produce rapid accurate minimum reflux solutions for ideal as well as highly non-ideal azeotropic systems. These methods suffer the drawback that an initial reboiler duty must be selected. This indicates that iterative steps must be taken within the method. It also indicates that some uncertainty arises whether the selected duty will produce a minimum reflux solution. The approaches adopted by Doherty and co-workers rely heavily on pinch points. The basic concept relies on the interaction of vectors between the pinch points of both the rectifying and stripping sections which sets a foundation for calculating the minimum reflux. For more work based on pinch points refer to Doherty and Malone (2001), Koehler et al. (1991), Urdaneta et al. (2004), Lucia et al. (2006) and Lucia et al. (2007).

The focus of this manuscript is to demonstrate a novel method, called Column Profile Maps Eigenvector (CPM-E) technique, in order to determine the minimum energy demand in any conventional column. However, the concepts of the method can be applied to almost any complex system such as the Petlyuk and Kaibel column. In addition to this, feasibility regions associated to select eigenvectors evaluated at the feed composition is demonstrated. The regions are developed from the profiles that portray linear behaviour through the feed composition, either entirely on the profiles of the stripping or rectifying section or a tangency condition on either of the sections. The feasible regions encompass sharp, non sharp splits and more importantly double feed pinch split.

### **2.1.1 General Overview of minimum energy demand methodologies**

Many of the current techniques discussed have practical limitations to the application based on the type of split. The localisation of pinch point based methods entail some amount of prior knowledge on the particular separation problem. The CPM-E technique presented here will hopefully eliminate these restrictions. In order to compare the new techniques to previously proposed methods, a brief overview of these important approaches is given.

#### ***2.1.1.1 Boundary Value Method***

Levy et al. (1985) introduced the boundary value method (BVM). The BVM, like so many other methodologies is based on solving a first order differential equation that is derived under constant molar over flow assumptions. The profiles of both column sections in a simple column can be determined when the products are fully specified and an arbitrary reflux or boil-up ratio is chosen. Since the reboiler duty (reflux ratio) is chosen arbitrarily, the resulting trajectories do not need to correspond to a feasible separation, as the profiles do not necessarily fulfil the criterion of intersecting within the Gibbs triangle or more commonly known Mass Balance triangle. If the profiles intersect, the point of intersection corresponds to the feed tray. Profiles that intersect and proceed to their respective pinch points

past the intersection point are regarded as over-refluxed columns i.e. more energy is put into the system than is necessary for the specified separation. Therefore, in order to determine minimum reflux with the BVM means to find the smallest reflux ratio which makes intersection of both profiles possible and thus allowing one profile to pinch (terminate) on the other. A feed pinch exists if one profile pinches on the other which occurs at the minimum reflux. The second type of pinch, called the saddle pinch exists if a profile has to pass through a saddle type node. This would mean that it makes ideal profiles linear as product specifications would have occurred at the boundary of the Gibbs triangle (sharp splits). The authors of BVM show that a co-linear condition of the pinches has to be satisfied at systems portraying extreme splits. This means, the reflux ratio that makes the feed pinch, saddle pinch and feed collinear is the minimum reflux. The co linearity criterion is exact for ideal systems and is only an approximation for non-ideal and azeotropic systems as the boundaries of non-ideal and azeotropic systems are not linear. The BVM is an iterative method, which can be time consuming if a continuously unsuitable reboiler duty is estimated. A manifold of profiles can be determined and has to be checked for intersection, when these components are varied. Due to the graphical nature of the BVM it cannot be applied to systems with more than four components, since checking whether profile intersection is present is mandatory. Though, for quaternary systems and lower order systems the BVM gives precise and accurate results.

### ***2.1.1.2 Zero Volume Criteria***

Julka and Doherty (1990) extended the work of BVM developed by Levy et al. (1985) to the Zero Volume criteria (ZVC). In addition to corresponding profile pinches of the rectifying section on the stripping section or vice versa and the collinear criteria described by the BVM, the ZVC uses all the pinches to completely describe the profiles associated to estimated reboiler duties and formulates a zero volume criteria of interacting nodes to satisfy minimum energy demand. For ternary systems, formulations would require certain nodes/pinch points of both sections to be collinear in order to satisfy minimum reflux as they do with BVM. For higher order systems, such as quaternary systems the authors

have shown that C-1 fixed points of the sections are used to construct a set of vectors. The value of reflux that makes the volume of these vectors zero corresponds to minimum reflux. This means, the minimum energy demand corresponds to the vectors from both column sections that have to be coplanar. The fact that the criterion can be verified from the determinant of the vectors evaluated at the stationary points that correspond to minimum reflux allows the ZVC to be applicable to any number of components. However, the criterion is only applicable if an intimate knowledge of the type of pinch and the location of the pinch which determines minimum reflux is known. This means that the method can only be applied to direct and indirect splits. The work of Fidkowski et al. (1991) closely resembles the BVM (Levy et al., 1985) for ternary and ZVC (Julka and Doherty, 1990) for quaternary systems. Fidkowski et al. (1991) identify a major practical limitation that arises on account of the tangent pinch developed by Levy et al. (1985). They show that this phenomenon is easily understood as a turning point and that a design method can be developed using an arc length continuation.

### ***2.1.1.3 Eigenvalue Criterion***

Poellmann et al. (1994) proposed a method based on eigenvalue theory that Bausa et al. (1998) regard as a combination of the BVM and ZVC. The procedure makes use of plate-to-plate calculation and only the regions close to the pinch points are considered. As a result of the fact that any nonlinear liquid profile can be accurately made linear near a pinch point due to the fact that the composition change from stage to stage near the pinch is very small, in addition to this, Poellmann et al. (1994) presented an optimization procedure to perform the assessment for the intersection of profiles, the Eigenvalue criterion is applicable to any number of components and can handle the most non-ideal systems. However, the selection of the pinch points actually occurring in the column profile is not a simple task. Frequently, the active pinches cannot be determined solely from the product specifications. In this case the column profile, which is not available at this stage of the procedure, needs to be analyzed in order to determine the loci of the trajectories and the relevant subset of active pinch points. When more than one

unstable eigenvector exists in one pinch point, a manifold of profiles can be calculated. For multi-component mixtures, multidimensional manifolds of column profiles have to be calculated and checked for intersection. Thus, the computational effort will increase drastically for higher numbers of components.

#### ***2.1.1.4 Rectification Body Method***

Bausa et al. (1998) proposed a method called the rectification body method (RBM) for the determination of minimum energy demands for multi-component distillation. The RBM has been considered as a generalisation of certain previously proposed techniques. In the opinion of Lucia et al. (2006) the RBM is more closely related to a combination of the eigenvalue method by Poellmann et al. (1994) and the BVM of Doherty and co-workers. Rectification body triangles are constructed from the pinch points of the rectifying and stripping sections. The nature of the node needs to be known, as the development of the rectification body is dependent on the direction of column profile trajectories originating from the predefined product specification. Minimum energy of the RBM is one where the triangles of both bodies touch one another. Due to estimated reboiler duties, the procedure of finding the minimum reflux is very similar to the BVM. This implies that the procedure is iterative and if a reflux ratio is poorly chosen it may cause a divergent solution, which forces a new selection of duty and the repeat of the procedure. Additional to this, the RBM requires feasible product specifications. Various procedures have been proposed to determine feasible products (Fidkowski et al., 1993; Poellmann et al., 1996; Safrit and Westerberg, 1997). Another aspect of the RBM that may cause some concern is the approximation of linear lines between nodes for highly non-ideal systems. Due to the approximation of the curved concentration profile, a large degree of inaccuracy may arise. The triangular rectifications bodies have recently been extended by Urdaneta et al. (2004) who have proposed a solution for minimum energy requirements for reactive distillation.

### 2.1.1.5 $V_{\min}$ Diagrams

$V_{\min}$  diagrams introduced by Halvorsen and Skogestad (2003a) is a graphical representation of the minimum energy consumption and show its relationship with the feed distribution for all possible operating points in a two-product conventional distillation column. The  $V_{\min}$  diagram is at this point a new application of the Underwood equations and can be visualised for any number of components (Halvorsen, 2001). The minimum vapour expression is derived for ideal mixtures under constant molar overflow and constant relative volatility, but is applicable to any zeotropic system. According to the authors, the distribution boundaries in the diagram will not be linear for a non-ideal system but is still applicable to the technique. This is made possible when the flow rates immediately above the feed stage are considered. Due to fact that the Underwood equations are only directly applicable to constant relative volatility systems; it would involve rigorous simulations to calculate non-ideal systems. The  $V_{\min}$  diagram methods have successfully been applied to more complex systems, such as the Petlyuk and Kaibel arrangements for ideal systems (Halvorsen and Skogestad, 2003b, 2003c).

### 2.1.1.6 Shortest Stripping Line

The shortest stripping line approach proposed by Lucia et al. (2006) and Lucia et al. (2008) illustrates that in a simple distillation column, energy efficiency of a configuration is directly related to length of the stripping line. That is, the authors begin with the intuitive belief that following the longest residue curve must somehow be related to the highest energy costs associated with performing a given separation. Furthermore, if the longest residue curve is the most costly separation, then the shortest curve should result in the use of the least amount of energy required for the given separation task. The Shortest Stripping Line technique makes use of distillation lines, which are equivalent to operating lines for finite separators under constant molar overflow as the authors noted that they are only interested in finite stages and finite internal flows of the columns. The shortest stripping line technique has been successfully applied to a variety of traditional distillation systems that show evidence of feed, saddle, or tangent

pinch points defined by Levy et al. (1985) reactive distillation columns, and columns that have minimum energy requirements that do not occur at a pinch point. Lucia et al. (2008) have applied the concept of shortest separation lines to multiunit reaction/separation/recycle (RSR) processes such as the production of MTBE from isobutene and methanol. In all these instances Lucia et al. (2008) have illustrated that the minimum energy requirements correspond to the shortest separation line. Lucia and co-workers have also demonstrated that both McCabe-Thiele method and the boundary value methods of Doherty and co-workers have shortest stripping line interpretations when they are used to determine minimum energy requirements. In more recent work, Lucia and co-workers have shown that Underwood's method also have a shortest stripping line interpretation and represents a global minimum in energy consumption for a specified set of light and heavy key component recovery fractions.

## 2.2 Background

### 2.2.1 Column Profile Maps

A Column Profile Map, introduced by Tapp et al. (2004), is produced from the Difference Point Equation shown by Equation 2.1. The derivation of the Difference Point Equation is shown in Appendix F. These Maps are composition trajectories generated for column sections for a pre-defined difference point ( $X_{\Delta}$ ) and reflux ratio ( $R_{\Delta}$ ). It should be noted that the work presented here has certain assumptions associated with it that makes the modelling process unambiguous; the Difference Point Equation is derived under constant molar over flow assumptions. The feed material is saturated liquid or saturated vapour conditions and perfect mixing is assumed over all mixing points.

The Difference Point Equation can model any vapour liquid equilibrium cascade defined within a column section and not only stripping and rectifying sections. These include absorption and stripping columns.

$$\frac{dX}{dn} = \left(1 + \frac{1}{R_{\Delta}}\right) (X - Y^*(X)) + \frac{1}{R_{\Delta}} (X_{\Delta} - X) \quad (2.1)$$

$$\text{Where: } X_{\Delta} = \frac{vY_T - LX_T}{\Delta}; \quad R_{\Delta} = \frac{L}{\Delta}; \quad \Delta = V - L$$

From the mathematical definitions given,  $\Delta$  is the difference between the vapour and liquid flows within a column section. It is better described as the net flow of material and is a pseudo stream flowing up or down in a column section. If the vapour flow were larger than the liquid flow in a column section,  $\Delta$  would be positive as we know it to be in a rectifying section (RS).

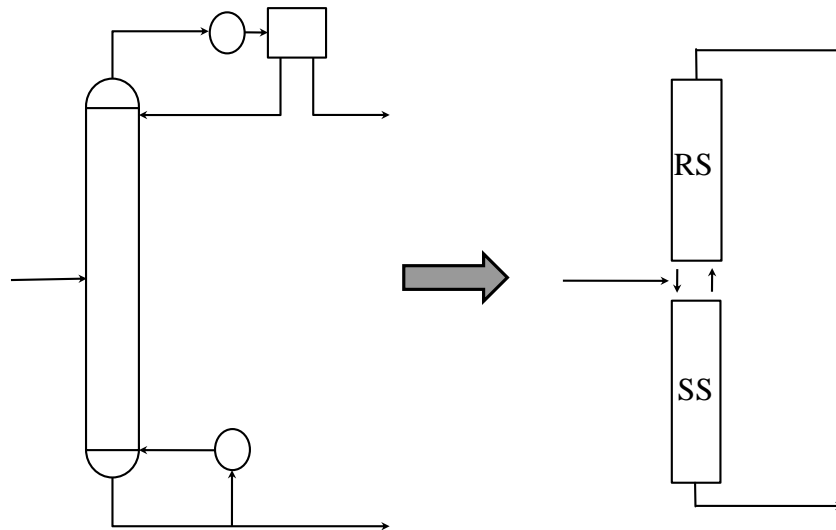


**Figure 2.1: Column section breakdown for the Conventional column.**

Conversely, if the vapour flow were smaller than the liquid flow in a column section,  $\Delta$  would be negative as we know it to be in a stripping section (SS). The difference point ( $X_{\Delta}$ ) is the pseudo composition vector of the net flow, and is physically valid anywhere in composition space.

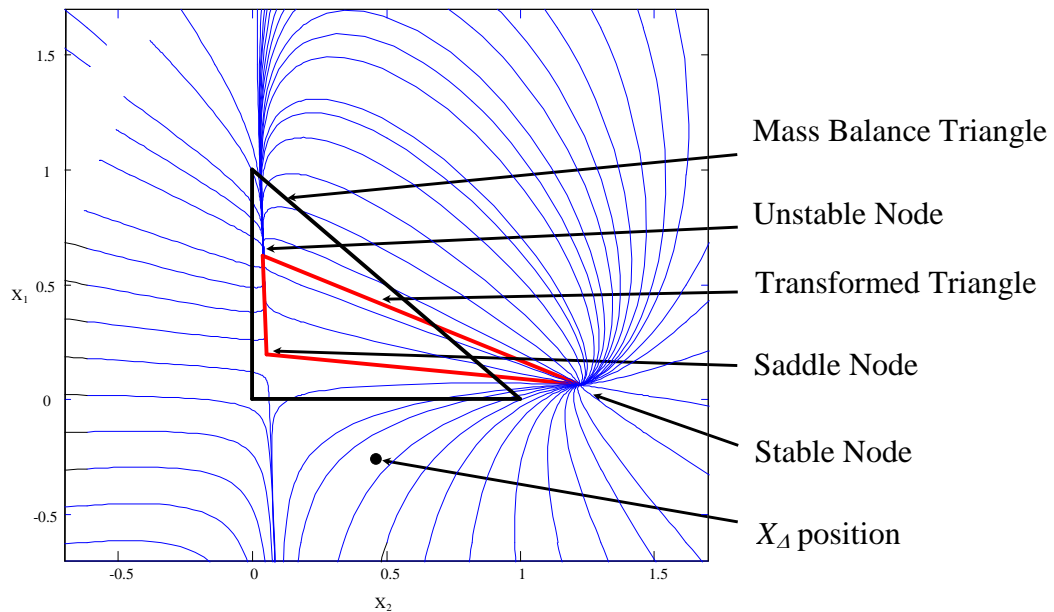


**Figure 2.2: Ternary Column Profile Map for  $X_A = [0.45 -0.25]$  and  $R_A = 6$ .**

**Note:  $x_1$  – Light Component,  $x_2$  – Heavy Component,  $x_3$  – Intermediate Component.**

The elements of the difference point sum to unity as they do for conventional compositions. A positive component value is a net flow of up and a negative value is a net flow of the component down the column section. The reflux ratio is defined as the ratio of liquid flowing down the column section to the net flow in the column section. Because of its dependence on  $\Delta$ ,  $R_\Delta$  can be either positive or negative.

To produce a Column Profile Map, the Difference Point Equation is solved at various initial conditions, throughout the composition space for a specific  $X_A$  and  $R_\Delta$  (where,  $n \rightarrow -\infty$  and  $n \rightarrow \infty$ ). A Column Profile Map for a three component system is illustrated in Figure 2.2. The resulting column trajectories either tend to infinity or terminate at a stationary point. For a ternary system, with constant relative volatility, there are three stationary point solutions present in a Column Profile Map. These are characterised as stable, unstable and saddle stationary points or nodes (See Figure 2.2). Unless otherwise stated, for convenience and simplicity, an ideal model with constant relative volatilities of [4 2 1] is used for the remainder of this paper.

### 2.2.2 $\Delta$ and $X_{\Delta}$ material balance within a conventional column

In the case of conventional columns, i.e. single feed and two products, the properties of the net flows, difference points and reflux ratios are constrained to suite and only produce feasible profiles that fall within the Mass Balance Triangle (MBT). In order to better understand this, we will take a closer look at the material balance within and around the column.

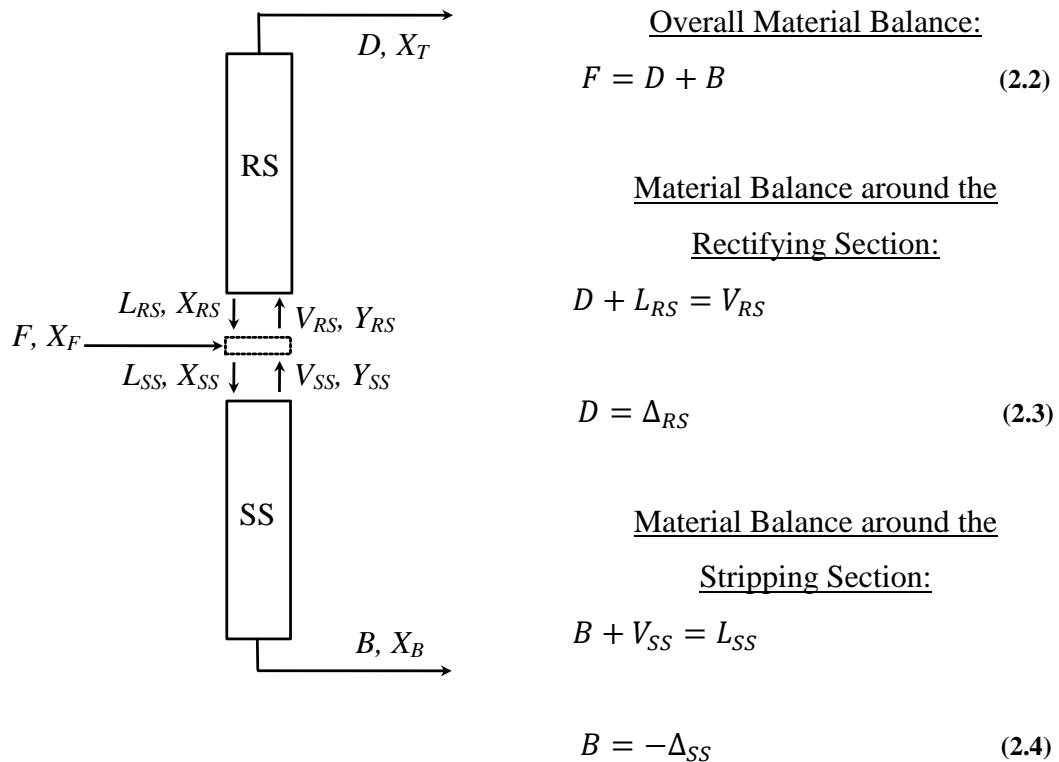


Figure 2.3: Material balance around feed point.

The net flows in conventional distillation columns are restricted to flow up ( $V > L$ ) in a RS (Equation 2.3) and flow down ( $V < L$ ) in a SS (Equation 2.4) (See Figure 2.1). This can be seen by performing a material balance around the column and around its individual column sections as shown by Figure 2.3 and Equations 2.2 to 2.4. Equation 2.3 indicates that the distillate product flow is equivalent to the positive net flow in the RS. Similarly, Equation 2.4 shows that the bottoms product flow is equal to the negative net flow in the stripping section. Both

equations demonstrate the constraints of the net flow and therefore the reflux ratio within the respective column sections. Let us now look at the remainder of the Difference Point Equation variables by performing an overall component material balance around various parts of the column.

Overall Component Material Balance:

$$FX_F = DX_D + BX_B \quad (2.5)$$

Component Material Balance around the Rectifying Section

$$\begin{aligned} DX_D + L_{RS}X_{RS} &= V_{RS}Y_{RS} \\ DX_D &= \Delta_{RS}X_{\Delta_{RS}} \end{aligned} \quad (2.6)$$

Component Material Balance around the Stripping Section

$$\begin{aligned} BX_B + V_{SS}Y_{SS} &= L_{SS}X_{SS} \\ BX_B &= -\Delta_{SS}X_{\Delta_{SS}} \end{aligned} \quad (2.7)$$

Substituting 2.6 and 2.7 into 2.5 gives

$$FX_F = \Delta_{RS}X_{\Delta_{RS}} - \Delta_{SS}X_{\Delta_{SS}} \quad (2.8)$$

The difference point selection, i.e. distillate composition and bottoms composition, cannot be selected outside the MBT as compositions selected outside the MBT cannot be achieved for a conventional column. This can be seen by performing a component material balance around the column and its individual column sections as shown by Equations 2.5 to 2.8. Substituting Equations 2.3 and 2.4 into Equations 2.9 and 2.7 respectively, we prove that the difference point of the rectifying section ( $X_{\Delta_{RS}}$ ) is the top product,  $X_D$ , and the difference point for the stripping section ( $X_{\Delta_{SS}}$ ) is the bottom product composition,  $X_B$ . The difference point selected in Figure 2.2 is not a feasible point for a rectifying or stripping section. An additional and very important detail we have not yet discussed from the material balances is the fact that the distillate product ( $X_{\Delta_{RS}}$ ), bottoms product ( $X_{\Delta_{SS}}$ ) and the feed composition lie on the same straight line (Equation 2.5). Their positions relative to one another are dependent on the net flow of RS and SS

governing them. This means mass balances will govern our selection of component difference point positions in the system. This will be discussed in greater detail later.

The reflux ratio relationship with net flow shows that in the same way as we are constrained to flow up in a RS and down in a SS tells us that we can only have reflux ratios that are positive in the RS and negative in the SS. Any other direction other than specified would result in an infeasible column profile intersection.

### 2.2.3 Eigenvector Maps

The use of eigenvalues and eigenvectors has proven to be very useful over the past decade to better describe and model distillation systems. The eigenvalues characterize the kind of singularity that can occur at that point in space where the eigenvalue is evaluated, while the eigenvectors characterize the asymptotic direction of the trajectories in the neighbourhood of the singularity. Holland et al. (2004b) introduced Eigenvalue and Eigenvector Maps and illustrated the usefulness of these maps for manipulating phase diagrams and therefore column profiles. The maps predict movement of the singularities based on the value of the design parameters of the difference point selected in the composition space and the reflux ratio. Eigenvectors shown in the maps are a product of the Jacobian Matrix of the separation vector evaluated at a singularity point. An eigenvector map can be obtained by plotting the eigenvectors over a range of  $x$  values, illustrated in Figure 2.4. (Refer to Appendix G for the mathematical background of eigenvectors)

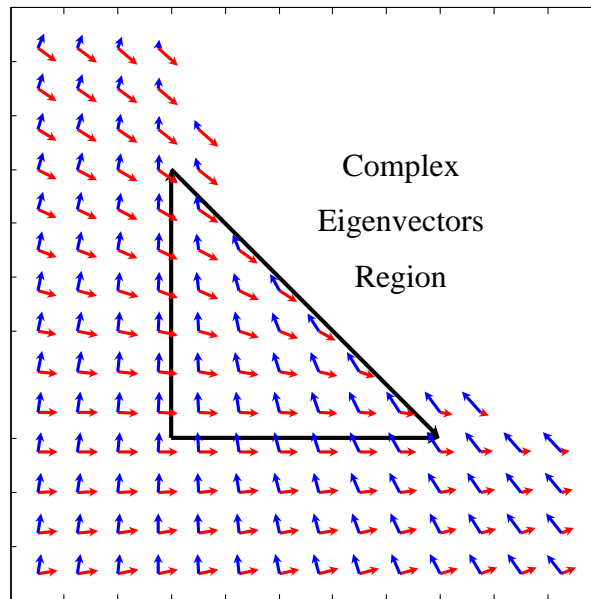


Figure 2.4: Eigenvector map for an ideal system. The compositions  $x_1$  and  $x_2$  are in the range  $X_i = [-0.5, +1.5]$ .

There exists a unique eigenvector map for each system modelled by a particular set of thermodynamic data because it is only a function of the separation vector i.e.  $X-Y^*(X)$  (Refer to Holland et al 2004a). The usefulness of these eigenvectors will be shown later.

### 2.3 Conditions for Minimum Reflux and Transformed Triangles

The design routines and methods followed and developed by many researchers in the field of separation technology have led to a great many different approaches for minimum reflux solutions. In this paper, we will make use the Difference Point Equation and eigenvector maps proposed by Tapp et al. (2004) and Holland et al. (2004) respectively to derive a generic method for finding minimum reflux ratios in ideal and zeotropic distillations as well as a simple and effective

approximation to minimum reflux for non-ideal and azeotropic systems which we have called Column Profile Map Eigenvector technique (CPM-E).

In order to establish and demonstrate the approach, it would be convenient to give a definition of minimum reflux conditions that applies to the graphical nature of the technique. It is well known that a conventional column is regarded as feasible, if the liquid profiles of the rectifying and stripping section intersect in the real composition space. Levy et al. (1985) defines the point of minimum reflux for a conventional distillation column as the condition at which one of the profiles just ends (pinches) as it reaches the other profile. This criteria and additional rules, that will be discussed, are pertinent to the CPM-E technique, as the CPM-E method is analogous to the Boundary Value Method (BVM) suggested by Levy et al. (1985).

In order to better understand the CPM-E technique it would be convenient to discuss another method in greater detail that uses ordinary differential equations and graphical techniques as we do to determine feasible columns and therefore columns under minimum reflux conditions. As described earlier, the approach taken by Levy et al. (1985), named, Boundary Value Method, was iterative but determined the minimum reflux accurately when compared to Underwood's methods. The BVM is implemented by identifying co-linearity of the lines drawn from the saddle node of the rectifying section through the feed (saddle pinch) and the unstable node through the feed (feed pinch) for direct splits. By plotting the liquid profiles for each section, showing that one of the profiles ends on the other and illustrating co-linearity of the feed pinch and saddle pinch lines, minimum reflux is determined. For indirect splits the saddle pinch and feed pinch are reversed, thus the rectifying section has a feed pinch and the stripping section has a saddle pinch.

By tracking the type of node and finding the correct node that satisfies co-linearity through the feed composition, we can determine the minimum reflux solution for

sharp splits. As mentioned previously, this process is iterative and requires rigorous solving routines.

Tapp et al. (2004) showed that the Column Profile Maps at finite reflux are simply transforms of the residue curve maps. The transform shifts the fixed points of the system in the space, maintaining (in constant relative volatility systems) the shape of the boundaries initially defined by the MBT (see Figure 2.2) i.e. the profiles connecting the fixed points are straight. This has resulted in the phenomenon being referred to as “Moving Triangles” or “Transformed Triangles” ( $TT_3$ ).

A typical example of a feasible liquid-phase composition profile is shown for a constant relative volatility system with their associated liquid  $TT_3$ 's in Figure 2.5a-c. The solid black line is the rectifying profile with its associated liquid  $TT_3$  shown as the blue triangle and the distillate composition given as the blue dot. The dashed black line is the stripping profile with its associated liquid  $TT_3$  shown as the pink triangle and the bottoms composition given as the pink dot. The green dot is the feed composition. These colours and notations will be adopted for the rest of this paper unless specified otherwise. Referring to Levy et al. (1985) description of co-linearity lines (CLL) at minimum reflux conditions, it can be seen by referring to Figure 2.5 a-c that it would be easier to track these saddle pinch and feed pinch which supplement co-linearity by using  $TT_3$ 's of the rectifying and stripping sections. In other words, there is no need to solve the differential equations and to plot the individual profiles, but it is more convenient to solve for the stationary points that define the nodes and rather plot the straight lines that join these nodes that are defined due to the fact that the  $TT_3$  retains all the qualitative topological information of the column profile. Solving for the stationary points is computationally simple and can in fact be done analytically for three component constant relative volatility systems. The stationary points are solved by equating the Difference Point Equation to zero and solving for the liquid compositions.

In Figure 2.5 a-b, the reflux ratio is greater than the minimum; the profiles cross and continue further on. The sections of the profile past the intersection are

meaningless, as shown by Lewis and Matheson (1932). The column that Figure 2.5b describes is subject to less energy input for the same product specifications as it is closer to the minimum reflux condition, since the overlap of the profiles is not as great as it is in the previous example (Figure 2.5a). Therefore, the desired structure that represents minimum reflux is shown in Figure 2.5c where the stripping profile ends or terminates on the rectifying profile. The point on the rectifying profile and stripping profile where they intersect is the feed stage.

Let us now focus our attention to the associated  $TT_3$ s of Figure 2.5a-c. The  $TT_3$ s of the associated profiles in Figure 2.5a overlap considerably. As we move closer to the minimum reflux condition, the associated  $TT_3$  overlap area is smaller (See Figure 2.5b). When we satisfy the minimum reflux condition as seen in Figure 2.5c, the associated  $TT_3$ s just touch. If a system is under-refluxed the profiles will not intersect and thus the  $TT_3$ s will not intersect or overlap at all. From this, the final criterion for the CPM-E technique is presented; the minimum reflux condition for any sharp split, direct or indirect, would be established by having the  $TT_3$ s of the rectifying and stripping section meet along a boundary. This criterion automatically satisfies the original definition proposed by Levy et al. (1985) where either the rectifying or stripping profile pinches on the other. Therefore the co-linearity criteria for the feed pinch and saddle pinch are also satisfied as we move to sharp split conditions.

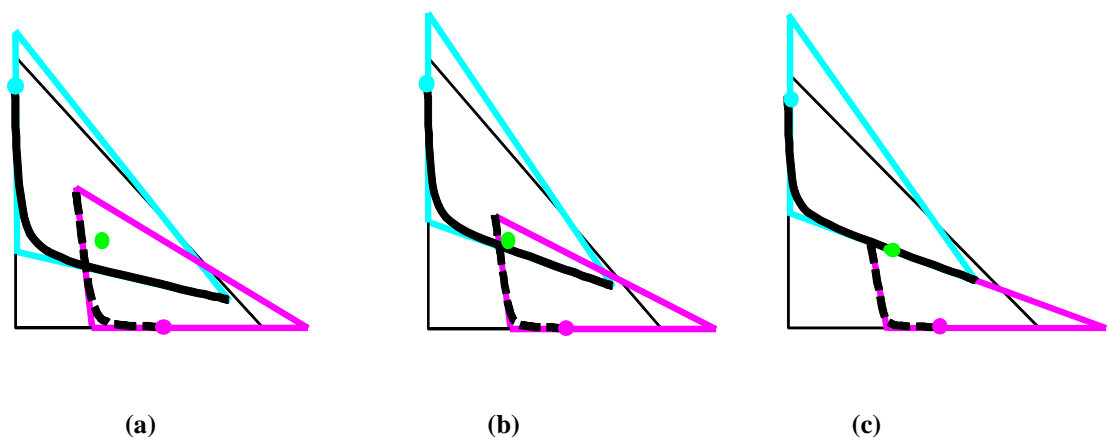


**Figure 2.5: Composition profiles and their associated transformed triangles in descending order of reflux. (a) Crossing Profiles with corresponding overlapping  $TT_3$ s. (b): Smaller reflux, but still over refluxed system. (c): System at minimum reflux conditions.**

## 2.4 Co-linearity Line Rule

In the previous section we dealt with the  $TT_{3s}$  of the individual sections in the column and found that, the last intersection of the  $TT_{3s}$  of the stripping and rectifying section is regarded as the minimum reflux for a conventional column. A more descriptive example of a minimum reflux solution can be seen in Figure 2.6. As the figure suggests, for a set product specification, when the column is over refluxed, the  $TT_{3s}$  of the RS and SS overlap. Reducing the reflux ratio moves the  $TT_{3s}$  of the individual sections so as to minimize the overlapping area. When minimum reflux is achieved, the  $TT_{3s}$  will just meet. The black dotted line indicates the line on which the  $TT_{3s}$  touch and is the combination of CLL discussed that have to pass through the feed composition (green dot Figure 2.6). The feed it seems is the last possible ‘point’ for the  $TT_{3s}$  to intersect. Any reflux selected above the minimum will result in an overlap of  $TT_{3s}$  and any reflux selected below the minimum will result in no overlap of the  $TT_{3s}$  (See Figure 2.7) and therefore no feasible intersection of profiles will occur. If we now consider our observations of the feed being the last ‘point’ for our  $TT_{3s}$  to intersect, then we can speculate that the CLL through the feed (dotted line-Figure 2.6 and Figure 2.7) is not a very strong function of the product specification. The feed placement in this case must be though. This is evident when we select another product specification with the same equimolar feed composition as we have in Figure 2.6 and Figure 2.7; we achieve the exact same co-linear line (Figure 2.8a and b). With the information we have discussed, the determination of the CLL will aid in achieving a minimum reflux solution. At specified feed conditions, distillate and bottoms compositions, the exact condition for minimum reflux is that the tangent to the saddle pinch profile at the feed pinch point is a straight line through  $X_F$ . In other words, the rectifying profile in this instance passes through the feed condition. This is true regardless of whether the mixture is ideal, non-ideal, or azeotropic. Levy et al (1985) demonstrate this by illustrating a proof that explains that a linear profile (ideal mixture with high-purity product) must pass through the feed composition at minimum reflux. Curved profiles (non-ideal and azeotropic mixtures) will pass close to the feed according to the amount of curvature.

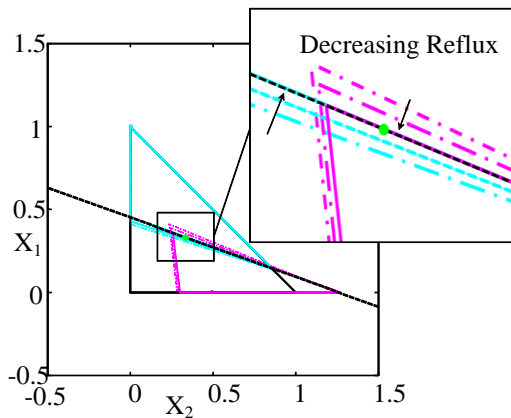


**Figure 2.6:** Multiple overlap of  $TT_3$  with decreasing reflux ratio. Line indicates the last possible intersection for a direct split.  $X_D = [1 \ 0]$ ,  $X_B = [0 \ 0.486]$ ,  $X_F = [1/3 \ 1/3]$ .

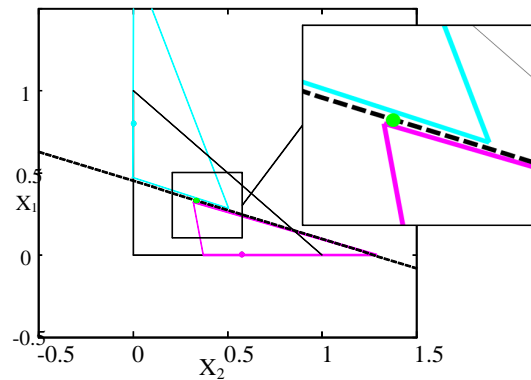
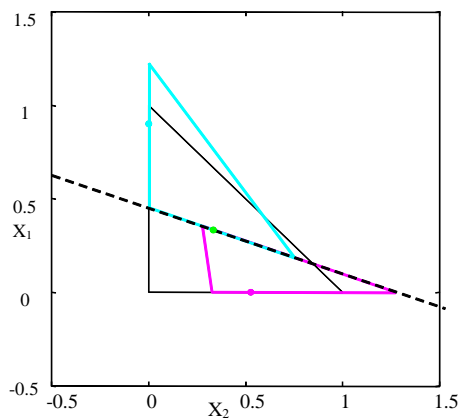
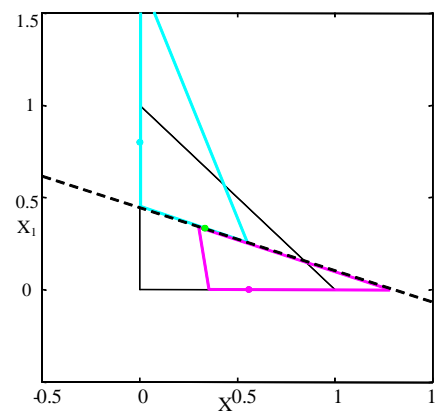


**Figure 2.7:** Reflux ratio selected below the minimum for a direct split.  $X_D = [1 \ 0]$ ,  $X_B = [0 \ 0.486]$ ,  $X_{Feed} = [1/3 \ 1/3]$ .



(a)



(b)

**Figure 2.8:** Different product specifications with the same feed composition produces the same CLL at minimum reflux (a)  $\alpha=[4 \ 1 \ 2]$ ,  $X_D = [0.9 \ 0]$ ,  $X_B = [0 \ 0.527]$ ,  $X_F = [1/3 \ 1/3]$ ,  $R_{\min} = 1.63$ . (b)  $\alpha=[4 \ 1 \ 2]$ ,  $X_D = [0.8 \ 0]$ ,  $X_B = [0 \ 0.556]$ ,  $X_F = [1/3 \ 1/3]$ ,  $R_{\min} = 1.04$ .

*Figure 2.8a-b illustrate that the same CLL exists for relatively high light product recovery to the distillate, but this ‘rule’ does not apply for relatively pure heavy product recovery to the bottoms. This issue is of immense importance and will be discussed in great detail later.*

## 2.5 Degrees of Freedom and Design Variables

The existence of a single CLL for a set feed composition and the relative pure lights distillate product suggests that a better, simpler and non-iterative solution for minimum reflux must exist. So far, to determine minimum reflux, we have had to undergo several important steps.

These steps include:

- (1) Selecting product specifications for a given feed.
- (2) Determining the minimum reflux by choosing a starting reflux ratio and reducing or increasing the reflux appropriately and plotting the  $TT_3$ s for each until the triangles just touch.
- (3) Once a minimum reflux is determined, calculate the reboil ratio based on the reflux using mass balance.

This methodology has certain degrees of freedom that limit the variables selected in order to determine the reflux. It is very important that the designer does not over specify the system as this could lead to multiple or incorrect solutions. With an appropriate design variable selection, this can be avoided. Let us now take a look at the degrees of freedom applied to graphical techniques and how it affects our selection of variables for conventional distillation.

The fact that Column Profile Map techniques and the CPM-E technique that will be introduced later is analogous to the BVM, allows us to say that the degrees of freedom for these methodologies are exactly the same. From this it was shown by Levy et al (1985) that for a given feed flow rate, feed composition ( $[X_{F1} X_{F2}]$ ) and pressure, four independent variables may be specified for a ternary system. E.g.  $X_{D1}$ ,  $X_{D2}$ ,  $X_{B1}$  and  $R_A$  - one of the product composition variables may be specified (i.e.  $X_D$  or  $X_B$ ), one overall material balance variable may be specified (i.e. distillate or bottoms rate) and one of the internal material balance variables may be specified (i.e. reflux ratio or boil-up ratio). In terms of individual product

component variables ( $X_D$  or  $X_B$ ) this is equivalent to four independent design parameters.

Under minimum reflux conditions, only three design parameters exist. The calculation at minimum reflux conditions will eliminate a design variable. In particular, an internal material balance variable. The CPM-E technique can only be applied if descriptions of the conditions at both ends of the column are specified (Levy et al., 1985; Julka and Doherty, 1990). In other words, in order to determine minimum reflux, we will either completely specify the top product composition and a product purity/impurity for a single component in the bottoms or completely specify the bottoms product specifications and a product purity/impurity for a single component in the distillate. Equation 2.8 and is used to determine the impurity composition of the fourth composition that does not fall under the category of degrees of freedom (DOF).

$$\frac{X_{F,2} - X_{SS,2}}{X_{F,1} - X_{SS,1}} = \frac{X_{F,2} - X_{RS,2}}{X_{F,1} - X_{RS,1}} \quad (2.9)$$

Equation 2.9 states that the feed, distillate, and bottoms compositions are co-linear when plotted on a triangular diagram, a fact that will be used repeatedly in this paper.

From our original definition of reflux as the ratio of liquid in a column section to the net flow in the column section, it would be more convenient to express the boil-up ratio as a reflux ratio. This would of course mean that the reflux ratio of the stripping section is determined from mass balance and is dependent on the feed phase. If the feed were liquid, the expression for the reflux ratio for the stripping section would be calculated by:

$$R_{\Delta SS} = \frac{L_{SS}}{\Delta_{SS}} = \frac{R_{RS}D + F}{-B} \quad (2.10)$$

This would not of course be the same for a vapour feed. The reflux ratio would then be calculated as:

$$R_{\Delta SS} = \frac{L_{SS}}{\Delta_{SS}} = \frac{R_{RS}D}{-B} \quad (2.11)$$

Equations 2.11 are derived by doing an overall flow material balance around the stripping section. Once the design variables are specified the distillate flow rate or bottoms flow rate can be calculated from the overall component material balance. The design routine needs component compositions; therefore, if we want to specify a distillate flow, then we can calculate the compositions from the material balance.

## 2.6 CPM-E Technique derivation and description

### 2.6.1 Eigenvector Application

The introduction to Eigenvectors has shown us that we can determine the direction of the trajectories in the region of a node. This means that, if we select a singularity point at the origin of the MBT and evaluate the eigenvectors, for a thermodynamically ideal system, the resulting vectors will point in the direction of the two remaining nodes (i.e. In this instance they would point at the stable and unstable nodes of the residue curve map). As mentioned previously, the eigenvectors for a predefined thermodynamic system is not a function of the reflux ratio or the difference point, but merely a function of the separation vector. This is a fascinating and extremely useful result, as we only have to determine the eigenvector map for a system once off to completely understand the movement of singularities (Holland et al., 2004). Let us now take a look at how we can use the idea of the eigenvectors to further our ability to determine minimum reflux solutions.

At this point it is quite evident that the CLL will eliminate the iterative steps taken previously in order to determine the minimum reflux. A pertinent question that should come to mind is: how can we determine this line without determining the required reflux first as we have previously. And if we can determine this line, how can it be used to determine minimum reflux?

Holland et al. (2004) demonstrated that the eigenvectors at the singularities, of constant-relative-volatility systems, always point along the direction of the  $TT_3$  boundaries. Because the boundaries are straight in these systems, the eigenvectors at each singularity point directly at the other singularities. Any point chosen along one of these boundaries will have eigenvectors that point directly at the same singularities, which define it (See Figure 2.9).

This implies that eigenvectors evaluated along the same  $TT_3$  boundary will produce directions co-linear with the  $TT_3$  boundary for ideal systems. It is evident at this point that the eigenvectors evaluated on the minimum reflux  $TT_3$  have to be co-linear with the CLL that we have discussed earlier. This of course solves the first problem we have encountered; we can now predetermine the CLL where the minimum reflux  $TT_3$ s touch. We demonstrated earlier how the CLL passes through the feed composition. Thus, if we evaluate the eigenvector at the feed composition, we have found all possible CLLs based on a specified feed condition (See Figure 2.10).

In addition to the eigenvector we have focussed on, there is another eigenvector with a larger slope that we have not yet considered, but is of immense importance and will be discussed in great detail. We will name the co-linearity line of smaller (absolute) gradient; derived from the red eigenvector, Co-Linearity Line 1 (CLL1) and the line of larger (absolute) gradient; derived from the blue eigenvector, Co-Linearity Line 2 (CLL2) (Blue) (see Figure 2.10).

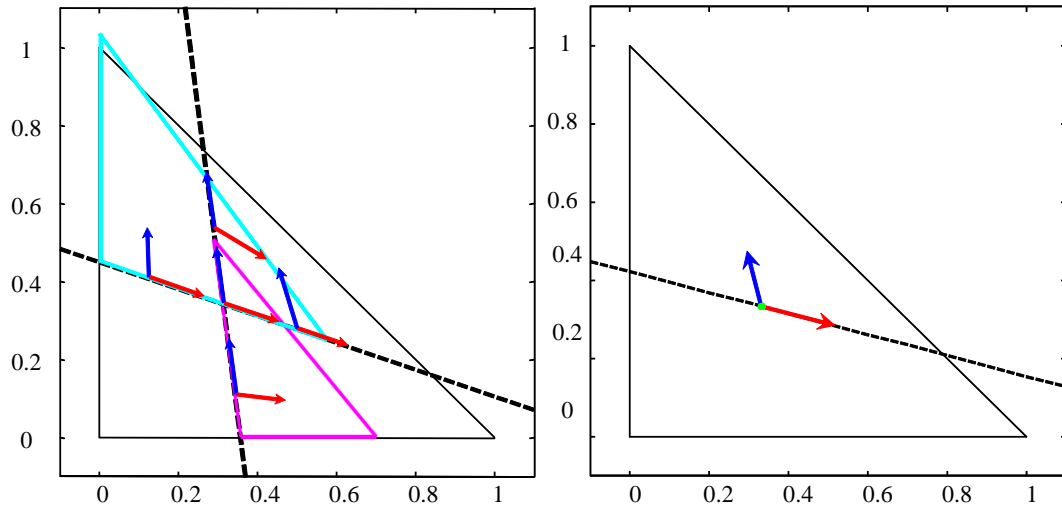


**Figure 2.9:** A point chosen along one of the eigenvector lines will have eigenvectors that point directly at the same singularities.

**Figure 2.10:** Eigenvector evaluated at the feed composition corresponds to CLL1.

### 2.6.2 CPM-E technique

The CLL determination for a given feed is now possible without knowing the minimum reflux solution. Even although CLL1 and CLL2 are very interesting observations at the minimum reflux solution, up to now we have not clarified why we need to find the CLLs. Finding these lines implies that we are a step closer to finding the stationary points where the profiles/TT<sub>3</sub>s of the minimum reflux coincides. Once we find at least one stationary point associated to a profile/TT<sub>3</sub> at minimum reflux conditions we can look at finding and quantifying the minimum reflux solution.

Earlier we described the process of determining stationary points. The course of this procedure involves knowing the difference point as well as the reflux ratio in order to determine the stationary points associated to the Column Profile Map. To find the stationary points, non-specific for a thermodynamically ideal ternary system, would involve solving the right hand side of the Difference Point Equation (Equation 2.1) for the liquid composition when it is equivalent to zero.

Taking a closer look at the terms in the Difference Point Equation, we identify two vectors. The first vector, called the separation vector is the difference between the liquid composition and the vapour composition in equilibrium with the liquid composition i.e.  $\tilde{s} = (X - Y^*(X))$ . The second vector is called the mixing vector and is the difference between the difference point and the liquid composition i.e.  $\tilde{m} = (X_{\Delta} - X)$ . In the instance of a stationary point determined by equating the Difference Point Equation to zero, it is noticed that the separation vector multiplied by the reflux ratio is equal to the mixing vector:

$$(R_{\Delta k} + 1)(X_i - Y_i^*(X_i)) = (X_i - X_{\Delta k,i}) \quad (2.12)$$

Geometrically this implies that the mixing vector is co-linear with the separation vector at the stationary point. This is illustrated in Figure 2.11.

Currently we know that we have to solve for the stationary point/s of the  $TT_3$  associated to the minimum reflux solution. The CLL is thus determined to aid our search for the node. Instead of searching the entire space for a solution of possible stationary points, the CLL narrows down the search to a straight line. We have found this line by evaluating the eigenvectors at the feed composition from the definitions of the minimum reflux condition. We also have the difference point placement, which we have shown is the distillate product composition. These and mathematical operators are the only tools that we have in order to determine the minimum reflux solution.

Simple geometry dictates, that, in order to determine a single point in two dimensions on a straight line, another straight line or curve has to intersect with this line. Equations of both lines should be known, and they have to be solved simultaneously for an intersecting point. The main aim is thus, to find a stationary point along the CLL. This of course means we have found one of these lines (CLL). The only other line that passes through the liquid stationary point is the mixing and separation vectors co-linear line discussed above (Equation 2.12) which is derived from the Difference Point Equation. All we know about this line

is that it comprises of three points that are co-linear, where two of them are unknown. But, one of the unknown points is a function of the other. The known point we have already discussed, and it is the difference point. The two known points are the liquid pinch point and the equilibrium vapour pinch point illustrated in Figure 2.11. Due to the fact that the vapour composition is only a function of the constant relative volatility and liquid composition, the only unknown is the liquid composition at the stationary point. In other words, the solution to the pinch point is found by equating the gradients of the mixing vector and separation vector, and then solving for the elements of the liquid composition simultaneously with the straight line equation of the CLL. This composition would be the stationary point solution on the CLL which is one of the stationary points on the minimum reflux  $TT_3$  solution (Figure 2.12).

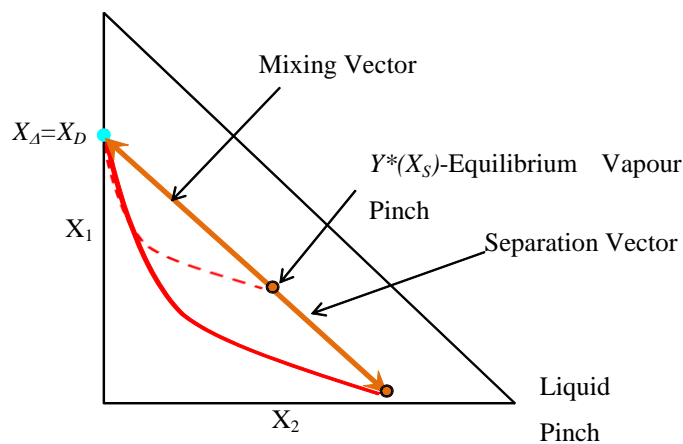


**Figure 2.11: Co-linear points evaluated at a liquid pinch point.**

The only unknown remaining is the reflux associated to the minimum reflux stationary point/s on the CLL. If the transformed triangle can be found algebraically by simply specifying the  $R_{\Delta}$  and  $X_{\Delta}$ , then the reverse must also be true. By knowing the fixed points of a Column Profile Map or its associated  $TT_3$  we must be able to determine  $R_{\Delta}$  and  $X_{\Delta}$ . There is no need to determine the difference point as it has already been specified. Therefore the only unknown is

the reflux ratio. The equation in order to determine the reflux ratio for a known difference point and a stationary point is the rearranged Difference Point Equation evaluated at a stationary point given by:

$$R_{\Delta k} = \frac{(X_S - X_{\Delta k})}{(X_S - Y_S^*(X_S))} - 1 \quad (2.13)$$

Where,  $X_S$  is the liquid stationary point. This equation is merely a rearrangement (Equation 2.12) by making the reflux ratio the subject of the formula. This is a very powerful result as the calculated reflux is the minimum reflux solution for a given feed. This result was found without iterations or tedious steps and is based on simple mathematics. We have only discussed the ternary system, but it will be shown in future publications, how the CPM-E technique can be applied to higher order systems such as the quaternary systems.

The results of the minimum reflux are illustrated in Figure 2.12. The liquid  $TT_3$  (solid blue line) is calculated and plotted using the solver routine described earlier and is the minimum reflux  $TT_3$ . The stationary point for the vapour  $TT_3$  (dashed blue line) is found from the equilibrium vapour points.

CLL1 is phase dependent. If vapour feed is added to the column, the vapour  $TT_3$  stationary points will line up along CLL1. The eigenvector directions in this case are not the eigenvectors of the standard separation vector as vapour profiles do not approach their pinch points along these directions. Vapour profiles approach pinch points along eigenvectors of the differential equations which have separation vectors expressed in terms of the vapour composition. i.e.  $(X^*(Y) - Y)$ . The figure illustrates the  $TT_3$ s of both the liquid and vapour in equilibrium with the liquid and shows the co-linear mixing vector ( $\tilde{m}$ ) and separation vector ( $\tilde{s}$ ).

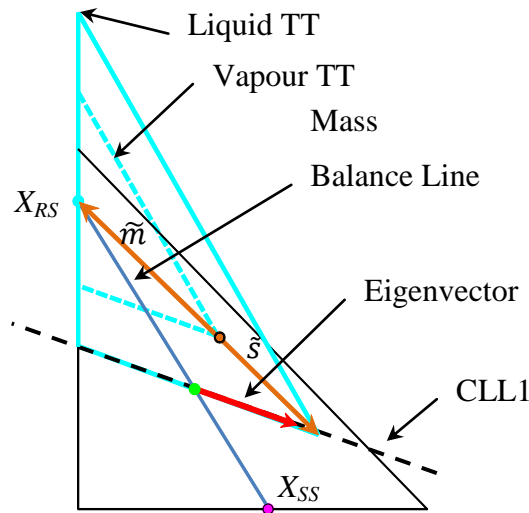


Figure 2.12: CLL stationary point with mixing and separation vector passing through the node of the transformed triangle for the minimum reflux solution.

## 2.7 Complete CPM-E Solutions

A non-iterative minimum reflux solution for graphical techniques is now possible. The solutions previously focused on include moderately pure lights recovery to the distillate product. The examples shown have not allowed for more than 20% of the intermediate in the top product and the material balance implies that no pure heavy bottoms product has even been considered. Previously it was mentioned that additional solutions exist other than the CLL1 that govern minimum reflux for different purities of either the distillate or bottoms product. We will now discuss the additional solutions that exist for the CPM-E technique.

The selection of  $X_D$  will affect the  $TT_3$  for each specified minimum reflux but will not affect the interaction properties of the  $TT_3$ s under minimum reflux conditions. Therefore, for each and every product selection, there is a specified  $TT_3$  that is related to a minimum reflux solution because of its association to the specified difference point placement. If we adopt the initial technique for determining the

minimum reflux by taking iterative steps after plotting successive  $TT_3$ s, as well as decrease the distillate composition from pure lights in the distillate to the indirect split we might be able to estimate the point where CLL1 doesn't apply anymore and cannot give a solution for the minimum reflux. This is illustrated in Figure 2.13.

Let us first focus on the top row of Figure 2.13. As the distillate composition is decreased in terms of lights product reporting to the top or shifted downwards towards the intermediate component along the light intermediate axis, the  $TT_3$ s of associated minimum reflux solution start shifting in such a way as to decrease the overlap of the RS and SS i.e. the stable node of the RS and unstable node of the SS move towards the feed composition on CLL1. This continues until the two nodes coincide and are one on top of the other coinciding with the feed composition. This point is extremely important and occurs when the profiles of the RS and SS both terminate on the feed. This point is known as the double feed pinch (Holland et al., 2009) or for sharp splits, preferred splits (Stichlmair, 1988).

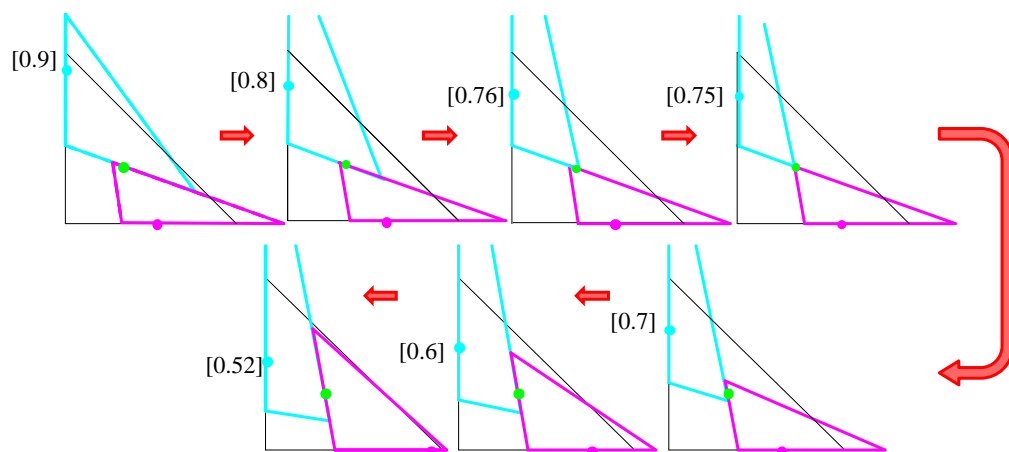


**Figure 2.13: Minimum reflux solution revealing the existence of CLL2 by shifting the distillate product towards the intermediate along the light intermediate axis for an equimolar feed.**

This point and others similar to it will be discussed in detail later. If we continue to shift the distillate composition downwards, we notice something extremely peculiar. The  $TT_3$ s that still resemble minimum reflux conditions interact and meet one another on a different line. The new interaction boundaries of the associated  $TT_3$ s will change the way the profiles of the respective column sections interact. This means that the profiles will also switch across to the ‘new’ meeting line. As we continue decreasing the lights recovery to the distillate product along the light intermediate axis the CLL remains constant and in its original position where as the stable node of the RS and unstable node of the SS of their  $TT_3$ s move further apart along the newly introduced CLL. This is the first application of other possible minimum reflux solutions developed from the CLL lines which we have named CLL2. The determination of CLL2 is equivalent to CLL1 i.e. determining the eigenvectors at the feed composition, but in this case using the eigenvector with the greater gradient (See Figure 2.14). Previous eigenvector calculations already suggested that CLL2 exists as the evaluation at the stationary point produced two eigenvectors (See Figure 2.10). CLL1 and CLL2 (See Figure 2.14) encompass all the feasible minimum reflux solution for sharp splits, from pure lightest key in the distillate to pure heaviest key in the bottoms. These are all the points for the distillate composition from the pure light vertex to the indirect split and therefore heavy vertex to the direct split for the bottoms product. It is important to note that we have not yet placed  $X_D$  in feasible regions inside the MBT (non-sharp splits), but thus far only along or as close to the light intermediate boundary as possible. I.e. direct splits, sharp splits and indirect splits.

CLL1 and CLL2 are distinct solutions, but as we will see later, they can work together under certain composition selections to produce additional solutions other than those already discussed. It is important to note that minimum reflux solutions derived from CLL1 produce  $TT_3$ s that interact along CLL1 (See Figure 2.15a). Therefore, minimum reflux solutions derived from CLL2 approach along CLL2 where the distillate product has lower concentrations of light key components (See Figure 2.16a). With this said, in order to simplify reference to minimum energy demand solutions from either CLL’s the solution will refer to a

‘common CLL’. Thus, minimum reflux solutions from CLL1 based on the smaller gradient eigenvector will be referred to as common CLL1 solutions and vice versa for CLL2.

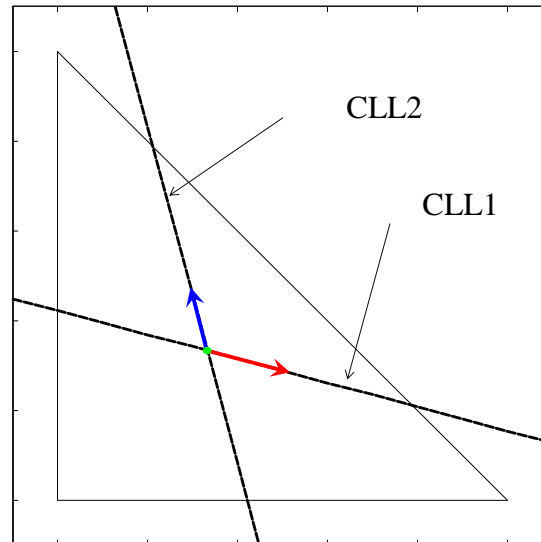
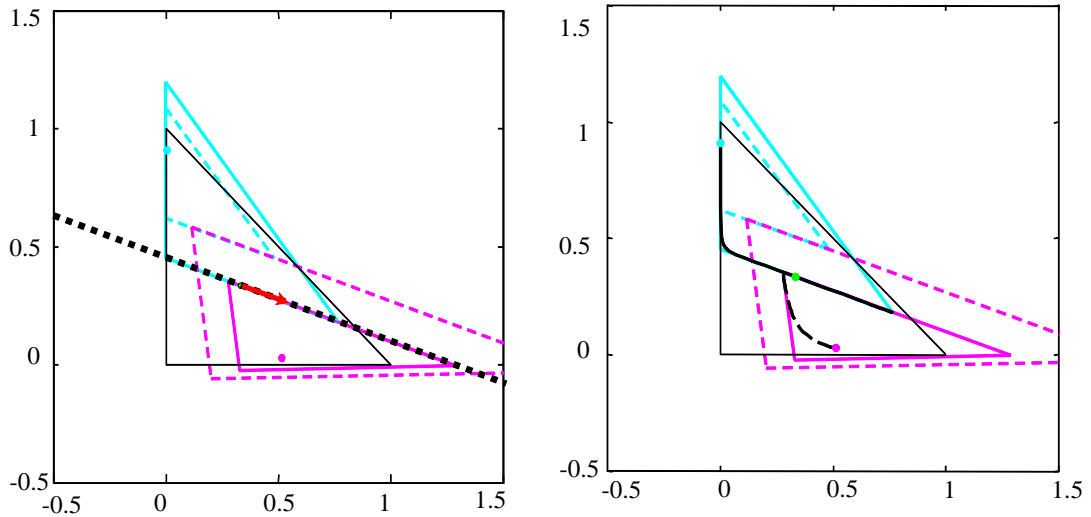


**Figure 2.14: CLL1 and CLL2 determined from eigenvectors evaluated at the feed composition.**

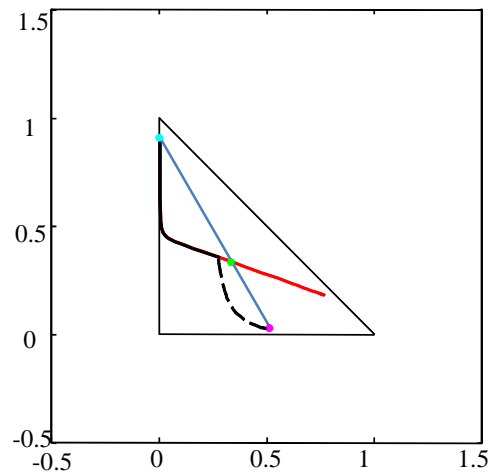
For an equimolar feed, as shown in Figure 2.15a-c and Figure 2.16a-c, the ‘swap-over’ from CLL1 to CLL2, along the light intermediate boundary is at  $X_D = [0.75 \ 0]$ . The sharp split that coincides with the point is regarded as the preferred split. It will be shown later how we can determine the preferred split boundary where the ‘swap-over’ phenomenon occurs for any feed composition and feasible product selection. The examples shown in Figure 2.15 and Figure 2.16 make use of common CLL1 and CLL2 respectively to obtain the minimum reflux solutions. Table 2.1 illustrates the operating parameters of each figure comprising the configuration. An analysis using  $V_{min}$ -diagrams introduced by Halvorsen and Skogestad (2003a) reveals that the CPM-E technique predicts exactly the same minimum reflux (See Table 2.1). Thus the CPM-E technique produces results that are identical to Underwood based procedures. The link between the CPM-E technique and  $V_{min}$ -diagrams (Underwood methods) will be explored in later publications. As illustrated by Figure 2.15b, the associated minimum reflux

profiles intersect on CLL1, where the SS terminates on the RS. Any profile beyond the intersecting point (feed stage) is irrelevant and cannot be utilized. The red lines in Figure 2.15c and Figure 2.16c illustrate this phenomenon.



(a)

(b)

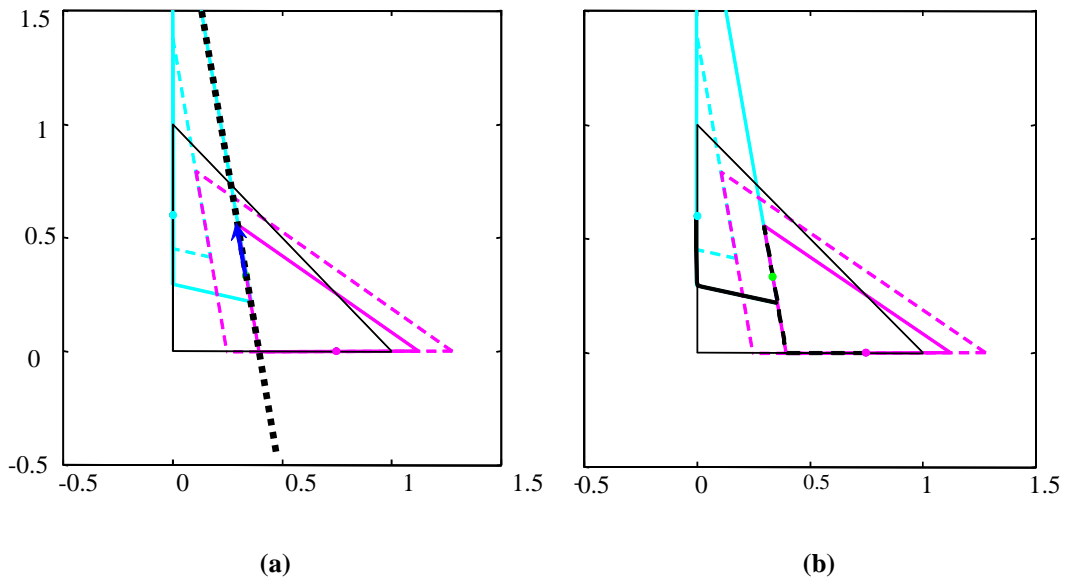


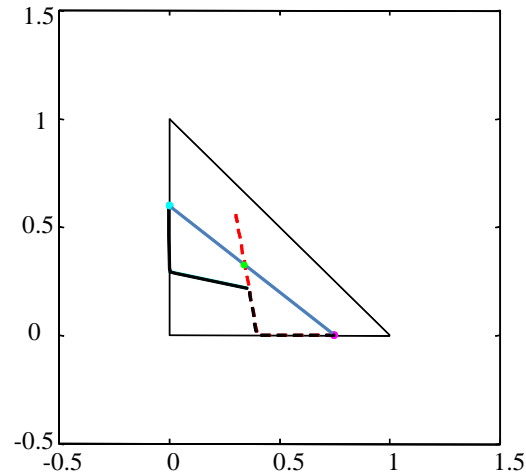
(c)

**Figure 2.15: Minimum reflux solution. (a) Minimum reflux  $TT_3$  solution along CLL1 (b) Associated minimum reflux profile termination on CLL1 and RS. (c) Profiles produced from CLL1 minimum reflux solution**

**Table 2.1: Solution values for examples discussed in Figure 2.15 and Figure 2.16.**

	Figure 2.15:	Figure 2.16:
$\alpha$	[4 2 1]	[4 2 1]
$X_F$	$[\frac{1}{3}, \frac{1}{3}]$	$[\frac{1}{3}, \frac{1}{3}]$
$X_D$	$[0.91, 10^{-4}]$	$[0.6, 10^{-3}]$
$X_B$	[0.027, 0.51]	$[10^{-7}, 0.758]$
$D/F$	0.65	0.56
$B/F$	0.35	0.44
$CPM-E R_{\Delta}$	1.68	0.92
$V_{\min} R_{\Delta}$	1.68	0.92





(c)

**Figure 2.16: Minimum reflux solution. (a) Minimum reflux  $TT_3$  solution along CLL1 (b) Associated minimum reflux profile termination on CLL1 and RS. (c) Profiles produced from CLL1 minimum reflux solution**

The black profiles in Figure 2.15c and Figure 2.16c are the composition profiles that model the composition change in a column operating at minimum reflux conditions. Figure 2.15 a-c and Figure 2.16 a-c illustrates a unique property of the profile intersection that allows the user to identify which CLL has been applied. That is, at minimum energy operation with infinite number of stages, the composition profile will have certain pinch-zones where there are no changes from stage to stage. Shiras (1950) denoted these as points of infinitude. If CLL1 is utilised, the SS terminates on the RS, where the pinch zone will actually appear from the feed stage and downwards, but we will see an abrupt composition change in the stages above the feed stage. If CLL2 is employed the roles will be exchanged. RS terminates on the SS and the pinch zone composition on the bottom will be invariant, but the pinch zone composition in the top will vary. This observation is useful as it demonstrates which column section is responsible for the additional energy that has to be applied to the system in order to achieve the necessary purity at the lowest possible energy demand.

## 2.8 Preferred Splits and Double Feed pinches

The preferred split represents a distinct minimum which illustrates the minimum energy operating condition for a conventional column. It is the minimum energy operation when we consider only sharp splits between the most heavy and most light components, while all the intermediates are distributed to both products. This means that the feed composition at this special minimum reflux solution has become a stationary point for both the RS and SS and therefore the preferred split will exhibit a pinch region on both sides of the feed stage and not individually as we have previously seen when either CLL1 or CLL2 are common.

The occurrence of the unstable node of the RS coinciding with the stable node of the SS at the feed composition causes the RS and the SS to terminate on one another at the feed composition. The profiles and their associated  $TT_3$ s at the preferred split are illustrated in Figure 2.17. The figure suggests that in the preferred split solution both CLLs are common as two boundaries of the associated  $TT_3$ s from both profiles of the column sections coincide with both CLL1 and CLL2. The intermediate-heavy boundary of the  $TT_3$  for the RS and light-heavy boundary of the  $TT_3$  for the SS coincide with CLL1, whereas the light-heavy boundary of the  $TT_3$  for the RS and light-intermediate boundary of the  $TT_3$  for the SS coincide with CLL2.



SS's  $TT_3$  meet. Holland et al. (2009) have described this phenomenon as “double-feed-pinches”. We will denote the line where the double feed pinches occur, as the DFP line. “Double-feed-pinch” minimum reflux solutions are illustrated in Figure 2.18a-b.

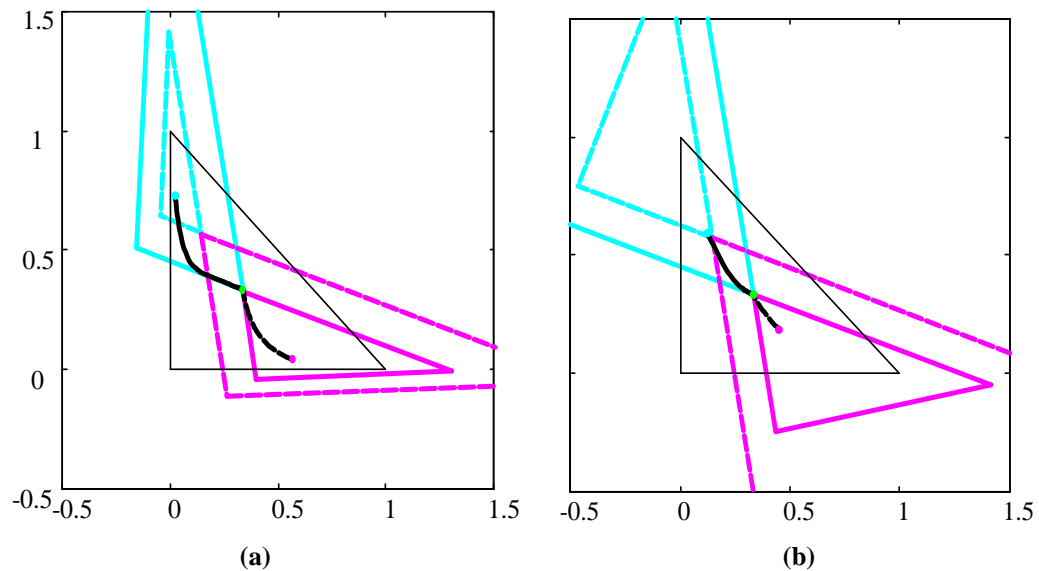


**Figure 2.18: Double Feed Pinch Solutions. (a) Double feed pinch solution for low heavy key impurity in distillate. (b) Double feed pinch solution for high heavy key impurity in distillate.**

A distinctive property that has been discussed and applies to the double-feed-pinch solutions due to eigenvector determination is the fact that the CLL boundaries remain fixed and are not a function of the product placement along the DFP line. Referring back to the previous case where the feed is a saturated liquid, would mean that the liquid boundaries of the  $TT_3$ s coincide with the CLLs. Due to the fact that the liquid  $TT_3$  boundaries coinciding with CLL remain fixed on the CLL indicates that the vapour boundaries at minimum reflux solution, although not coinciding with the CLLs, remain fixed in position with a change in product placement as well (See Figure 2.18a-b). With this said, intuitively it is clear that a limit should arise merely from the fact that the CLLs are constant for any product placement. If we refer again to Figure 2.18a-b, note that the difference points of the distillates are selected inside the vapour  $TT_3$  (Blue dashed triangle). It is

important that the reflux in the RS has to be positive (as shown by Equation 2.3) and the SS reflux must be negative (As shown by Equation 2.4) as material balance dictates this. Therefore distillate product selection outside of the vapour  $TT_3$  will result in negative reflux ratios within the RS and vice versa for the SS. The sign of the reflux as a condition for feasibility would be one of the important criteria to determine which feasible  $X_D$  placement would apply to common CLLs in order to limit our search for the constraint mentioned above.

*NOTE: The “double-feed-pinch” point is phase dependent. Vapour feed columns will exhibit a vapour profile “double-feed-pinch” point - although it should be noted that both phases in both cases will pinch.*

## 2.9 Minimum Reflux Regions

### 2.9.1 Complete minimum reflux regions

The minimum reflux solutions demonstrated using the CPM-E technique have all been based on the definition of the sharp split in either the distillate compositions or bottoms compositions. The solutions derived are all regarded as the sloppy split minimum reflux as opposed to approximations thereof, which are analogous to non sharp splits for the CPM-E technique. Certain limiting criterion constrains difference point selection within the MBT. We will now discuss all the limiting difference point choices and develop regions that produce feasible, minimum refluxes.

An evident set of boundaries that will confine all the possible difference points in any conventional distillation, minimum or over refluxed, system is the bow-tie region (Fien and Liu, 1994). The bow tie region is the red shaded region illustrated in Figure 2.19. Bow-tie regions give the feasible combinations of distillate and bottoms compositions for a specified feed composition (Van

Dongen, 1983; Van Dongen and Doherty, 1985). In other words, a bow-tie region gives the feasible distillation column mass balance lines for a specific feed (Fien and Liu, 1994).

Previous discussions have shown that the sign of the reflux in each column section is of great importance and will limit our choices of difference points in the MBT. Considering that a common CLL for a set of minimum reflux solutions remain the same, and as a result the contact boundaries of the liquid  $TT_3$ s and therefore the vapour  $TT_3$ s of the associated solutions remain the same as well, selecting difference points outside the vapour  $TT_3$ , but within the MBT will result in oppositely signed refluxes in the column sections. This sets another limit for each CLL employed. This means that the vapour boundary that is associated with the coincident CLL is the last lines of possible  $X_D$  selection points which we will call vapour CLLs. This phenomenon is illustrated in Figure 2.20a-c. Figure 2.20a is the positive reflux region when CLL1 is utilised and Figure 2.20b is the positive reflux when CLL2 is utilised. If the fact that SSs reflux ratio is negative, the remaining MBT region not occupied by the positive minimum reflux, is associated to the SS. The complete vapour CLL is illustrated in Figure 2.20c. Due to the fact that the preferred split is the point where the minimum reflux ratio solution swaps over from the CLL to the next unused CLL means that if a limiting point along the DFP exists for one CLL, intuitively it must occur at the same point when the other unused CLL is applied. This fact is true and is evident from Figure 2.20c.

Three distinct boundaries, besides the obvious MBT that will limit our search for feasible minimum reflux solutions have been discussed. They include: the DFP, the bow-tie region and the vapour CLL depending on which column section is chosen to analyse. The DFP is significant as it not only separates minimum reflux solutions of different topology but the line itself is a special minimum reflux solution that incorporates both CLLs to find a minimum reflux solution. This means, that if a CLL is chosen to find a reflux solution based on the product selection i.e. high light key purity in distillate uses CLL1 and high heavy key in

bottoms uses CLL2, then only the region that applies to the utilised CLL will produce feasible solutions and any region outside this one will not produce anything useful. By superimposing the three boundaries (DFP, bow tie region and vapour CLL), three defining feasible regions arise. The feasible region will include the DFP line that produces feasible minimum reflux solutions. The interaction of the CLLs with the feed and each other is a significant aspect for the number of components. This means that if there were for example four components, more than three feasible regions would exist.

The combinations of the three defining regions are shown in Figure 2.21a-c. The red regions indicate infeasible difference point selection under minimum reflux conditions. The green regions are the feasible regions that are associated to difference points for the RS that produce feasible minimum reflux solutions. The blue regions are the feasible regions that are associated to the difference points for the SS. From a DOF point of view selecting a distillate product point in the green region implies only an impurity based on the light or heavy component, below the feed composition can be selected.

The fact that the bow-tie and vapour CLL regions are dependent on the feed composition and in the case where the phase of the CLL is utilised, the feed phase, implies that the feasible regions developed for viable minimum reflux solutions, shown in Figure 2.21a-c, are dependent on the feed conditions. The regions will stretch and contract depending on the feed point placement in the real composition space.

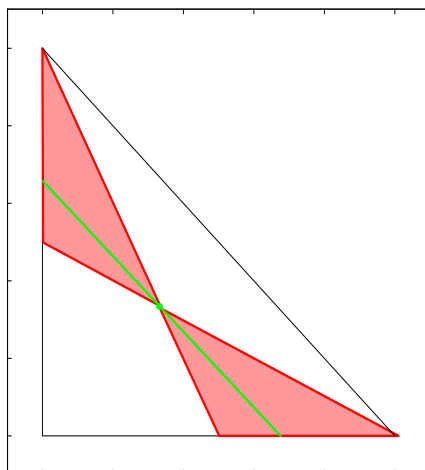


Figure 2.19: Bow-tie region for equimolar feed with associated preferred split.

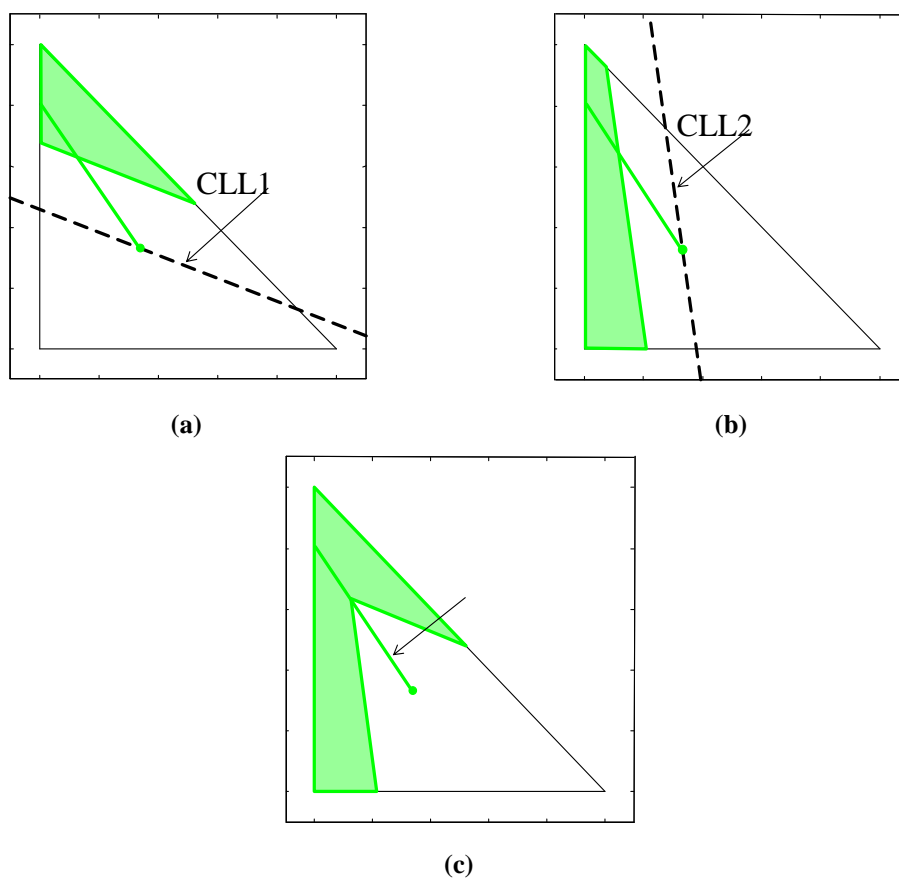


Figure 2.20: (a) Rectifying sections positive reflux regions associated to common CLL1. (b) Rectifying sections positive reflux regions associated to common CLL2. (c) Combined positive reflux regions.

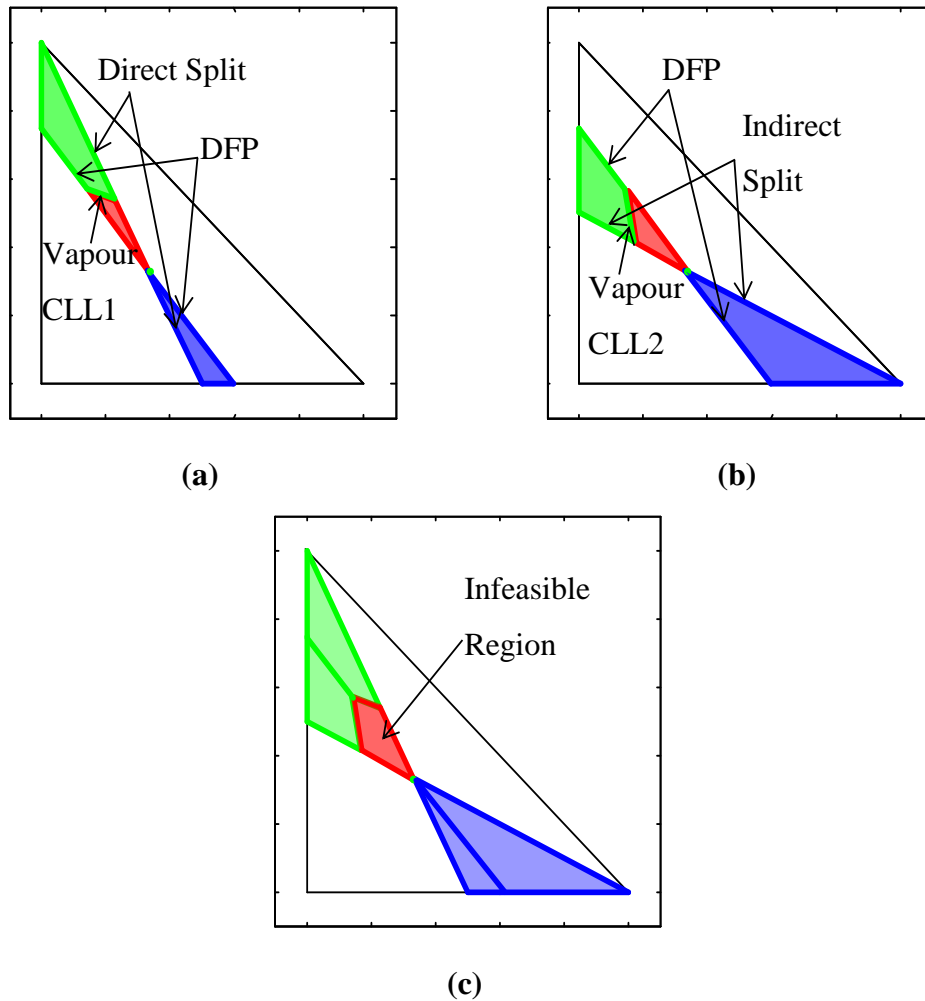


Figure 2.21: (a) Feasible and infeasible regions associated to common CLL1. (b) Feasible and infeasible regions associated to common CLL2. (c) Combination of CLL1 and CLL2 regions of interest.

### 2.9.2 Sloppy split minimum reflux regions

It is of great importance to note that the regions in Figure 2.21a-c are based on all possible minimum reflux solutions which include sloppy split minimum and approximations of minimum reflux solutions based on the CPM-E technique. The sloppy split minimum reflux solutions are associated to sharp split separations either in the distillate product or bottoms product, and depend purely on the CLL used and thus the region of feasibility used in order to determine the minimum reflux solution. This means that if for instance CLL1 were to be used, not the

entire green region characterised in Figure 2.21a produces sloppy split minimum reflux solutions. Only the sharp split in the distillate composition i.e. light-intermediate axis that coincides with the feasible region produces accurate solutions. The bottoms compositions undergo similar behaviour when CLL2 is utilised. The sharp split i.e. heavy-intermediate axis coinciding with the blue region in Figure 2.21b represents sloppy split minimum.

Although CLL1 distillate region illustrated in Figure 2.21a is reduced to a line does not mean that the blue region associated to the bottoms composition when CLL1 is used is reduced to the sharp split criterion. Due to the fact that the SS profile terminates on the RS profile or equivalently the  $TT_3$  of the SS means that the impurity is based on any component pertaining to the material balance can be selected within the feasible region. The opposite argument is true for CLL2s feasible region. Due to the fact that the RS terminates on the SSs  $TT_3$  means any profile associated to a difference point in the distillate that pertains to the feasible region is feasible as long as it obeys mass balance and the bottoms profile split is sharp. In this way we reduce the regions depicted in Figure 2.21a-c to the sloppy split minimum reflux regions.

The combined sloppy split minimum reflux solution regions are illustrated in Figure 2.22. In this figure the individual colours correspond to the three different solutions for the sloppy split minimum. I.e. Blue line for distillate and blue region for bottoms correspond to CLL1 reflux solutions. The red region is the infeasible region based on the incorrect sign of the column sections. The black dotted line is the feasible DFP line and the black dot at the extremities of the DFP line is the preferred split. Selection of the difference points found in Figure 2.21a-b that are not shown in Figure 2.22, although not incorrect, will produce non-intersecting profiles as these profiles do not trace the necessary  $TT_3$ s of the associated column sections.

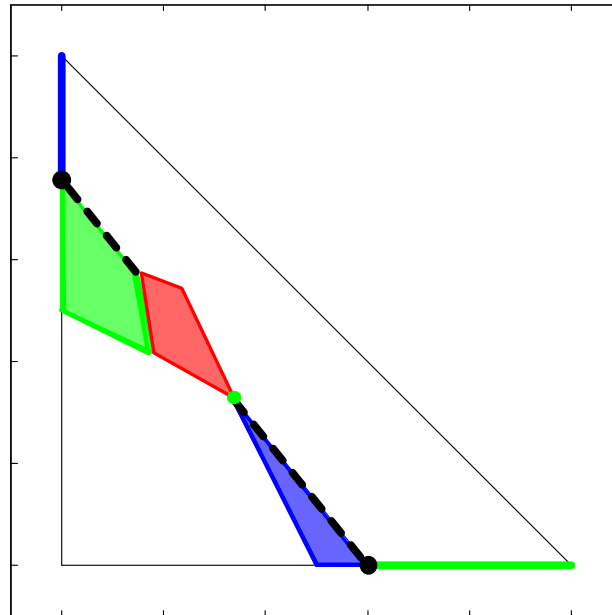


Figure 2.22: Sloppy Split minimum reflux regions.

## 2.10 Application to higher order systems

The CPM-E method is applicable to higher order systems. The concepts discussed in Chapters 4 and 5 provide a good illustration of the application of the CPM-E method to quaternary systems. The extrapolation to sloppy-split, higher order, ideal systems is fairly straightforward. The main aspect when dealing with higher order, minimum reflux systems is the interaction of the rectifying and stripping sections boundaries. It has been illustrated that a ternary systems boundary is a straight line or a point based on the co-linearity requirement for sloppy splits minimum reflux solutions. If we now extend this idea to three dimensional space containing four species that produce tetrahedrons, it is clear that the interaction of the rectifying and stripping sections is either along a plane, a line or a point. As with ternary systems, the product specification predefines what interaction the profiles will have (Refer to section 2.9).

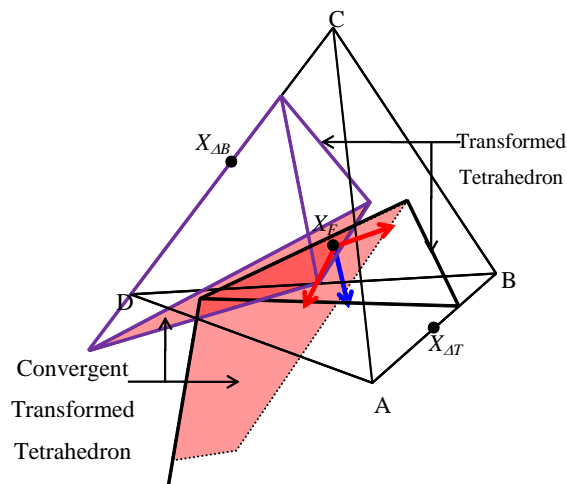
The interactions of the transformed tetrahedrons under minimum reflux conditions provide a unique, geometric opportunity for evaluating the feasibility of a certain

column. For the quaternary system, a minimum reflux solution is based on interactions of the planes of the transformed tetrahedrons. More specifically, the minimum reflux solution is found when the planes of the rectifying and stripping sections are co-planar through the feed. Thus, the eigenvectors evaluated at the feed condition provides the co-planar surface where the transformed tetrahedrons interact under minimum reflux conditions. If the feed is liquid, the planes of the liquid transformed tetrahedrons will pass through the feed and naturally vice versa for a vapour feed. Therefore by evaluating the eigenvectors at the given feed creates the co-planar surface where the saddle pinch and feed pinch lie on the plane through the feed. The eigenvector evaluation at the feed composition thus produces a condition to determine the stationary points along the co-planar surface and therefore the reflux associated to the minimum transformed tetrahedrons.

The commonality of the co-planar surface eigenvectors and the co-linear mixing and separation vectors allows for the determination of the stationary point associated to the minimum reflux transformed tetrahedrons. This feasibility criterion using the eigenvectors is depicted in Figure 2.23: A design for an equimolar quaternary mixture in a simple column for the component AB-CD split. At minimum reflux the planes of the transformed tetrahedrons intersect, created from the eigenvectors evaluated at the feed condition..

The extension to the equivalent higher order systems minimum reflux solution is based on the same principles as the ternary and quaternary systems. As mentioned previously the minimum reflux solution for the ternary system is based on the linear interactions of the eigenvectors, mixing vectors and separation vectors. The quaternary solution is based on the planar interactions of the transformed tetrahedrons for the rectifying and stripping sections and the evaluated eigenvectors at the feed. In the same way as we evaluated the eigenvectors at the feed composition and produced the co-linear and co-planar where the transformed triangles/tetrahedrons met, the eigenvector evaluation at the feed composition for higher order systems produces the co-hyper-planar boundaries where the

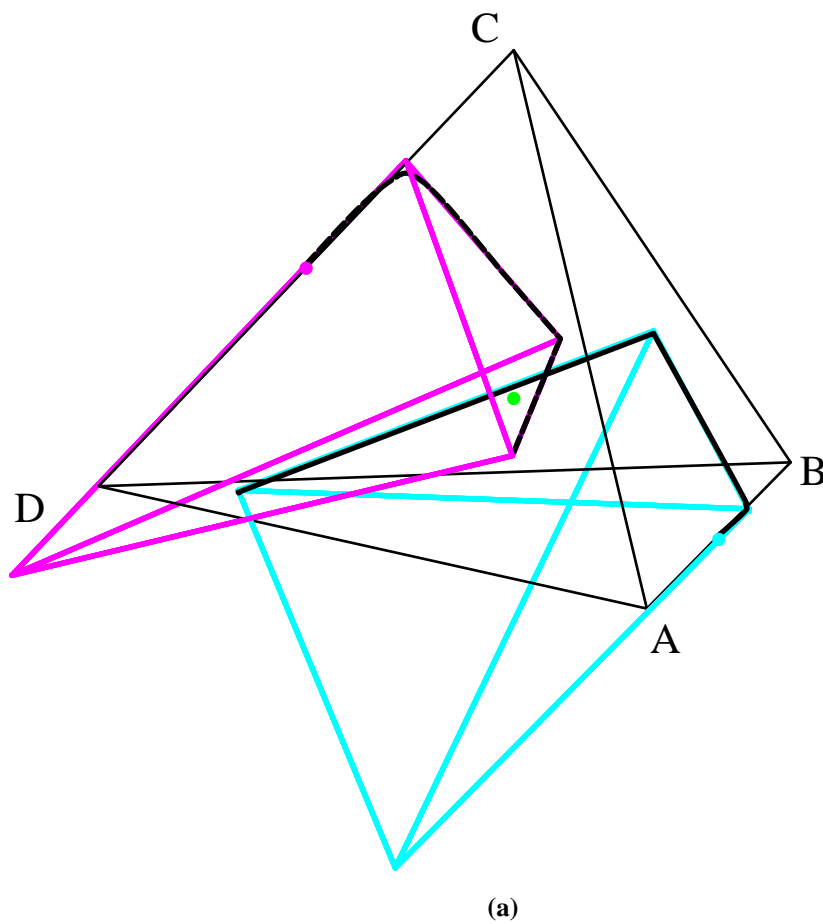
transformed hyper planes touch. In order to determine higher order system minimum reflux solutions the stationary points must therefore interact on hyper planes of the desired number of components as required. In order to determine the pinch point of the transformed hyper planes (profile termination point), the point where the co-linear mixing and separation vector intersects with the co-hyper-planar boundary is one of the minimum reflux stationary points. The exact same solution as mentioned above for different quality of feeds is applicable to any higher order system, but cannot be graphically visualised. Importantly, the solutions obtained using the CPM-E techniques described above for finding minimum reflux is exactly equivalent to the minimum reflux solutions predicted by the Underwood method.

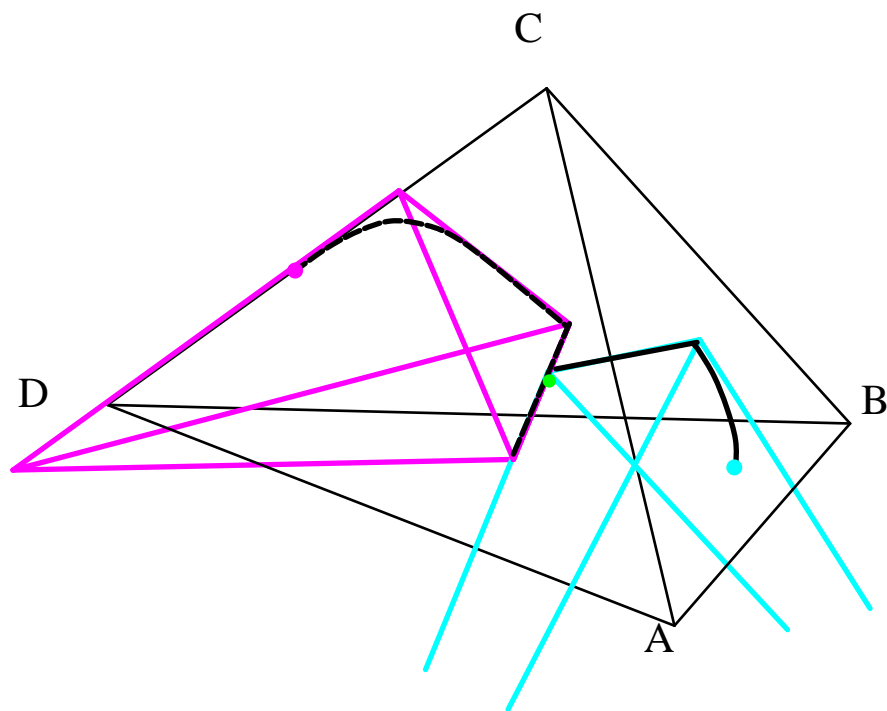


**Figure 2.23: A design for an equimolar quaternary mixture in a simple column for the component AB-CD split. At minimum reflux the planes of the transformed tetrahedrons intersect, created from the eigenvectors evaluated at the feed condition.**

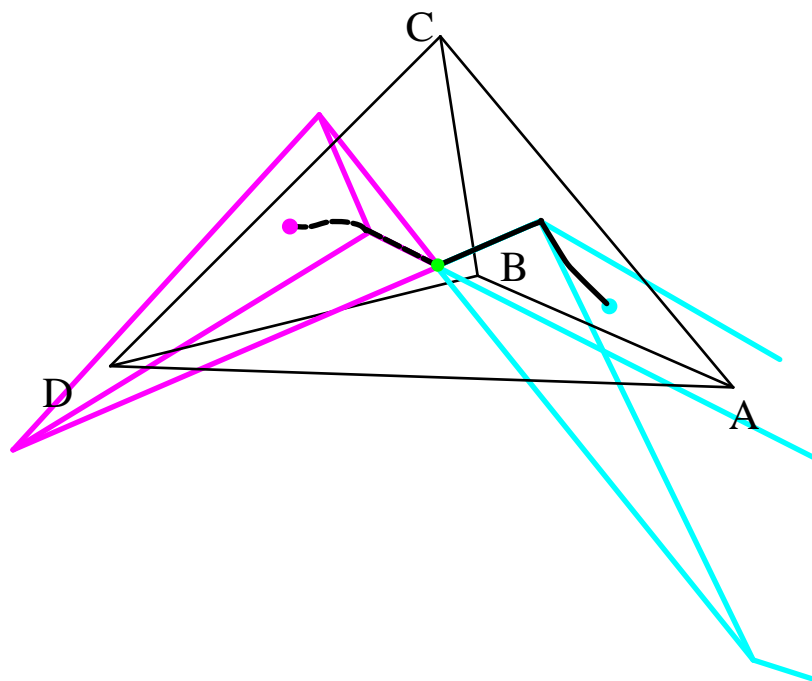
It has been shown that an ideal ternary system has two different classes of minimum reflux solutions. As the evaluation of the eigenvectors at the feed composition produces two eigenvectors, a solution on each eigenvector as well as a solution utilising both eigenvectors simultaneously (double feed pinch and preferable slit) is present. For a quaternary system, evaluation of eigenvectors at

the feed composition produces three independent eigenvectors. Thus, the tetrahedrons interact not only on the edges, but also along the planes of the tetrahedrons. Intuitively three classes of solutions are present which are defined by the selection of the product specifications for a quaternary system. Since three eigenvectors exist, six different solutions exist. A solution where the rectifying and stripping section tetrahedrons interact on two different planes, three different edges and a single point at the feed composition (Double feed pinch and preferred split). The three classes of solutions for a quaternary system at minimum reflux is illustrated in below.





(b)



(c)

Figure 2.24: Three classes of a quaternary systems minimum reflux solutions. (a) Plane interaction. ( $\alpha = [6 \ 4 \ 2 \ 1]$ ,  $X_F = [\frac{1}{4} \ \frac{1}{4} \ \frac{1}{4} \ \frac{1}{4}]$ ,  $X_T = [0.5 \ 0.5 \ 0 \ 0]$ ,  $X_B = [0 \ 0 \ 0.5 \ 0.5]$ ,  $R_{min} = 1.21$ ). (b) Edge interaction ( $\alpha = [6 \ 4 \ 2 \ 1]$ ,  $X_F = [\frac{1}{4} \ \frac{1}{4} \ \frac{1}{4} \ \frac{1}{4}]$ ,  $X_T = [0.439 \ 0.436 \ 0.125 \ 0]$ ,  $X_B = [0 \ 0.004 \ 0.416 \ 0.58]$ ,  $R_{min} = 0.47$ ). (c) Point interaction depicting a double feed pinch solution ( $\alpha = [6 \ 4 \ 2 \ 1]$ ,  $X_F = [\frac{1}{4} \ \frac{1}{4} \ \frac{1}{4} \ \frac{1}{4}]$ ,  $X_T = [0.55 \ 0.33 \ 0.12 \ 0]$ ,  $X_B = [0 \ 0.18 \ 0.36 \ 0.46]$ ,  $R_{min} = 0.44$ ).

## 2.11 Simulation and Methodology Comparison

Simulation programs often aid in providing a definitive answer regarding the accuracy as well as the shortcomings of a methodology, as most of these simulation programs such as ASPEN Plus utilise direct iterations. The ASPEN Plus simulations were initialised using the results of the CPM-E techniques and are illustrated in Figure 2.25.

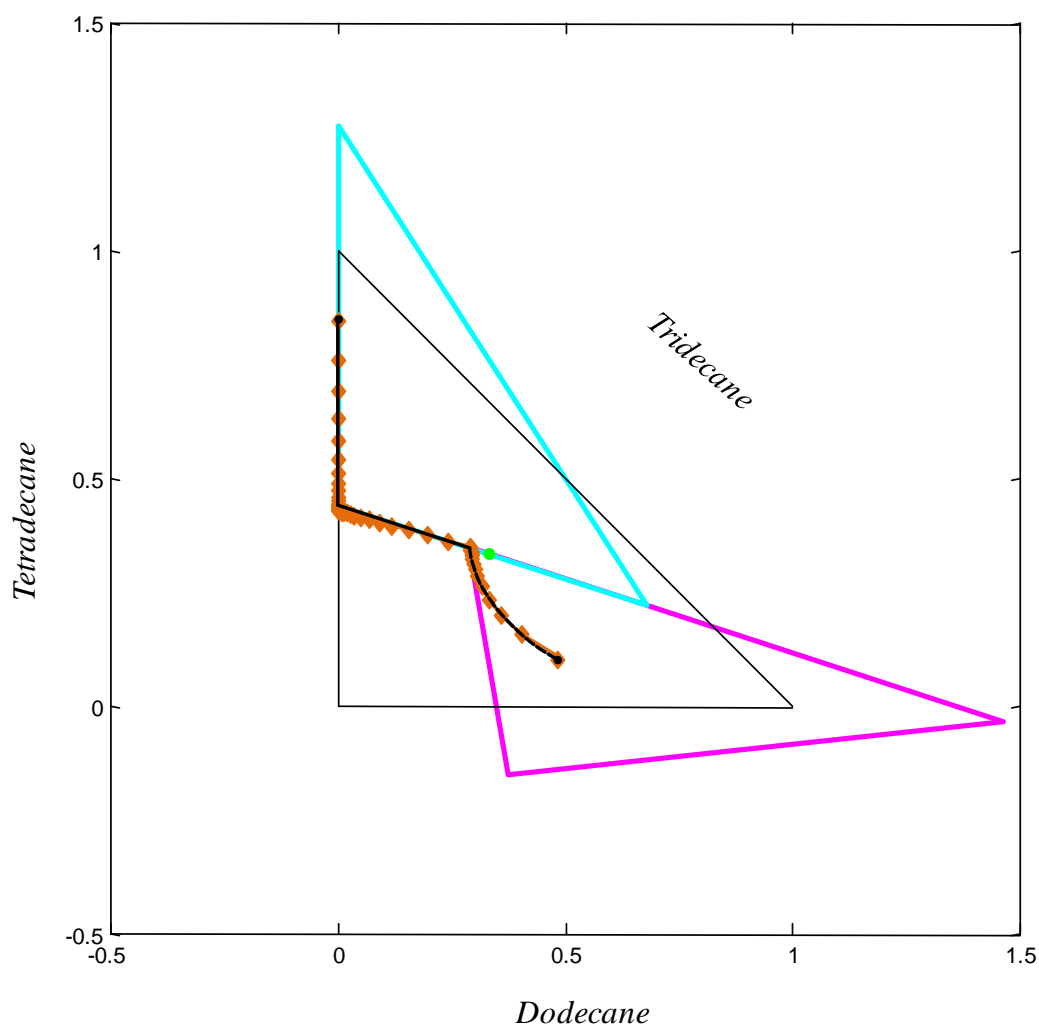


Figure 2.25: Comparison of the CPM-E technique to an ASPEN Plus simulation using a Dodecane, Tridecane and Tetradecane system. Equimolar feed,  $\alpha_{\text{equivalent}} = [2.41 \ 1 \ 1.55]$  and  $X_T = [0.85 \ 0]$ ,  $X_B = [0.1 \ 0.48]$  Reflux = 2.72.

As a real system is required to simulate a comparison, the Dodecane-Tridecane-Tetradecane ( $C_{12}H_{26}$ ,  $C_{13}H_{28}$  and  $C_{14}H_{30}$ ) ternary system was selected. These species are all present in Fischer Tropsch Synthesis and define a consecutive series of hydrocarbons that fall on the cusp of two main products (Diesel and Heavy Naphtha) in an intermediate product recover sequence. As the interaction of an Alkanes mixture portrays ideal behaviour, the selection of these species is suitable for our requirements.

The solid black line and dotted line in Figure 2.25 are the rectifying and stripping section  $R_{\min}$  profiles determined from the CPM-E technique. The continuous orange diamond shaped profile is the ASPEN Plus simulation initialised from the results of the CPM-E technique. These profiles are almost identical and show that the CPM-E technique has immense merit and can be utilised to determine  $R_{\min}$  accurately without tedious and onerous calculations.

The comparison to current methodologies to calculate minimum reflux is useful as these comparisons show how well the method under observation portrays opportunities for close collaboration to a method as well as the accuracy of the method. The comparison of the  $R_{\min}$  calculated by utilising the CPM-E technique produces exactly the same results as compared to the result of the Underwood equations (See Table 2.2). Table 2.2 shows the comparison between the Underwood method, the boundary value method (BVM) introduced by Levy et al. (1985) and the CPM-E technique. The results of the BVM are in strong agreement with Underwood's method and therefore the CPM-E method.

**Table 2.2: Comparison of the CPM-E techniques to valued methods.**

Relative volatilities		Feed composition		Product compositions		Reflux ratio		
$\alpha_{12}$	$\alpha_{13}$	$X_{F1}$	$X_{F2}$	$X_{D1}$	$X_{B1}$	Underwood	BVM	CPM-E
1.25	1.5	0.3	0.3	0.95	0.01	9.08	9.1	9.08
2.37	12.67	0.3	0.3	0.999	0.001	1.52	1.54	1.52

## 2.12 $R_{\min}$ for Non-Sharp Split, Non-Ideal and Azeotropic Systems

### 2.12.1 Non-Sharp Solutions

Regions of feasibility have shown that non sharp solutions are merely an approximation of the real minimum reflux when the CPM-E technique is implemented. The untracked  $TT_3$ s of the most important profiles that are associated to a category of solutions based on the CLLs chosen, is the motivation that only parts of the feasible region is an estimation of the real minimum reflux. Even although the solutions based on the CPM-E technique for non-sharp solutions is not the quantitative reflux value, the solutions established on the technique are very close to the actual value. The methods adopted by Levy et al. (1985) and Julka and Doherty (1990) have shown that the refluxes calculated for non sharp solutions can be approximated by having reflux multipliers that give closer values to the real solution. The graphical nature of the CPM-E technique and BVM allows for the reproducibility of this method. Although this isn't a unique science, the applicability of the CPM-E technique allows for more rapid solutions without the need of iterative steps. Intuitively we would expect that the solutions based on the CPM-E technique for non-sharp solutions wouldn't satisfy profile intersection criterion as the methodology is based on a specific phase of  $TT_3$ s intersecting one another. This means that although the respective  $TT_3$ s intersect, the profiles will not, unless the  $TT_3$ s of these column sections overlap instead of touch along a CLL. The degree at which the  $TT_3$ s have to overlap to ensure that the profiles intersect is dependent on the sharpness of the split. If a relatively large amount of heavy impurity were found in the distillate, the overlap would be quite extensive.

Although it is not our intention in this paper to completely solve and find a direct solution for all non-sharp minimum reflux solutions as we have for the sharp split case, the CPM-E methodology can be used in conjunction with pinch point loci to

solve for them. Any minimum reflux solution is based on the termination of either profile on the other. This means that if we select distillate compositions in CLL1 region (See Figure 2.21a), the unstable node of the SSs  $TT_3$  has to coincide with the RS profile and vice versa when CLL2 is utilised. Figure 2.26a-b illustrates a non-sharp minimum reflux solution. Once again, from the form of the intersection it is quite easy to recognise which CLL is employed for the minimum reflux solution based on the order of intersection of the profiles.

The minimum reflux solution of Figure 2.26a-b is based on a distillate composition consisting of 90% lights component, and 2% heavies and 10% lights impurity in the bottoms for an equimolar feed. The non-sharp solution clearly indicates an overlap of  $TT_{3s}$  other than the  $TT_{3s}$  touching. Using the CPM-E technique produces a calculated  $R_{\min\text{-calc}}$  of 2.2. The actual  $R_{\min\text{-actual}}$  is 3.01 and this suggests that the multiplier is approximately 1.37. The low value of the multiplier indicates that the CPM-E technique produces a close approximation to the actual reflux. As with the sharp split solution, the non sharp solution is based on calculating the linear dependency on the system and evaluating the appropriate nodes that coincide with the straight line.

### 2.12.2 Non-Ideal and Azeotropic Solutions

The methods and rules discussed can therefore be extended to more complex systems. These include non sharp minimum reflux calculations which we have already discussed. Along with these systems, the use of the CPM-E technique can be applied to non-ideal and azeotropic systems. Holland et al. (2004) have shown as a result of the thermodynamics, there is a great change in direction of the eigenvectors in some areas along the light intermediate axis. Hence changing the position of the nodes by transforming the space will result in a great variety of phase diagrams. This as a result makes the azeotropic systems difficult to analyse under any finite reflux conditions. If we simplify the systems by looking at regions defined within the residue curve map (infinite reflux) of the system, it is possible to apply the CPM-E to each region depending on what purity the

designer specifies. This means an azeotropic system can have a feasible/infeasible region as we have shown for ideal and zeotropic systems for predefined feed conditions. Again this region is found by finding limiting conditions within each region of the system.

As for the ideal systems, these limiting boundaries consist of the DFP line, bow-tie region and CLL lines which are based on the sign of the reflux. By evaluation of the eigenvectors at the feed condition, we can find the CLL based on the distillate and bottoms composition selection, which will be utilised to find  $R_{min}$ . It is important to note that for ideal systems any point chosen along the eigenvector boundaries will have eigenvectors that point directly at the same singularities, which define it. This is not true for non-ideal systems, as the boundaries between nodes are not straight other than at infinite reflux. Although the eigenvectors do not point in the exact same direction, they are very similar even for systems that portray regions of great curvature such as the acetone-benzene-chloroform (ABC) system.

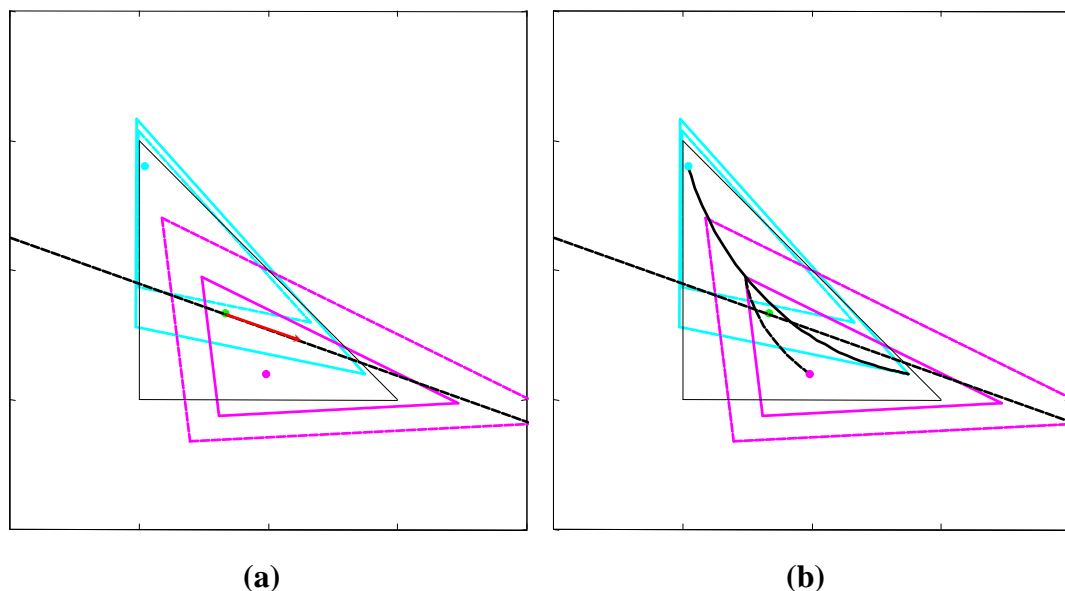


**Figure 2.26:** (a)  $TT_3$  overlap for feasible non sharp minimum reflux. (b) Non sharp solution with SS profile termination on RS profile.

The ABC system has a distillation boundary due to the existence of a binary low boiling azeotrope between chloroform and acetone. It has been shown (Levy et al., 1985; Doherty and Perkins, 1977, 1978a, b, 1979a, b; Van Dongen and Doherty, 1984; Van Dongen and Doherty, 1985; Furter et al., 1972) that the curvature of the distillation boundary in the ABC system is of the worst case ever encountered. In general, distillation boundaries are much less curved than the one presented in the ABC system, and consequently the profiles are more linear. An important aspect when using the CPM-E technique is of course that the straight line that passes through the saddle node of a profile and the feed composition (CLL) is used to determine the minimum reflux. This application suggests that the linear combination should exist, and if it does not, it will only be an approximation to the actual reflux. The extent of accurate approximations at this point is solely dependent on the degree of error to which the curves can be estimated to be straight lines. Thus, when the CPM-E technique is applied to a system such as the ABC system a degree of inaccuracy will exist. As the profiles become more linear, the approximation of the CPM-E technique improves dramatically.

## 2.13 Discussion and Conclusion

In this work we have illustrated a general method for calculating minimum reflux ratios through the use of Column Profile Maps named CPM-E technique. The techniques and methods we have developed are extremely powerful and versatile tools that do not suffer some of the fundamental shortcomings of currently employed short-cut techniques. The method applies to ideal, non-ideal, and azeotropic distillations, becoming identical with Underwood's method for ideal mixtures.

The technique makes use of eigenvectors evaluated at the feed composition in order to find a linear relationship between the saddle node and feed conditions. This line, called the co-linearity line (CLL) is the line where two sets of nodes

from each column section intersect when minimum reflux conditions are present. The evaluation of the eigenvector at a stationary point produces two vectors that point in the direction of other nodes in the vicinity of the stationary point. Thus two CLLs exist, one for each eigenvector.

Three distinct solutions exist for the CPM-E technique. A solution that arises when each of the individual CLLs are common and a special solution when both CLLs are common. The solution based on both CLLs being common produces a line of solutions called the double feed pinch line that passes through the preferred split. The three solutions are associated to feasible regions within the mass balance triangle. These regions are areas that are associated to either CLL utilised and is solely dependent on the purity of the products selected. As a result, the regions produced from each solution allow the user the freedom to select non-sharp products as these solutions are based on the original eigenvector boundary selected.

The paper focuses on ideal ternary systems, but due to the nature of the non-iterative CPM-E solution that arises from the eigenvector boundaries, the CPM-E technique can be applied to higher order systems such as quaternary and even pentenary system. These will be illustrated in publications in the future.

In non-ideal and azeotropic mixtures, the saddle pinch profile will not be linear, but the nonlinearity in the profile is typically weak. Therefore, a proficient approximation to the exact condition for finding the minimum reflux in these mixtures is through the CPM-E technique which makes the stable/unstable stationary point, the saddle pinch point, and the feed composition collinear. In this way, a single, general purpose method provides a minimum reflux solution regardless of the ideal or non-ideal thermodynamic nature of the mixture.

Holland (2006) has shown that infeasible sharp split separations can never be made feasible without increasing the reflux ratio. As a result distributed feeds can only be applied to non-sharp splits. As the CPM-E method is only applicable to

sharp and sloppy splits, application of the CPM-E method to a distributed feed system is not applicable and no additional insight into a distributed feed column can be found. This is not only a limitation to the CPM-E technique but to all minimum reflux methods.

The CPM-E technique can be applied to higher order systems. The simplicity originates from uncomplicated mathematics combined with graphical interpretation. Every column can be broken down into column sections and modelled according to Column Profile Maps, which makes the CPM-E technique a versatile tool for solving minimum energy requirements. This is not only true for conventional columns, but for any thermally-coupled systems. This means that the concepts of the CPM-E techniques can without a doubt be applied to more complex systems such as the Petlyuk and Kaibel columns.

## Chapter 3: Complex Column Design - Sharp Split Petlyuk Column

*The first application of the CPM-E technique is applied in this chapter in order to determine the region of feasibility in the split ratio space and hence the minimum reflux conditions for the coupled sections of the Petlyuk column. The work has been published in Industrial and Engineering Chemistry Research (see Holland et al., 2010). Although my name appears as the second author on this paper, the work is almost exclusively Dr. Simon Holland's and can also be found in his thesis (Holland, 2005).*

---

### **Abstract**

Currently employed short-cut design techniques tend to be configuration specific. Few can be employed on complex distillation configurations. In this work we will demonstrate, in detail, the use of column profile maps (CPMs) for the comprehensive analysis and design of complex distillation systems by applying the CPM technique to the design of the fully thermally coupled (Petlyuk) distillation column at sharp-split conditions. It is shown that for set product composition specifications and set reflux ratio, only a small region of key parameters (vapour and liquid split ratios) result in feasible separations. These results and hence the CPM design procedure are validated by the work of Halvorsen and Skogestad (2001). It is also shown that the minimum reflux solution can be found using the methodology. The results are valid for all zeotropic separation synthesis

---

### 3.1 Introduction

Distillation is one of the most utilised large scale industrial methods of mixture separation. It is a very energy intensive process and accounts for a significant percentage of plant utility costs. A survey (Ognisty, 1995) conducted in the mid 1990's estimates that energy inputs to distillation columns in the United States accounts for approximately 3% of the countries entire energy consumption. It is clear that the efficiency of the separation can have a substantial influence on the profitability of a process and methods of improving the energy efficiency of distillation systems are, therefore, constantly sought.

One alternative, to the energy intensive, traditional distillation configurations, which has offered promise, are the thermally coupled distillation columns. These include side-strippers, side-rectifiers and fully thermally coupled configurations also known as Petlyuk columns. The energy demand of these and traditional columns has been well studied over the years: Petlyuk et al (1965); Stupin and Lockhart (1972); Hendry et al (1973); Doukas and Luyben (1978); Tedder and Rudd (1978); Westerberg (1985); Fidkowski and Krolikowski (1987); Glinos and Malone (1988); Carlberg and Westerberg (1989); Rudd (1992); Triantafyllou and Smith (1992); Wolff and Skogestad (1995); Westerberg and Wahnschafft (1996); Finn (1996). It has been shown analytically (Fidkowski and Krolikowski, 1987) that for three component zeotropic separations, the Petlyuk column has the lowest overall energy demand. The other thermally coupled configurations also require less energy than the traditional direct and indirect splits.

Thermally coupled configurations offer, not only, the potential for utility savings but for capital savings as well. Traditional direct and indirect configurations require two shells, two condensers and two reboilers for three component zeotropic separations. Side-rectifiers and side-strippers eliminate the requirement of one reboiler and one condenser respectively, while the Petlyuk column eliminates the requirement of one of each. Furthermore the two shell Petlyuk arrangement can be replaced with a single shell containing an internal divider or

wall. This is known as the dividing wall (Wright, 1949) or partitioned column and is thermodynamically equivalent to the Petlyuk column if there is no heat transfer through the dividing wall.

Clearly the Petlyuk column has many qualities which make it an attractive alternative to traditional configurations and yet relatively few have actually been employed industrially. Until fairly recently BASF was the sole industrial proponent of the dividing wall column (Kaibel, 1988, 1995). In the last few years, Sumito Heavy Industries Co. together with Kyowa Yuka (Parkinson, 1998) and MW Kellogg Limited together with BP Amoco (Lestak et al., 1999) have employed dividing wall columns. Other recent examples include German (Kolbe and Wenzel, 2002), American (Schultz, 2002) and South African companies. The major concern over the use of Petlyuk or dividing wall columns appears to be related to the efficient design and control of these arrangements.

The standard Petlyuk arrangement, of pre-fractionator and main column, suffers from the drawback that the pressure in the pre-fractionator is neither uniformly higher nor uniformly lower than the pressure in the main column. The vapour draw in the main column is required to be at a higher pressure than that at the bottom of the pre-fractionator while the vapour feed from the top of the pre-fractionator is required to be at a higher pressure than at the corresponding feed point in the main column (see Figure 3.4). New arrangements have been suggested (Agrawal and Fidkowski, 1998) that remove this issue by having unidirectional vapour flow either from the first to the second shell or vice versa. In these arrangements either the bottoms or the distillate is taken from the feed column. The dividing wall column can also suffer controllability problems due to the pressure differential across the dividing wall. This issue can be resolved by simply making use of equal stages on either side of the partition and hence enforcing an equal pressure drop on either side of the divide. A number of studies (Wolff and Skogestad 1995; Halvorsen and Skogestad, 1997, 1999; Abdul Mutalib and Smith, 1998a, 1998b) have been performed on the control and operation of the dividing wall column. Theoretical studies (Halvorsen and

Skogestad, 1997, 1999) suggest that maintaining column product specifications while operating close to the minimum column energy requirement is difficult without good control strategies. A pilot plant study (Abdul Mutalib and Smith, 1998b) of the control issue reported stable column responses, to feed disturbances, using temperature control. A product purity offset was reported, however.

The industrial reservations regarding the efficient design of the Petlyuk and dividing wall columns are likely related to the difficulty involved in rigorous simulation. Due to the thermal coupling of the pre-fractionator and main column a number of internal variables such as flows and compositions are required to be estimated when using iterative simulation packages. This requires advance knowledge of the solution output in order to achieve the solution. The less accurate the estimate of the unknown parameters, the less likely the iterative routine will converge to a solution. This issue, as well as general design issues, have been addressed in literature (Fonyo et al, 1974; Tedder and Rudd, 1978; Spadoni and Stramigioli, 1983; Triantafyllou and Smith, 1992; Amminudin et al, 2001), with varying success, but without a comprehensive understanding of the form of the Petlyuk solution and operating parameters.

One of the fundamental breakthroughs regarding the understanding of the dynamics and steady state operation of the Petlyuk column was the development of the analytical solution for minimum vapour requirement for sharp-splits (Fidkowski and Krolikowski, 1987). The solution makes use of the Underwood equations (Underwood, 1948) and the “carry-over” of the Underwood roots from one column section to another. This methodology, used to derive the minimum vapour flow equations, was then used to derive the Petlyuk “optimality region” for infinite stages and sharp splits (Halvorsen and Skogestad, 1997). The “optimality region” is a section of parameter space defined by the Petlyuk’s vapour and liquid split ratios containing all feasible split ratios for set sharp/pure product specifications and set reflux ratio. The form of the “optimality region” was studied at various reflux ratios, feed compositions, feed qualities and relative volatilities. In terms of a general understanding of the column dynamics and

steady state, the study of the “optimality region” has been very successful. In terms of its use for design purposes, however, the methodology does suffer a number of drawbacks when put to practical use. It is only directly applicable to constant relative volatility systems as the Underwood equations are only valid for this set of thermodynamics. The generation of individual Petlyuk solutions from values within the “optimality region” still requires iterative solving methods. The non-sharp “optimality region” cannot be generated without extensive direct simulation.

It is our intention in this work to detail the use of Column Profile Maps (CPMs) (Tapp et al, 2004) as a design and optimisation tool for the Petlyuk column and to generate the “optimality region” for all zeotropic thermodynamics and product specifications. We will, however, refer to the “optimality region” as the “feasible region” as it is the set of split ratios resulting in feasible Petlyuk separations. The generation of the feasible region will be performed from a topological perspective and the net flow of components within the Petlyuk column will be analysed in detail. Although we will also make use of constant relative volatility assumptions, the graphical nature of the procedure will allow for the methodology’s applicability to all zeotropic thermodynamics. The sharp-split solution and topological phenomena will be used to generate non-sharp split solutions where infinite stages are not necessarily required. The non-sharp minimum reflux solution will be detailed with reference to the sharp-split minimum reflux solution. This chapter will deal, solely, with the sharp-split solution and will lay down fundamental concepts and definitions which will be employed in the following chapter which addresses the non-sharp Petlyuk problem. By employing the CPM technique it will be shown that all required design parameters, even total required stages, feed stage and side-draw stage come “naturally” from the solution.

**Assumptions:**

- We will address the three component problem in this work.
- Constant molar overflow is assumed for all distillation modelling.

- An assumption of constant relative volatility is also made although the results are applicable to all three component zeotropic thermodynamics.
- Feed material is assumed to be at saturated liquid or saturated vapour conditions.
- Perfect mixing is assumed over all mixing points.

### 3.2 Column Profile Maps

CPMs, which were introduced by Tapp et al (2004), are maps of composition trajectories generated for a column section with constant net-molar-flow using the difference point equation (see Equation 6.1 below). The difference point equation (DPE) for column section (CS)  $k$  is defined as follows:

$$\frac{dX}{dn} = \left( \frac{1}{R_{\Delta k}} + 1 \right) [X - Y^*(X)] + \frac{1}{R_{\Delta k}} [X_{\Delta k} - X] \quad (3.1)$$

$$\text{Where: } X_{\Delta k} = \frac{V_k Y^T - L_k X^T}{\Delta_k} \quad \text{and} \quad R_{\Delta k} = \frac{L_k}{\Delta_k}$$

$X$  is a liquid phase composition vector

$Y^*(X)$  is the equilibrium vapour composition vector

$R_{\Delta k}$  is the reflux ratio of CS  $k$

$V_k$  is the vapour flow rate of CS  $k$

$L_k$  is the liquid flow rate of CS  $k$

$\Delta_k$  is the net flow of CS  $k$  defined as  $\Delta_k = V_k - L_k$

$n$  is a stage number equivalent

$X^T$  is the liquid composition vector at the top of the CS

$Y^T$  is the vapour composition vector at the top of the CS

$X_{\Delta k}$  is the difference point of CS  $k$

The derivation of the Difference Point Equation is shown in Appendix F. To produce a CPM, the DPE is solved at various initial conditions, throughout

composition space (for  $n \rightarrow \infty$  and  $n \rightarrow -\infty$ ), after the selection of constants  $X_{\Delta k}$  and  $R_{\Delta k}$ . A CPM can be seen in Figure 3.1 below. The solutions or composition profiles/trajectories tend to infinity or terminate at stationary points. For three-component, constant relative volatility, systems there are three stationary point solutions present in a CPM. These are characterised as unstable, saddle point or stable nodes (see Figure 3.1). The stationary points of a system are equivalent to pinch point compositions in a CS. We can draw straight lines through the stationary points of the system. The boundaries thus formed separate regions of qualitatively different topology.

The position of these stationary points (and boundaries) and subsequently the qualitative form of the CPM, for a particular system, is dependent on  $X_{\Delta k}$  and  $R_{\Delta k}$ . For a set reflux ratio ( $R_{\Delta k}$ ), the stationary points can be “shifted” around composition space by varying  $X_{\Delta k}$ . Similarly, for a constant  $X_{\Delta k}$  value the stationary points can be “shifted” around composition space (along pinch point curves) by varying  $R_{\Delta k}$ . As  $R_{\Delta k} \rightarrow \infty$ , the stationary points tend to the pure component values of the mass balance triangle (\*MBT) and the DPE collapses to the residue curve equation (see Equation 3.2). At these conditions, the boundaries of the CPM lie on the axes and the CPM becomes topologically equivalent to the residue curve map (RCM).

$$\frac{dX}{dn} = [X - Y^*(X)] \quad (3.2)$$

The CPM is in fact a simple transform of the RCM. The topology present in each region of the RCM (defined between the axes) is “transformed” at finite reflux and shifted around composition space (see Figure 3.2 and Figure 3.3).

---

\* The MBT is defined by:  $0 < x_1 < 1$  ;  $0 < x_2 < 1$  ;  $0 < x_3 < 1$

By analysing the position of the stationary points, Tapp et al (2004) identified seven regions of  $X_{\Delta k}$  placement that resulted in qualitatively different CPMs. These seven regions correspond to regions of the RCM with differing topology (seen Figure 3.2). Because the different topology of the residue curve map corresponds to the regions of  $X_{\Delta}$  placement and the form of this topology is retained in the CPM, we can identify the shifted topology by referring to “*transformed regions*”. A transformed region simply represents topology that is qualitatively similar to topology present in the residue curve map within a particular difference point region. Figure 3.3 shows the seven transformed regions of a CPM.

The fact that the form of the RCM topology is retained at finite reflux implies that we do not need to solve the DPE to determine the qualitative form of the CPM. We need only solve for the stationary points. This is computationally simple and can in fact be done analytically for three component constant relative volatility systems. By extending straight lines between the points we can produce a “*transformed triangle*” ( $TT_3$ ). The  $TT_3$  retains all the qualitative topological information of the CPM (see Figure 3.3).

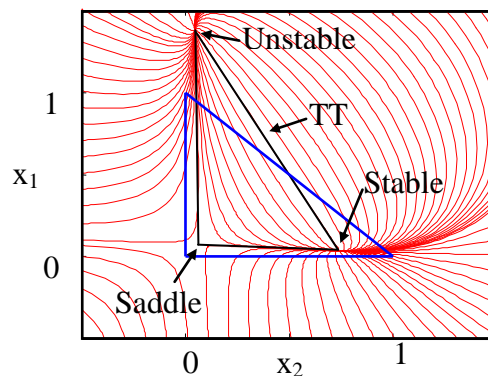


Figure 3.1: Column Profile Map for  $X_A = [0.3, -0.2]$  and  $R_A = 9$ .

Note:  $x_1$  – Light Component,  $x_2$  – Heavy Component,  $x_3$  – Intermediate Component

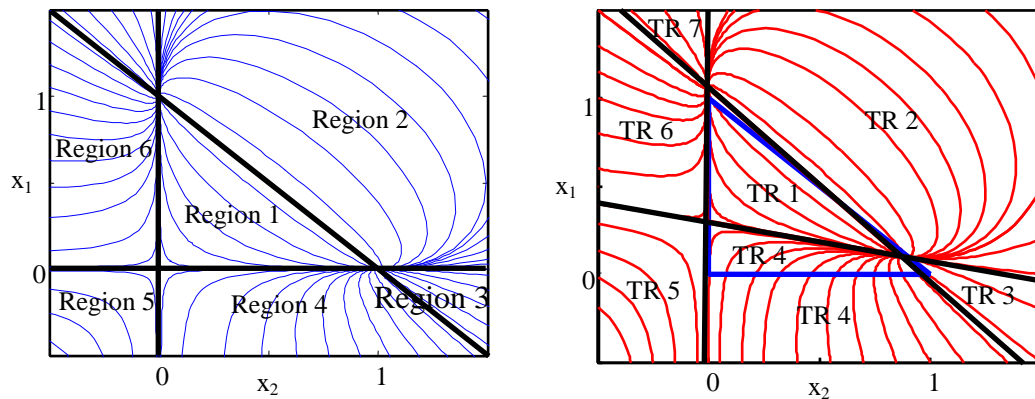


Figure 3.2: Difference point regions of Residue Curve Map

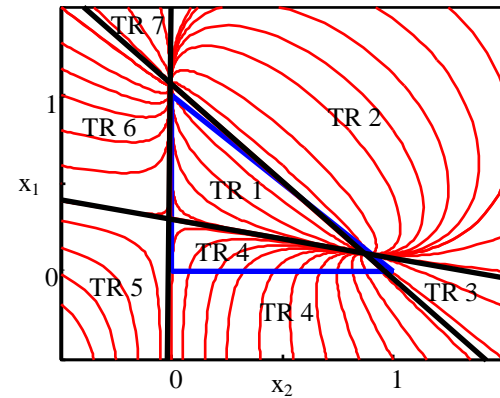


Figure 3.3: Transformed regions of Column Profile Map

### 3.3 Properties of $\Delta_k$ , $X_{\Delta k}$ and $R_{\Delta k}$

$\Delta_k$  which is defined as the difference between the vapour and liquid flows in CS  $k$  is a net flow of material within the column section. This net flow can be thought of as a pseudo stream flowing up or down the CS. If  $V_k > L_k$ , then  $\Delta_k > 0$  which means we have a net flow or pseudo stream flowing up the CS. But if  $V_k < L_k$ , then  $\Delta_k < 0$  and we have a net flow or pseudo stream flowing down the CS. The value of  $\Delta_k$  is the same at any point along the length of the CS.

The difference point ( $X_{\Delta k}$ ) can be thought of as the pseudo composition vector of  $\Delta_k$ , and is physically valid anywhere in composition space – both inside and outside the MBT. Because  $X_{\Delta k}$  is a pseudo composition, the elements sum to 1 i.e.

$$\sum_{i=1}^3 X_{\Delta k-i} = 1. \quad X_{\Delta k-i}, \text{ is the composition of element } i \text{ in the pseudo stream } \Delta_k \text{ and}$$

$\Delta_k X_{\Delta k-i}$  is the net flow of component  $i$  within CS  $k$ . A positive value is a net flow of component  $i$  up and a negative value is a net flow of component  $i$  down the column section. If  $X_{\Delta k-i}$  is negative, the direction of the net flow of component  $i$  is opposite to that of the  $\Delta_k$  and the sum of the remaining components is greater than 1.

The reflux ratio is defined as the ratio of liquid flowing down the CS to the net flow in the CS. Because of its dependence on  $\Delta_k$ ,  $R_{\Delta k}$  can be either positive (when  $\Delta_k > 0$ ) or negative (when  $\Delta_k < 0$ ). CPMs generated for a fixed difference point and positive reflux ratios are qualitatively different from those generated with the same difference point and negative reflux ratio.

### 3.4 CPM Design Methodology

Holland et al (2004 b) first introduced the methodology for distillation system design using CPMs. They illustrated the design of the Petlyuk column at overall infinite reflux. The outline for the methodology they introduced is as follows:

- Break column configuration into column sections.
- Choose difference points ( $X_{\Delta}$ ) and reflux ratio ( $R_{\Delta}$ ) for the most important column sections
- By material balance determine the difference points and reflux ratios of the remaining sections.
- Produce column profile maps (CPMs) for each of the sections and superimpose them to determine feasible operating profiles (if they exist).

We will address the finite reflux problem in a similar way. The above procedure cannot be employed directly due to the difficulty involved with choosing operating parameters (such as reflux ratios) for the pre-fractionator. It is very difficult to intuitively choose reflux ratios for the pre-fractionator column sections that will result in feasible designs. The general idea, nevertheless, is fundamental to our methodology. The column will be broken into column sections in the same way. Difference points will be chosen for the most important column sections – when the degrees of freedom are available. Feasibility of designs will always be determined by the superimposition of CPMs for each section.

To simplify the task a sharp-split specification on all products will be made i.e. the distillate product is assumed to contain effectively no heavy component material, the bottoms product is assumed to contain effectively no light component material and the side-draw product is assumed to be effectively pure intermediate component material. The non-sharp split problem will be addressed in future work.

It will be shown that, by employing this design methodology, it is possible to find all solutions (if they exist) for a particular overall column reflux ratio (rectifying reflux ratio) and product choice. An understanding of column parameter dynamics can also be gleaned. When feasible solutions do not exist, the method allows the designer to determine when or why they do not exist. Furthermore, analysis of the column using the method allows a minimum overall column reflux ratio to be determined.

### **3.5 Column Section Breakdown and Net Flow**

We shall begin the design process by breaking the Petlyuk column down into column sections. A schematic representation of the column can be seen in Figure 3.4 below. We can apply the column section breakdown approach used by Tapp et al (2004a) to identify individual column sections within the configuration. Tapp et al (2004a) defined column sections as lengths of column between points of addition or removal of material and/or energy. Using this definition, we can identify six column sections in the configuration. The column section breakdown is seen in Figure 3.5 below.

Column section 1 (CS 1) is a standard rectifying section terminated by a total or partial condenser. Column section 6 (CS 6) is a standard stripping section terminated by a total or partial reboiler. Column sections 2-5 will be referred to as the “*coupled column sections*”.

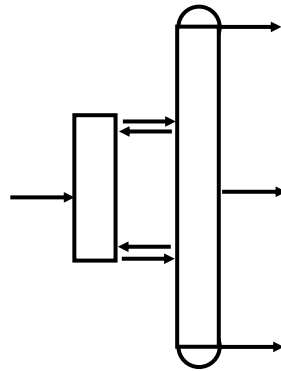


Figure 3.4: Petlyuk column (main column with pre-fractionator)

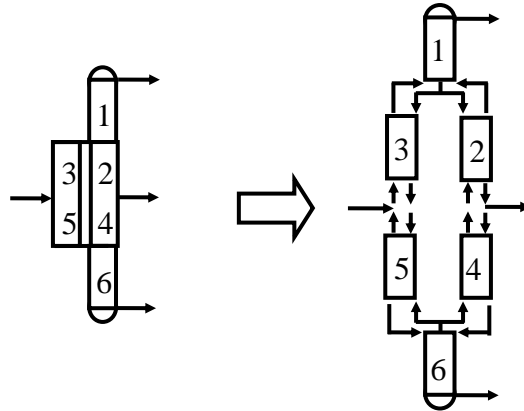
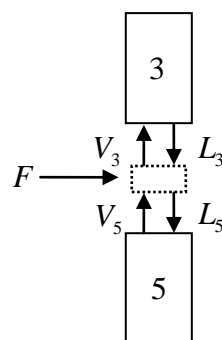


Figure 3.5: Column section breakdown for the Petlyuk column

## 3.6 Net Flow and Difference Point Material Balances in the Petlyuk Column

### 3.6.1 Net Flow and the Material Balance

$\Delta_k$  is a pseudo stream within a column section. Because of this  $\Delta_k$  has to obey the material balance in the same way that real streams do. This can be seen by performing a material balance at the point where feed material is added between two column sections (CS 3 and CS 5). See Figure 3.6 below.



$$L_3 + V_5 + F = L_5 + V_3$$

Rearranging we obtain :

$$V_5 - L_5 + F = V_3 - L_3$$

$$\text{But, } \Delta_k = V_k - L_k$$

Therefore :

$$\Delta_5 + F = \Delta_3$$

$$\Delta_3 - \Delta_5 = F$$

(3.3)

Figure 3.6: Mixing point between Column Section 3 and 5.

As mentioned above,  $\Delta_k$  can be positive or negative depending on the magnitude of the vapour and liquid flow rates. Equation 6.3 can be satisfied by various combinations of, positive and negative,  $\Delta_3$  and  $\Delta_5$  values. For example certain positive values of both  $\Delta_3$  and  $\Delta_5$  would satisfy Equation 6.3, as would certain negative values.  $\Delta_3$  could also be positive and  $\Delta_5$  negative. Negative  $\Delta_3$  and positive  $\Delta_5$  values, however, would violate the material balance. These net flow scenarios are illustrated in Figure 3.7a-d below.

COLUMN SECTION 3 AND 5:

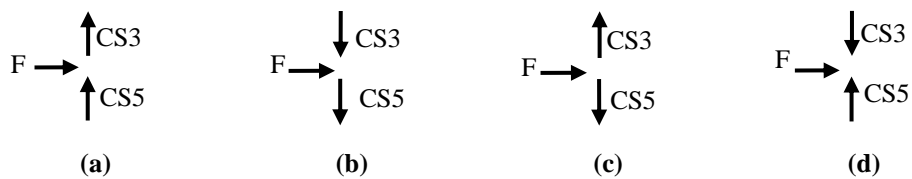


**Figure 3.7: Feasible net flow patterns at the point of feed addition. (a)  $\Delta_3 > 0$ ,  $\Delta_5 > 0$ , Feasible. (b)  $\Delta_3 < 0$ ,  $\Delta_5 < 0$ , Feasible. (c)  $\Delta_3 > 0$ ,  $\Delta_5 < 0$ , Feasible. (d)  $\Delta_3 < 0$ ,  $\Delta_5 > 0$ , Infeasible.**

This may seem like a trivial result, unless we recall that the reflux ratio for a column section is a function of  $\Delta_k$  and can be positive or negative. This result suggests that there are multiple reflux ratio combinations possible in the Petlyuk configuration. These combinations result in multiple, qualitatively different, CPMs that may be employed for the design. Some of the available combinations may provide more efficient separations. This implies that the net flow within the configuration may be advantageous or disadvantageous to the separation.

Let us now analyse the net flow combinations of the remaining mixing points in the configuration.

COLUMN SECTION 1, 2 AND 3: Column section 1 (CS 1) is a standard rectifying section. It produces a product - the distillate. The distillate flow is equal to the net flow in CS 1 because these streams are defined in the same way. To produce a product  $V_1$  is always greater than  $L_1$ ; hence the net flow can only be positive in CS 1. The net flows in CS 2 and 3 can be either positive or negative. The various combinations are seen in Figure 3.8a-d below.

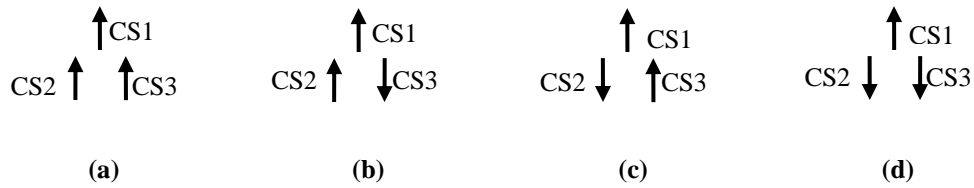


**Figure 3.8: Feasible net flow patterns at the mixing point of the rectifying section. (a)  $\Delta_2 > 0, \Delta_3 > 0$ , Feasible. (b)  $\Delta_2 > 0, \Delta_3 < 0$ , Feasible. (c)  $\Delta_2 < 0, \Delta_3 > 0$ , Feasible. (d)  $\Delta_2 < 0, \Delta_3 < 0$ , Infeasible.**

COLUMN SECTION 4, 5 AND 6: Column section 6 (CS 6) is a standard stripping section. It produces a product - the bottoms. The bottoms flow has equal magnitude but opposite sign to the net flow in CS 6 because the bottoms is defined as  $L_6 - V_6$ . Since  $L_6$  must be greater than  $V_6$  to produce a product, the net flow can only be negative in CS 6. The net flows in CS 4 and 6 can be either positive or negative. The various combinations are seen in Figure 3.9a-d below.

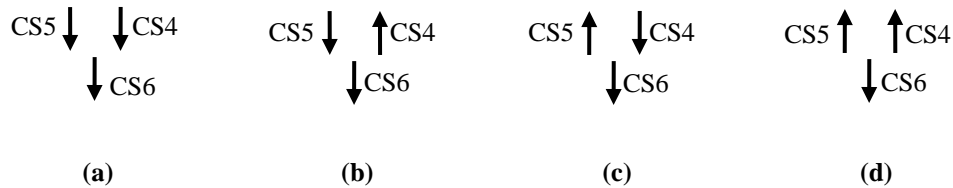


**Figure 3.9: Feasible net flow patterns at the mixing point of the stripping section. (a)  $\Delta_4 < 0, \Delta_5 < 0$ , Feasible. (b)  $\Delta_4 > 0, \Delta_5 < 0$ , Feasible. (c)  $\Delta_4 < 0, \Delta_5 > 0$ , Feasible. (d)  $\Delta_4 < 0, \Delta_5 < 0$ , Infeasible.**

Column Section 2 and 4: The net flows in CS 2 and 4 can be either positive or negative. The various combinations are seen in Figure 3.10a-d below.

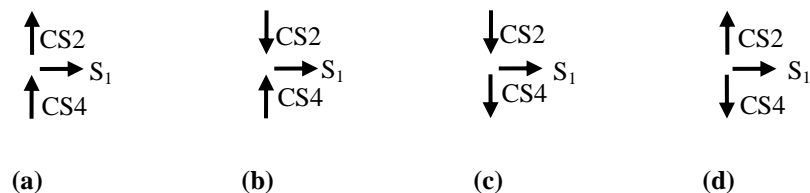


**Figure 3.10: Feasible net flow patterns at the first side draw. (a)  $\Delta_2 > 0, \Delta_4 > 0$ , Feasible. (b)  $\Delta_2 < 0, \Delta_4 > 0$ , Feasible. (c)  $\Delta_2 < 0, \Delta_4 < 0$ , Feasible. (d)  $\Delta_2 > 0, \Delta_4 < 0$ , Infeasible.**

By combining the feasible net flow scenarios in each column section and disregarding those that are infeasible we see that there are, in fact, *five possible net flow patterns in the Petlyuk column*. This result is quite surprising in light of the single flow pattern possible in a two product column (up in the rectifying section and down in the stripping section). These five flow patterns will, undoubtedly, allow profiles from a much wider range of qualitatively different CPMs to be sampled. The five scenarios are named net flow pattern 1 through 5 and are illustrated in Figure 3.11 a-e.

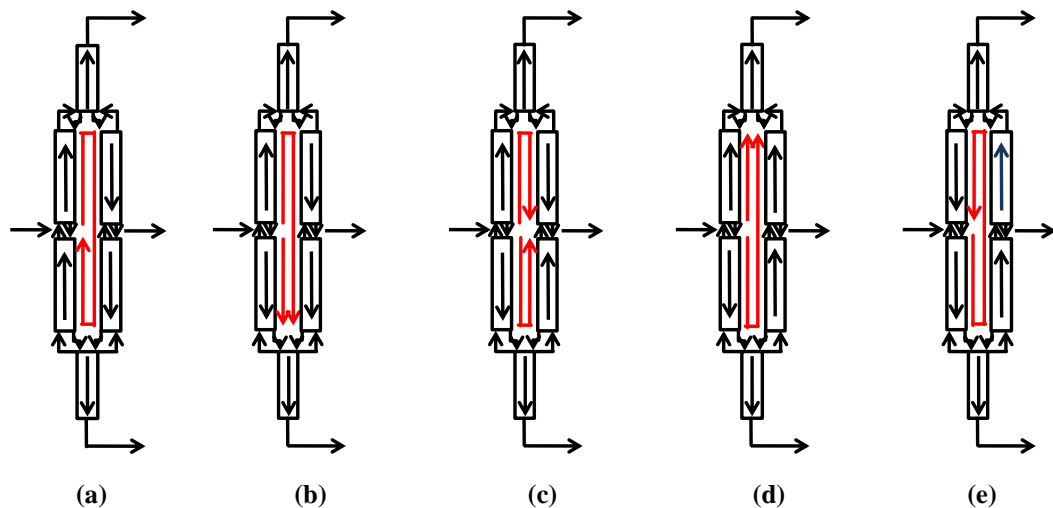


**Figure 3.11: Various Flow patterns that arise due to feasible net flow combinations. (a) Flow Pattern 1. (b) Flow Pattern 2 (c) Flow Pattern 3. (d) Flow Pattern 4. (e) Flow Patter 5.**

Physically these flow patterns are induced by control on the vapour and liquid split ratios into the coupled column sections (CS 2-5) from the stripping and rectifying sections, respectively. The net flow of material within the column can also be thought of in terms of the distributions of feed material.

The feed material in Figure 3.11c is distributed between the top and bottom halves of the column, so that there is net flow of material in both directions. If the net amount of material directed to the bottom half of the column is increased, the case

in Figure 3.11d is achieved. In this case, in order to maintain material balance, the material must be directed upwards, on the product side, in both CS 2 and 4. This is due to the fact that the side-draw flow rate is not large enough to change the direction of the net flow from CS 4 to CS 2. If the net amount of material directed to the top half of the column is increased, however, the case in Figure 3.11b is achieved. This case is the exact opposite of that in Figure 3.11d. The net flow of material on the product side is downwards for the same reasons given above. By increasing the material directed to the top half even further, the material eventually circulates (anti-clockwise in Figure 3.11a) within the coupled sections, flowing upwards in CS 5 instead of downwards. Conversely, if the material directed downwards on the feed side is increased further, the case in Figure 3.11e is achieved where material is circulated in the opposite direction (clockwise in Figure 3.11e).

The largest drawback to the configuration being operated with the net flow patterns 1, 2, 4 and 5 (Figure 3.11a, b, d and e) is that the net flow in the column sections at the side-draw (CS 2 and CS 4) is in the same direction. This results in the reflux ratios of the sections having the same sign. The side-draw has the effect of lowering the reflux from one column section to the other. If both refluxes are negative, the reflux of CS 4 will have a larger magnitude than that of CS 2. If the magnitude of the reflux of CS 2 is to be large enough to have the column operating on specification, the CS 4 reflux must be very high. *This ultimately means that CS 1 and CS 6 must operate at a fairly high reflux and the column will be energy intensive.* This is also true if both refluxes are positive. The net flow pattern 3 (Figure 3.11c) does not have this drawback and is therefore likely to be the most energy efficient operating mode.

### 3.6.2 Difference Points and the Material Balance

Because difference points are like pseudo compositions, they obey linear mixing rules. This can be shown by performing a component material balance at the feed point between CSs 3 and 5. See Figure 3.12.

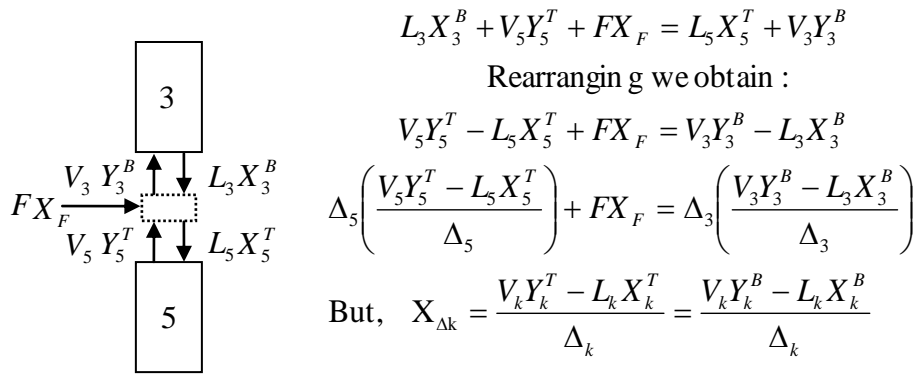


**Figure 3.12: Component mixing point between column Section 3 and 5**

Therefore :

$$\Delta_5 X_{\Delta 5} + F X_F = \Delta_3 X_{\Delta 3} \quad (3.4)$$

Geometrically this is equivalent to difference points  $X_{\Delta 3}$  and  $X_{\Delta 5}$  lying on a straight line through  $X_F$ , in composition space. Their relative positions will depend on the sign and magnitude of  $\Delta_3$  and  $\Delta_5$ . Table 3.1 summarises the various possibilities for CS 3 and 5.

The dependence of the difference point positions on the net flow implies that there will be as many relative difference point placement scenarios as there are net flow patterns. This is, indeed, the case and these will be explored in more detail later.

Table 3.1: Geometric Interpretation of Material Balance over CS 3 and 5			
Net Flow Pattern	$\Delta_3$	$\Delta_5$	Relative Positions of Difference Points
1	+	+	$X_{\Delta 5} \quad X_{\Delta 3} \quad X_F$ ●————●————●
2, 3, 4	+	-	$X_{\Delta 5} \quad X_F \quad X_{\Delta 3}$ ●————●————●

5	-	-	
	-	+	Infeasible

### 3.7 Composition Matching Criteria

The approach of treating the Petlyuk column as a number of column sections and piecing the solutions to these (the CPMs) together, as opposed to finding the solution to the entire column through iteration, results in the designer having to be mindful of certain composition matching criteria which need to be satisfied. Composition matching is required at all points where column sections meet. We will now discuss the required criteria at each of these four mixing points.

COMPOSITION MATCHING CRITERION 1: The liquid profiles from CS 1, CS 2 and CS 3 must all intersect if they are to be considered as possible operating profiles. This is simply due to the fact that the liquid leaving the bottom of CS 1 is divided between CS 2 and CS 3; hence this composition must exist on all three profiles. If CS 1 was not a standard rectifying section and the CPMs of all three column sections were superimposed, any three intersecting profiles from these maps could be thought of as possible solutions to the three-column section system. The situation is somewhat simplified by the fact that CS 1 is a rectifying section as only one profile on this CPM is valid. Rectifying sections have to operate on profiles that pass through the distillate composition or the composition in equilibrium with this stream, hence only one profile is valid. Any profiles from the CPMs of CS 2 and CS 3 intersecting on this solution are valid however.

COMPOSITION MATCHING CRITERION 2: The vapour profiles of the CS 4, CS 5 and CS 6 must all intersect because CS 4 and CS 5 are both fed vapour by CS 6, which is a standard stripping section. Only one profile of the CS 6 vapour CPM is

valid as the vapour stripping profile must pass through either the bottoms composition or composition in equilibrium with this stream. Any profiles from the vapour CPMs of CS 4 and CS 5 intersecting on this solution are valid.

COMPOSITION MATCHING CRITERION 3: Both the liquid and vapour profiles of CS 2 and CS 4 must intersect. There is no composition change in either the vapour or liquid material from the bottom of CS 2 to the top of CS 4. This is because material is removed from, not added to, the liquid or vapour streams. Valid profiles must intersect at the side-draw composition.

COMPOSITION MATCHING CRITERION 4: The liquid or vapour profiles of CS 3 and CS 5 must intersect. If the feed material is vapour then we assume that it mixes perfectly and instantly with the vapour stream from CS 5 to produce the bottom vapour stream of CS 3. It is assumed that there is no mass transfer to the liquid stream leaving CS 3 and that this composition is the same as the top liquid composition in CS 5. Similarly if the feed is liquid, it is assumed that the vapour composition at the top of CS 5 is the same as that at the bottom of CS 3. It is important to note that if the composition at which the matching criterion, of one phase is satisfied, is identified on CPM  $k$  and CPM  $k+1$  and the difference points used to generate the two CPMs satisfy the material balance, the compositions of associated passing streams will satisfy the material balance required of that phase. This means that if we superimpose CPMs to determine where the matching criteria are satisfied, we need not worry about satisfying the material balance and finding associated compositions of the other phase. These will automatically be satisfied and can easily be calculated, if required, using the definitions of the difference point and net flow of the particular CS.

The numerous matching criteria discussed above are depicted in Figure 3.13.

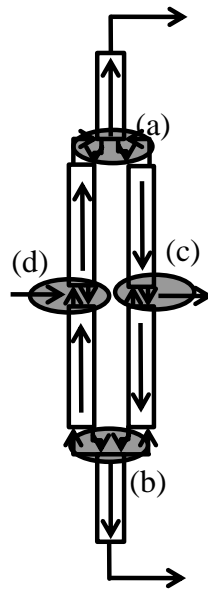


Figure 3.13: Various compositions matching criterion. (a) Matching criteria 1 (b) Matching criteria 2. (c) Matching criteria 3. (d) Matching criteria 4

### 3.8 Feasible Topology

It would be very useful during the design process to be able to determine ranges of feasible column parameters (such as reflux ratio etc) without generating every possible solution in doing so. Unfortunately, however, there is no analytical way of tracking arbitrary solutions within each CPM and determining whether or not they produce feasible Petlyuk column solutions, unless an explicit function exists for these profiles.

In this chapter, to bypass this problem, we will look at the case where there is a sharp-split on all the products. Restricting ourselves to this class of solution enables us to determine the exact position of all viable column section profiles for any set of parameters. We will now investigate why this is possible by analysing the effects of each sharp product specification.

Firstly, however, we must clarify the definition of individual sharp product specifications.

- A *sharp distillate product specification* is one in which the light and intermediate components appear in finite quantities, but the heavy component appears in infinitesimal quantities.
- A *sharp bottoms product specification* is one in which the heavy and intermediate components appear in finite quantities, but the light component appears in infinitesimal quantities.
- The side-draw product can be sharp in terms of the light component (infinitesimal light component material but finite intermediate and heavy component material), sharp in terms of the heavy component (infinitesimal heavy component material but finite intermediate and light component material) or sharp in terms of the light and heavy components (effectively pure intermediate component material). For this work, a *sharp side-draw product specification* will be taken as one which is sharp in terms of both the light and heavy components.

With clarified definitions we are now in a position to analyse the topological effects of the sharp product specifications.

### 3.8.1 Implications of Sharp Distillate Product Specifications

A sharp distillate product specification means that the distillate product ( $X_D$ ) is effectively confined to the light-intermediate axis ( $x_1$  axis).

But  $X_D = \frac{V_1 Y_1^T - L_1 X_1^T}{D} = X_{\Delta I}$  i.e. the difference point of CS 1 ( $X_{\Delta I}$ ) is equal to

the distillate composition. *This means that  $X_{\Delta I}$  is a real composition in the column and is confined to the light-intermediate axis.*

If we analyse the rectifying profile as well as the movement of the CS 1 transformed triangle (TT<sub>3</sub>) - which is equivalent to analysing the movement of the stationary points - while varying  $X_{\Delta I}$  (at constant  $R_{\Delta I}$ ), we notice that as the

difference point is moved closer to the light-intermediate axis, the profile and one of the  $TT_3$  boundaries approach the axis as well. The  $TT_3$  boundary, defined between the unstable node and the saddle point, approaches the axis from negative heavy component space, while the rectifying composition profile approaches from positive heavy component space. When the difference point is effectively on the axis, the afore-mentioned  $TT_3$  boundary lies here too and *the rectifying profile runs along the boundaries of this triangle*. Figure 3.14a-c illustrates this phenomenon.

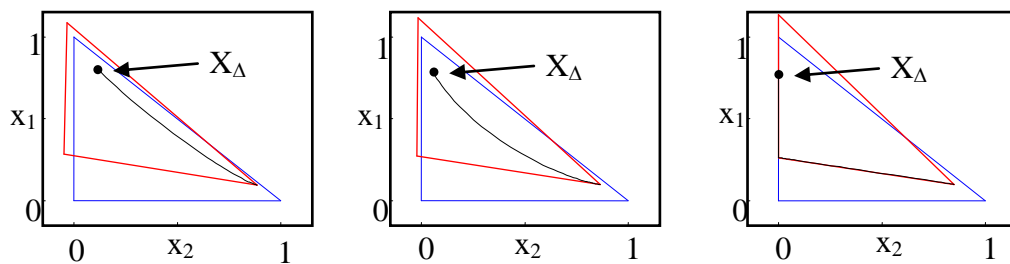


**Figure 3.14 a-c: Rectifying profiles for difference points at varying distances from the light-intermediate axis. Implications of Sharp Bottoms Product Specifications**

A sharp bottoms product specification means that the bottoms product ( $X_B$ ) is effectively confined to the heavy-intermediate axis ( $x_2$  axis).

$$\text{But } X_B = \frac{V_6 Y_6^B - L_6 X_6^B}{-B} = \frac{V_6 Y_6^B - L_6 X_6^B}{\Delta_6} = X_{\Delta_6} \quad \text{i.e. the difference point of CS 6}$$

( $X_{\Delta_6}$ ) is equal to the bottoms composition. *This means that  $X_{\Delta_6}$  is a real composition in the column and is confined to the intermediate-heavy axis.*

If we analyse the stripping profile and CS 6  $TT_3$ , in the same way as we did for the sharp distillate specification, we notice that as we move  $X_{\Delta_6}$  towards the intermediate-heavy axis the stripping profile and one of the  $TT_3$  boundaries move towards each other and the axis as well. When  $X_{\Delta_6}$  lies effectively on the axis, the  $TT_3$  boundary defined between the saddle-point and stable node lies here too and *the stripping profile runs along the boundaries of this triangle*. Figure 3.15a-c illustrates this phenomenon.

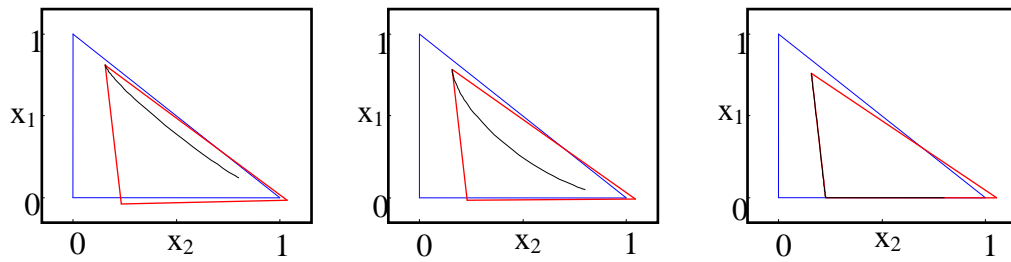


**Figure 3.15: Stripping profiles for difference points at varying distances from the intermediate-heavy axis.**

### 3.8.2 Implications of Sharp Side-Draw Product Specifications

Analysis of the CS 2 and 4  $TT_3$ s is not possible until we have discussed the feasible placements of  $X_{\Delta 2}$  and  $X_{\Delta 4}$ . For now, however, it will suffice to state that because the CS 2 profile has to satisfy matching criteria 1 and 3 it will *run effectively on the light-intermediate axis and also along the boundaries of the CS 2  $TT_3$* . Similarly, the CS 4 profile has to satisfy composition matching criteria 2 and 3 and will *run effectively on the intermediate-heavy axis and the CS 4  $TT_3$  boundaries*.

### 3.8.3 Implications of Sharp Product Specifications for CS 3 and CS 5

Because the product placement forces composition matching criteria 1 and 2 to be satisfied close to the axes, the CS 3 and CS 5 profiles, respectively, will be forced to satisfy these compositions too. We will see later that the difference points of these sections must also lie on the axes and these profiles therefore run along the boundaries of their respective  $TT_3$ s.

### 3.8.4 Summary of the Topological Effects of Sharp-Split Specifications

The topological effect of a sharp product specification is, clearly, to force the composition profile of the CS, from which the product is drawn, to operate on the boundary of its associated  $TT_3$ . By specifying all products as sharp we force, not

only the composition profiles of these product CSs but *all the configuration composition profiles to operate on their associated  $TT_3$ s*.

This means we need only produce the  $TT_3$ s, instead of the entire CPM, for any set of parameters, to immediately determine whether or not all the column section solutions will satisfy the Petlyuk matching criteria and therefore produce a feasible column design. Instead of focusing on the intersection of many individual solutions, we can simply focus on the overlap of the  $TT_3$ s concerned. We need, in fact, only analyse the liquid  $TT_3$ . It is a product of the vapour-liquid equilibrium that if a  $TT_3$  for one phase overlaps, the other will overlap also (see Appendix A for details).

### 3.9 General form of the Petlyuk Composition Profiles

If the development of a design tool is to be successful, we need a qualitative understanding of the form Petlyuk composition profiles would take for ideal systems. We can look at each of the six column sections separately and postulate what an efficient well designed profile would look like.

CS 1 is a rectifying section. Profiles for this section will run from the distillate composition, along the light-intermediate axis, getting rapidly richer in the intermediate component and slowly richer in the heavy component. We know that these profiles run along the boundaries of their  $TT_3$ s (for sharp-splits) and should therefore run through the saddle point composition. At the saddle point, they will “tear” away from the light-intermediate axis ( $x_1$  axis) and quickly gain in the heavy component until the composition profile pinches within the MBT. We know that the profiles must pinch within the MBT by analysing the, positive reflux, pinch point curves for qualitatively different  $X_{\Delta k}$  placement produced by Tapp et al. (2004). The stable nodes of CPMs, produced for difference points within difference point region 1, always lie within the MBT (for ideal systems). The probable form of the liquid and vapour solutions can be seen in Figure 3.16a

below. Using the profiles as a basis, the probable form of the  $TT_{3s}$  will be similar to that seen in Figure 3.16b.

Solutions for the stripping section (CS 6) will behave in the same way with respect to the intermediate composition moving away from the product (in this case the bottoms composition) and will “tear” away from the intermediate-heavy axis ( $x_2$  axis) at a saddle point but now becoming rapidly richer in the light component. The stripping profiles will pinch at unstable nodes within the MBT. This is ascertained, again, by consulting the pinch point curves (for negative reflux ratios) produced by Tapp et al (2004). The stripping profiles can be seen in Figure 3.17a. Again using the profiles as a basis the probable form of the  $TT_{3s}$  will be similar to that of Figure 3.17b.

The main purpose of CS 2 is to transport the intermediate component from the top half of the column to the side-draw. The amount of heavy component transported here should be minimal. The composition trajectories for CS 2 must, therefore, run (along the light-intermediate axis) from the side-draw composition (high purity intermediate composition) gaining in the light component until they reach the rectifying trajectories and satisfy composition matching criterion 1. It is possible for these profiles to pinch at the top of the CS. If this were to happen, the pinch point would be an unstable node. The probable form of the trajectories would be similar to those seen in Figure 3.18a. The  $TT_{3s}$  are likely of the form seen in 6.18b.

CS 4 transports the intermediate from the bottom half of the column to the side-draw. Very little light component material should be transported in this section. The profiles for CS 4 should run from the side-draw, along the intermediate-heavy axis, to meet up with the stripping section profiles and satisfy composition matching criterion 2. It is feasible for these profiles to pinch at the bottom of the CS. In this case the pinch point would be a stable node. The resulting profiles would look like those in Figure 3.19 a-b the corresponding  $TT_{3s}$  would likely be of the form seen in Figure 3.19b.

CS 3 is required to transport both light-component material to CS 1 and intermediate material to CS 2. As these sections must process as little heavy-component material as possible (for product purity purposes) this material must be minimised in CS 3 as well. Potential profiles for CS 3 will run from the point where CS 2's profile meets the rectifying profile, along the light-intermediate axis, towards a saddle point and then tear away from the boundary towards the feed composition, where either the liquid or vapour profile will intersect the CS 5 profile as shown in Figure 3.20a and Figure 3.20b.

CS 5 must transport heavy component material to CS 6 and intermediate component material to CS 4 with minimal light material. Potential profiles will run from the point where CS 4's profile meets the stripping profile, along the intermediate-heavy axis, towards a saddle point and then tear away from the boundary towards the feed composition, where they meet up with the CS 3 profiles as shown in Figure 3.21a and Figure 3.21b.

The complete set of composition profiles and corresponding  $TT_3$ s for the Petlyuk column can be seen in Figure 3.22 a-b, respectively. Figure 3.22b, clearly shows how all composition matching criteria (required for a feasible design) are satisfied by the overlap of the liquid  $TT_3$ s concerned.

With an understanding of the probable form of Petlyuk solutions we are now in a position to test column parameters for potential feasibility. Values for these parameters which result in dramatically different topological phenomena, for each CS, from that discussed above and do not result in the satisfaction of the composition matching criteria required can be discarded.

**Note:** Unless otherwise stated, within composition diagrams a solid line will denote the liquid phase while a dotted line will denote vapour phase (except lines CLL1 and CLL2 – defined later). Red lines (within composition diagrams) are associated with CS 1, pink with CS 2, green with CS 3, black with CS 4, blue with

CS 5 and yellow with CS 6. The light component composition ( $x_1$ ) will always be represented on the y-axis while the heavy component composition ( $x_2$ ) will be represented on the x-axis. The MBT will always be represented by a blue triangle.

**Table 3.2: Profile and  $TT_3$  Legend of Composition Diagrams**

	Liquid composition CS 1		Vapour composition CS 1
	Liquid composition CS 2		Vapour composition CS 2
	Liquid composition CS 3		Vapour composition CS 3
	Liquid composition CS 4		Vapour composition CS 4
	Liquid composition CS 5		Vapour composition CS 5
	Liquid composition CS 6		Vapour composition CS 6

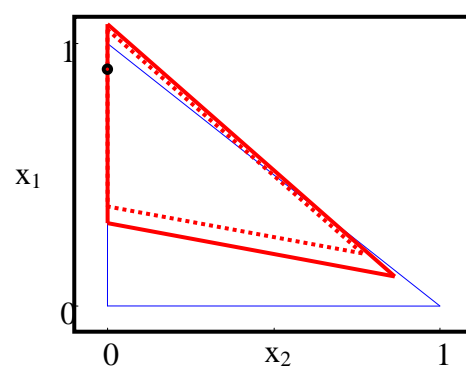
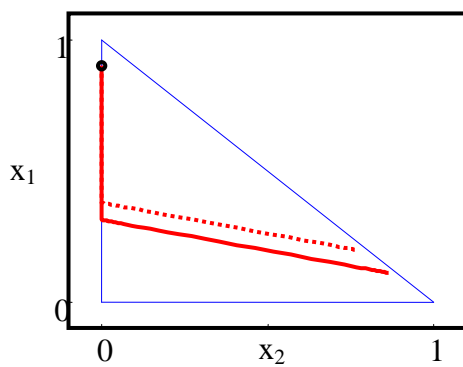


**Figure 3.16a: Rectifying composition profiles**      **Figure 3.16b: Rectifying section  $TT_{3s}$  profiles**

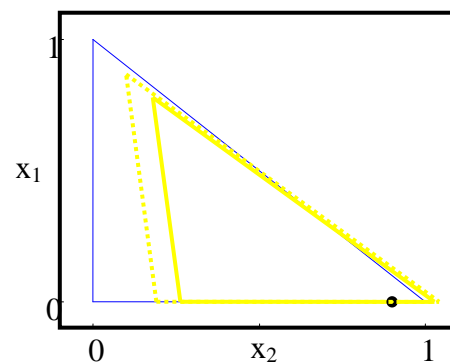
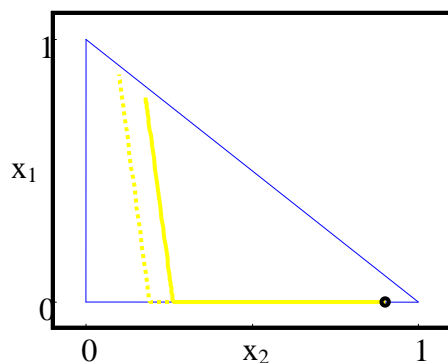


**Figure 3.17a: Stripping composition profiles**      **Figure 3.17b: Stripping section  $TT_{3s}$  profiles**

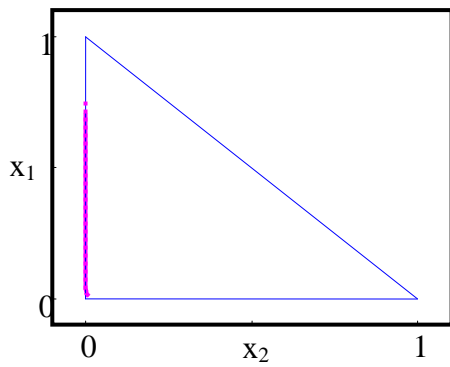


Figure 3.18a: CS 2 composition profiles

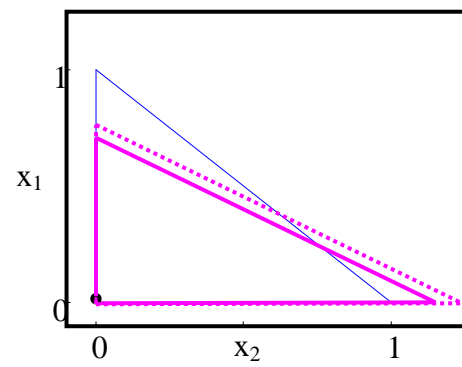


Figure 3.18b: CS 2  $TT_3s$

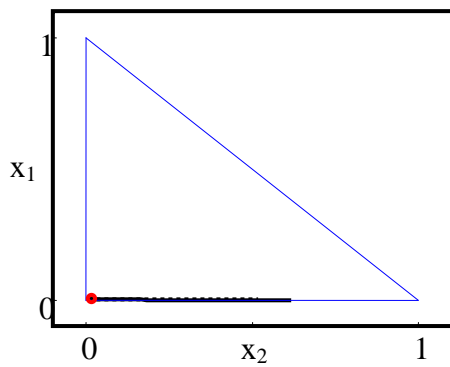


Figure 3.19a: CS 4 composition profiles

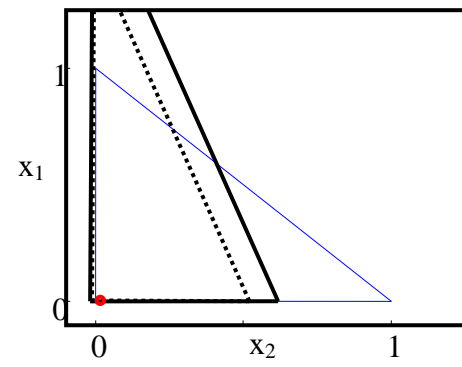


Figure 3.19b: CS 4  $TT_3s$

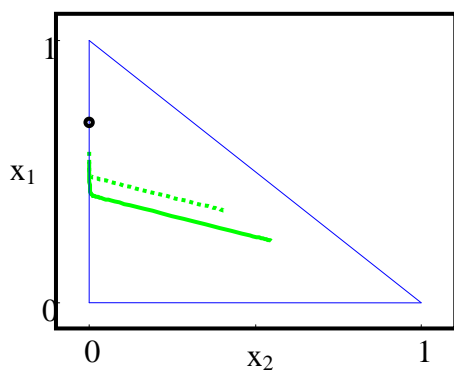


Figure 3.20: CS 3 composition profiles

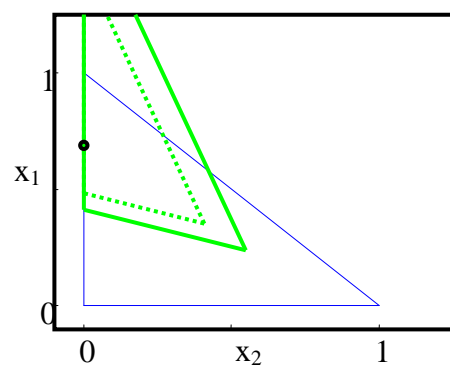


Figure 3.20b: CS 3  $TT_3s$

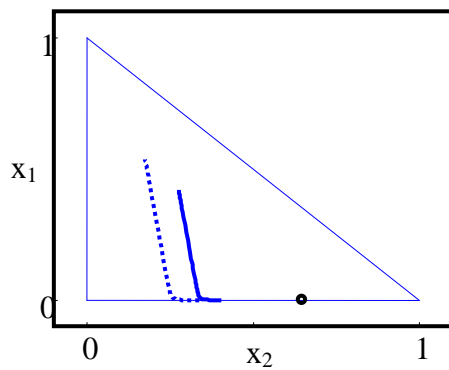


Figure 3.21a: CS 5 composition profiles

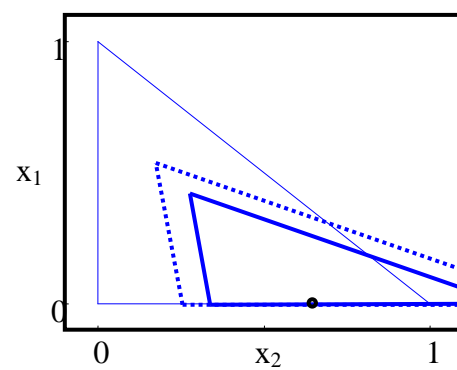
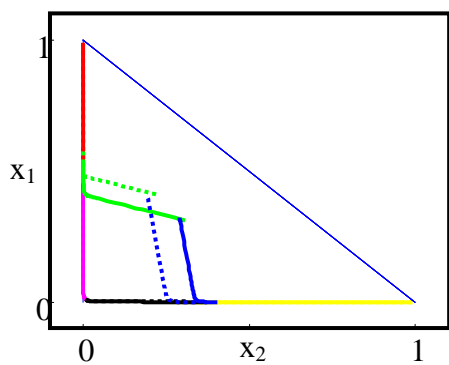
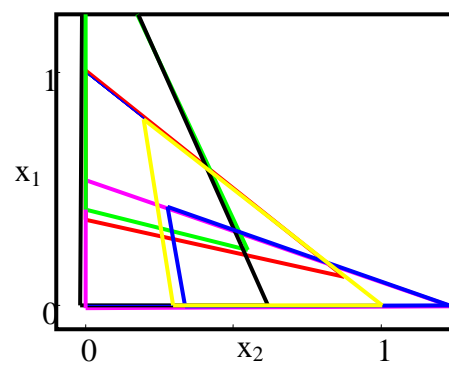
Figure 3.21b: CS 5 TT<sub>3s</sub>

Figure 3.22a: Petlyuk composition profiles

Figure 3.22b: All six column section TT<sub>3s</sub>

## 3.10 Degrees of Freedom and Variable Selection

### 3.10.1 Degrees of Freedom

The Petlyuk column, due to the thermal coupling of the main column with a pre-fractionator, is a fairly complicated column to design. This complication arises as a result of the multiple degrees of freedom (DOF) introduced to the design by the coupling. In distillation systems, for simplicity, we can divide these DOF into composition variables, overall material balance variables and internal material balance variables. With simple distillation columns, for a given feed, there are

only three degrees of freedom - one of the product composition variables may be specified (i.e.  $X_D$  or  $X_B$ ), one overall material balance variable may be specified (i.e. distillate or bottoms rate) and one of the internal material balance variables may be specified (i.e. reflux ratio or boil-up ratio).

For the Petlyuk column, however, for a given feed there are two product compositional DOF, two overall material balance DOF, one internal compositional DOF and three internal material balance DOF (two in the coupled sections and one in either the rectifying or stripping sections). In total eight DOF. This, clearly, adds many levels of complexity to the design process.

It is important to note that the total required stages, feed stage and side-draw stage are not considered as degrees of freedom when designing using the CPM technique. These variables result as a solution from the process once all other DOF have been specified. They can be determined by tracking variable  $n$  in the difference point equation (Equation 6.1) for any particular Petlyuk solution.

Some of the possible design variables include:

$R_{\Delta k}$	CS k reflux ratio
$X_{\Delta k}$	CS k difference point
$D$	Distillate flow rate
$B$	Bottoms flow rate
$S$	Side-draw flow rate
$L_k$	CS k internal liquid flow rate
$V_k$	CS k internal vapour flow rate
$\Phi_V$	Vapour split ratio ( $V_2/V_1$ )
$\Phi_L$	Liquid split ratio ( $L_2/L_1$ )
$\Phi_V'$	Vapour split ratio ( $V_4/V_6$ )
$\Phi_L'$	Liquid split ratio ( $L_4/L_6$ )

Of the multiple possible design variables only eight may be specified. We will now discuss the selection of these variables and their effects on the design.

### 3.10.2 Variable Selection

It is important in this geometric based design process to work with, where possible, variables whose effects on the entire configuration are understood. Variables such as the reflux ratio, for instance, are useful when analysing a single column section, as we can intuitively comprehend its effects on the composition profile. However, the influence of changes of reflux ratio in one column section on the composition profile of another column section may be more difficult to understand. Generally, the interaction of variables becomes more and more complex as they are coupled by the connection of column sections. For this reason the design approach we will take, although fairly intuitive, will be used in an attempt to “uncouple” the rectifying and stripping sections from the remainder of the column by specifying either of these sets of variables independently.

As mentioned previously we shall be dealing with sharp splits on all products. The distillate will be chosen to contain almost no heavy material, the bottoms product will be chosen to contain effectively no light material and the flow rates of these product streams will be chosen such that the side-draw will, effectively, be pure intermediate product. Specifying these variables ( $\Delta_1$ ,  $X_{\Delta 1}$ ,  $\Delta_6$ ,  $X_{\Delta 6}$ ) satisfies four DOF; two compositional and two overall material balance DOF. If we now specify an internal variable (e.g. reflux) of either the rectifying (CS 1) or stripping sections (CS 6), both sections will be completely satisfied and no freedom will exist for the selection of other variables in either. We will specify the reflux of CS 1 ( $R_{\Delta 1}$ ), as opposed to that of CS 6, although this is completely arbitrary. Once  $R_{\Delta 1}$  is specified the reflux of CS 6 can be determined by material balance. Five DOF have now been specified. The conditions within the coupled sections (CS 2-5) are dependent on the conditions of the rectifying and stripping sections and the remaining three DOF.

Of the three remaining DOF, one is a compositional DOF and two are internal material balance DOF. As CS 1 and CS 6 are completely specified, these

remaining variables must be specified in CS 2 to CS 5. The choice of compositional variable will be discussed in greater detail later, but for now it will suffice to state that we will specify the difference point of CS 2 ( $X_{\Delta 2}$ ). The remaining variables, both internal material balance variables, are the most difficult to choose. As mentioned above working with reflux, although convenient for single column sections, becomes less useful when multiple sections are connected. If we decided to work with the reflux ratio of one of the coupled column sections it would not be obvious what effect changes to this variable would have on the other sections. Another issue would be the choice of column section to work with. Although this may be more obvious for other variables, it does present an issue here.

The variables we will choose to work with are  $\Phi_V$  and  $\Phi_L$ , which are defined, respectively, as the ratio of vapour and liquid in CS 2 to that in CS 1. We will refer to these variables as split ratios although  $\Phi_V$  is, in fact, a mixing ratio. Similar variables can be defined in terms of vapour and liquid flow rates in CS 6. The decision to work with the CS 1 definition is simply a matter of convenience. The use of  $\Phi_V$  and  $\Phi_L$  will lead to a very useful representation of coupled column section variables as well as feasible column solutions.

### 3.11 Difference Point Placement for the Petlyuk Column

With all the external DOF specified we must now turn our attention to the remaining internal DOF. We are required to specify one internal composition variable. The available composition variables are the difference points ( $X_{\Delta k}$ ) of the coupled column sections, the placement of which are critical to the feasibility of the design. The behaviour of the  $TT_3$  is dependent on two variables, namely the difference point ( $X_{\Delta}$ ) and the reflux ratio ( $R_{\Delta}$ ). The form of the CPM changes as the placement of the difference point changes. It is crucial that the difference point for a column section is placed correctly so that the resulting CPM satisfies all required feasible column criteria. It is, however, impossible to have all difference points in the Petlyuk configuration placed optimally as only one DOF remains but

we can place one point such that it facilitates the composition matching of the others.

In making the choice of difference point, it is necessary to identify sections for which the required design specifications are more difficult to achieve with arbitrary parameter sets. If we consider that CS 2 and CS 4 are required to achieve a product specification, it is logical that the difference point of either of these two sections is chosen such that the intermediate product composition can be achieved. We will arbitrarily choose to place the difference point of CS 2 (although placing  $X_{\Delta 4}$  would be just as effective).

To determine the optimal placement of  $X_{\Delta 2}$  the requirements of this column section must be understood. Firstly, CS 2 is required to achieve a particular composition, specifically the side-draw composition; therefore the CPM for CS 2 must provide trajectories which intersect this composition point. Secondly, the profile is required to intersect the rectifying profile; therefore it should run from the side-draw composition, close to the light-intermediate axis and cross the rectifying profile.

From a material transport perspective the main purpose of CS 2 is the transport of the intermediate component to the side-draw. If the side-draw composition is required to be very “pure”, CS 2 should not transport large quantities of light or heavy component material i.e. the pseudo composition of the net flow ( $X_{\Delta 2}$ ) should have a high intermediate component percentage. This does not exclude difference points with non-zero light and heavy components, however. High purities are possible in a column section even if the net flow does involve large “impurity” flows because a single phase can be sampled. This can be explained if we consider that at a difference point the vapour and liquid compositions are equal (this is shown in Equation 3.6), but as compositions away from the difference point are sampled a “gap” opens up between the vapour and liquid compositions (as shown in Equation 3.7). Difference points associated with large impurities

can, therefore, generate trajectories of one phase achieving high purities while the other does not. An illustration of this is seen in Figure 3.23 below.

The difference point is defined as :

$$X_{\Delta k} = (1 + R_{\Delta k}) Y_k^T - R_{\Delta k} X_k^T$$

Rearranging

$$Y_k^T = \frac{X_{\Delta k} + R_{\Delta k} X_k^T}{(1 + R_{\Delta k})} \quad (3.5)$$

$$\text{If } X_k^T = X_{\Delta k} \Rightarrow Y_k^T = \frac{X_{\Delta k} + R_{\Delta k} X_{\Delta k}}{(1 + R_{\Delta k})} = X_{\Delta k} \quad (3.6)$$

$$\text{If } X_{k-3}^T \approx 1 \text{ but } X_{\Delta k-3} < 1 \Rightarrow Y_{k-3}^T = \frac{X_{\Delta k} + R_{\Delta k} X_{k-3}^T}{(1 + R_{\Delta k})} \neq X_{k-3}^T \neq X_{\Delta k-3} \quad (3.7)$$

Minimising difference point impurities should improve overall performance though, by the simple logic that if there is a smaller net flow of “impurity” material through the section, there is less to be separated from the intermediate component. If we consider this argument only, the difference point for CS 2 should be placed near the intersection of the  $x_1$  and  $x_2$  axes (pure intermediate).

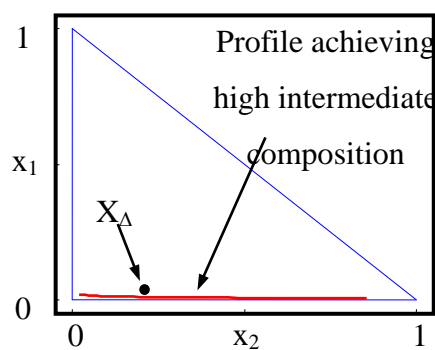


**Figure 3.23: Low intermediate purity difference point with liquid profile sampling high intermediate purity**

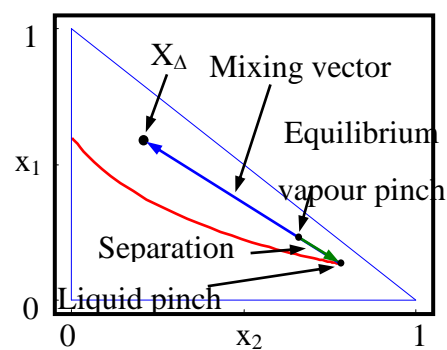


**Figure 3.24: Mixing and separation vector collinearity**

It is possible to use geometrical ideas to confirm our intuitive net flow arguments above. Tapp et al (2004) illustrated that a qualitative understanding of the CPM could be achieved by studying the pinch point curves resulting from difference points placed arbitrarily in each of the 7 qualitatively different regions of the composition space that were identified (see Figure 3.2). By noting where the nodes of the system move, we can identify which (difference point) regions of the space would result in favourable trajectories at the side-draw. As mentioned above the required profile in CS 2 needs to intersect the rectifying profile. The rectifying profile will run close to the light-intermediate axis (see Figure 3.16a), so any profile running from a high purity side-draw composition to the rectifying profile will do likewise (see Figure 3.18a-b). If the column section operates at negative reflux the profile will reach an unstable node stationary point close to the light-intermediate axis of the MBT (see Figure 3.18b). If it is operated at positive reflux, the profile will terminate outside the MBT but also close to the axis (see Figure 3.25a and b).  $X_{\Delta 2}$  must produce a pinch point curve that runs close to this boundary. We can determine areas of possible  $X_{\Delta 2}$  placement geometrically by using the co-linearity condition of the mixing and separation vectors at the pinch point. Pinch points only occur in composition space when the mixing vector ( $X_{\Delta} - X$ ) is collinear with the separation vector ( $X - Y^*(X)$ ) (see Figure 3.24).

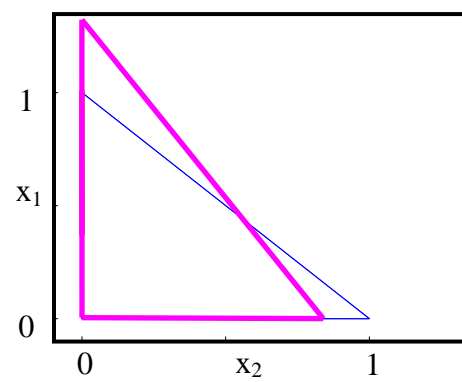
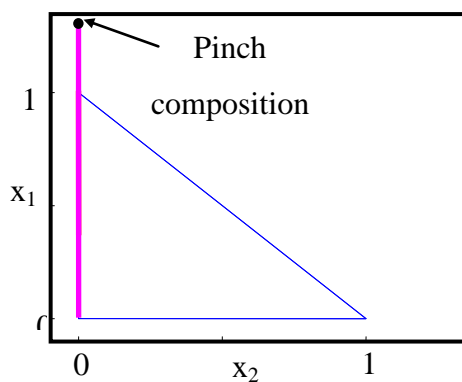


**Figure 3.25a: CS 2 profile pinching outside MBT for  $R_{A2} > 0$**       **Figure 3.25b:  $TT_3$  for CS 2 for  $R_{A2} > 0$**

All that is required is to choose (desirable) potential pinch points on the residue curve map and extend lines along the direction of the tangent of individual residue curves at these points (separation vectors are tangential to the residue curve at their liquid composition). If we extend straight lines, from points close to the light-intermediate axis, along the residue curve tangents we can find lines of possible  $X_{\Delta 2}$  values. illustrates lines of  $X_{\Delta 2}$  values that satisfy three arbitrarily chosen pinch points. Pinch points chosen close to the axis produce lines of  $X_{\Delta}$  close to the axis, therefore if the  $X_{\Delta 2}$  is placed close to the light-intermediate axis the pinch point curve will run very close to this boundary and consequently so will potential profiles. This will satisfy the side-draw composition requirement as well as the rectifying profile intersection.

As was illustrated previously, difference points obey linear mixing rules. The CS 2 and CS 4 difference points must lie on a straight line running through the side-draw composition. If the placement of  $X_{\Delta 2}$  is to be finalised we must determine the implications of this placement on  $X_{\Delta 4}$ . If  $X_{\Delta 2}$  is placed at an arbitrary position along the light-intermediate axis and  $X_S$  is placed very close to the pure intermediate composition, linear mixing rules will force  $X_{\Delta 4}$  to lie along the light-intermediate axis as well. However, if  $X_{\Delta 4}$  was chosen independently we would, by the same logic applied to the placement of  $X_{\Delta 2}$  position  $X_{\Delta 4}$  along the intermediate-heavy axis (CS 4 profiles must run from the side-draw composition along this axis to the stripping profile). The only possible way to satisfy the requirements for both difference points, for sharp-splits on the side-draw, is if  $X_{\Delta 2}$  and  $X_{\Delta 4}$  are placed very close to both axes i.e. close to the pure intermediate component. Because the side-draw is placed very close to the pure intermediate component all three points must in fact exist at the same composition. This result agrees with the intuitive net flow arguments made above. Suitable difference point placements for each of the column sections, for each net flow pattern, are seen in Figure 3.27a-e. The relative positioning of the difference points is dependent on the net flow in each column section and subsequently the final positioning of  $X_{\Delta 3}$  and  $X_{\Delta 5}$  is a function of the remaining internal material balance variables which will be discussed next. Because difference points obey linear mixing rules,  $X_{\Delta 3}$  is,

however, constrained to the material balance line though the distillate composition ( $X_{\Delta 1}$ ) and  $X_{\Delta 2}$ , while  $X_{\Delta 5}$  is constrained to the material balance line through the bottoms composition ( $X_{\Delta 6}$ ) and  $X_{\Delta 4}$ .

It fascinating to note, that for net flow patterns 1, 2, 4 and 5  $X_{\Delta 3}$  or  $X_{\Delta 5}$  must operate outside of the MBT. This forces the net flow of some of the components within CS 3 and CS 5 to flow in opposite directions. The fact that these difference points operate outside the MBT also introduces the potential for interesting topology to be shifted into the MBT for these column sections.

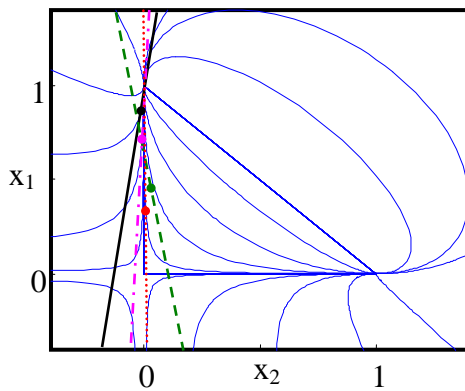


Figure 3.26: Residue curve tangent lines at potential pinch points

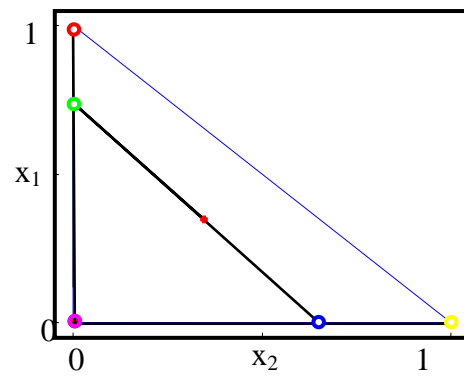


Figure 3.27a: Material balance – net flow pattern 3

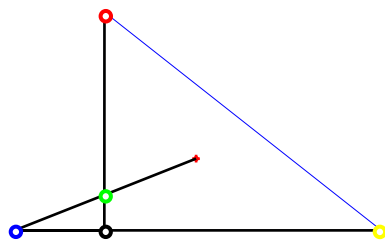


Figure 3.27b: Material balance – net flow pattern 1

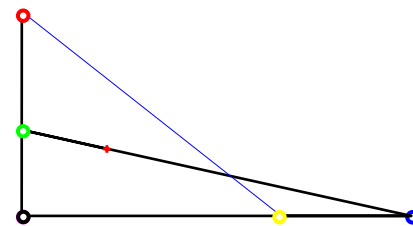


Figure 3.27c: Material balance – net flow pattern 2

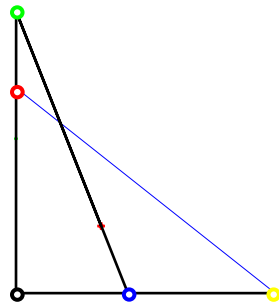


Figure 3.27d: Material balance – net flow pattern 4

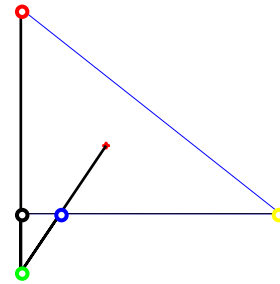


Figure 3.27e: Material balance – net flow pattern 5

Table 3.3: Legend Figure 3.27a-e	
●	$X_{A1}$
●	$X_{A2}$
●	$X_{A3}$
●	$X_{A4}$
●	$X_{A5}$
●	$X_{A6}$

### 3.12 Variable Representation in $\Phi_V$ vs. $\Phi_L$ Space

The split ratios were introduced in our discussion of variable selection above and are the internal material balance variables chosen for the design process. Our choice of other variables was largely based on our intuitive understanding of their effects. Because we do not have this advantage with our choice of  $\Phi_V$  and  $\Phi_L$  we shall represent coupled-column-section variables we do understand in split ratio space. We shall also define boundaries in this space that represent physical limits on the column section internal flows. These representations will help effect an intelligent selection of the liquid and vapour splits.

### 3.12.1 Net Flow Regimes in $\Phi_V$ vs. $\Phi_L$ Space

The various net flow patterns can be controlled or achieved by manipulating the split ratios. The regimes can readily be visualised, in  $\Phi_V$  vs.  $\Phi_L$  space, by producing lines of zero net flow for the coupled column sections (see Figure 3.28). The dependence of the net flow, for each of the coupled column sections, on the vapour and liquid split ratios from CS 1 can be seen in the Equation 6.8-6.11 below. The split ratios for both the liquid and vapour are defined, as mentioned previously, in terms of the respective flows from CS 1. As a consequence, all the equations below are functions of the reflux ratio in CS 1. The CS 4 and CS 5 zero net flow lines are both functions of the distillate flow rate as well as the side-draw flow rate and feed flow rate respectively.

$$\Delta_2 = \Phi_V \Delta_1 (R_{\Delta 1} + 1) - \Phi_L \Delta_1 R_{\Delta 1} = 0 \Rightarrow \Phi_L = \frac{(R_{\Delta 1} + 1)}{R_{\Delta 1}} \Phi_V \quad (3.8)$$

$$\Delta_3 = (1 - \Phi_V) \Delta_1 (R_{\Delta 1} + 1) - (1 - \Phi_L) \Delta_1 R_{\Delta 1} = 0 \Rightarrow \Phi_L = \frac{(R_{\Delta 1} + 1)}{R_{\Delta 1}} \Phi_V - \frac{1}{R_{\Delta 1}} \quad (3.9)$$

$$\Delta_4 = \Phi_V (\Delta_1 R_{\Delta 1} + \Delta_1) - \Phi_L \Delta_1 R_{\Delta 1} + S = 0 \Rightarrow \Phi_L = \frac{(R_{\Delta 1} + 1)}{R_{\Delta 1}} \Phi_V + \frac{S/\Delta_1}{R_{\Delta 1}} \quad (3.10)$$

$$\begin{aligned} \Delta_5 = (1 - \Phi_V) (\Delta_1 R_{\Delta 1} + \Delta_1) - (1 - \Phi_L) \Delta_1 R_{\Delta 1} - F = 0 \\ \Rightarrow \Phi_L = \left( \frac{R_{\Delta 1} + 1}{R_{\Delta 1}} \right) \Phi_V + \left( \frac{F/\Delta_1 - 1}{R_{\Delta 1}} \right) \end{aligned} \quad (3.11)$$

By dividing up the  $\Phi_V$  vs.  $\Phi_L$  space with lines of zero net flow for each of the coupled sections, we can identify regions within the space of different overall net flow pattern. These are labelled 1 to 5 in Figure 3.28. Above the  $\Delta_5 = 0$  line (blue) values of  $\Phi_V$  and  $\Phi_L$  produce values of  $\Delta_5 > 0$ , while below the line values of  $\Delta_5 < 0$  are produced. Similarly for the  $\Delta_3 = 0$  line (green), above the line are values of  $\Delta_3 > 0$ , while below are values of  $\Delta_3 < 0$ . The inverse is true for lines  $\Delta_2 = 0$  (pink) and  $\Delta_4 = 0$  (black). Above these lines negative values are produced, while below positive values are produced.

Each of the regions between these lines and between the lines and the boundaries of the space produce a different net flow pattern in the coupled sections. These are the flow patterns illustrated in Figure 3.11a-e. This behaviour, described above, is summarised in Table 3.4 below.

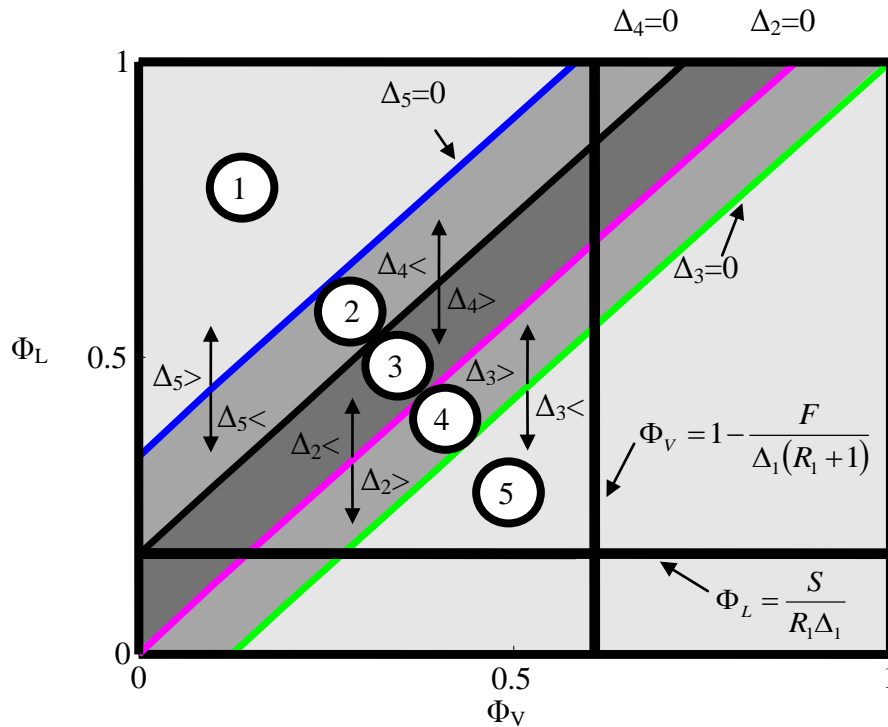


Figure 3.28: Net Flow Regimes in  $\Phi_V$  vs.  $\Phi_L$

Table 3.4: Summary of net flow regions illustrated in Figure 3.28

Region From Figure 3.28	$\Delta$ Direction CS2	$\Delta$ Direction CS3	$\Delta$ Direction CS4	$\Delta$ Direction CS5	Illustrated By
1	- ve	+ ve	- ve	+ ve	Figure 3.11a
2	- ve	+ ve	- ve	- ve	Figure 3.11b
3	- ve	+ ve	+ ve	- ve	Figure

					3.11c
4	+ ve	+ ve	+ ve	- ve	Figure 3.11d
5	+ ve	- ve	+ ve	- ve	Figure 3.11e

### 3.12.2 Physical Limits on $\Phi_V$ and $\Phi_L$

Because of the definition of the split ratios, there are values of both  $\Phi_V$  and  $\Phi_L$ , which cannot be produced. The vapour split ratio, at which the vapour flow in CS 3 is equal to the feed rate, represents an upper physical limit on the value of  $\Phi_V$  for a column with vapour feed. The exact value of this limit can be calculated using Equation 6.12.

$$\Phi_V = 1 - \frac{F}{\Delta_1(R_{\Delta 1} + 1)} \quad (3.12)$$

Material balances calculated with values of  $\Phi_V$  greater than this upper limit will produce negative vapour flow values in CS 5. Similarly, for a column with liquid side-draw, if the liquid split ratio is specified such that the value for the liquid flow in CS 2 is smaller than the side-draw rate, negative liquid flows in CS 4 will result in any material balance. The split ratio value at which the liquid flow in CS 2 is equal to the side-draw rate, therefore, represents a lower limit on the value of  $\Phi_L$ . This limiting value can be calculated with Equation 6.13.

$$\Phi_L = \frac{S}{R_{\Delta 1} \Delta_1} \quad (3.13)$$

Both these limits are illustrated in Figure 3.28.

### 3.12.3 Reflux Ratio in $\Phi_V$ vs. $\Phi_L$ Space

The reflux ratio of the coupled sections can also be conveniently represented in the  $\Phi_V$  vs.  $\Phi_L$  space. Because of the definitions of the split ratios, lines of constant reflux are straight. The equations for the constant reflux lines for each of the coupled column sections are seen below (Equations 3.14-3.19). These equations are also all functions of  $R_{\Delta 1}$ . The form of the  $R_{\Delta 4}$  and  $R_{\Delta 5}$  equations are dependent on the phase of the side-draw and feed material respectively.

$$R_{\Delta 2} = \frac{\Phi_L R_{\Delta 1}}{\Phi_V (R_{\Delta 1} + 1) - \Phi_L R_{\Delta 1}} \Rightarrow \Phi_L = \Phi_V \frac{R_{\Delta 2} (R_{\Delta 1} + 1)}{R_{\Delta 1} (R_{\Delta 2} + 1)} \quad (3.14)$$

$$R_{\Delta 3} = \frac{(1 - \Phi_L) R_{\Delta 1}}{(1 - \Phi_V) (R_{\Delta 1} + 1) - (1 - \Phi_L) R_{\Delta 1}} \Rightarrow \Phi_L = (\Phi_V - 1) \frac{R_{\Delta 3} (R_{\Delta 1} + 1)}{R_{\Delta 1} (R_{\Delta 3} + 1)} + 1 \quad (3.15)$$

$R_{\Delta 4}$  - Liquid side-draw

$$R_{\Delta 4} = \frac{\Phi_L R_{\Delta 1} - S/\Delta_1}{\Phi_V (R_{\Delta 1} + 1) - \Phi_L R_{\Delta 1} + S/\Delta_1} \Rightarrow \Phi_L = \Phi_V \frac{R_{\Delta 4} (R_{\Delta 1} + 1)}{R_{\Delta 1} (R_{\Delta 4} + 1)} + \frac{S}{\Delta_1 R_{\Delta 1}} \quad (3.16)$$

$R_{\Delta 4}$  - Vapour side-draw

$$R_{\Delta 4} = \frac{\Phi_L R_{\Delta 1}}{\Phi_V (R_{\Delta 1} + 1) - \Phi_L R_{\Delta 1} + S/\Delta_1} \Rightarrow \Phi_L = \Phi_V \frac{R_{\Delta 4} (R_{\Delta 1} + 1)}{R_{\Delta 1} (R_{\Delta 4} + 1)} + \frac{SR_{\Delta 4}}{\Delta_1 R_{\Delta 1} (R_{\Delta 4} + 1)} \quad (3.17)$$

$R_{\Delta 5}$  - Liquid Feed:

$$R_{\Delta 5} = \frac{(1 - \Phi_L) R_{\Delta 1} + F/\Delta_1}{(1 - \Phi_V) (R_{\Delta 1} + 1) - (1 - \Phi_L) R_{\Delta 1} - F/\Delta_1} \Rightarrow \Phi_L = (\Phi_V - 1) \frac{R_{\Delta 5} (R_{\Delta 1} + 1)}{R_{\Delta 1} (R_{\Delta 5} + 1)} + 1 + \frac{F}{\Delta_1 R_{\Delta 1}} \quad (3.18)$$

$R_{\Delta 5}$  - Vapour Feed:

$$R_{\Delta 5} = \frac{(1 - \Phi_L) R_{\Delta 1}}{(1 - \Phi_V) (R_{\Delta 1} + 1) - (1 - \Phi_L) R_{\Delta 1} - F/\Delta_1} \Rightarrow \Phi_L = (\Phi_V - 1) \frac{R_{\Delta 5} (R_{\Delta 1} + 1)}{R_{\Delta 1} (R_{\Delta 5} + 1)} + 1 + \frac{FR_{\Delta 5}}{\Delta_1 R_{\Delta 1} (R_{\Delta 5} + 1)} \quad (3.19)$$

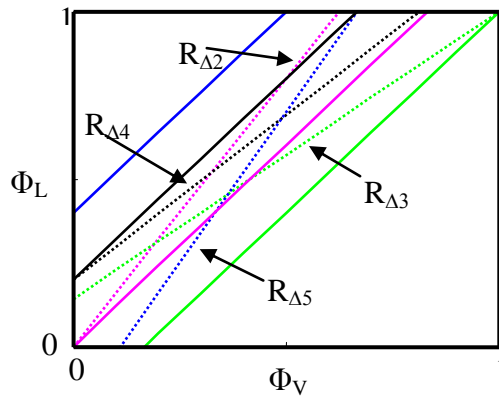


Figure 3.29: Constant reflux lines in  $\Phi_V$  vs.  $\Phi_L$

The sign of the reflux is dependent on the sign of the net flow, therefore the regions of the space corresponding to positive and negative net flow, for each of the sections, correspond to positive and negative reflux for those sections as well. Infinite reflux lines originate from the zero net flow lines (both positive and negative infinite reflux). The lines fan out, away from their respective zero net flow lines, as the absolute value of the reflux is reduced (see Figure 3.29). These representations enable us to intuitively determine the effects of a particular choice of  $\Phi_V$  and  $\Phi_L$  on the reflux of coupled sections.

### 3.12.4 Constant $X_{\Delta}$ in $\Phi_V$ vs. $\Phi_L$ Space

It is possible to find split ratio lines that result in constant  $X_{\Delta k-i}$  for the coupled-column-sections i.e. varying the split ratios along these lines does not shift the difference points. This can be useful if we wish to design a column that directs individual components within the coupled column sections in a specific way. We are confined to values for the variable difference points ( $X_{\Delta 3}$ ,  $X_{\Delta 5}$ ) along straight lines between the distillate and bottoms product compositions and  $X_{\Delta 2}$  (see Figure 3.27a-e above), but we can control exactly where along these lines a particular difference point lies. Below is an expression for one of these constant  $X_{\Delta}$  lines (Equation 6.20) – this equation has been generated for CS 3, but similar expressions can be derived for CS 5.

$$\Phi_L = \frac{(R_{\Delta 1} + 1)}{R_{\Delta 1}} \Phi_V + \frac{1}{R_{\Delta 1}} \left( \frac{X_{\Delta 3-i} - X_{\Delta 1-i}}{X_{\Delta 2-i} - X_{\Delta 3-i}} \right) \quad (3.20)$$

where  $X_{\Delta 3-i}$  is a control on component  $i$  for the difference point of CS3.

Again we notice that this line is straight. Its slope is of equal gradient to the zero net flow expressions generated above. Figure 3.30 below illustrates an example of a constant  $X_{\Delta}$  line at an  $X_{\Delta 3-1}$  value of 0.6 (light component). We can see that in this particular case this value is only satisfied in region 3 of split ratio space.

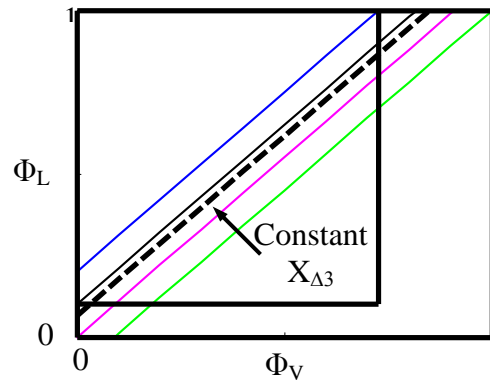


Figure 3.30: Constant  $X_{\Delta}$  lines in  $\Phi_V$  vs.  $\Phi_L$  space.

### 3.13 Constructing Split Ratio Regions of Feasibility

The design procedure thus far has involved the allocation of product composition and flow, the reflux ratio of CS 1 as well as the difference point of CS 2. Let us assume for now that our arbitrary choice of  $R_{\Delta 1}$  will result in a potentially feasible Petlyuk solution i.e. solutions exist for this reflux ratio. Following the discussion of the representation of net flow pattern regions and reflux ratios in  $\Phi_V$  vs.  $\Phi_L$  space we are now in a position to choose values for the vapour and liquid split ratios. We have a number of tools at our disposal. We can generate the net flow regions for our choice of  $R_{\Delta 1}$  and products. This immediately allows us to narrow

down our range of choice of values for  $\Phi_V$  and  $\Phi_L$  by deciding on our region of operation. Furthermore we now have an understanding of the effects of our choice on the reflux ratios of the coupled column sections.

Note: Transformed Triangle Boundary Definitions

For the following sections it will be convenient to label the boundaries of the  $TT_3$ s. A boundary defined between an unstable node and a saddle point of  $TT_3$  “ $k$ ” will be referred to as boundary “ $A_k$ ”. A boundary defined between a stable node and a saddle point of  $TT_3$  “ $k$ ” will be referred to as boundary “ $B_k$ ”. The final boundary defined between an unstable node and a stable node will be referred to as boundary “ $C_k$ ” of the  $TT_3$ . Figure 3.31 below illustrates these boundary definitions. Unless otherwise stated this will always refer to liquid  $TT_3$  boundaries. Vapour  $TT_3$  boundaries will be referred to as “vapour boundary  $A_k$ ”, etc.

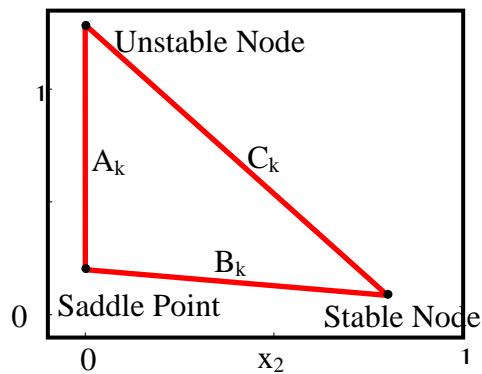


Figure 3.31: Transformed triangle boundary definitions

### 3.13.1 Coupled Column Section Minimum Reflux and binary CPM-E technique

Let us assume that we have allocated all variables including  $\Phi_V$  and  $\Phi_L$  and that the resulting solutions are the superimposed  $TT_3$ s of Figure 3.22b. For this solution we can see that all the required matching criteria are satisfied.

TT<sub>3</sub>s of CS 1, CS 2 and CS 3 overlap.

TT<sub>3</sub>s of CS 2 and CS 4 overlap.

TT<sub>3</sub>s of CS 3 and CS 5 overlap.

TT<sub>3</sub>s of CS 4, CS 5 and CS 6 overlap.

The reflux ratios of CS 1 and CS 6 are specified parameters and as such their TT<sub>3</sub>s are fixed. The TT<sub>3</sub>s of CS 2 and CS 4 produce a substantial overlap with these, so it is clear that their reflux ratios are higher than is required for feasibility. These refluxes are set by our choice of  $\Phi_V$  vs.  $\Phi_L$ . If we allowed these values to be changed we could vary other parameters. If we were to reduce  $R_{\Delta 2}$ , until boundary C<sub>2</sub> just touched boundary B<sub>1</sub> (see Figure 3.32) a minimum reflux ratio for CS 2 could be found. This is possible because  $X_{\Delta 2}$  is fixed and the corresponding TT<sub>3</sub> is only a function of  $R_{\Delta 2}$ . The same is true for CS 4.  $X_{\Delta 4}$  is fixed because  $X_{\Delta 2}$  was placed at the side draw composition – hence  $X_{\Delta 4}$  is constrained to this value for all choices of  $R_{\Delta 4}$  and  $\Phi_V$  and  $\Phi_L$ . We can reduce  $R_{\Delta 4}$  until the boundary C<sub>4</sub> just touches boundary A<sub>6</sub> (see Figure 3.33) and find a minimum  $R_{\Delta 4}$ .

An alternative to the incremental increase and decrease solution discussed above of refluxes in order to achieve a minimum reflux for CS 2 with CS 1 and CS 4 with CS 6 would of course be to apply the CPM-E technique described in Chapter 2. In this case, because we are limited to the boundaries of the MBT in each section of the column, the splits are binary interactions. This means, as described earlier, the profile of CS 2 and CS 1 are confined to the light-intermediate axis where as CS 4 and CS 6 are confined to the heavy- intermediate axis. By evaluating the eigenvectors at the saddle node of CS 1 TT<sub>3</sub>, we have found the intersection boundary where CS 2 and CS 1 will touch. Any node from CS 2 interacting or intersecting with the extension of the eigenvector is used to determine the reflux pertaining to the minimum reflux for the coupled sections. The same will apply to the interaction of CS 4 and CS 6.

*Note: Because two eigenvectors occur at the evaluation point, only one can be utilised. The eigenvector on the co-linear boundary of the MBT is of no interest to us and is neglected as it has no effect to the TT<sub>3</sub> interaction.*

These minima can both be represented in  $\Phi_V$  vs.  $\Phi_L$  space as illustrated before (see Figure 3.36). The  $R_{\Delta 2MIN}$  defined above is always  $< 0$  and  $R_{\Delta 4MIN}$  is always  $> 0$ . Any value of  $\Phi_V$  and  $\Phi_L$  between the minimum  $R_{\Delta 2}$  line (dashed pink) and the CS 2 zero net flow line (solid pink) will produce an overlap of TT<sub>3</sub> 2 and TT<sub>3</sub> 1 with a value of  $R_{\Delta 2} < 0$ . No  $\Phi_V$  and  $\Phi_L$  values above the minimum  $R_{\Delta 2}$  line will ever produce an overlap and hence a feasible Petlyuk design for our chosen  $R_{\Delta I}$  and products, so we can discard this entire region when choosing our split ratios. Similarly, the region between the minimum  $R_{\Delta 4}$  line (dashed black) and the CS 4 zero net flow line (solid black) will produce an overlap of TT<sub>3</sub> 4 and TT<sub>3</sub> 6. The value of  $R_{\Delta 4}$  here is  $> 0$ . Values of  $\Phi_V$  and  $\Phi_L$  below the minimum  $R_{\Delta 4}$  line can be discarded.

It should be noted that we cannot immediately discard the regions below the CS 2 or above CS 4 zero net flow lines. These regions produce reflux ratios with opposite sign ( $R_{\Delta 2} > 0$ ,  $R_{\Delta 4} < 0$ ) to the minima discussed above as they are in different net flow regions. Because of this both sets of matching criteria are satisfied. The overlap of TT<sub>3</sub> 2 and TT<sub>3</sub> 1 is automatically satisfied because the unstable node of CPM 2 lies outside the MBT above the unstable node of CPM 1 (see Figure 3.34). This topological phenomenon is always true for CPMs produced from positive differences points with positive reflux ratios. The overlap of TT<sub>3</sub> 4 and TT<sub>3</sub> 6 is also satisfied because the stable node of CPM 4 lies outside the MBT beyond the stable node of CPM 6 (see Figure 3.35). This topological phenomenon is always true for CPMs produced from positive differences points with negative reflux ratios. Although these guaranteed overlaps might seem like an advantage, they cannot be achieved simultaneously - the resulting net flow pattern is infeasible (up in CS 2 and down in CS 4). One of the CSs must operate with a reflux ratio of the same sign as its minimum reflux ratio. This means that the only region of  $\Phi_V$  vs.  $\Phi_L$  space that will satisfy both matching criteria and produce feasible net flow patterns in sections 2 and 4 is between the minimum reflux ratio lines of both CSs (above  $R_{\Delta 4MIN}$  and below  $R_{\Delta 2MIN}$ ). No value picked

outside this range will ever produce a feasible Petlyuk solution, whether the split is sharp or not.

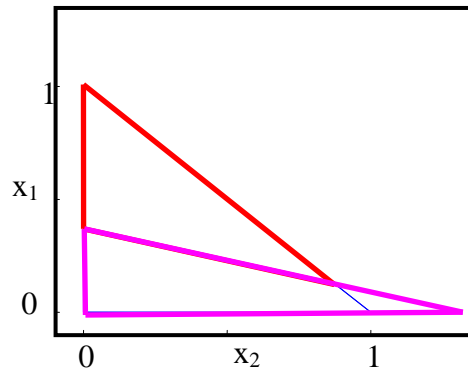


Figure 3.32:  $TT_3$  for CS 1 and CS 2 at minimum  $R_{\Delta 2}$

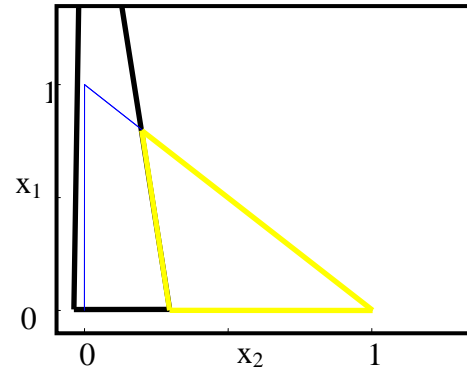


Figure 3.33:  $TT_3$  for CS 4 and CS 6 at minimum  $R_{\Delta 4}$

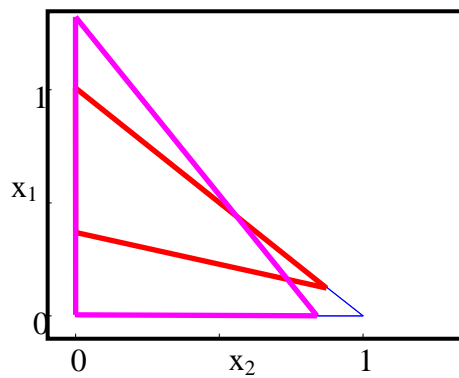


Figure 3.34:  $TT_3$  for CS 1 and CS 2 for positive  $R_{\Delta 2}$

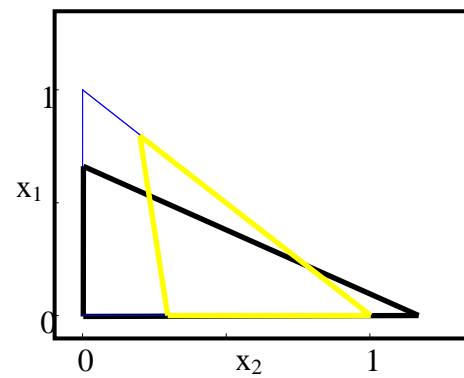


Figure 3.35:  $TT_3$  for CS 4 and CS 6 for negative  $R_{\Delta 4}$

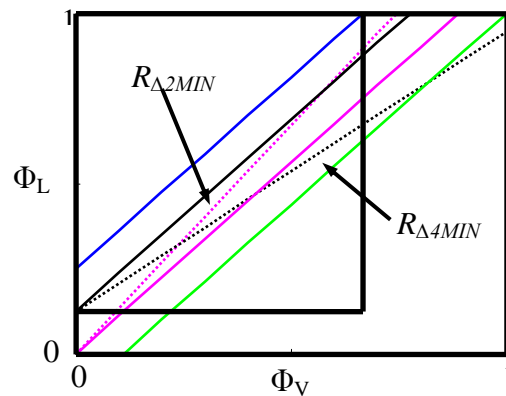


Figure 3.36: Minimum  $R_{\Delta 2}$  and  $R_{\Delta 4}$  in  $\Phi_V$  vs.  $\Phi_L$  space

### 3.13.2 Limiting Conditions for Overlap of TT<sub>3</sub> 3 and TT<sub>3</sub> 5 and ternary CPM-E technique

We have substantially reduced the range of possible split ratio choices by identifying regions (in  $\Phi_V$  vs.  $\Phi_L$  space) resulting in negative vapour or liquid flows, categorising regions of differing net flow patterns and producing lines of minimum reflux ratio for CS 2 and CS 4 based on two of the required matching criteria. We will now turn our attention to another of the matching criteria; the overlap of TT<sub>3</sub> 3 and TT<sub>3</sub> 5. The split ratios chosen for the example in Figure 3.22b produced a large overlap of these TT<sub>3</sub>s. If we start at these split ratios and increase the vapour split incrementally at constant liquid split, the TT<sub>3</sub>s of CS 3 and CS 5 will shift as seen in Figure 3.37a-b below. At a certain value, boundaries B<sub>3</sub> and C<sub>5</sub> of TT<sub>3</sub> 3 and TT<sub>3</sub> 5 respectively will actually be collinear. This represents the final  $\Phi_V$  value at the constant  $\Phi_L$  value, previously chosen, that will produce an overlap of these TT<sub>3</sub>s. Conversely, if we incrementally increase  $\Phi_L$  at constant  $\Phi_V$  the TT<sub>3</sub> will shift as seen in Figure 3.38a-b. Eventually a value of  $\Phi_L$  will be reached at which boundary C<sub>3</sub> and boundary A<sub>5</sub> just touch and are also collinear. Another remarkable property of the material balance is that these collinear boundaries will, in fact, always pass through the feed composition for constant-relative-volatility systems (vapour TT<sub>3</sub> boundaries for vapour feed and

liquid  $TT_3$  boundaries for liquid feed). Consequently, we immediately have an idea of their placement for all values of  $\Phi_L$  and  $\Phi_V$ .

Holland et al (2004 b) discussed the eigenvector fields underlying systems whose vapour-liquid-equilibrium can be modelled using the separation vector:

$$\tilde{\mathbf{s}} = [\mathbf{X} - \mathbf{Y} * (\mathbf{X})] \quad (3.21)$$

The eigenvectors of the difference point equation and the residue curve equation are only a function of the separation vector and completely independent of the difference point and reflux ratio. The eigenvector field, therefore, is the same for all CPMs of a particular system. Any liquid composition profile terminating at a stationary point approaches (the node) along the direction of the eigenvector at the point. Holland et al (2004 b) demonstrated that the eigenvectors at the singularities, of constant-relative-volatility systems, always point along the direction of the  $TT_3$  boundaries. Because the boundaries are straight in these systems, the eigenvectors at each singularity point directly at the other singularities. Any point chosen along one of these boundaries will have eigenvectors that point directly at the singularities, which define it. If we calculate the direction of the two eigenvectors at the feed composition we can immediately determine the two lines of co-linearity of the boundaries of  $TT_3$  3 and  $TT_3$  5. We will name the co-linearity line of smaller (absolute) gradient, Co-Linearity Line 1 (CLL1) (see Figure 3.39) and the line of larger (absolute) gradient, Co-Linearity Line 2 (CLL2) (see Figure 3.40). Once we know these two lines we can solve for all values of  $\Phi_L$  and  $\Phi_V$  that result in  $TT_3$  3 and  $TT_3$  5 bordering each other. This is done by simply choosing points along the co-linearity lines and, realising that these points must be satisfied by nodes of either of the  $TT_3$ s, determining the associated values of  $\Phi_L$  and  $\Phi_V$ . This solution is the first application of the CPM-E technique applied to a ternary system as developed by Chapter 1. Ultimately the node locations that produce feasible difference point solutions for either CS 3 or CS 5, is the minimum reflux solution (See Chapter 1). The interaction of the transformed triangle along the CLL produced from the eigenvector evaluation at

the feed point can be extended to any number of components through the basic interaction lines, planes and hyper planes depending on the number of eigenvectors presents and hence the number of components. Higher order minimum reflux solutions, for the relevant coupled sections as well as the overall system discussed, based on the application of the CPM-E technique in order to find the minimum reflux solutions are dealt with in Chapter 5 and 6.

These values can be plotted in  $\Phi_L$  vs.  $\Phi_V$  space. Figure 3.41 illustrates an example of these lines of  $\Phi_L$  and  $\Phi_V$  solutions, which divide values resulting in TT<sub>3</sub> 3 and TT<sub>3</sub> 5 overlap from those resulting in no overlap. There are of course two lines of solutions corresponding to the two co-linearity lines through the feed point. These lines are straight due to the linearity of CLL1, CLL2 and the material balance. The red line represents all points resulting in the lining-up of boundaries B<sub>3</sub> and C<sub>5</sub> of TT<sub>3</sub> 3 and TT<sub>3</sub> 5 respectively (i.e. generated from CLL1). We will refer to this line generated from CLL1 as Phi-Eigenvector-Boundary-1 (PEB1). To the left of PEB1 the boundary B<sub>3</sub> will be below CLL1 and boundary C<sub>5</sub> will be above it – a potential overlap. This is only a potential overlap because the stable node of TT<sub>3</sub> 3 might lie further “left” than the unstable node of TT<sub>3</sub> 5 – i.e. closer to the light-intermediate axis. To the right of PEB1 the relative positions of boundary B<sub>3</sub> and boundary C<sub>5</sub> will be inverted - hence no potential overlap. The blue line represents all points resulting in the lining-up of boundaries C<sub>3</sub> and A<sub>5</sub> (i.e. generated from CLL2). We will refer to this line generated from CLL2 as Phi-Eigenvector-Boundary-2 (PEB2). Below PEB2 boundary C<sub>3</sub> will lie to the right of CLL2 and boundary A<sub>5</sub> will lie to the left – potential overlap. Again this is only a potential overlap because the unstable node of TT<sub>3</sub> 5 might lie “below” the stable node of TT<sub>3</sub> 3 (closer to the intermediate-heavy axis). Above PEB2 boundary C<sub>3</sub> will lie to the left of CLL2 and boundary A<sub>5</sub> will lie to the right – hence no potential overlap. If we focus our attention on the area between PEB1 and PEB2, on the side of potential overlaps for both, we find that the uncertainty in this region for one line is removed by the other. An overlap of TT<sub>3</sub> 3 and TT<sub>3</sub> 5 is guaranteed for values of  $\Phi_L$  and  $\Phi_V$  chosen here.

Note: CLL1 and CLL2 (and consequently PEB1 and PEB2) are phase dependent. If vapour feed is added to the column, vapour boundaries  $B_3$  and  $C_5$  will line up along CLL1 while vapour boundaries  $C_3$  and  $A_5$  will line up along CLL2. The eigenvector directions in this case are not the eigenvectors of the standard separation vector as vapour profiles do not approach their pinch points along these directions. Vapour profiles approach pinch points along, and vapour  $TT_3$  boundaries line up along, eigenvectors of the differential equations which have separation vectors expressed in terms of the vapour composition.

$$\text{i.e. } \tilde{s} = [X * (Y) - Y]$$

### 3.13.3 Satisfying the Remaining Matching Criteria

In our development of the minimum reflux line for CS 2 we neglected the third column section involved in the required composition matching.  $TT_3 3$  must overlap not only  $TT_3 5$  but also  $TT_3 2$  and  $TT_3 1$ . An intersection with  $TT_3 1$  is always guaranteed in region 1, 2 and 3, however, as  $X_{\Delta 3}$  is within the MBT and operates with a positive reflux ratio. The same reasoning, as discussed previously for positive reflux in CS 2, prevails (see Figure 3.34).  $TT_3 1/TT_3 3$  overlaps, as we will see later, only occur in regions 4 and 5 under specific circumstances. The overlap of  $TT_3 3$  with  $TT_3 2$  is more difficult to guarantee. What we can show, though, is that when a node of  $TT_3 2$  (unstable) lies on top of a node from  $TT_3 1$  (saddle), a  $TT_3 3$  node (saddle) must lie at this same point and the respective boundary lines must then be collinear (Appendix B). It can also be shown that when these nodes lie on top of each other and the split ratios are adjusted along lines of constant  $X_{\Delta}$  (i.e. making the changes of the  $TT_3$ 's only a function of the changes to  $R_{\Delta}$ ),  $R_{\Delta 3}$  decreases, shifting boundary  $B_3$  away from the intermediate boiler and towards the light boiler. The rate at which  $R_{\Delta 3}$  decreases is smaller than the rate at which  $R_{\Delta 2}$  increases, however, and we can therefore infer that  $TT_3 1, 2$  and  $3$  will overlap for all split ratio values in regions 1, 2 and 3 below the minimum  $R_{\Delta 2}$  line (see Appendix C for details). If we assume that this movement of  $TT_3$ s is true not only for situations in which nodes are directly on top of each

other, but also for situations when boundaries touch we can be certain that if  $TT_3$  2 and  $TT_3$  1 overlap, all three  $TT_3$ s will overlap.

Similar logic to that used above for the matching criteria of CS 1, 2 and 3 can be used for that of CS 4, 5 and 6.  $TT_3$  5 is always guaranteed of overlapping  $TT_3$  6, in region 3, 4 and 5, by the same reasoning used for the overlap of  $TT_3$  4 with  $TT_3$  6 at negative  $R_{\Delta 4}$  (see Figure 3.35).  $X_{\Delta 5}$  lies within the MBT and  $R_{\Delta 5}$  is negative in region 3, 4 and 5. Also using reflux arguments, as above, it can be shown that  $TT_3$  4 overlaps  $TT_3$  5 for all values of split ratio space in regions 3, 4 and 5 above the minimum  $R_{\Delta 4}$  line.

The final matching criterion is the requisite overlap of the  $TT_3$ s of CS 2 and CS 4. This criterion is automatically satisfied because the difference points of CS 2 and CS 4 have the same value. For ideal systems, positive difference points always lie within their respective transformed triangles. As these points are the same for both sections, the  $TT_3$ s have to overlap by default.

### 3.13.4 Overall Column Feasibility in $\Phi_V$ vs. $\Phi_L$ Space

We have considered all the required composition matching criteria and found regions of split ratio space that satisfy them. We are now in a position to determine if there are regions that satisfy all requirements simultaneously and hence yield feasible Petlyuk designs. Figure 3.42 below illustrates examples of the PEB1 and PEB2 lines. Superimposed on these lines are the minimum reflux lines for CS 2 and CS 4. If we consider all these lines together and the individual regions of feasibility for each matching criterion, we can see that there is a region that satisfies all matching criteria for our selection of  $R_{\Delta i}$  and products. Any choice of  $\Phi_L$  and  $\Phi_V$  within this region will result in a feasible Petlyuk column design. This is extremely powerful because we no longer have to guess values for the split ratios. We have a method to actually calculate feasible split ratio combinations and understand their implications, for the design. From a very large range of potential split ratio values (0 to 1 for both), we have reduced the possible

choices to a very small region. It is clear that, for this choice of reflux ratio, it is very difficult to arbitrarily choose split ratios that would result in a feasible design. We will discuss the effects of  $R_{\Delta I}$  in depth later, but for now it will suffice to say that this region grows in size if  $R_{\Delta I}$  is increased and shrinks if  $R_{\Delta I}$  is decreased. This result holds with our intuitive understanding of distillation, which is that separations are more difficult at low reflux than at high reflux.

The feasible region of split ratios is bound on each side by one of the lines generated from the matching criteria. Because these boundaries represent limiting conditions for certain column sections it is useful to explore the conditions along these boundaries further.

Along the  $R_{\Delta 2MIN}$  line,  $TT_3 2$  borders  $TT_3 1$ . If we disregard the default infinite stage requirement of sharp-split separations, we can immediately conclude that, in this special case, it will take an infinite number of stages for the CS 2 composition profile to reach the rectifying profile because the unstable node pinch point lies on the boundary of  $TT_3 1$ . All split ratios chosen along the section  $R_{\Delta 2MIN}$  line between point “A” and “B”, in Figure 3.42, will result in an infinite number of required stages for CS 2 and hence an unstable pinch point at the top of CS 2. Similarly, all split ratios chosen between points “A” and “D” along the  $R_{\Delta 4MIN}$  line will result in an infinite number of required stages for CS 4. This condition results in a stable pinch at the bottom of the CS.

The intersection of the  $R_{\Delta 2MIN}$  line and the  $R_{\Delta 4MIN}$  line is more interesting. This specific choice of split ratios is denoted the “balanced main column”. This operating point is characterised by minimum feasible vapour flow through CS 2 and CS 4. At these conditions  $TT_3 2$  borders  $TT_3 1$  and  $TT_3 4$  borders  $TT_3 6$ . There are two pinching column sections – an unstable node at the top of CS 2 and a stable node at the bottom of CS 4.

Between points “B” and “C” along PEB2, boundary  $C_3$  borders boundary  $A_5$ . CS 3 is at minimum reflux conditions along this line. The line does not result in a

single minimum reflux value as in  $R_{\Delta 2MIN}$  and  $R_{\Delta 4MIN}$ , but a series of minimum  $R_{\Delta 3}$  values corresponding to different values of  $X_{\Delta 3}$ . This minimum reflux is characterised by a stable node pinch point at the bottom of CS 3 (in the middle of the pre-fractionator).

At the intersection of PEB2 and the  $R_{\Delta 2MIN}$  line (point “B”) both CS 2 and CS 3 will pinch (an unstable node at the top of CS 2 and a stable node at the bottom of CS 3).

Between points “C” and “D” along PEB1, boundary  $C_5$  borders boundary  $B_3$ . CS 5 is at minimum reflux along this line. The line, also, does not result in a single minimum reflux value but a series of minimum  $R_{\Delta 5}$  values corresponding to different values of  $X_{\Delta 5}$ . The top of CS 5 will terminate at an unstable pinch point.

At the intersection of PEB2 and the  $R_{\Delta 4MIN}$  line (point “D”), CS 4 will pinch in a stable node at the bottom and CS 5 will terminate in an unstable pinch point at the top.

At point “C”, PEB1 and PEB2 intersect. This point is denoted the “preferred split” and is characterised by minimum feasible vapour flow through the pre-fractionator. This particular set of split ratio values will result not only in a stable pinch point for CS 3 and an unstable pinch point for CS 5, but in these points coinciding, at the feed composition, in a “double-feed-pinch” point. Figure 3.43 illustrates the  $TT_3s$  of a “double-feed-pinch” Petlyuk column. The “double-feed-pinch” point is of course phase dependent. Vapour feed columns will exhibit a vapour profile “double-feed-pinch” point - although it should be noted that both phases in both cases will pinch.

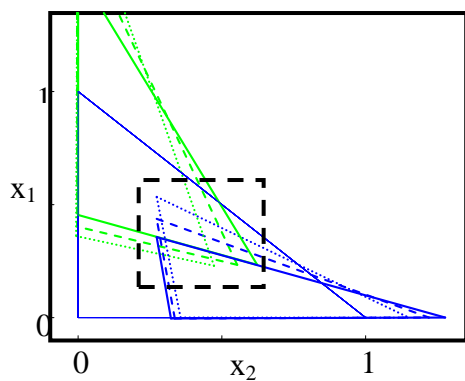


Figure 3.37a: Liquid TT<sub>3</sub> 3 and TT<sub>3</sub> 5 shift at constant  $\Phi_L$  varying  $\Phi_V$

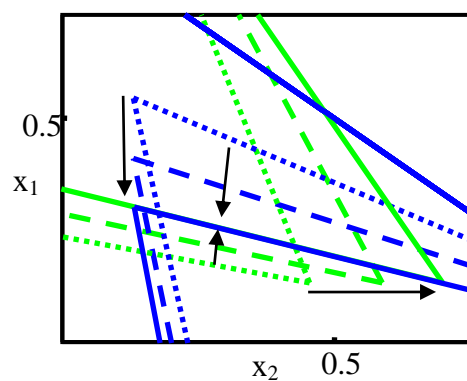


Figure 3.37b: Zoom of highlighted area from figure 6.37a

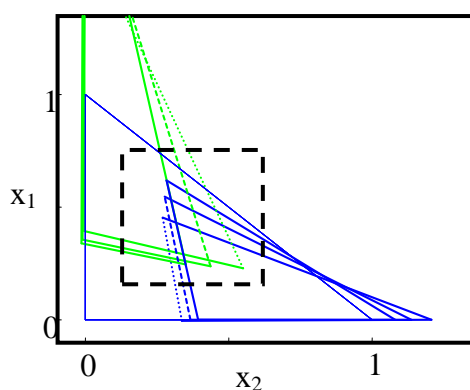


Figure 3.38a: Liquid TT<sub>3</sub> 3 and TT<sub>3</sub> 5 shift at constant  $\Phi_V$  varying  $\Phi_L$

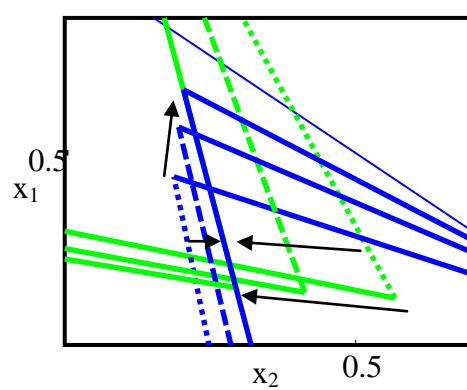


Figure 3.38b: Zoom of highlighted area from Figure 3.38a

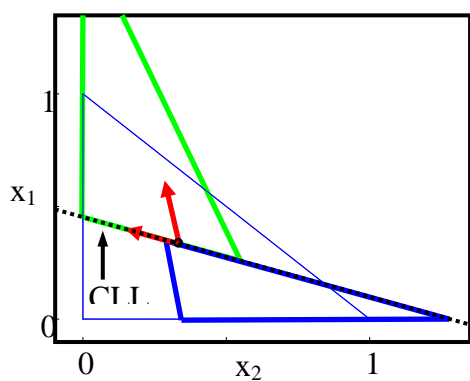


Figure 3.39: Triangles bordering along CLL1

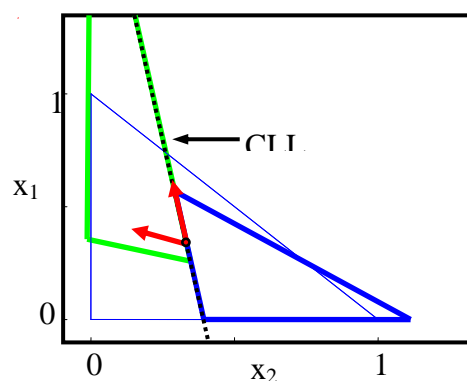


Figure 3.40: Triangles bordering along CLL2

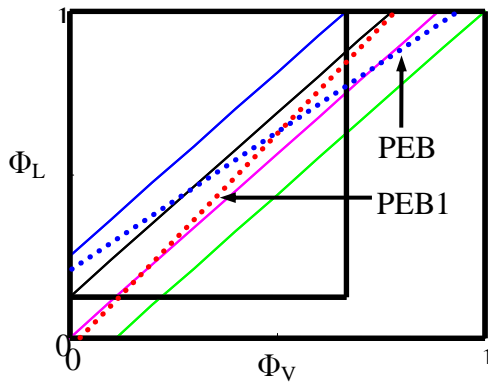
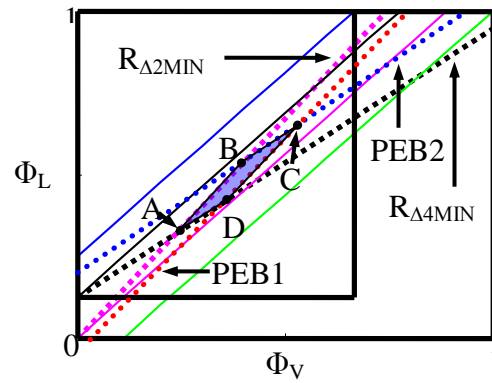


Figure 3.41: PEB1 and PEB2

Figure 3.42: Region of  $\Phi_L$  and  $\Phi_V$  space resulting in feasible Petlyuk solutions.

### 3.14 Overall Minimum Reflux

Throughout this work so far we have assumed that the overall column reflux ratio,  $R_{\Delta 1}$ , is large enough to produce a feasible solution. The design procedure described above is a waste of time if the column reflux ratio is not high enough. A trial and error approach of choosing a reflux ratio and testing for feasible solutions is definitely not desirable. Fidkowski and Krolikowski (1987) derived analytical expressions for the sharp-split Petlyuk column minimum reflux ratio with saturated liquid feed. Halvorsen and Skogestad (2001) modified these expressions to include feed material of any quality. It was shown that the overall column minimum reflux for sharp splits is equal to the maximum of two sharp simple column splits namely: light component to the intermediate-heavy axis and heavy component to light-intermediate axis. These expressions are applicable to constant relative volatility systems only. It would be useful to gain an understanding the topological implications of the minimum reflux solution so that any zeotropic system may be handled. We will now revisit two of the composition matching criteria and try and understand their implications for minimum column reflux ratio.

Earlier we showed that if  $TT_3 2$  and  $TT_3 1$  touch, boundary  $B_3$  must be collinear with  $C_2$  and  $B_1$  (see Appendix B) – the matching criteria of these column sections is then satisfied. We also showed that the last overlap of  $TT_3 3$  and  $TT_3 5$  occurs when boundaries of these triangles are collinear and run through the feed point (at  $CLL1$  and  $CLL2$ ). It is clear that we cannot satisfy both these situations with any arbitrary choice of column reflux ratio ( $R_{\Delta 1}$ ). If  $R_{\Delta 1}$  is too small  $TT_3 3$  will not be able to simultaneously overlap  $TT_3 1$  and  $2$  as well as  $TT_3 5$  (see Figure 3.44, Figure 3.45 and Figure 3.46). The same problem is evident in the required composition matching at the bottom half of the column i.e. the matching of compositions in CS 4, 5 and 6 (see Figure 3.47, Figure 3.48 and Figure 3.49). The main problem is that the two sets of collinear lines – the first set being the CS 2 and 4 minimum reflux collinear boundaries and the second being  $CLL1$  and  $CLL2$  - will occur in the wrong position relative to each other in composition space. The CS 2 minimum reflux line will lie “above”  $CLL1$ , closer to the light component. This means that any adjustment of split ratios in favour of satisfying the  $TT_3 3$  and  $TT_3 5$  overlap will reduce the reflux of CS 2 at a higher rate than the reflux of CS 3 and hence make satisfying the  $TT_3 1, 2, 3$  matching criterion impossible (the inverse argument to that made in Appendix C). In this case the minimum  $R_{\Delta 2}$  line will lie below  $PEB1$  in split ratio space, so overall column feasibility is impossible (see Figure 3.50). The key to resolving the minimum  $R_{\Delta 1}$  issue lies with boundary  $B_1$  (or boundary  $A_6$ ) and the feed composition point.

Let us attempt to resolve the issue of satisfying matching criteria at the top half of the column. Boundary  $B_1$  acts as a “watershed”, with intersection of the  $TT_3$ s on one side and no intersection on the other. When  $R_{\Delta 2}$  is reduced from the minimum,  $TT_3 1$  and  $2$  will not overlap and neither will  $TT_3 2$  and  $3$ .  $TT_3 3$ , however, shifts “down” and must shift in this direction to overlap  $TT_3 5$ . The “watershed” needs therefore to be shifted down far enough that when  $TT_3 3$  is shifted to overlap  $TT_3 5$  for the “first time”, in the co-linearities  $CLL1$  and  $CLL2$  at the feed point, it has not yet reached the point when its boundary is collinear with boundary  $B_1$ . This indicates that boundary  $B_1$  must be closer to the intermediate-heavy boundary than the feed composition – the feed point must be contained within the boundaries of

the  $TT_3$  1. The minimum column reflux ratio will then be the value resulting in boundary  $B_1$  running through the feed point. Obviously, because the matching criteria of CS 3 and 5 is feed phase dependent, the relevant CS 1  $TT_3$  defining the column overall minimum reflux is also phase dependent – if the feed is vapour, the vapour boundary  $B_1$  will run through the feed composition. We can conclude, by similar logic that the feed point must lie within the  $TT_3$  6 (of relevant phase). The true minimum column reflux ratio will be the smallest value that allows the feed to be contained within both  $TT_3$  1 and 6 – i.e. contained within one and situated on the border of the other. The  $TT_3$ s for a column at minimum reflux is shown in Figure 3.51. This topological observation explains, from a composition profile perspective, why the sharp-split Petlyuk minimum reflux ratio is equal to the maximum of the two simple column splits.

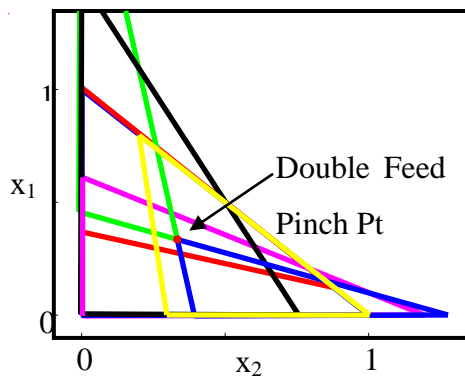


**Figure 3.43: Double feed pinch column  $TT_3$ s – saturated liquid feed**

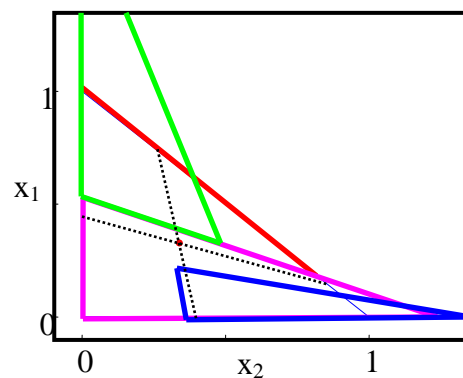


**Figure 3.44: Matching criterion 1 satisfied but criterion 4 is not**

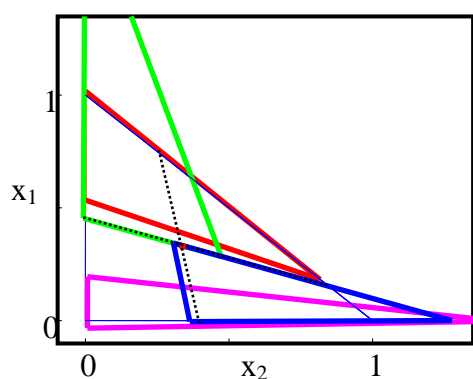


Figure 3.45: Matching criterion 4 satisfied along CLL1 but criterion 1 is not.

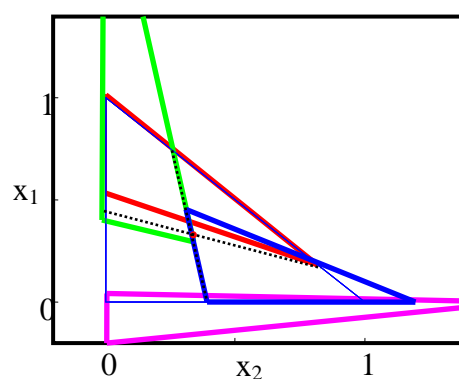


Figure 3.46: Matching criterion 4 satisfied along CLL2 but criterion 1 is not.

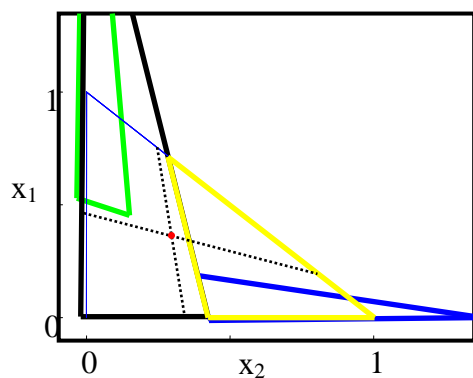


Figure 3.47: Matching criterion 2 satisfied but criterion 4 is not

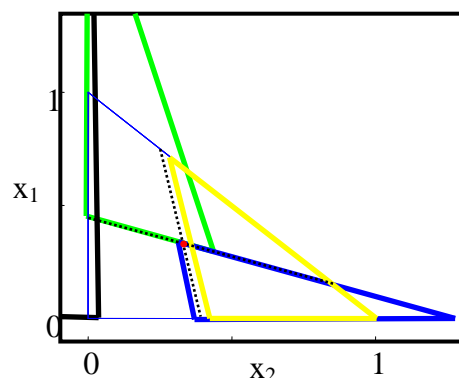


Figure 3.48: Matching criterion 4 satisfied along CLL1 but criterion 2 is not.

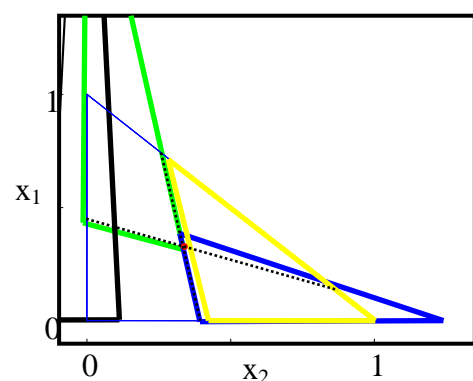


Figure 3.49: Matching criterion 4 satisfied along CLL2 but criterion 2 is not.

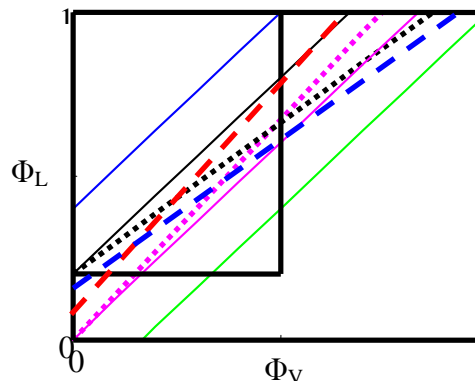


Figure 3.50: No overlap of feasible regions in split ratio space below min column reflux.

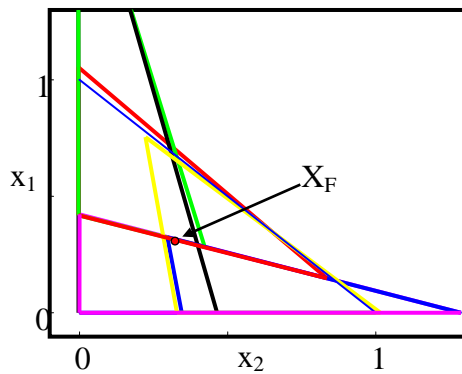


Figure 3.51:  $TT_3$  for column at minimum reflux

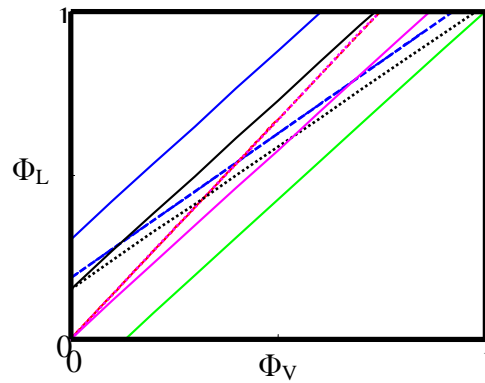


Figure 3.52: Region of feasibility shrinks to line at minimum reflux

### 3.15 The Effect of Varying $R_{\Delta I}$

Halvorsen and Skogestad (2001) performed an extensive analysis of the feasible/optimality region at various reflux ratios, feed qualities and relative volatilities. We will now outline the more common feasible region effects for saturated liquid feed as well as changes to the zero net flow lines and negative flow boundaries upon variation of reflux ratio.

#### 3.15.1 CS 2 and CS 4 minimum reflux

When the value of  $R_{\Delta I}$  is increased the area of  $TT_3$  1 inside the MBT increases, as boundary  $B_1$  moves away from the light component. The value of  $R_{\Delta 2MIN}$  required for  $TT_3$  2 to border  $TT_3$  1 is, therefore, reduced as boundary  $C_2$  is much closer to  $X_{\Delta 2}$ . We find that  $R_{\Delta 4MIN}$  is similarly reduced because  $R_{\Delta 6}$  is increased the moment  $R_{\Delta 1}$  is increased - to maintain material balance. The net result of the reduction in the values of  $R_{\Delta 2MIN}$  and  $R_{\Delta 4MIN}$  is that these lines, in split ratio space, now fan out further from their respective zero net flow lines (infinite reflux lines). See Figure 3.53 below. For our choice of relative volatilities and product points, the  $R_{\Delta 2MIN}$  line shifts much slower than the  $R_{\Delta 4MIN}$  line.

### 3.15.2 Negative Flow Boundaries

The negative flow boundaries are described by Equation 6.6 and Equation 6.7. It is clear that the value of  $\Phi_V$ , in Equation 6.6, must increase as  $R_{\Delta I}$  increases, because the second term in this equation is negative and its magnitude decreases. The negative flow boundary in split ratio space must therefore shift to the right - closer to  $\Phi_V = 1$ . The value of  $\Phi_L$ , in Equation 6.7, on the other hand, must decrease as the denominator increases. The negative flow boundary, described by Equation 6.7, will shift downwards towards  $\Phi_L = 0$  as  $R_{\Delta I}$  increases. (See Figure 3.54)

### 3.15.3 Zero Net Flow Boundaries

Each of the zero net flow lines shifts towards the  $\Phi_L = \Phi_V$  line as  $r_{\Delta I}$  is increased. This occurs because the gradients of these straight lines, described by Equation 6.2 to Equation 6.5, tend to 1 and the  $\Phi_L$ -intercepts tend to 0 as  $R_{\Delta I} \rightarrow \infty$ . As a consequence the area of net flow regions 2,3 and 4 decrease. (See Figure 3.56 and Figure 3.57)

### 3.15.4 PEB1 and PEB2

With increasing  $R_{\Delta I}$  the slope of PEB1 decreases slightly and its  $\Phi_L$ -intercept shifts downwards. The slope of PEB2 also decreases, but its  $\Phi_L$ -intercept increases, moving upwards along the  $\Phi_L$  axis. For our choice of products and constant relative volatilities, we again see a marked difference in the rate of change of two boundaries of the same type, in split ratio space. PEB1 shifts far more rapidly than PEB2. (See Figure 3.55)

### 3.15.5 Feasible $\Phi_L$ and $\Phi_V$ regions

The shifting of the various boundaries in split ratio space combine to increase the overall area of the feasible  $\Phi_L$  and  $\Phi_V$  region as  $R_{\Delta I}$  is increased (see Figure 3.58). This effectively makes the separation easier as a larger range of split ratios result in feasible designs than before. At minimum overall column reflux the feasible region has zero area (see Figure 3.52). The region effectively “grows” from this zero area at minimum reflux as  $R_{\Delta I}$  is increased - as would be expected. The most interesting effect of the increase of the feasible region area is that at high enough  $R_{\Delta I}$  values, the region crosses into the four remaining net flow regions (see Figure 3.59 and Figure 3.62). The associated net flow patterns can therefore be produced in feasible designs if  $R_{\Delta I}$  is sufficiently large. We have now confirmed the intuitive arguments about the required magnitude of the column reflux ratio for net flow patterns 1, 2, 4 and 5 discussed previously. These flow patterns are indeed only possible at high reflux ratio. Figure 3.60, Figure 3.61, Figure 3.63 and Figure 3.64 each show the six liquid TT<sub>3</sub>s of a feasible Petlyuk design for net flow patterns 1, 2, 4 and 5.

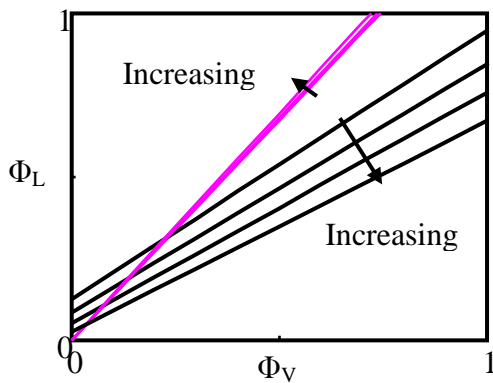


Figure 3.53:  $R_{\Delta 2MIN}$  and  $R_{\Delta 4MIN}$  at varying reflux

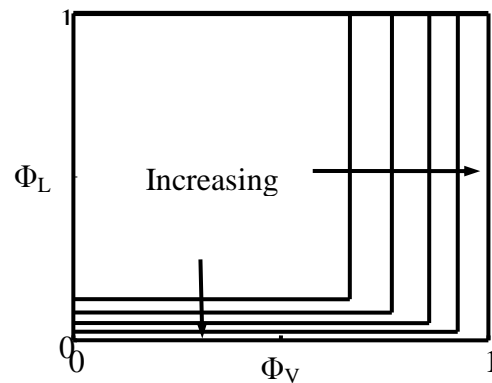


Figure 3.54: Negative flow boundaries at varying reflux

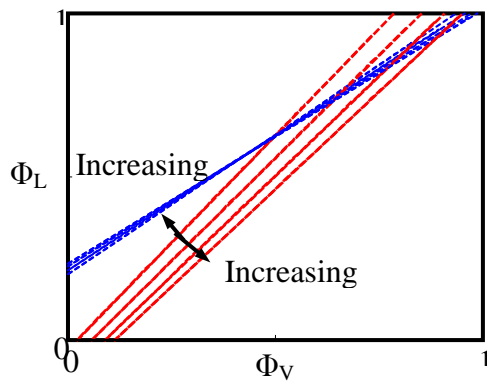


Figure 3.55: PEB1 and PEB2 varying reflux

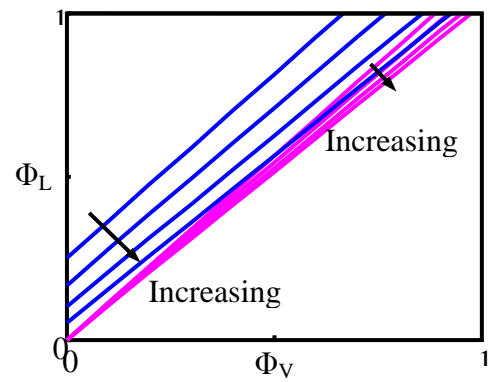


Figure 3.56:  $\Delta_5$  and  $\Delta_2$  zero net flow lines varying reflux

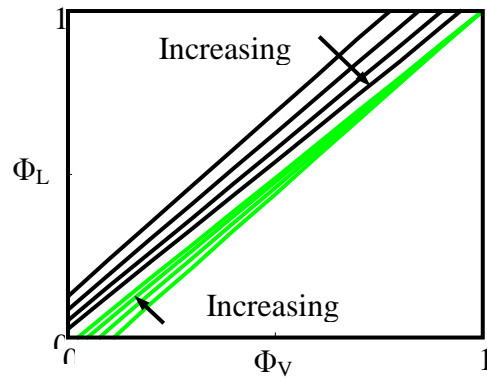


Figure 3.57:  $\Delta_3$  and  $\Delta_4$  zero net flow lines varying reflux

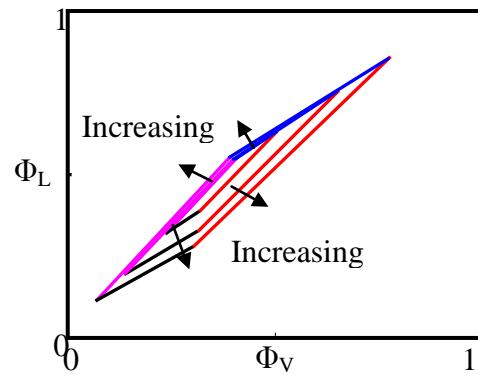


Figure 3.58: Feasible region varying reflux

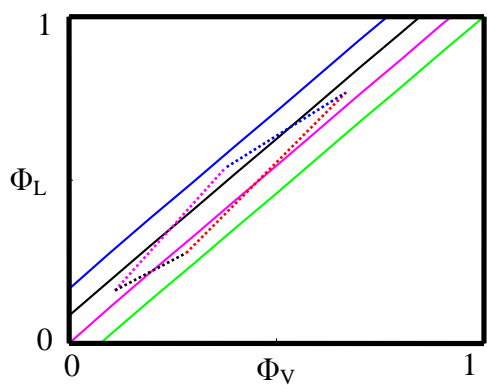


Figure 3.59: Feasible solutions in region 2, 3 and 4

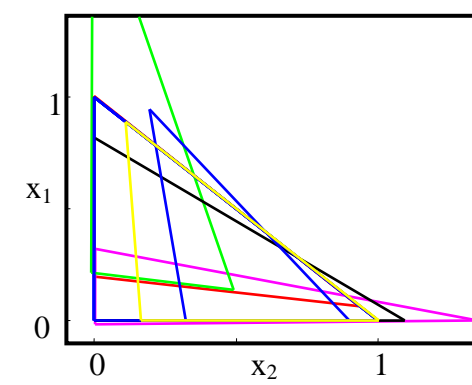


Figure 3.60: Feasible  $TT_3$ s for net flow pattern 2

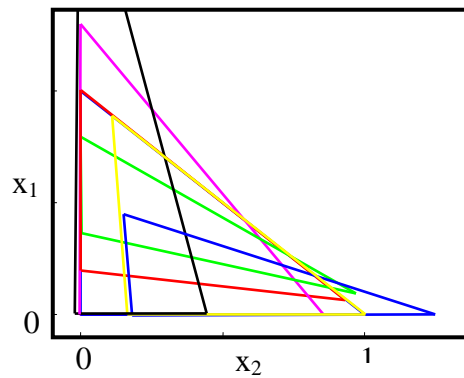


Figure 3.61: Feasible  $TT_3$ s for net flow pattern 4

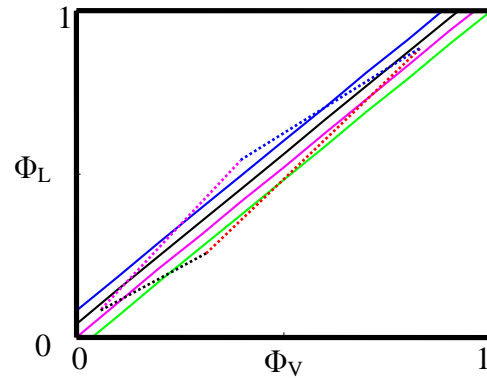


Figure 3.62: Feasible solutions in region 1, 2, 3, 4 and 5

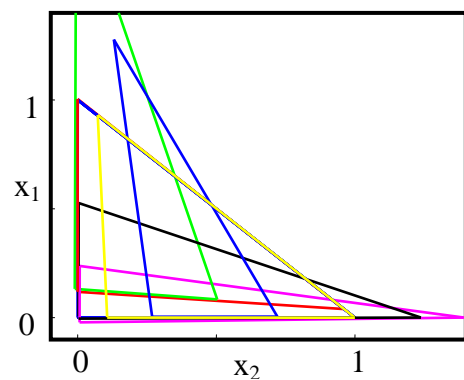


Figure 3.63: Feasible  $TT_3$ s for net flow pattern 1

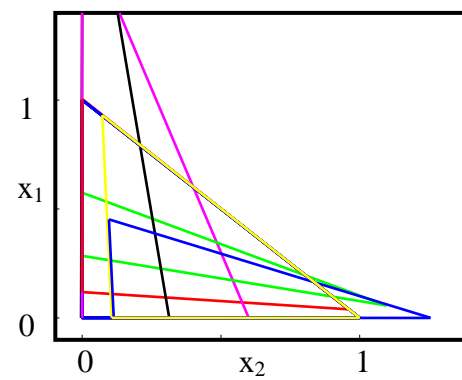


Figure 3.64: Feasible  $TT_3$ s for net flow pattern 5

### 3.16 Discussion

In this work we have successfully modelled the Petlyuk column. The column is broken down into column sections and a CPM is produced for each of these sections using the difference point equation. These CPMs can then be superimposed and feasible operating profiles found.

This design procedure is graphical but can be performed quickly and with little computational effort. Instead of producing entire CPMs, the procedure can be performed by simply tracking the stationary solutions of the difference point equation. Using these stationary solutions a transformed triangle can be produced that enables us to track all regions of CPM topology without solving the difference point equation.

The importance of the reflux ratio to the qualitative form of the CPM/TT<sub>3</sub> has led to a comprehensive analysis of the feasible net flow patterns in the Petlyuk configuration. We have shown that there are *five* possible net flow patterns. These are flow patterns 1 to 5. The net flow pattern within the column is determined by the choice of vapour and liquid split ratios. Regions, of split ratio space, resulting in each of these flow patterns can be found by producing zero net flow lines for the coupled column sections.

Net flow pattern 3 is the most efficient mode of operation. Feasible column solutions can be produced at lower reflux ratio for this flow pattern than for the other four patterns. This fact leads to a very useful analytical test of Petlyuk operation. *If the operating split ratios result in flow patterns other than net flow pattern 3 we can immediately conclude that the column is operating inefficiently.*

Variables other than net flow can be represented in split ratio space. In fact, the representation of variables in split ratio space is a very powerful tool for analysing and understanding Petlyuk column parameters. We can very simply produce lines of split ratios corresponding to coupled-column section reflux ratios, lines of constant difference point values and also generate regions corresponding to negative internal flow rates. However, the most powerful result is that by producing PEB 1 and 2 as well as minimum reflux ratio lines for CS 2 and 4 we can construct a region of split ratios that result in feasible Petlyuk column designs. These boundaries (PEB 1 and 2 and minimum refluxes for CS 2 and 4) are constructed from the eigenvector evaluation at the appropriate points. The eigenvector predicts the line of intersection at minimum reflux for intersection

CSs (i.e. CS 1 and CS 2, CS3 and CS 5, CS 4 and CS 6). *These regions contain all feasible split ratios values that allow the design specifications to be met.*

The feasible region, of split ratio solutions, is exactly equivalent to the optimality region defined by Halvorsen and Skogestad (2001). The CPM methodology is broader in scope, however, as it can be applied to all zeotropic systems. Although the topological boundaries, between stationary points, of non-ideal systems have a degree of curvature, straight lines offer very good approximations to these boundaries. As such feasible regions can be generated for these systems with a fair degree of accuracy. The methodology also allows the generation of individual solutions containing all the required design parameters as well as composition profiles.

Feasible regions illustrate that the choice of vapour and liquid split ratios, in the Petlyuk column, cannot be made arbitrarily. For reflux ratios above the minimum, only a very small region of split ratio space results in feasible designs. The designer would be very fortunate to arbitrarily choose a feasible split ratio pair. The choice of split ratios within this feasible region can also not be made arbitrarily. Values, chosen along the boundaries of the region, result in an infinite number of required stages. Although we have analysed sharp-split separations in this work, which, by their nature, require infinite stages, the feasible region boundaries can be generated for non-sharp-splits as well. These non-sharp-split boundaries also coincide with an infinite number of required stages.

From a stage number and split ratio perspective it is clear why producing Petlyuk designs, for desired separations, is difficult using iterative solving methods. Convergence problems aside, without an understanding of the effects of parameters such as reflux ratio and the split ratios it is exceedingly difficult to determine the required number of stages for a separation. For a set number of stages the designer would typically choose arbitrary split ratios and reflux ratios. These are very unlikely to produce the desired separation and the designer must resort to trial and error. If we now couple this trial and error approach with

iterative convergence problems it is evident that current design methods are not particularly efficient. The CPM approach on the other hand has allowed us to not only generate individual solutions, but find *all possible solutions* for a set of column parameters (reflux ratio and product flow rates). For non-sharp splits, parameters like the total number of required stages, feed stage and side-draw stage are a natural product of the process. These can be determined by tracking variable  $n$  along each composition profile of a column section.

Determining column minimum reflux ratio, for any zeotropic thermodynamics, is one of the most powerful results of the methodology. We can determine this value directly by analysing the position of the feed point relative to the boundaries of  $TT_3 1$  and  $TT_3 6$  as described previously. We can, however, also determine if a design is infeasible by analysing the boundaries in split ratio space. If the boundaries of the split ratio feasible region occur in the wrong position relative to each other, the designer can immediately infer that the design at the chosen parameters is infeasible. In this case, either the column reflux ratio or product flow rates must be altered in order to make the separation feasible.

At minimum reflux the feasible region has zero area. It is simply a line at these conditions. As the reflux is increased, the area of the feasible region increases i.e. more split ratios become feasible for operation. This holds with the intuitive understanding that separation by distillation becomes easier as the reflux ratio is increased. If the designer wishes to operate the column with net flow patterns 1, 2, 4 or 5, it is simple to determine the minimum column reflux ratio required. When the feasible region crosses into the relevant net flow region (of split ratio space), after increasing  $R_{\Delta I}$ , this flow pattern becomes feasible. Although these flow patterns hold no obvious advantages for zeotropic systems, they do, in fact, hold very exciting advantages for azeotropic systems. *These flow patterns allow for the sampling of very “unusual” difference points which quite often allow distillation boundaries to be crossed.*

---

In summary the CPM methodology for Petlyuk design is very powerful and efficient. The procedure for generating the feasible/optimality region and minimum reflux is not quite as elegant as the analytical methods employed by Halvorsen and Skogestad (2001), but does allow the determination of all feasible solutions and minimum reflux ratio, for all zeotropic systems. On selecting a reflux ratio and split ratio pair, individual column solutions can be generated without requiring iteration. Parameters such as feed stage placement, side-draw stage placement, total required stages, column section stage requirements as well as internal vapour and liquid traffic are a natural outcome of the procedure. The solutions generated from the procedure can be used for the effective initialisation of rigorous iterative simulation packages such as ASPEN Plus and do not vary drastically from the solutions generated using these packages.

## Chapter 4: Complex Column Design - Sharp Split Kaibel Column

*This chapter is an extension of the Petlyuk column. Much of the guidance in this chapter was offered by Dr. Simon Holland, for which I am extremely thankful. Parts of the concepts of this chapter have been published in Computers and Chemical Engineering (See Hildebrandt et al. (2010)). This publication was originally work presented at the FOAPD 2009 conference held in Breckenridge, Colorado.*

---

### **Abstract**

The Kaibel Column is a fully-thermally coupled column with an adiabatic wall dividing the column into two equal halves for the production of four product streams. The Kaibel Column allows for a feed mixture of four or more components from which it produces a distillate, bottoms and two product side streams. Compared to the conventional 3 column direct split sequence, the Kaibel column can be built in a single shell, making it an attractive alternative in terms of capital cost savings along with its counterpart; the Petlyuk Column. Furthermore, the reduction in the number of reboilers and condensers' required leads to improved operating costs. In this paper we demonstrate the use of Column Profile Maps (CPMs) for the comprehensive analysis and design of Kaibel Columns by applying the CPM technique for a system at sharp-split conditions. From the results of the topological analysis, it is shown that, for set product composition specifications, when using an ideal system (constant relative volatilities), there is only one set of feasible operating parameters.

---

## 4.1 Introduction

Distillation is the most widely used separation technique in the chemical process industry and is the largest energy consumer among process separation units. There are an estimated 40 000 distillation columns in the U.S. that consume approximately 18% of all of the energy in the manufacturing sector (Eldridge et al., 2005). This fact has provided a continuous incentive towards the search for more energy-efficiency distillation systems.

An option to design non-conventional distillation schemes with better energy efficiencies is the use of thermal coupling. A thermally coupled structure involves an interconnection between two columns with a liquid or vapour extraction from the first column and a recycle stream from the other column in the other phase. Such interconnections can be implemented in place of a reboiler, condenser or both. A large body of work has been developed (Segovia-Hernández et al., 2005; Hernández et al., 2003; Kim, 2004; Annakou and Mizsey, 1996; Caballero and Grossmann, 2004; Kolbe and Wenzel, 2002; Agrawal and Fidkowski, 1998) investigating the separation of ternary and quaternary mixtures, with three thermally coupled systems gaining special interest, specifically, the side-rectifier which eliminates the use of one reboiler; the side-stripper which eliminates the use of one condenser, and the fully thermally coupled distillation system (Wright, 1949; Cahn et al., 1962; Petlyuk et al., 1965; Kaibel, 1987) that eliminates the requirement of one reboiler and condenser.

It has been shown (Fidkowski and Krolikowski, 1987) that for a three component zeotropic separation, the Petlyuk column has the lowest overall energy demand when compared to conventional schemes and even when comparing among the thermally coupled schemes (Segovia-Hernández et al., 2005). Lower energy consumption levels, which equates to lower annual costs of thermally coupled systems with respect to conventional sequences have been studied and reported (Fidkowski and Krolikowski, 1990; Glinos and Malone, 1988; Tedder and Rudd, 1978; Yeomans and Grossmann, 2000; Petlyuk et al., 1965; Stupin and Lockhart,

1972; Westerberg, 1985; Westerberg and Wahnschafft, 1996; Fidkowski and Krolkowski, 1987; Carlberg and Westerberg, 1989; Rudd, 1992; Triantafyllou and Smith, 1992).

The Kaibel column, introduced at BASF (Kaibel, 1987), separates four products in a single shell with a dividing wall and only comprises of a single reboiler and condenser. The Kaibel column is an extension of the Petlyuk arrangement (Petlyuk et al., 1965), and both the Petlyuk and the similar dividing wall column (DWC) (Wright, 1949) having been extensively investigated. The original thermally coupled arrangement consisting of the two shells (pre-fractionator and main column) that separate a four component mixture was first proposed by Cahn et al. (1962). The Kaibel column offers large savings in energy and investment costs compared to the conventional distillation configurations for multi-component systems. A similar sequential distillation setup would require three columns to separate four components. Hence, it also has the potential of saving space. Savings of 35 %, 25 % and 40 %, have been reported for operating cost, investment cost and plot space respectively (Wenzel and Röhm, 2003).

Even though the Kaibel column has shown potentially large savings in capital and operational costs, it has taken a long time for the industry to implement the ideas. However, the last 25 years have seen the technology come into use industrially and there are now more than 90 divided wall columns in operation around the world (Kaibel et al., 2007). Over the past 15 years Julius-Montz GmbH gained a strong position in DWC technology through its long association with BASF. Before this alliance was present BASF was the sole industrial promoters of the DWC (Kaibel, 1987). The growing market has attracted additional competitors, notably Sulzer Chemtech Ltd, from Switzerland, ExxonMobil from Texas and Koch-Glitsch in Kansas. Sulzer has installed more than 20 DWCs worldwide and Koch-Glitsch has built approximately 10 (Parkinson, 2009). Linde AG in Germany has built several DWCs and has the particular distinction of having installed the world's tallest, at approximately 100 m and 5.5 m in diameter. This

column was installed for Sasol, South Africa, which is used to recover petrochemicals from Fischer-Tropsch, based feed stocks (Parkinson, 2009).

The successful implementation of DWC concept represents an example of a recent technological breakthrough in the field of distillation and separation processes with potential for further exciting developments. Upon implementation of ‘un-fixed’ or more commonly known ‘un-welded’ wall (Kaibel et al., 2007) technology, which enabled significant expansion of the application and led to a major increase in utilisation of DWC, it became a very attractive option, not only for the separation of three and four component mixtures but also of mixtures containing larger number of components within a single shell.

Despite the incentive on energy and equipment savings provided by thermally coupled schemes; their industrial implementation has been constrained because of the potential control problems associated with the operation of a more complex configuration (Dünnebieber and Pantelides, 1999). Nevertheless, some works have been reported (Abdul Mutalib and Smith, 1998a, 1998b; Hernández and Jiménez, 1999a; Jiménez, Hernández, Montoy, and Zavala-García, 2001; Segovia-Hernández, Hernández, and Jiménez, 2002; Wolff and Skogestad, 1995) on the dynamic properties of thermally coupled systems that have shown a rather promising perspective on the operational characteristics of such systems.

Fidkowski and Krolikowski (1987) detailed one of the fundamental breakthroughs regarding the understanding of steady state operation of the thermally coupled columns. This in particular was the development of the analytical solution for minimum vapour requirement for sharp-splits which made use of the Underwood methodologies (Underwood, 1948). These ideas were then re-emphasised by Carl and Westerberg (1989a, 1989b) who also detailed that the Underwood roots “carry over” from the top of the first column to the second column in the fully thermally coupled columns. The drawback from this solution was that it did not encompass all the possible solutions, but merely one set of solutions regarding conventional flows within a column. Halvorsen (2001) extended the idea of the

“carry over” of Underwood roots and developed an implicit set of solutions for reverse flows within the column by developing the V-min diagram. This methodology, used to derive the minimum vapour flow equations, was then used to derive the Petlyuk and extended Petlyuk columns “optimality region” for infinite stages and sharp splits for multi-component separations (Halvorsen and Skogestad, 1997; Halvorsen and Skogestad, 2003). Although the methodology is quite useful and viewed as a new approach based on Underwood’s method, for multi component, non-ideal mixtures, construction of the V-min diagram requires the use of meticulous simulation techniques.

The focus of this manuscript is to show the use of Column Profile Maps (CPMs) (Tapp et al., 2004) as a design technique for higher order systems such as the Kaibel column that separates quaternary mixtures in any proportion. In addition to this, this work will also set a foundation for construction and generation of the optimality regions for higher order systems. Topological net flow of individual components as well as overall material flow arguments will be used to generate the feasible region for the Kaibel column. This paper is an extension of the Petlyuk solution generated by Holland et al. (2010) and will only deal with sharp split solutions that are analogous with infinite number of stages, but will lay down fundamental theory and definitions for non-sharp splits. The graphical nature of the CPM procedure allows for the methodology’s applicability to all zeotropic thermodynamics. The work covered makes use of constant relative volatility system.

## 4.2 CPMs for Ternary and Quaternary Systems

Column Profile Maps (CPM), introduced by Tapp et al. (2004), are generated using the difference point equation (DPE) (see Equation 4.1 below). They are maps of liquid composition trajectories generated for a column section  $k$  ( $CS_k$ ) with a constant net-molar flow and are defined for a single difference point ( $X_\Delta$ ) and reflux ratio ( $R_\Delta$ ). The DPE for  $CS_k$  is defined as follows:

$$\frac{dX}{dn} = \left(1 + \frac{1}{R_{\Delta k}}\right) (X - Y^*(X)) + \frac{1}{R_{\Delta k}} (X_{\Delta k} - X) \quad (4.1)$$

$$\text{Where: } X_{\Delta k} = \frac{V_k Y_T - L_k X_T}{\Delta_k} \quad (4.2)$$

$$R_{\Delta k} = \frac{L_k}{\Delta_k} \quad (4.3)$$

$$\Delta_k = V_k - L_k \quad (4.4)$$

A CPM is produced, using the DPE which is solved at various initial conditions, throughout the composition space for selected  $X_{\Delta k}$  and  $R_{\Delta k}$  (where  $n \rightarrow -\infty$  and  $n \rightarrow \infty$ ). The derivation of the Difference Point Equation is shown in Appendix F. A CPM for a three component system can be seen in Figure 4.1. The resulting column profiles/trajectories either tend to infinity or terminate at a stationary point. For a three component (ternary) system, with constant relative volatility, there are three stationary point solutions present in a CPM namely the pure components. These are characterised as stable, unstable and saddle stationary points or nodes (See Figure 4.1). For a four component (quaternary) system, with constant relative volatility, there are 4 stationary points.

For the purpose of simplicity, this paper considers the 4-component feed ( $F$ ) with pure components A (light), B (light intermediate), C (heavy intermediate) and D (heavy) and their respective relative volatilities as [6 4 2 1]. An example of a quaternary CPM is shown in Figure 4.2. It is evident from Figure 4.2; the entire map is not populated with curves, as this will be too confusing to observe graphically.

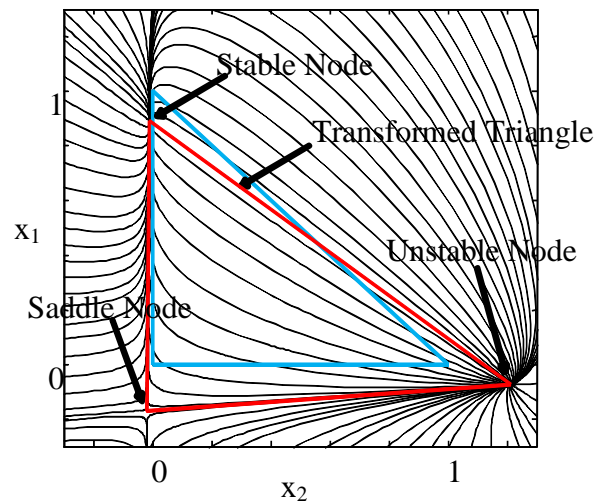


**Figure 4.1: Ternary Column Profile Map for  $X_{\Delta k} = [-0.3, 0.2]$  and  $R_{\Delta k} = 10$ . Note:  $x_1$  – Heavy Component,  $x_2$  – Light Component,  $x_3$  – Intermediate Component**

As for the ternary system, the quaternary system with constant relative volatilities allows us to draw straight lines through the nodes (See Figure 4.2). The boundaries formed from these intersected nodes form regions of qualitatively different topology (See Figure 4.1 and Figure 4.2).

It is important to note that the DPE is defined under constant molar over flow assumptions and is used for all distillation modelling. Feed material is assumed to be at saturated liquid or saturated vapour conditions and perfect mixing is assumed over all mixing points.

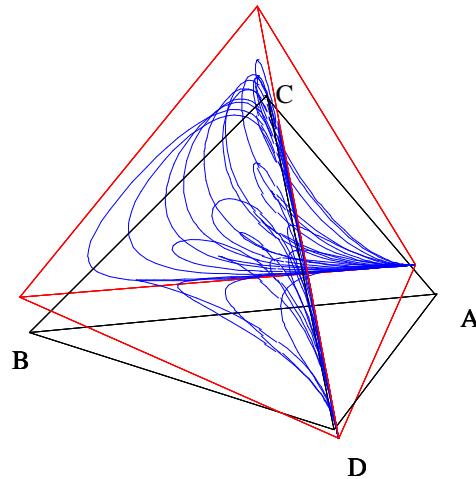


**Figure 4.2: Quaternary Column Profile Map for  $X_{\Delta k} = [0.3, -0.2, -0.3]$  and  $R_{\Delta k} = 9$ .**

**Note: D – Heavy Pure Component, A – Light Pure Component, B– Light Intermediate Pure Component, C – Heavy Intermediate Pure Component.**

The position of these stationary points and boundaries for a particular system are dependent on  $X_{\Delta k}$  and  $R_{\Delta k}$ . For a set  $R_{\Delta k}$ , the stationary points can be ‘shifted’ around the composition space by varying  $X_{\Delta k}$ . Similarly, by setting a constant  $X_{\Delta k}$ , the stationary points can be ‘shifted’ around, on pinch point curves, by varying  $R_{\Delta k}$ . As  $R_{\Delta k}$  tends to infinity, the stationary points tend to the residue curve map stationary points, which are the pure components on the mass balance triangle (MBT). The DPE collapses to the general form of the residue curve equation, given by equation 2.2 below. The boundaries for these conditions, for the CPM lie on the axes and the CPM becomes topologically equivalent to a residue curve map (RCM).

$$\frac{dX}{dn} = (X - Y^*(X)) \quad (4.5)$$

This shows that the CPM is a ‘transform’ of the RCM. By analysing the stationary points for the quaternary system, fifteen regions of  $X_{\Delta k}$  placement result in qualitatively different CPMs. These fifteen regions correspond to regions of the RCM with differing topology. The fifteen different regions can be seen in

Figure 4.3 a, b and c. Due to the fact that we are dealing with a 4 component system, these regions are better seen when separated by planes as illustrated in Figure 4.3a, which is the isometric drawing of the combined planes in the mass balance space.

Figure 4.3b is the top view as shown by the downward arrow of the isometric view.

Figure 4.3c is the bottom view as shown by the upward arrow of the isometric view. Figure 4.4 shows the Mass Balance Triangle (MBT) for a quaternary system, with the lines extending through the respective nodes. A CPM (plotted for a finite reflux) is merely a simple transform of the RCM (plotted at infinite reflux) and the form of the RCM topology is completely retained at finite reflux. This allows one to simplify the calculations by plotting the locations of the stationary point solutions only. By extending lines between the analytically determined quaternary, constant relative volatility stationary points, we can produce a ‘transformed tetrahedron’ ( $TT_4$ ). All the topological information about a CPM for a set of conditions ( $X_{Ak}$  and  $R_{Ak}$ ) can be shown and is retained by plotting the  $TT_4$  (see Figure 4.2).

#### 4.2.1 Quaternary System Boundary definition

The six boundaries (see Figure 4.4) which are defined by four planes (see Figure 4.3) which arise from the four surfaces of the quaternary Gibbs tetrahedron, produces fifteen regions where a  $X_{Ak}$  placement in each of these regions produce qualitatively different CPM. These fifteen regions correspond to regions of the RCM with differing topology. These six boundaries will be referenced several times in the chapter and are worth labelling. The boundary between the unstable node (Pure A) and the first light intermediate (Pure B) will be referred to as the light–light intermediate axis or (L–LI).

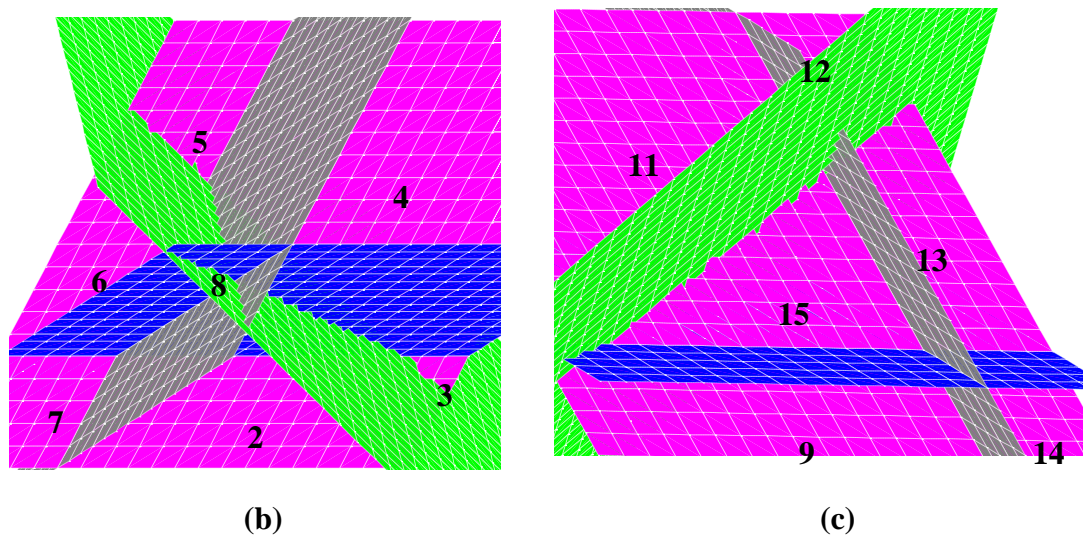
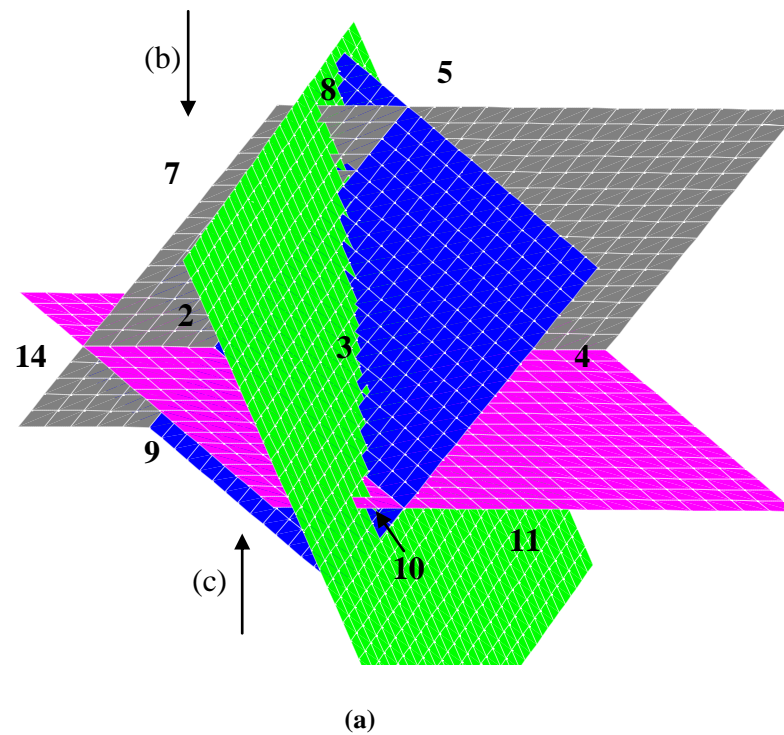
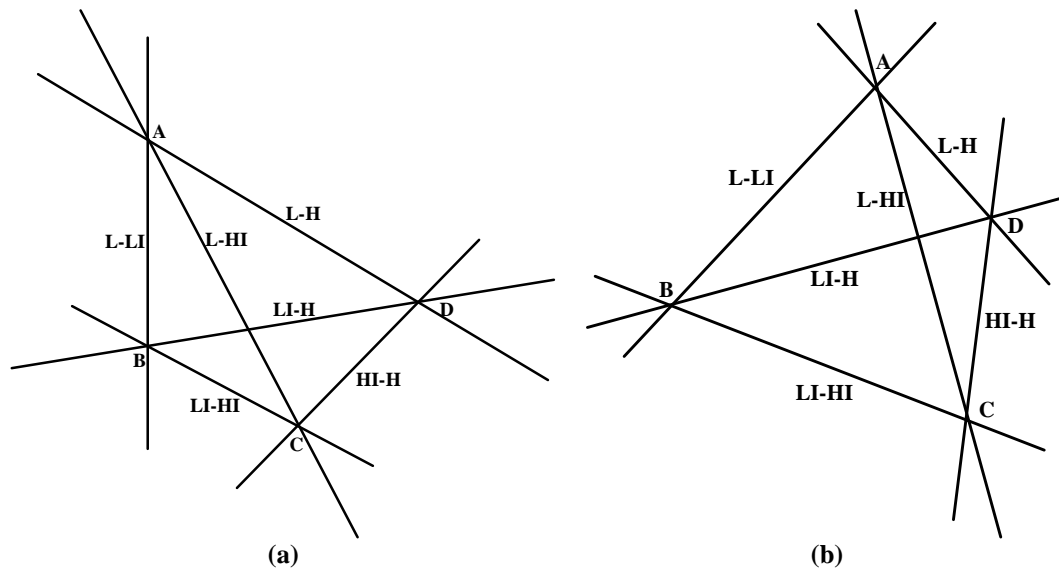


Figure 4.3: Fifteen regions of the RCM with differing topology.

The boundary between the first light intermediate saddle (Pure B) and the second light intermediate saddle (Pure C) will be referred to as the light intermediate–heavy intermediate axis or (LI-HI axis). The boundary between the second light

intermediate saddle (Pure C) and the stable node (Pure D) will be referred to as the heavy intermediate–heavy axis or (HI-H axis). The boundary between the unstable node (Pure A) and the stable node (Pure D) will be referred to as the light–heavy axis or (L-H axis).



**Figure 4.4: (a) Quaternary right angled tetrahedron boundary definitions. (b) Quaternary equilateral tetrahedron boundary definitions**

The boundary between the unstable node (Pure A) and the second heavy intermediate saddle node (Pure C) will be referred to as the light–heavy intermediate axis or (L-HI axis). And finally the boundary between the first light intermediate saddle node (Pure B) and the unstable node (Pure D) will be referred to as the light intermediate - heavy axis or (LI-H axis). Figure 4.4 illustrates these boundary definitions. Figure 4.4 (b) is a transform of Figure 4.4 (a) from a right angle tetrahedron to an equilateral tetrahedron.

#### 4.2.2 Properties of internal material

$\Delta_k$  which is defined as the difference between the vapour and liquid flows in  $CS_k$  is a net flow of material within the column section. This net flow can be thought

of as a pseudo stream flowing up or down the CS. If  $V_k > L_k$ , then  $\Delta_k > 0$  and therefore a net flow or pseudo stream flowing up is achieved in the  $CS_k$ . But if  $V_k < L_k$ , then  $\Delta_k < 0$  and thus a net flow or pseudo stream flowing down is achieved in the  $CS_k$ . The value of  $\Delta_k$  is constant within a  $CS_k$  and is thus the same at any point along the length of the  $CS_k$ .

The difference point ( $X_{\Delta k}$ ) can be thought of as the pseudo composition vector of  $\Delta_k$ , and being a difference between two compositions is physically valid anywhere in composition space – both inside and outside the MBT. Because  $X_{\Delta k}$  is a pseudo composition, the elements must sum to 1 i.e.  $\sum_{i=1}^C X_{\Delta k-i} = 1$ .  $X_{\Delta k-i}$  is the composition of element  $i$  in the pseudo stream  $\Delta_k$  and  $\Delta_k X_{\Delta k-i}$  is the net flow of component  $i$  within  $CS_k$ . A positive value is a net flow of component  $i$  up and a negative value is a net flow of component  $i$  down the column section. If  $X_{\Delta k-i}$  is negative, the direction of the net flow of component  $i$  is opposite to that of the  $\Delta_k$  and the sum of the remaining components is greater than 1.

The reflux ratio is defined as the ratio of liquid flowing down the CS to the net flow in the CS. Because of its dependence on  $\Delta_k$ ,  $R_{\Delta k}$  can be either positive (when  $\Delta_k > 0$ ) or negative (when  $\Delta_k < 0$ ). CPMs generated for a fixed difference point and positive reflux ratios are qualitatively different from those generated with the same difference point and negative reflux ratio.

### 4.3 CPM Design Methodology

Holland et al (2004b) illustrated the design of the Petlyuk column at overall infinite reflux. As shown in the previous chapter as well as in this paper the finite reflux problem is dealt with in a similar way. The procedure cannot be employed directly due to the difficulty that arises when choosing operating parameters (such as reflux ratios) for the pre-fractionator. The general idea, nevertheless, is fundamental to our methodology. The column will be broken into column sections

in a similar way. Difference points will then be chosen for each of the column sections where the degrees of freedom are available to do so. Feasibility of designs will always be determined by the superimposition of CPMs for each section. A feasible design is one which the appropriate profiles (liquid and/or vapour) intersect to yield a fully integrated process.

To simplify the task a sharp-split specification on all products will be made. The non-sharp split and variations of that will be addressed in future work.

It will be shown that, by employing the design methodology it is possible to find all solutions (if they exist) for a particular overall column reflux ratio (i.e. rectifying reflux ratio) and product choice. When feasible solutions do not exist, the method allows the designer to determine when or why they do not exist. Furthermore, analysis of the column using the method allows a minimum overall column reflux ratio to be determined which is discussed in the chapter that follows.

#### **4.4 Column Section Breakdown**

The design process will be initiated by breaking the Kaibel column down into column sections. A schematic representation of the column can be seen in Figure 4.5 below. The CPM technique enables one to apply the column section breakdown approach used by Tapp et al (2004a) to identify individual column sections within the configuration. Tapp et al (2004) defined column sections as lengths of column between points of addition or removal of material and/or energy. Using this definition, we can identify seven column sections in the configuration. The column section breakdown is seen in Figure 4.6 below.

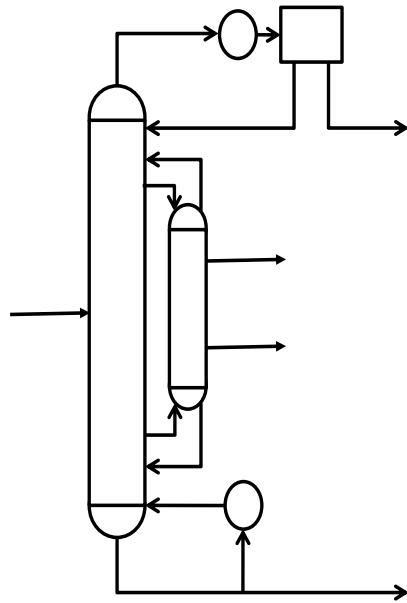


Figure 4.5: Kaibel column (main column with post-fractionator).

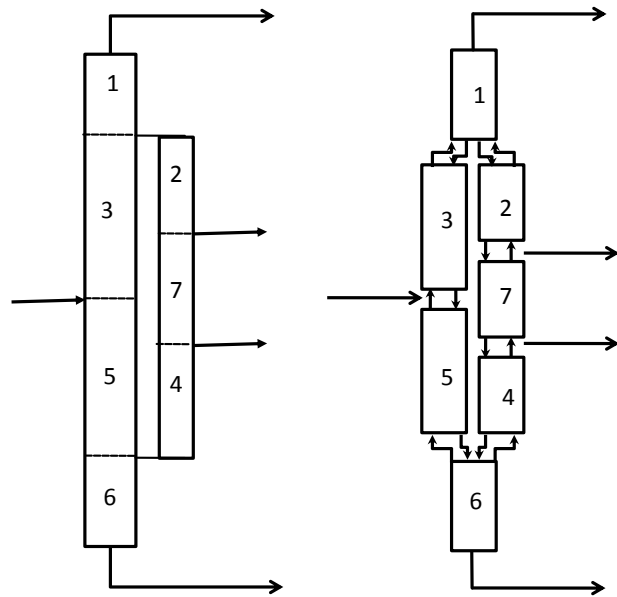


Figure 4.6: Column section breakdown for the Kaibel column

If a Single Dividing Wall Column (DWC) were utilised, the CS breakdown would be exactly the same. The fact that the definition of a DWC is that of a Thermally Coupled Column when taking into consideration that there is no or minimal energy transfer across the dividing wall, it would be expected that the CS breakdown would be exactly the same.

Column section 1 (CS1) is a standard rectifying section terminated by a total or partial condenser. Column section 6 (CS6) is a standard stripping section terminated by a total or partial reboiler. The group of column sections from 2-7 will be referred to as the “*coupled column sections*”.

## 4.5 Net Flow and Mass Balances in the Kaibel Column

As discussed previously, the net flow ( $\Delta_k$ ) is defined as the difference between the vapour and liquid flows in CS $k$  is the net flow of material within the CS and can be thought of as a pseudo stream. Because of this the net flow has to obey material

balances. When a material balance is performed around the feed point (between CS3 and CS5), we can see that this statement holds (Figure 4.7).

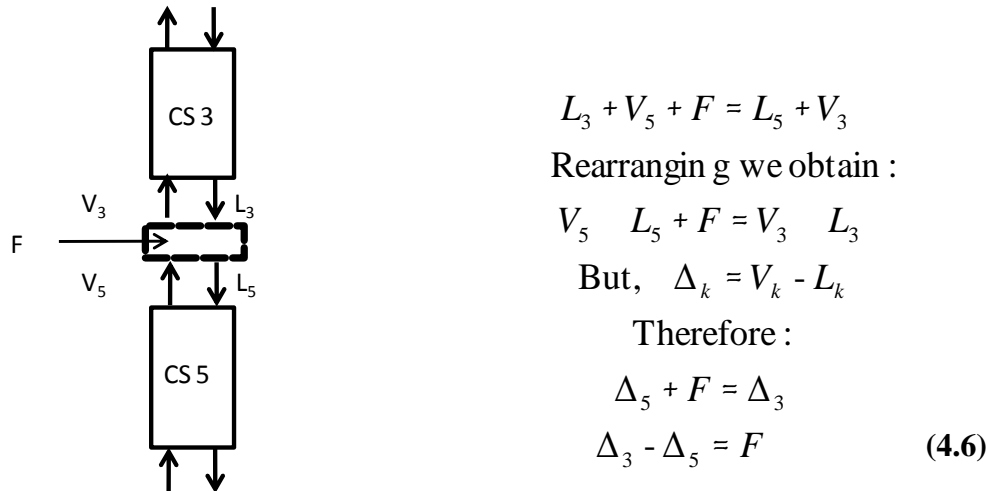
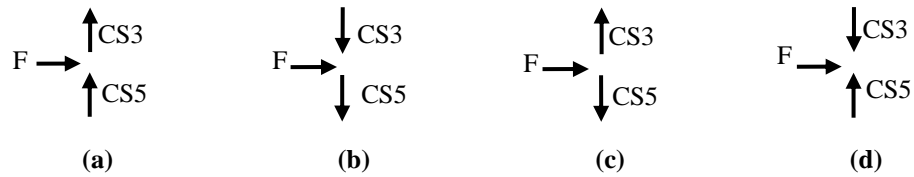


Figure 4.7: Kaibel column feed point material balance

As mentioned previously, the  $\Delta_k$  can be either positive or negative depending on the magnitude of liquid and vapour in CS $k$ . Thus, there are several combinations of positive or negative  $\Delta_3$  and  $\Delta_5$  values that would satisfy Equation 4.6. If  $\Delta_3$  and  $\Delta_5$  were both positive, they would satisfy Equation 4.6, as would certain negative values.  $\Delta_3$  could also be positive and  $\Delta_5$  negative. Negative  $\Delta_3$  and positive  $\Delta_5$  values, however, would not satisfy the material balance and is regarded as '*infeasible*'. The feasible net flow scenarios are illustrated in Figure 3.7 a-d below. The results in this section are analogous to the Petlyuk solution shown in the previous paper in this series.

COLUMN SECTION 3 AND 5: Taking into consideration that the reflux ratio is a function of the net flow in a CS, implies that there are multiple reflux ratio combinations possible for the Kaibel Column. Thus, these combinations of reflux ratios result in multiple qualitatively different CPM selections that may be employed for design. We can also say that a selection of net flow combinations may or may not be advantageous to the separation. Let us now take a look at flow combinations for the remaining CS mixing points within the Kaibel Column.



**Figure 4.8: Feasible net flow patterns at the point of feed addition. (a)  $\Delta_3 > 0$ ,  $\Delta_5 > 0$ , Feasible. (b)  $\Delta_3 < 0$ ,  $\Delta_5 < 0$ , Feasible. (c)  $\Delta_3 > 0$ ,  $\Delta_5 < 0$ , Feasible. (d)  $\Delta_3 < 0$ ,  $\Delta_5 > 0$ , Infeasible.**

COLUMN SECTION 1, 2 AND 3: CS1 is a rectifying section and produces the distillate product. The distillate flow is equal to the net flow in CS1 as they are defined in the same way. To produce any product from CS1, the vapour flow in CS1 has to be greater than the liquid flow, which makes  $\Delta_1 > 0$ . CSs 2 and 3 net flows may either be positive or negative. These various combinations of net flows are seen in Figure 4.9 a-d.

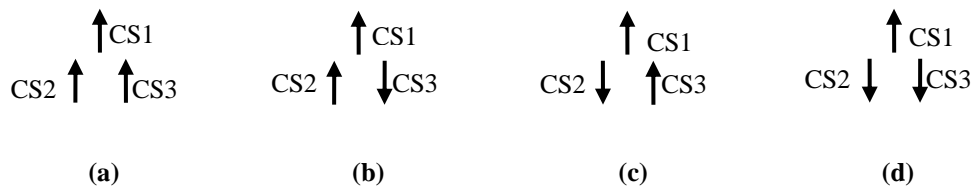


**Figure 4.9: Feasible net flow patterns at the mixing point of the rectifying section. (a)  $\Delta_2 > 0$ ,  $\Delta_3 > 0$ , Feasible. (b)  $\Delta_2 > 0$ ,  $\Delta_3 < 0$ , Feasible. (c)  $\Delta_2 < 0$ ,  $\Delta_3 > 0$ , Feasible. (d)  $\Delta_2 < 0$ ,  $\Delta_3 < 0$ , Infeasible.**

COLUMN SECTION 2 AND 7: CS2 and 7 are responsible for achieving the light intermediate product, and just like the mixing point discussed, these section's net flow may either be positive or negative and produce feasible and infeasible net flow combinations. The various flow combinations can be seen in Figure 4.10 a-d.

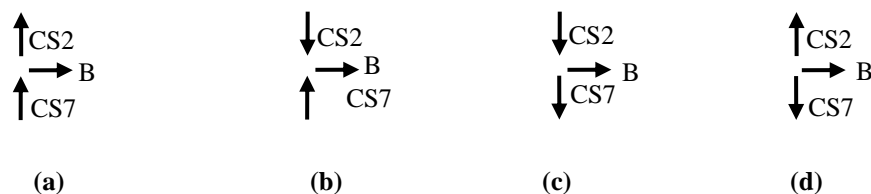


**Figure 4.10: Feasible net flow patterns at the first side draw. (a)  $\Delta_2 > 0$ ,  $\Delta_7 > 0$ , Feasible. (b)  $\Delta_2 < 0$ ,  $\Delta_7 > 0$ , Feasible. (c)  $\Delta_2 < 0$ ,  $\Delta_7 < 0$ , Feasible. (d)  $\Delta_2 > 0$ ,  $\Delta_7 < 0$ , Infeasible.**

COLUMN SECTION 4 AND 7: CS4 and 7 are responsible for achieving the heavy intermediate product. The net flows in these sections may once again be either positive or negative. The various flow combinations can be seen in Figure 4.11 a-d.



**Figure 4.11: Feasible net flow patterns at the second side draw. (a)  $\Delta_4 > 0$ ,  $\Delta_7 > 0$ , Feasible. (b)  $\Delta_4 < 0$ ,  $\Delta_7 > 0$ , Feasible. (c)  $\Delta_4 < 0$ ,  $\Delta_7 < 0$ , Feasible. (d)  $\Delta_4 > 0$ ,  $\Delta_7 < 0$ , Infeasible.**

COLUMN SECTION 4, 5 AND 6: CS6 is a stripping section and produces the bottoms product. The bottoms flow is equal to the net flow in CS6 as they are defined in the same way. To produce any product from CS6, the vapour flow in CS6 has to be smaller than the liquid flow, thus making  $\Delta_6 < 0$ . CSs 4 and 5 net flows may either be positive or negative. These various combinations of net flows are seen in Figure 4.12 a-d.

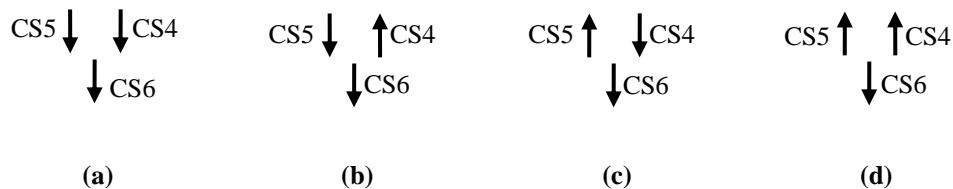


**Figure 4.12: Feasible net flow patterns at the mixing point of the stripping section. (a)  $\Delta_4 < 0$ ,  $\Delta_5 < 0$ , Feasible. (b)  $\Delta_4 > 0$ ,  $\Delta_5 < 0$ , Feasible. (c)  $\Delta_4 < 0$ ,  $\Delta_5 > 0$ , Feasible. (d)  $\Delta_4 < 0$ ,  $\Delta_5 < 0$ , Infeasible.**

A conventional column with a rectifying and stripping section will only have net flow up in the rectifying and down in the stripping section. But, by combining feasible net flow configurations above and disregarding those that are infeasible, we see that 'six net flow patterns in the Kaibel Column' are in fact possible. It will be sufficient to say that, these six different flow patterns will allow us to sample profiles from a wider range of qualitatively different CPMs. The above mentioned

flow patterns, are named net flow pattern (FP) 1 through 5 and are illustrated in Figure 3.11a-f. FP 3 consists of two flow patterns, due to the fact that the net flow in CS7 changes direction; negative in FP 3a and positive in FP 3b, whilst the remaining sections net flow direction are the same.

Physically these flow patterns are induced by control on the vapour and liquid split ratios into the coupled column sections (CS2-7) from the stripping and rectifying sections, respectively. The net flow of material within the column can also be thought of in terms of the distributions of feed material (Holland et al. (2010)). In FP 3b (Figure 3.11d) the feed is distributed between the top and bottom half of the entire column, so that there is a net flow of material in both direction where material flows in a circular motion in the coupled CSs and meets at the mixing point of CS2 and 7. If material were to be directed to the bottom half of the column, FP 4 would be achieved (Figure 3.11e). In order to maintain mass balances, the material needs to be directed upwards on the product side in CSs 2, 7 and 4. This is due to the fact that the side-draw flow rates are not large enough to change the direction of the net flow from CS4 through to CS2. If material were to be directed to the top half of the column, FP 2 would however be achieved (Figure 3.11b). In order to maintain mass balances, the material needs to be directed downwards on the product side for the same reasons as above and is the exact opposite of FP4.

If less material than described above were to be directed to the top half of the column, FP 3a (Figure 3.11c) would be achieved, where CS7 net flow direction would change (negative) due to the fact that the light intermediate flow is not large enough to change the direction in CS7. By increasing the material directed to the top half of the column even more, FP 1 (Figure 3.11a) will be achieved. Where the material circulates in a clock wise direction in the coupled sections, where the net flow in CS5 is upwards. Conversely, if a large amount of material were directed to the bottom half of the column, FP 5 (Figure 3.11f) would be achieved where material circulates in an anti-clockwise direction.

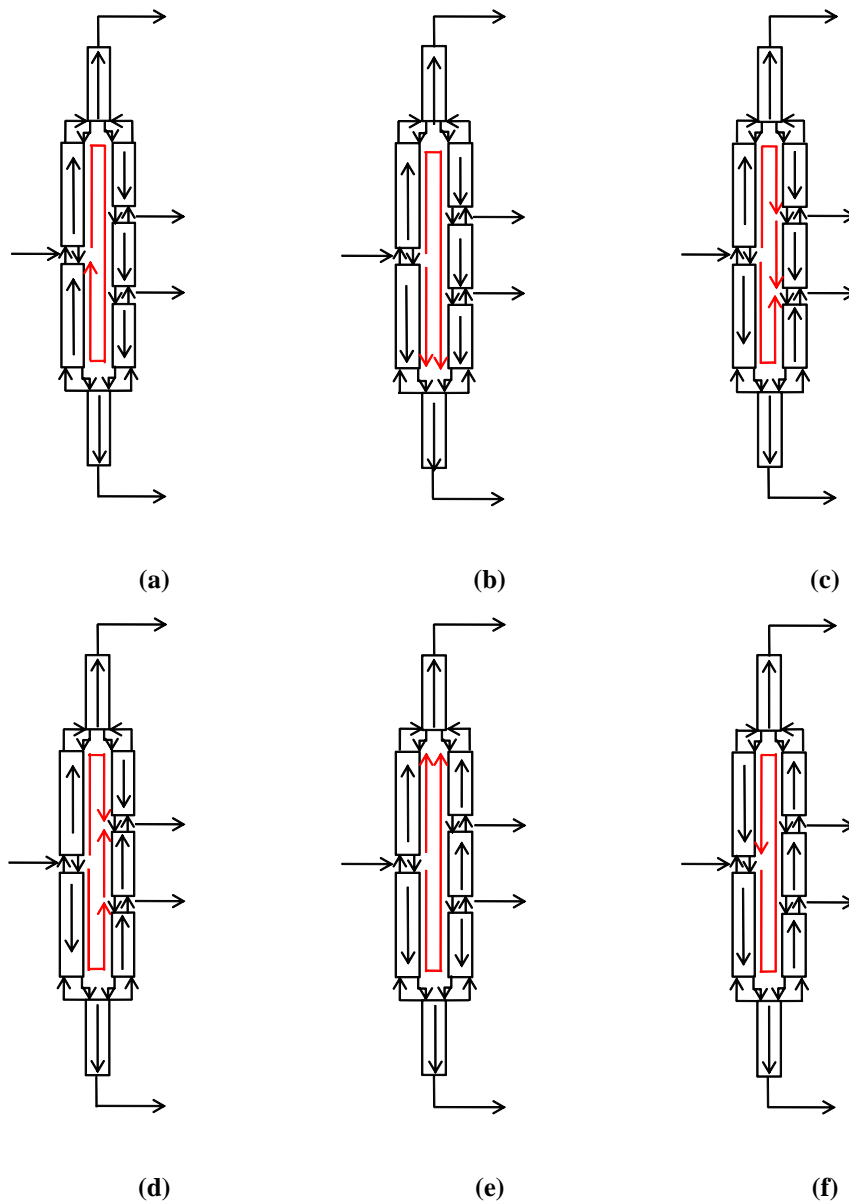


**Figure 4.13: Various Flow patterns that arise due to feasible net flow combinations. (a) Flow Pattern 1. (b) Flow Pattern 2 (c) Flow Pattern 3. (d) Flow Pattern 4. (e) Flow Patter 5. (f) Flow Pattern 6.**

The largest drawback to the configuration being operated with net flow patterns 1, 2, 4 and 5 (Figure 3.11a, b, e and f) is that the net flows in the column section adjacent to the side draws are in the same direction. This means these sections will result in the reflux ratios having the same sign. Side-draws have the effect of lowering the reflux from one column section to the other. If the refluxes for CS2, 4 and 7 all are negative, the reflux of CS4 will have a larger magnitude than that

of CS7 and the reflux of CS7 will have a larger magnitude than that of CS2. If the magnitude of the reflux of CS2 is to be large enough to have the column operating on specification, the CS7 reflux must be very high and thus CS4 even higher. This ultimately means that CS1 and CS6 must operate at a fairly high reflux and the column will be very energy intensive. This is also true if the refluxes are positive. It can thus be deduced that FP3 (as was similarly done by Holland et al. (2010)) that Petlyuk Column equivalent net flow pattern 3 does not have this drawback and is therefore likely to be the most energy efficient operating mode. This will hold for the Kaibel Column under the same argument.

## 4.6 Difference Point and Mass Balances in the Kaibel Column

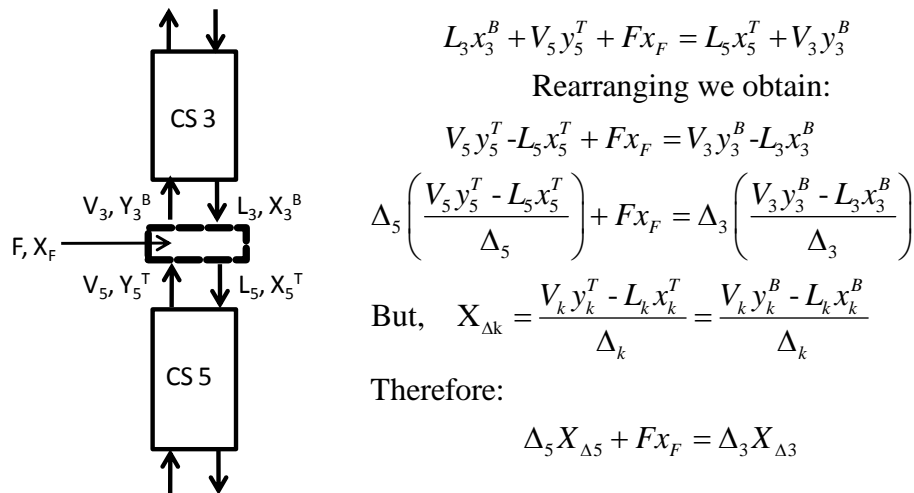


Figure 4.14: Kaibel column feed point component material balance.

The difference point ( $X_{\Delta k}$ ) is physically valid anywhere in composition space, so they have to obey mixing rules as conventional compositions do. By doing a component material balance at the feed point (CS3 and CS5), we can see that this is true Figure 4.14

We can see, that this result is the equivalent to the difference points  $X_{\Delta 3}$  and  $X_{\Delta 5}$  lying on a straight line through  $x_F$  in composition space. Their positions relative to one another are dependent on the net flow of CS3 and CS5 governing them. This is true for all mixing points in the column e.g.  $X_{\Delta 2}$ ,  $X_{\Delta 7}$  and  $X_B$  will be on a straight line in composition space as well. This means mass balances will govern our selection of  $X_{\Delta k}$  positions in the system. The use of this idea will be explored in more detail later.

## 4.7 Kaibel Column Composition Matching Criteria

Composition matching criteria is a pre-requisite for the designer and is required at all mixing points. We will now show and discuss the criterion by using the CS breakdown and piece together column profiles that intersect at the correct compositions.

MATCHING CRITERIA 1: As discussed earlier, CS1 is a rectifying section and is responsible for achieving a product, namely the distillate. The liquid leaving the bottom of CS1 divides to CS2 and CS3. It is possible to say that the liquid profiles from sections 1, 2 and 3, thus, have to intersect within the composition space. If CS1 was not a rectifying section, the superimposed CPMs of the three column sections in question would be feasible at any three intersecting profiles. I.e. any three intersecting profiles from these maps would be possible solutions to the three-column section system. The situation is somewhat simplified by the fact that CS1 is a rectifying section. Only one profile is valid, because this is the section that has to operate on profiles that passes through the distillate composition or the composition in equilibrium with this stream. However, any liquid profiles from the CPMs of CS2 and CS3 intersecting on CS1 profile at one point are valid.

MATCHING CRITERIA 2: The profiles intersection of CSs 2 and 7 have to occur at the light intermediate side draw composition. Due to the fact that there is no

composition change in either vapour or liquid composition when drawing components out the bottom of CS2 and top of CS7 where these profiles intersect, both the liquid and vapour profiles have to intersect for CS2 and CS7. If material had to be added to either the liquid or vapour streams, this would not hold.

MATCHING CRITERIA 3: The profiles intersection of CSs 4 and 7 have to occur at the heavy intermediate side draw composition. As discussed in Matching Criteria 2, due to the fact that there is no composition change in either vapour or liquid composition when drawing components out the bottom of CS7 and top of CS4 where these profiles intersect, both the liquid and vapour profiles have to intersect for CS4 and CS7. If material had to be added to either the liquid or vapour streams, this would not hold.

MATCHING CRITERIA 4: As discussed earlier, CS6 is a stripping section and is responsible for achieving a product, namely the bottoms. The vapour leaving the top of CS6 divides to CS4 and CS5. It is possible to say that the vapour profiles from sections 4, 5 and 6, thus, have to intersect within the composition space. If CS6 was not a stripping section, the superimposed CPMs of the three column sections in question would be feasible at any three intersecting profiles as with the liquid profiles of matching criteria 1. Thus, only one profile is valid, the profiles that pass through the distillate composition or the composition in equilibrium with this stream. And any vapour profiles from the CPMs of CS4 and CS5 intersecting on CS6 profile are valid.

MATCHING CRITERIA 5: CS 3 and CS 5 liquid or vapour profiles have to intersect, depending on the nature of the feed. Due to the fact that the bottom of CS3 and the top of CS5 is a point of feed addition and we assume instantaneous perfect mixing from section to section, the sum of individual compositions have to lie on a straight line as discussed in the previous section. Thus, with the current assumptions as well as assuming that there is no mass transfer from the vapour to the liquid streams, at the point of feed input, if the feed is liquid, the vapour

profiles of CS3 and CS5 must intersect. Conversely, if the feed is vapour, the liquid profiles of CS3 and CS5 have to intersect.

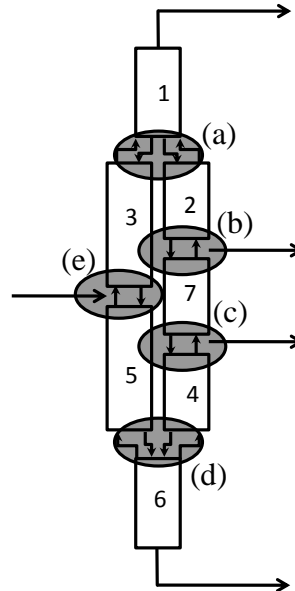


**Figure 4.15: The Range of Matching Criterion. (a) Matching Criteria 1. (b) Matching Criteria 2. (c) Matching Criteria 3. (d) Matching Criteria 4. (e) Matching Criteria 5.**

It is important to note that, if we superimpose CPMs to determine where the matching criteria are satisfied, we need not worry about satisfying the material balance and finding associated compositions of the other phase as they are a result of the superimposed CPMs. These will automatically be satisfied and can easily be calculated, if required, using the definitions of the difference point and net flow of the particular CS.

## 4.8 Sharp Splits and related Feasible Topology

In this work, we will look at the sharp split solution, on all products, solution for the Kaibel Column. This means that we have significantly reduced the complexity of the problem by setting a product specification to unity or close to unity. Restrictions, like the sharp split solution, enables one to determine the exact

position of all viable column section profiles for any set of parameters. Before continuing, it will be useful to specify exactly what is meant by sharp split and define individual sharp split products.

- A sharp distillate product specification is one in which the light and light intermediate components appear in finite quantities, but the heavy intermediate and heavy component appears in infinitesimal quantities.
- A sharp bottoms product specification is one in which the heavy and heavy intermediate components appear in finite quantities, but the light and light intermediate components appears in infinitesimal quantities.

The heavy and light intermediate side draws sharp split have several definitions. Let us first look at the light intermediate.

- The light intermediate side-draw product can be sharp in terms of the light component, which is, infinitesimal light component material but finite heavy and light intermediate.
- Sharp in terms of the heavy intermediate component. Infinitesimal heavy intermediate component material but finite light intermediate and light component material present in the product.
- Sharp in terms of both, light and heavy intermediate components, which is, effectively pure intermediate component material.

The heavy intermediate side draws sharp split are as follows.

- The heavy intermediate side-draw product can be sharp in terms of the light component, which is, infinitesimal light intermediate component material but finite heavy and light intermediate components.
- Sharp in terms of the heavy component. Infinitesimal heavy intermediate component material but finite light intermediate and heavy component material present in the product.
- Sharp in terms of both, light intermediate and heavy components. This is effectively pure intermediate component material. For this work, a *sharp light intermediate side-draw product specification* will be taken as one

which is sharp in terms of both the light and heavy intermediate components and a *sharp heavy intermediate side-draw product specification* will be taken as one which is sharp in terms of both the light intermediate and heavy components.

The definition of the sharp splits for all product draw off's as described above (light, light intermediate, heavy intermediate and heavy products), are loosely defined in the same manner as Fien and Liu (1994) have. This comes from the use of direct and indirect splits for a given feed composition.

#### 4.8.1 Sharp Distillate and Bottoms Specifications

From the definition of sharp distillate product specifications, the distillate composition is confined to the light-light intermediate axis (L-LI) (see Figure 4.4). Holland et al. (2010) (Chapter 2) show by mass balance, that the distillate composition is equivalent to the difference point for CS1 ( $X_{AI}$ ) in the Petlyuk system. The exact same argument applies to the Kaibel Column, where,  $X_{AI}$  is a real composition and is confined to the L-LI axis.

Holland et al. (2010) show, for the Petlyuk system, that by analysing the movement of the transformed triangle ( $TT_3$ ) - while varying  $X_{\Delta k}$  (at constant  $R_{\Delta k}$ ), it is noticed that as the difference point is moved closer to an axis, the profile and one of the  $TT_3$  boundaries approach the axis and both eventually effectively coincide with the MB boundary.

For the 4 component system, when the difference point of CS1 is effectively on the axis, the same phenomenon occurs as it has to obey mass balance according to the DPE, and thus the transformed tetrahedron ( $TT_4$ ) boundary lies here too. Thus, the rectifying profile runs along the boundaries of this tetrahedron when the difference point is set on the boundary. The  $TT_4$  boundary, defined between the unstable node and the light intermediate saddle point, approaches the axis from negative heavier component space. Figure 4.16 illustrates this observable fact.

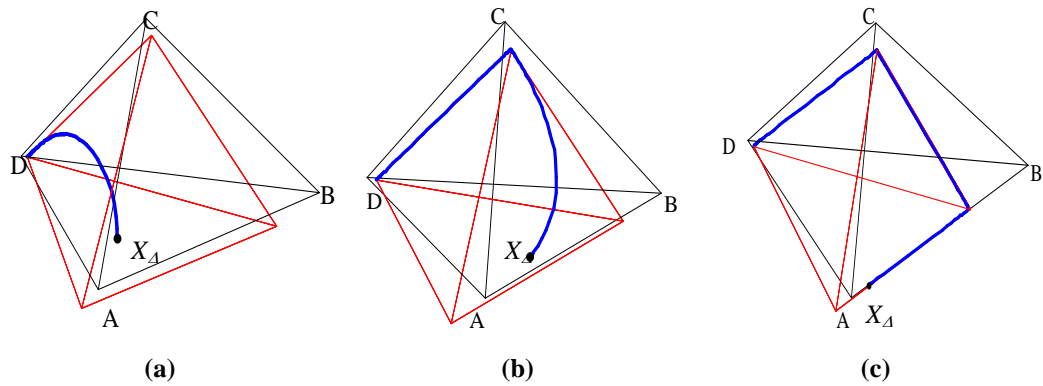


**Figure 4.16 a-c: Rectifying profiles for difference points at varying distances from the L-LI axis.**

The definition of sharp bottoms product specifications, stipulates that the bottoms composition is confined to the heavy intermediate-heavy axis (HI-H) (see Figure 4.4). Holland et al. (2009) shows that the bottoms composition is equivalent to the difference point for CS6 ( $X_{\Delta 1}$ ) in the Petlyuk system. Like the rectifying section, an analogous argument applies to the Kaibel Column, where,  $X_{\Delta 6}$  is a real composition and is confined to the HI-H axis.

If we analyse the stripping profile and CS6  $TT_4$ , in the same way as we did for the sharp distillate specification, we notice that as we move  $X_{\Delta 6}$  towards the HI-H axis the stripping profile and one of the  $TT_4$  boundaries move towards each other and the axis as well. When  $X_{\Delta 6}$  lies effectively on the axis, the  $TT_4$  boundary defined between the saddle-point and stable node lies here too and the stripping profile runs along the boundaries of this triangle. Figure 4.17 illustrates this occurrence.

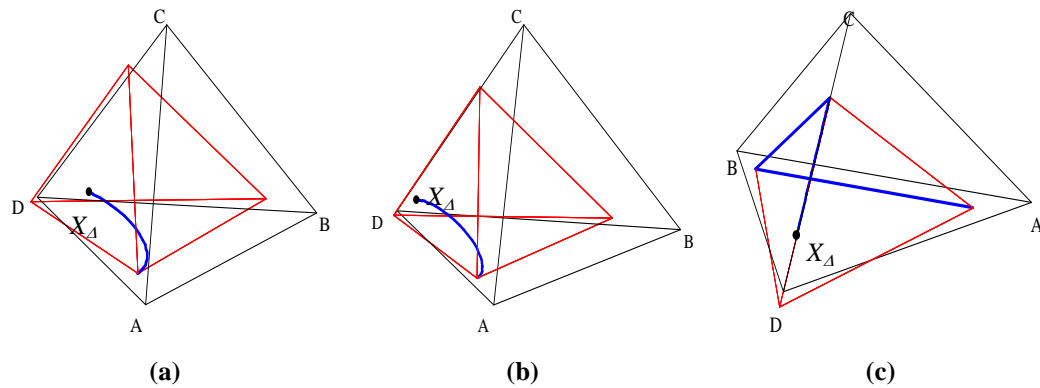


Figure 4.17 a-c: Stripping profiles for difference points at varying distances from the HI-H axis.

### 4.8.2 Sharp Side Draw Specifications

We have shown that the distillate and bottoms profiles have to run along the L-LI and HI-H respectively if the sharp specifications are to be met. Due to this, and the fact that CS2 have to satisfy matching criteria 1 and 2, it is possible to say that the profile of CS2 has to lie on the L-LI axis in-order to intersect with the distillate profile and the light intermediate side draw. Similarly, CS4 has to satisfy matching criteria 3 and 4, where CS6 profile runs along the HI-H axis. Thus, it is possible to say that CS4 profile has to run along the HI-H axis. CS7 profile will be dealt with in greater detail later.

### 4.8.3 Implications of Sharp Product Specifications on CS 3 and CS 5.

As discussed previously, mass balance govern our selection of  $X_{\Delta k}$  positions in the system. CS3 has to satisfy matching criteria 1 and 5. CS5 has to satisfy matching criteria 4 and 5. From this and taking into consideration that the other intersecting profiles are practically on the MB axes, CS3 and CS5 difference points must also lie on the MB axes. Due to the sharp split implications on the other coupled CSs, CS3 and CS5 will not only touch but run on their  $TT_4$  boundaries.

#### 4.8.4 $TT_4$ and Topological Effects of Sharp-Split Specifications.

We have discussed that, CS1 and CS6 have to lie on their respective axes and will effectively run along their  $TT_4$ . CS2 and CS4 profiles will also run along their respective boundaries in order to satisfy their matching criteria's. Clearly, for sharp split specifications, the topological effect is to force the compositional profiles of the CSs to operate on the boundaries of their respective  $TT_4$  i.e. by having specified a sharp split constraint, all CS profiles will operate on their  $TT_4$  boundaries. This means that we do not have to solve the entire CPM for each set of parameters chosen or given, but only the  $TT_4$  to immediately determine whether or not all the CS solutions will satisfy the matching criteria's and therefore produce a feasible column design. Instead of focusing on the intersection of many individual solutions, we can simply focus on the overlap of the  $TT_{4s}$  concerned.

### 4.9 Design parameters

There are multiple design variables and combinations of these variables that can be chosen in order to fully design a Kaibel Column. In the case of the Kaibel Column with a post-fractionator or pre-fractionator, and the thermodynamically equivalent single dividing wall column, many design parameters are eliminated due their relationship with limiting criteria of other parameters. This will be shown in sections which follow. The exact combination/s of design parameters that enable us to solve directly for a Kaibel solution will not be given, but rather, all the parameters than can be chosen in order to achieve a solution are shown below. These parameters are exactly the same as for the Petlyuk Column, but the Kaibel Column parameters have an additional side draw flow rate.

Some of the possible design variables include:

$R_{\Delta k}$  CS  $k$  reflux ratio

$X_{\Delta k}$  CS  $k$  difference point

---

D	Distillate flow rate
B	Bottoms flow rate
S <sub>1</sub>	First Side-draw flow rate
S <sub>2</sub>	Second Side-draw flow rate
L <sub>k</sub>	CSk internal liquid flow rate
V <sub>k</sub>	CSk internal vapour flow rate
$\Phi_V$	Vapour split ratio ( $V_2/V_1$ )
$\Phi_L$	Liquid split ratio ( $L_2/L_1$ )
$\Phi_V'$	Vapour split ratio ( $V_4/V_6$ )
$\Phi_L'$	Liquid split ratio ( $L_4/L_6$ )

It is important to note that the total required stages, feed stage and side-draw stage are not considered as design parameters when designing simple or complex columns using the CPM technique. These variables result as a solution from the process once all other necessary parameters have been specified. They can be determined by tracking variables in the difference point equation (Equation 4.1) for any particular solution.

## 4.10 $X_{\Delta}$ Placements for the Kaibel Column

### 4.10.1 $X_{\Delta}$ Placement for the Distillate and Bottoms column sections

Column Section 1 is a rectifying section. Profiles for this section will run from the distillate composition, along the L-LI axis, getting rapidly richer in the light intermediate component and slowly richer in the heavy intermediate. As discussed before the profiles run along the boundaries of their TT<sub>4</sub>s as specified by sharp split constraints and should therefore run through the light intermediate saddle point composition of its TT<sub>4</sub>. We know that the profiles must pinch within the MBT by analysing the, positive reflux, pinch point curves for qualitatively different  $X_{\Delta k}$  placement produced by Tapp et al. (2004) and Holland et al. (2010).

The stable nodes of CPMs, produced for difference points within difference point region 1, always lie within the MBT for ideal systems.

Solutions for the stripping section (CS6) will behave in the same way with respect to the heavy intermediate composition moving away from the product (in this case the bottoms composition) and will deviate from the HI-H axis at a saddle point but now becoming rapidly richer in the light intermediate component. The stripping profiles will pinch at unstable nodes within the MBT. This is ascertained, again, by consulting the pinch point curves (for negative reflux ratios) produced by Tapp et al (2004) and Holland et al. (2010).

#### 4.10.2 $X_{\Delta}$ Placement for the Coupled Column Sections

If we consider that CS2 and CS7 are required to achieve a product specification, light intermediate, it is logical that the difference point of either of these two sections is chosen such that the light intermediate product composition can be achieved.

To determine the optimal placement of  $X_{\Delta 2}$  the requirements of this column section must be understood. Firstly, CS2 is required to achieve a particular composition, specifically the first side-draw composition; therefore the CPM for CS2 must provide trajectories which intersect this composition point. Secondly, the profile is required to intersect the rectifying profile; therefore it should run from the first side-draw composition, close to the L-LI axis and cross the rectifying profile.

From a material transport perspective, the main purpose of CS2 is the transport of the light intermediate component to the first side-draw. If the side-draw composition is required to be very “pure”, CS2 should not transport large quantities of light, heavy intermediate or heavy component material i.e. the pseudo composition of the net flow ( $X_{\Delta 2}$ ) should have a high light-intermediate component percentage. High purities are possible in a column section even if the net flow does involve large “impurity” flows because a single phase can be

sampled. This can be explained if we consider that at a difference point the vapour and liquid compositions are equal, but as compositions away from the difference point are sampled a “gap” opens up between the vapour and liquid compositions.

Decreasing the difference point impurities would improve overall performance, and by the simple logic, if there is a smaller net flow of “impurity” material through the section, there is less to be separated from the light intermediate component. If we consider this argument only, the difference point for CS2 should be placed in the vicinity of the intersection of the L-LI, LI-HI and LI-H axes.

If we tighten the product specification constraints and specify that the first side draw has to be very pure in light-intermediate component and do the same for the heavy intermediate component with regard to the second side draw, we can say that CS7 has to separate only the light intermediate and heavy intermediate as well as satisfy matching criteria 2 and 3. Understanding that CS7 is a binary separation, we can conclude that CS7 profile is confined to the LI-HI axis only, and that its difference point, if it exists, will be placed on this axis.

CS4 is required to achieve a particular composition, specifically the second side-draw composition; therefore the CPM for CS4 must provide trajectories which intersect this composition point. Secondly, the profile is required to intersect the stripping profile; therefore it should run from the second side-draw composition, close to the HI-H axis and cross the stripping profile.

From a material transport perspective the main purpose of CS4 is the transport of the heavy intermediate component to the second side-draw. If the side-draw composition is required to be very “pure”, CS4 should not transport large quantities of light, light intermediate or heavy component material i.e. the pseudo composition of the net flow ( $X_{\Delta 4}$ ) should have a high heavy-intermediate component percentage. As explained with CS2, decreasing the difference point impurities would improve overall performance, and by the simple logic, if there is a smaller net flow of “impurity” material through the section, there is less to be separated from the heavy intermediate component. Again, if we consider this

argument only, the difference point for CS4 should be placed near the intersection of the LI-HI, L-HI and HI-H axes.

Let us now take into consideration the linear mixing rules of difference points to finally determine CS2 and CS4  $X_A$ 's. The placement of  $X_{A2}$  affects the placement of the  $X_{A4}$  due to the fact that a profile exists that connects these sections and obeys matching criteria 2 and 3, named CS7. By limiting the description and possible solutions to sharp split and confining CS2 profile to the L-LI axis and CS4 profile to the HI-H axis, we can see from Figure 4.18 a, that, by shifting the difference point of CS2 onto this axis, CS4 difference point shifts off the HI-H axis, into region 7 composition and therefore does not satisfy sharp split conditions due to component material balance constraints. As we move  $X_{A2}$  closer to the pure light intermediate (closer to Pure B), we can see from Figure 4.18b that the sharp split criteria for CS4 is becoming more realistic. When the difference point of CS2 is on the pure light intermediate component, it will thus force the difference point of CS4 to lie on the pure heavy intermediate.

With this knowledge and taking into consideration that CS7 is a binary separation between light and heavy intermediates as described, we can finally conclude, that, the only way to satisfy sharp split conditions for both intermediate products is to have the difference points of CS2 and 4 at the light and heavy intermediate pure compositions respectively (Figure 4.18b).

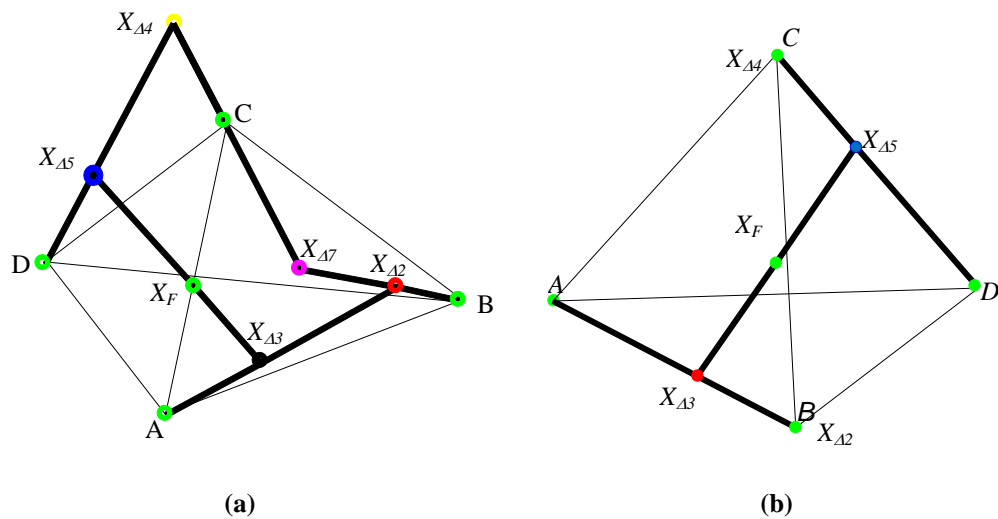


**Figure 4.18: Material balance for Kaibel Column. (a) Infeasible Material balance. (b) Feasible Material balance**

Holland et al. (2009) showed that, the relative positioning of the difference points is dependent on the net flow in each column section and subsequently the final positioning of the adjacent CS's difference points is a function of the remaining internal material balance variables in the Petlyuk configuration. We can speculate that due to the fact that we have six Net Flow Patterns and by the same logic above the relative positioning of the difference points for each of the CSs is dependent on the net flow in each CS and subsequently the final positioning of CS3 and CS5 difference points. This means  $X_{A3}$  and  $X_{A5}$  is fundamentally dependant on these Flow Patterns in the Kaibel configuration. If we take a closer look at Figure 4.18 b, we can see that this depicts a specific flow pattern, specifically FP 3. This is very interesting, as, any combination of information that describe a specific FP (FP 1, FP 2, FP 4 or FP 5) will always reduce to FP 3, if CS2 and CS4 difference points are at the pure components of the side draws. Determining which of the FP 3 will be utilised, FP 3a or FP 3b, is shown and discussed in greater detail later.  $X_{A3}$  is, however, constrained to the material balance line though the distillate composition ( $X_{\Delta 1}$ ) and  $X_{A2}$ , while  $X_{A5}$  is constrained to the material balance line through the bottoms composition ( $X_{\Delta 6}$ ) and  $X_{A4}$ . This means that because we already have CS1, CS2, CS4 and CS6

difference point placements, CS3 and CS5 difference points are predetermined for a given feed compositions and feed flow as shown by Equation 4.7.

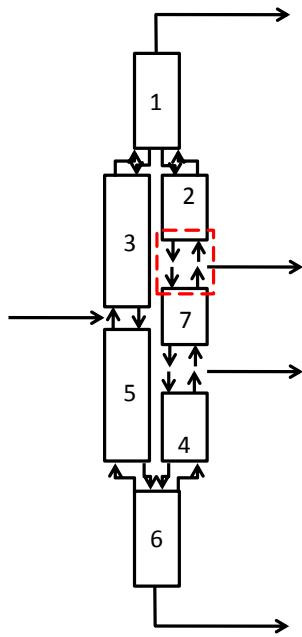
## 4.11 Consequences of $X_{\Delta}$ Placement on Net Flow

### 4.11.1 Implications on Net Flow

So far we have discussed and illustrated the difference point placements of the rectifying and stripping sections as well as some of the coupled column sections difference point placements, which we have established are “locked” for a set product specification, in our case, sharp split products and given feed conditions. We have recognized that the different FPs give rise to different relative difference point placement for all CSs. We will now, however, take a closer look at the effect the placements of these difference points have on the net flows in the CSs.

Let us start by doing a general component material balance around CS2 and CS7 mixing point, specifically for the light intermediate component, as illustrated below in Figure 4.19

We can see from this result that the net flow in CS7 is a function of its difference point for light intermediate component, first side draw flow rate and net flow in CS2 if the side draw is pure. Let us now extend this idea, and perform another component material balance, again on the light intermediate component around CS7 and CS4 which is illustrated in Figure 4.20 below.



$$L_2 X_{2,2}^B + V_7 Y_{7,2}^T = L_7 X_{7,2}^T + V_2 Y_{2,2}^B + S_1 X_{2,2}$$

Rearranging we obtain:

$$V_7 Y_{7,2}^T - L_7 X_{7,2}^T = V_2 Y_{2,2}^B - L_2 X_{2,2}^B + S_1 X_{2,2}$$

From the definition of the difference point and net flow that:

$$\Delta_7 X_{\Delta 7,2} = \Delta_2 X_{\Delta 2,2} + S_1 X_{2,2}$$

We know that:

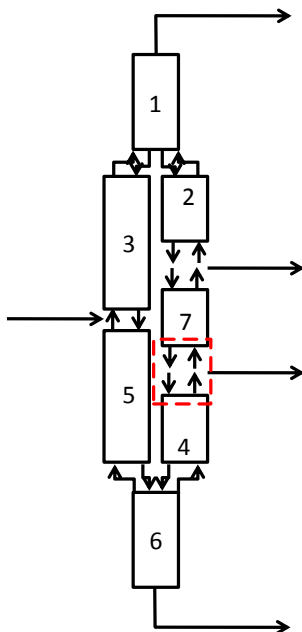
$$X_{\Delta 2,2} = X_{2,2} = 1$$

Therefore:

$$\Delta_7 = \frac{\Delta_2 + S_1}{X_{\Delta 7,2}}$$

(4.8)

**Figure 4.19: General Component Material Balance on Light Intermediate Component across CS2 and CS7.**



$$L_7 X_{7,B}^B + V_4 Y_{4,B}^T = L_4 X_{4,B}^T + V_7 Y_{7,B}^B + C X_{C,B}$$

Rearranging we obtain:

$$V_4 y_{4,2}^T - L_4 x_{4,2}^T = V_7 y_{7,2}^B - L_7 x_{7,2}^B + C x_{C,2}$$

From the definition of the difference point and net flow that:

$$\Delta_4 X_{\Delta 4,2} = \Delta_7 X_{\Delta 7,2} + C x_{C,2}$$

We know that:

$$X_{\Delta 4,2} = x_{C,2} = 0$$

Therefore:

$$\Delta_7 = 0$$

(4.9)

**Figure 4.20: General Component Material Balance on Light Intermediate Component over CS7 and CS4.**

This result shows that with sharp split specifications, the net flow in CS7 has to be zero. In other words, the vapour and liquid flows in this section are exactly the same. This means that Equation 4.9 can only be satisfied completely if  $X_{\Delta 7, 2}$  is infinitely big in Equation 4.8. Note that this result is only due to the net flow in CS7 being equal to zero and not visa-versa. Meaning that an infinitely big  $X_{\Delta}$  in CS7 did not formulate the net flow in CS7 zero, but rather, the zero net flow in CS7 induced a tendency for the difference point of CS7 to go to infinity.

This is a very powerful result, as we can now say that sharp split constraints can only be adhered to when the net flow in CS7 is zero ( $\Delta_7 = 0$ ), or rather, the flow of liquid and vapour between the light intermediate and heavy intermediate side draws has to be equal ( $V_7=L_7$ ).

From a graphical Net Flow Pattern point of view, CS7 net flow is omitted from the Pattern. Figure 4.21 shows FP 4 (as an example) with the missing flow in this section.

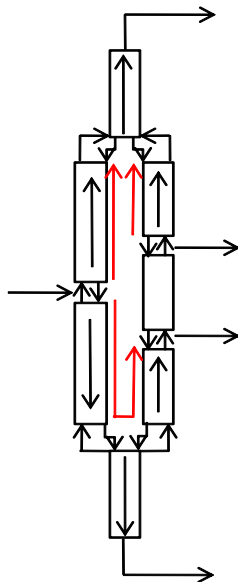


**Figure 4.21: Infeasible FP 4 with zero net flow in CS7.**

We mentioned previously that, if more material is directed to the bottom, in order to maintain mass balance, the material needs to be directed upwards on the product side in CSs 2, 7 and 4 (FP 4). This is due to the fact that the side-draw flow rates are not large enough to change the direction of the net flow from CS4 through to CS2. As we can see, this is impossible to achieve as the mass balance at the point where light intermediate product is drawn off will not hold (Infeasible). Taking a closer look at other flow patterns, other than FP 3, the same or similar impossibilities occur. Now no material is able to flow upwards above the light intermediate side draw, only downwards. For a sharp split Kaibel Column design, CS7 will always have a zero net flow, implying that CS2 net flow will be negative.

Extending this idea to the other net flows means that CS4 net flow has to be positive, CS3 net flow positive and CS5 negative. Thus only a combination of FP 3a and FP 3b is allowable and exact. Figure 4.22 illustrates this result in hierarchical manner. Figure 4.22 shows all the Net Flow Patterns including the CS7 zero net flow, which is called FP 3. On the right hand side of FP 3 are the FPs that will be achieved by having a net increase of material to the bottom half of the column with non-sharp splits. On the left hand side of FP 3 are the FPs that will be achieved by having a net increase of material to the top half of the column with Non-Sharp Splits. The non-sharp split case will be dealt with in later publications.

Previously, it was said that the largest drawback to the configuration being operated with the net flow patterns 1, 2, 4 and 5 (Figure 5.9a, b, e and f) is that the net flows in the column section by the side draws are in the same direction. By having a sharp split configuration, this eliminates this shortcoming completely.

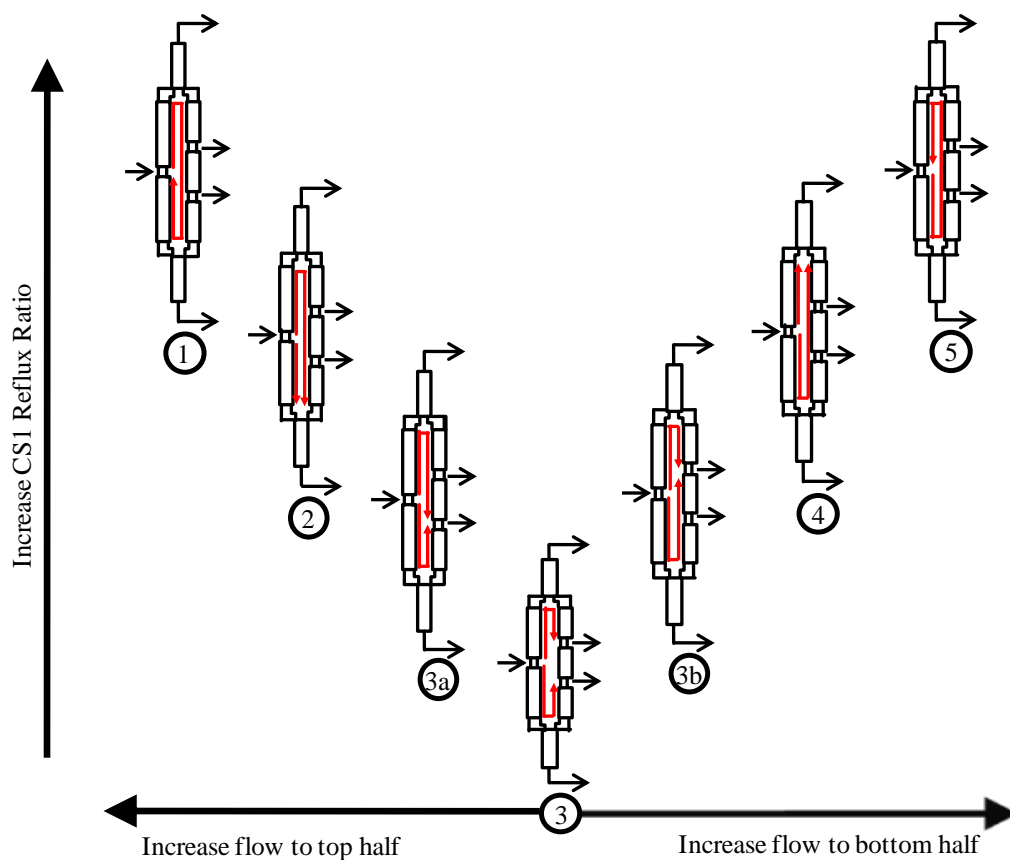


Figure 4.22: Sharp Split reduction diagram illustrating all the FPs for the Kaibel Column.

### 4.11.2 Zero Net Flow Implications on Column Section Profile

Holland et al. (2004c) illustrates the use of the DPE in the design of a complex column under infinite reflux condition ( $\Delta = 0$ ). They show how the original DPE reduces to the infinite reflux DPE as shown in Equation (4.10) below:

$$\frac{dx}{dn} = [X - Y^*(X)] + \delta_k \quad (4.10)$$

$$\text{Where } \delta_k = [Y_k^T - X_k^T] = [Y_k^B - X_k^B] \quad (4.11)$$

$\delta_k$  is the difference in composition between the vapour and liquid streams and is called the difference vector for the CS. The difference vector is constant in direction and magnitude along the length of a CS.

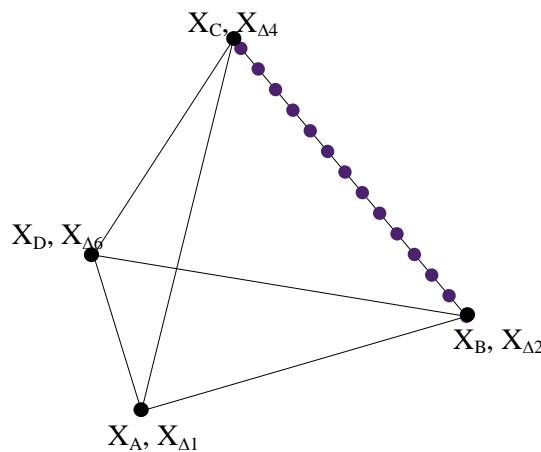


**Figure 4.23: Column Section 7, residue curve between light and heavy intermediate pure components.**

Due to the fact that, CS7 is an infinite reflux CS, we would expect the profile to fall under the infinite reflux case as described above. It has been established that CS7 profile has to satisfy matching criteria 2 and 3. CS2 and CS4 liquid and vapour profiles have to intersect with their respective pure components. With this said, and taking into consideration that CS7 is responsible for a binary split only,

we can conclude that the difference vector for CS7 is zero ( $Y_k^T = X_k^T$ ). Thus CS7 profile is a residue curve between the light and heavy intermediate pure components as illustrated in Figure 4.23.

## 4.12 Variable Representation in Liquid vs. Vapour Split Ratio Space

Liquid and vapour split ratios ( $\Phi_L$  and  $\Phi_V$  respectively) were introduced in our discussion of design parameters above. Liquid and vapour split ratios are the independent internal material balance variables chosen for the design process.

Our choices of variables such as difference points and reflux ratios are based on our insight and understanding around these variables when they are altered or adjusted. For the split ratio ( $\Phi_V$  and  $\Phi_L$ ) parameters, this does not apply and we cannot make an intuitive decision on the variables, based on the effects these parameters have on the system. Thus, we will represent variables we do understand in the split ratio space ( $\Phi_L$  vs.  $\Phi_V$ ). The variable representation in the split ratio space will limit and therefore help select liquid and vapour splits that produce a feasible solution.

### 4.12.1 Net Flow regimes in $\Phi_V$ vs. $\Phi_L$ Space

The various net flow patterns can be controlled or achieved by manipulating the split ratios. The regimes can be visualised, in  $\Phi_V$  vs.  $\Phi_L$  space, by producing lines of zero net flow for the coupled column sections (see Figure 4.24). The dependence of the net flow, for each of the coupled column sections, on the vapour and liquid split ratios from CS1 can be seen in the Equation 4.12 – 4.16 below. The split ratios for both the liquid and vapour are defined, as mentioned previously, in terms of the respective flows from CS1. As a consequence, all the equations below are functions of the reflux ratio in CS1. As seen from these equations additional to the reflux ratio in CS1, CS7 net flow line is a function of

the distillate flow rate ( $\Delta_I$ ) and the light intermediate side draw flow rate as well. CS4 zero net flow line is a function of the distillate flow rate ( $\Delta_I$ ), light intermediate side draw flow rate ( $S_I$ ) as well as the heavy intermediate side-draw ( $S_2$ ) flow rate and CS5 zero net flow line is a function of the distillate flow rate ( $\Delta_I$ ) and feed flow rate.

$$\Delta_2 = (R_{\Delta I} + I)\Delta_I\Phi_V - R_{\Delta I}\Delta_I\Phi_L = 0 \Rightarrow \Phi_L = \frac{(R_{\Delta I} + 1)}{R_{\Delta I}}\Phi_V \quad (4.12)$$

$$\Delta_3 = \Delta_I(R_{\Delta I} + I)(1 - \Phi_V) - R_{\Delta I}\Delta_I(1 - \Phi_L) = 0 \Rightarrow \Phi_L = \frac{(R_{\Delta I} + 1)}{R_{\Delta I}}\Phi_V - \frac{1}{R_{\Delta I}} \quad (4.13)$$

$$\Delta_4 = \Delta_I(R_{\Delta I} + I)\Phi_V - R_{\Delta I}\Delta_I\Phi_L + (S_1 + S_2) = 0 \Rightarrow \Phi_L = \frac{(R_{\Delta I} + 1)}{R_{\Delta I}}\Phi_V - \frac{(B+C)/\Delta_I}{R_{\Delta I}} \quad (4.14)$$

$$\begin{aligned} \Delta_5 = \Delta_I(R_{\Delta I} + I)(1 - \Phi_V) - R_{\Delta I}\Delta_I(1 - \Phi_L) - F = 0 \\ \Rightarrow \Phi_L = \frac{(R_{\Delta I} + 1)}{R_{\Delta I}}\Phi_V - \left[ \frac{F/\Delta_I - 1}{R_{\Delta I}} \right] \end{aligned} \quad (4.15)$$

$$\Delta_7 = \Delta_I(R_{\Delta I} + I)\Phi_V - R_{\Delta I}\Delta_I\Phi_L + S_1 = 0 \Rightarrow \Phi_L = \frac{(R_{\Delta I} + 1)}{R_{\Delta I}}\Phi_V - \frac{S_1/\Delta_I}{R_{\Delta I}} \quad (4.16)$$

By dividing up the  $\Phi_V$  vs.  $\Phi_L$  space with lines of zero net flow for each of the coupled sections, we can identify regions within the space of different overall net flow pattern. These are labelled 1 to 5 in Figure 4.24.

Above the  $\Delta_5 = 0$  line (orange) values of  $\Phi_V$  and  $\Phi_L$  produce values of  $\Delta_5 > 0$ , while below the line values of  $\Delta_5 < 0$  are produced. Similarly for the  $\Delta_3 = 0$  line (red), above the line are values of  $\Delta_3 > 0$ , while below are values of  $\Delta_3 < 0$ . The inverse is true for lines  $\Delta_2 = 0$  (blue),  $\Delta_7 = 0$  (green) and  $\Delta_4 = 0$  (purple). Above these lines negative values are produced, while below positive values are produced. Each of the regions between these lines and the boundaries of the space produce a different net flow pattern in the coupled sections. These are the flow patterns illustrated in Figure 4.13 a-f. This behaviour is summarised in Table 4.1 below.

### 4.12.2 Limits in $\Phi_V$ vs. $\Phi_L$ Space

There are values of both  $\Phi_V$  and  $\Phi_L$ , which cannot be utilised in order to find feasible profile intersections. Based on a vapour feed to the column, a limit would exist where the flow of vapour into the column is equal to the vapour flow in CS 3. If the flow of vapour in CS 3 were bigger than the flow of vapour into the column the vapour flow in CS 5 would be negative (i.e. If  $V_3 > F$  then  $V_5 < 0$ ). The exact value of this limit can be calculated using Equation 4.17.

$$\Phi_V = 1 - \frac{F}{\Delta_1(R_{\Delta 1} + 1)} \quad (4.17)$$

Similarly, for a column with liquid side-draws, if the liquid split ratio is specified such that the value for the liquid flow in CS2 is smaller than the side-draw rates, negative liquid flows in CS4 will result. The lower limit therefore exists where the liquid split ratio value at which the liquid flow in CS2 is equal to the side-draw rate (i.e. If  $L_2 < S$  then  $L_4 < 0$ ). This limiting value can be calculated with Equation 4.18.

$$\Phi_L = \frac{S_1 + S_2}{R_{\Delta 1} \Delta_1} \quad (4.18)$$

Both these limits are illustrated in Figure 4.24 and are shown for a defined reflux in CS1.

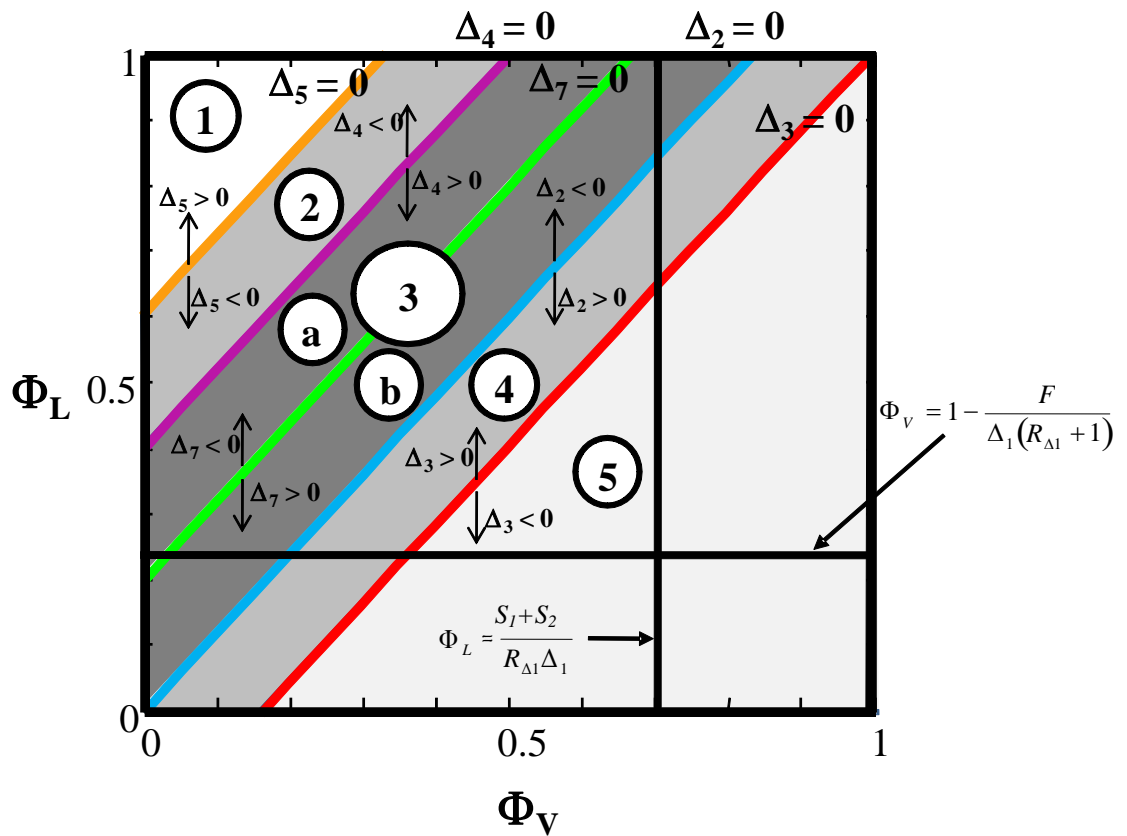


Figure 4.24: Net Flow Regimes in  $\Phi_V$  vs.  $\Phi_L$  for the Kaibel Column.

Table 4.1: Summary of net flow regions illustrated in Figure 4.24.

Region From Figure 4.24	$\Delta$ Direction CS2	$\Delta$ Direction CS3	$\Delta$ Direction CS4	$\Delta$ Direction CS5	$\Delta$ Direction CS7
1	-ve	+ve	-ve	+ve	-ve
2	-ve	+ve	-ve	-ve	-ve
3	a	+ve	+ve	-ve	-ve
	b	-ve	+ve	+ve	-ve
4	+ve	+ve	+ve	-ve	+ve
5	+ve	-ve	+ve	-ve	+ve

### 4.12.3 Reflux Ratio in $\Phi_V$ vs. $\Phi_L$ Space

The reflux ratio of the coupled sections can also be conveniently represented in the  $\Phi_V$  vs.  $\Phi_L$  space. Because of the definitions of the split ratios, lines of constant reflux are straight. The equations for the constant reflux lines for each of the coupled column sections are seen below (Equations 4.19 – 4.28). These equations are also all functions of  $R_{\Delta 1}$ . From the definition of the split ratios,  $R_{\Delta 7}$ ,  $R_{\Delta 4}$  and  $R_{\Delta 5}$  (Equations 4.20 - 4.25 and 4.27 – 4.28) are dependent on the phase of the side-draws and feed material respectively.

$$R_{\Delta 2} = \frac{\Phi_L R_{\Delta 1}}{\Phi_V (R_{\Delta 1} + 1) - \Phi_L R_{\Delta 1}} \Rightarrow \Phi_L = \Phi_V \frac{R_{\Delta 2} (R_{\Delta 1} + 1)}{R_{\Delta 1} (R_{\Delta 2} + 1)} \quad (4.19)$$

#### $R_{\Delta 7}$ – Liquid side-draw ( $S_1$ )

$$R_{\Delta 7} = \frac{\Phi_L R_{\Delta 1} + S_1 / \Delta_1}{\Phi_V (R_{\Delta 1} + 1) + \Phi_L R_{\Delta 1} + S_1 / \Delta_1} \Rightarrow \Phi_L = \Phi_V \frac{R_{\Delta 7} (R_{\Delta 1} + 1)}{R_{\Delta 1} (R_{\Delta 7} + 1)} + \frac{S_1}{\Delta_1 R_{\Delta 1}} \quad (4.20)$$

#### $R_{\Delta 7}$ – Vapour side-draw ( $S_1$ )

$$R_{\Delta 7} = \frac{\Phi_L R_{\Delta 1}}{\Phi_V (R_{\Delta 1} + 1) + \Phi_L R_{\Delta 1} + S_1 / \Delta_1} \Rightarrow \Phi_L = \Phi_V \frac{R_{\Delta 7} (R_{\Delta 1} + 1)}{R_{\Delta 1} (R_{\Delta 7} + 1)} + \frac{S_1 R_{\Delta 7}}{\Delta_1 R_{\Delta 1} (R_{\Delta 7} + 1)} \quad (4.21)$$

#### $R_{\Delta 4}$ – Liquid side-draw ( $S_1$ ) and Liquid side-draw ( $S_2$ )

$$R_{\Delta 4} = \frac{\Phi_L R_{\Delta 1} - (S_1 + S_2) / \Delta_1}{\Phi_V (R_{\Delta 1} + 1) - \Phi_L R_{\Delta 1} + (S_1 + S_2) / \Delta_1} \Rightarrow \Phi_L = \Phi_V \frac{R_{\Delta 4} (R_{\Delta 1} + 1)}{R_{\Delta 1} (R_{\Delta 4} + 1)} + \frac{S_1 + S_2}{\Delta_1 R_{\Delta 1}} \quad (4.22)$$

#### $R_{\Delta 4}$ - Vapour side-draw ( $S_1$ ) and Liquid side-draw ( $S_2$ )

$$R_{\Delta 4} = \frac{\Phi_L R_{\Delta 1} - \frac{S_2}{\Delta_1}}{\Phi_V (R_{\Delta 1} + 1) - \Phi_L R_{\Delta 1} + \frac{(S_1 + S_2)}{\Delta_1}} \Rightarrow \quad (4.23)$$

$$\Phi_L = \Phi_V \frac{R_{\Delta 4} (R_{\Delta 1} + 1)}{R_{\Delta 1} (R_{\Delta 4} + 1)} + \frac{S_1 R_{\Delta 4}}{\Delta_1 R_{\Delta 1} (R_{\Delta 4} + 1)} + \frac{S_2 / \Delta_1}{R_{\Delta 1}}$$

$R_{\Delta 4}$  - Liquid side-draw ( $S_1$ ) and Vapour side-draw ( $S_2$ )

$$R_{\Delta 4} = \frac{\Phi_L R_{\Delta 1} - \frac{S_1}{\Delta_1}}{\Phi_V (R_{\Delta 1} + 1) - \Phi_L R_{\Delta 1} + \frac{(S_1 + S_2)}{\Delta_1}} \quad (4.24)$$

$$\Rightarrow \Phi_L = \Phi_V \frac{R_{\Delta 4} (R_{\Delta 1} + 1)}{R_{\Delta 1} (R_{\Delta 4} + 1)} + \frac{S_2 R_{\Delta 4}}{\Delta_1 R_{\Delta 1} (R_{\Delta 4} + 1)} + \frac{S_1 / \Delta_1}{R_{\Delta 1}}$$

$R_{\Delta 4}$  - Vapour side-draw ( $S_1$ ) and Vapour side-draw ( $S_2$ )

$$R_{\Delta 4} = \frac{\Phi_L R_{\Delta 1}}{\Phi_V (R_{\Delta 1} + 1) - \Phi_L R_{\Delta 1} + \frac{(S_1 + S_2)}{\Delta_1}} \quad (4.25)$$

$$\Rightarrow \Phi_L = \Phi_V \frac{R_{\Delta 4} (R_{\Delta 1} + 1)}{R_{\Delta 1} (R_{\Delta 4} + 1)} + \frac{(S_1 + S_2) R_{\Delta 4}}{\Delta_1 R_{\Delta 1} (R_{\Delta 4} + 1)}$$

$$R_{\Delta 3} = \frac{(1 - \Phi_L) R_{\Delta 1}}{(1 - \Phi_V)(R_{\Delta 1} + 1) - (1 - \Phi_L) R_{\Delta 1}} \Rightarrow \Phi_L = (\Phi_V - 1) \frac{R_{\Delta 3} (R_{\Delta 1} + 1)}{R_{\Delta 1} (R_{\Delta 3} + 1)} + 1 \quad (4.26)$$

$R_{\Delta 5}$  - Liquid Feed

$$R_{\Delta 5} = \frac{(1 - \Phi_L) R_{\Delta 1} + \frac{F}{\Delta_1}}{(1 - \Phi_V)(R_{\Delta 1} + 1) - (1 - \Phi_L) R_{\Delta 1} + \frac{F}{\Delta_1}} \quad (4.27)$$

$$\Rightarrow \Phi_L = (\Phi_V - 1) \frac{R_{\Delta 5} (R_{\Delta 1} + 1)}{R_{\Delta 1} (R_{\Delta 5} + 1)} + 1 + \frac{F}{\Delta_1 R_{\Delta 1}}$$

$R_{\Delta 5}$  - Vapour Feed

$$R_{\Delta 5} = \frac{(1 - \Phi_L) R_{\Delta 1}}{(1 - \Phi_V)(R_{\Delta 1} + 1) - (1 - \Phi_L) R_{\Delta 1} - \frac{F}{\Delta_1}} \quad (4.28)$$

$$\Rightarrow \Phi_L = (\Phi_V - 1) \frac{R_{\Delta 5} (R_{\Delta 1} + 1)}{R_{\Delta 1} (R_{\Delta 5} + 1)} + 1 + \frac{F R_{\Delta 5}}{\Delta_1 R_{\Delta 1} (R_{\Delta 5} + 1)}$$

The sign of the reflux is dependent on the sign of the net flow, therefore the regions of the space corresponding to positive and negative net flow, for each of the sections, correspond to positive and negative reflux for those sections as well. Infinite reflux lines originate from the zero net flow lines (both positive and negative infinite reflux). These equations are only used to calculate the reflux for each section, and not in a graphical manner. In the following papers to follow, these equations will be utilised more extensively to describe limiting operating conditions for the system under minimum reflux conditions.

## 4.13 Feasibility in the Split Ratio Region

### 4.13.1 Determining feasibility in $\Phi_L$ vs. $\Phi_V$

As discussed, to operate a Kaibel column at sharp split specifications, the column has to be controlled such that the net flow in CS7 is zero. This would mean that the zero net flow line in the split ratio space, given by Equation 4.16, is the only possible solution for the Kaibel Column. This is extremely powerful because we no longer have to guess values for the split ratios. We have a method to actually calculate probable split ratio combinations and understand their implications, for the design. From a very large range of potential split ratio values (0 to 1 for both), we have reduced the possible choices to a very small region. This is illustrated in Figure 4.25. As can be seen from Figure 4.24, zero net flow of CS7 corresponds to net flow pattern 3 that is described in greater detail in Figure 4.22. Note that it is not mentioned that the entire  $\Delta_7=0$  line is feasible when attempting a sharp split, but only that it is closer prospect for a feasible solution.

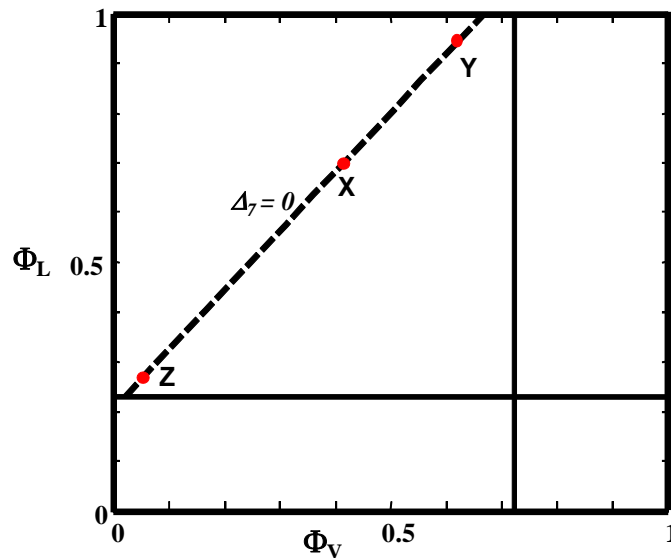


Figure 4.25: Feasible operating line in  $\Phi_V$  vs.  $\Phi_L$  for the Sharp Split Kaibel Column.

In Figure 4.25 we can see that we have vapour and liquid split ratio limitations. These limitations have an effect on the operating line. Depending on the reflux ratio chosen for CS1 ( $R_{A1}$ ), may depend on how much of the line is completely eliminated from the space entirely. At higher refluxes more of the operating line is visible between the maximum bounds of the original  $\Phi_L$  vs.  $\Phi_V$  region. This result holds with our intuitive understanding of distillation systems, which is that separations are more difficult at low reflux than at high reflux. The example given in Figure 4.25 is thus derived from a fairly high reflux ratio in CS1.

Let us now take a closer look at how we design the column using a single point on the operating line. Each vapour and liquid split ratio combination on the  $\Delta_7 = 0$  operating line is thus a possible combination closer to a ‘feasible’ operating point for the Sharp Split Kaibel Column.

If we select a point, and apply Equations 4.12–4.16 and 4.19–4.28, using the relevant feed and products specifications (feed and products phases) we will achieve a particular solution for each CS in the column. Thus, from these equations we determine the net flows and reflux ratios for each CS. These results

can be seen qualitatively by showing the  $TT_4$  for all the relevant sections pertaining to select matching criteria's.

As a first example let us select a point close to the intersection of liquid split ratio limit line and zero vapour split ratio, but still on the zero net flow operating line (given by point (Z) in Figure 4.25). Matching criteria 1, 4 and 5 are represented using  $TT_4$  in Figure 4.26, Figure 4.27 and Figure 4.28. Matching criteria 2 and 3 are always satisfied as the  $X_A$ 's for CS2 and CS4 is on the pure components for sharp split separations. It is evident that matching criteria 1 is not satisfied as CS1 (red) and CS2 (blue) liquid profiles do not overlap (See Figure 4.26). Matching criteria 4 is not satisfied either as CS6 (light blue) and CS4 (pink) vapour profiles do not overlap (See Figure 4.27). We can see from Figure 4.28, matching criteria 5 is satisfied completely as the  $TT_4$  of CS3 (green) and CS5 (yellow) overlap. Holland et al. (2010) show that for a ternary system the overlapping of vapour  $TT_3$  boundaries are associated to a vapour feed and liquid  $TT_3$  boundaries overlapping for liquid feed. The exact same can be said about 4 component systems although they now overlap in three dimensions and not two as for the ternary case. In our examples, we have a liquid feed as the liquid  $TT_4$  of CS3 and CS5 are shown (solid lines) and in this case satisfy matching criteria 5.

Point (Y) as our next point of operation, which is located close to the intersection of the maximum liquid split ratio ( $\Phi_L=1$ ) and the vapour split ratio limit line, shows very different results. In this case matching criteria 1 is satisfied as CS1 and CS2 liquid profiles intersect (See Figure 4.29). Matching criteria 4 is satisfied as well, as CS6 and CS4 vapour profiles intersect (See Figure 4.30). We can now see from Figure 4.31, matching criteria 5 is not satisfied as the  $TT_4$  of CS3 and CS5 do not overlap at all. It is evident that neither point Z nor point Y are satisfactory split ratio combinations to operate the column that give us feasible operating conditions as not every single matching criteria is satisfied.

*Note: Unless otherwise stated, within composition and CPM diagrams a solid line will denote the liquid phase while a dotted line will denote vapour phase*

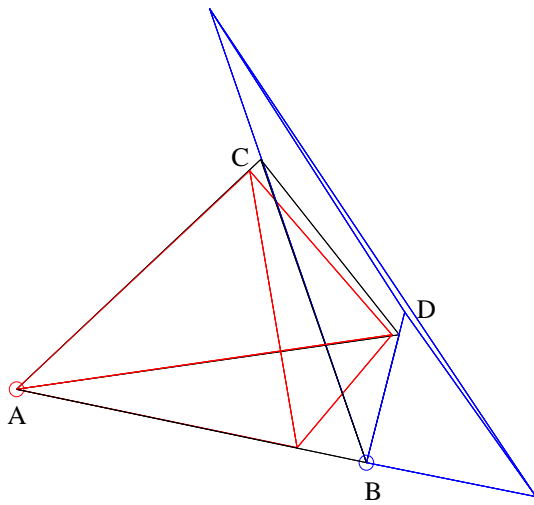


Figure 4.26:  $TT_4$  for CS1 and CS2 not satisfying matching criteria 1.

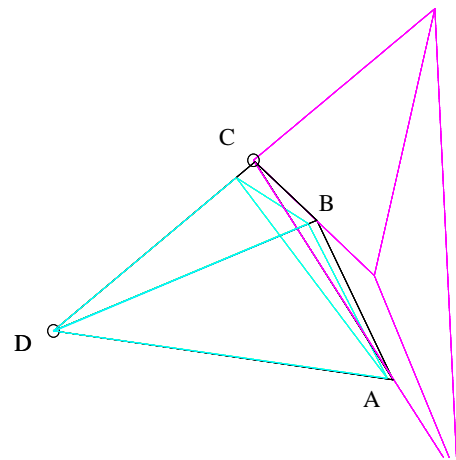


Figure 4.27:  $TT_4$  for CS4 and CS6 not satisfying matching criteria 4.

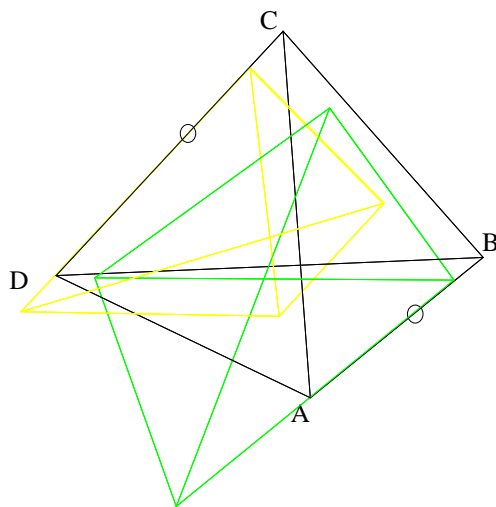


Figure 4.28:  $TT_4$  for CS3 and CS5 satisfying matching criteria 5.

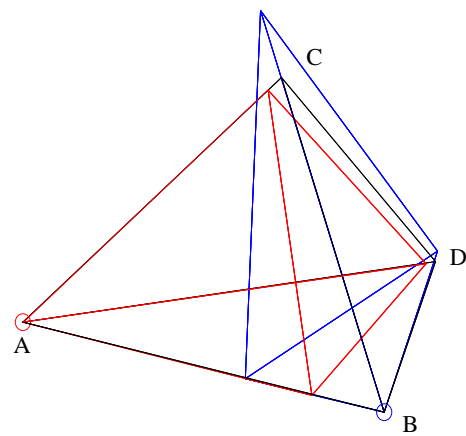
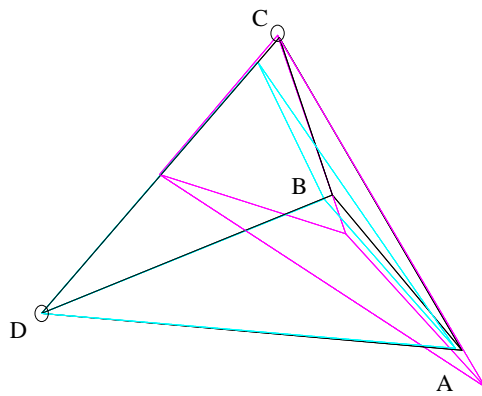
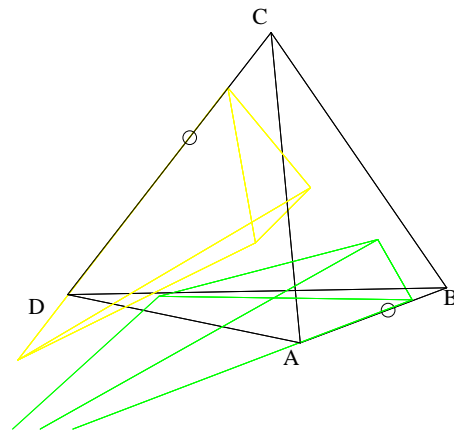


Figure 4.29:  $TT_4$  for CS1 and CS2 satisfying matching criteria 1.



**Figure 4.30:  $TT_4$  for CS4 and CS6 satisfying matching criteria 4.**



**Figure 4.31:  $TT_4$  for CS3 and CS5 not satisfying matching criteria 5.**

Point X is an arbitrarily chosen point in the middle of the operating line in the split ratio space. By investigating the feasible  $TT_4$  for all the relevant CSs produces significantly better results. Matching criteria 1 is satisfied as CS1 and CS2 liquid profiles intersect. Matching criteria 4 is satisfied as well, as CS6 and CS4 vapour profiles intersect. Matching criteria 5 is now once again satisfied as the  $TT_4$  of CS3 and CS5 overlap.

From these examples we can see that even although we are operating the column on the  $\Delta_7 = 0$  line in the split ratio space, not every combination of these split ratios give us feasible intersections of profiles in the CSs. If we increase the vapour split ratio in systematic steps when we are situated at point Z but still remain on the operating line at all the points we will eventually achieve a point where all the CSs overlap and all matching criteria's are satisfied. Figure 4.32, Figure 4.33 and Figure 4.34 illustrates this phenomenon. If we now decrease the vapour split ratio in systematically small steps when we are situated at point Y but still remain on the operating line at all the selected points we will again achieve a point where all the CSs overlap and all matching criteria's are satisfied. Figure 4.35, Figure 4.36 and Figure 4.37 illustrates this phenomenon.

As we increase the vapour and liquid split ratio along the operating line we can see from Figure 4.32 and Figure 4.33 eventually we create an overlap of CS1 and 2, as well as CS4 and 6 respectively (direction of arrow is an increase in split ratios). Conversely, when we decrease the vapour and split ratio along the operating line we can see from Figure 4.37 how we eventually achieve an overlap with CS3 and CS5. Figure 4.34 illustrates that CS3 and CS5 will always overlap if we increase the vapour and liquid split ratio along the operating line until we achieve a feasible split ratio combination. We can also see that from Figure 4.35 showing the overlap of CS1 and CS2 will always be achieved when decreasing the vapour and liquid split ratios along the operating line until we achieve a feasible split ratio combination. The same holds for Figure 4.36 that illustrates the overlap for CS4 and CS6.

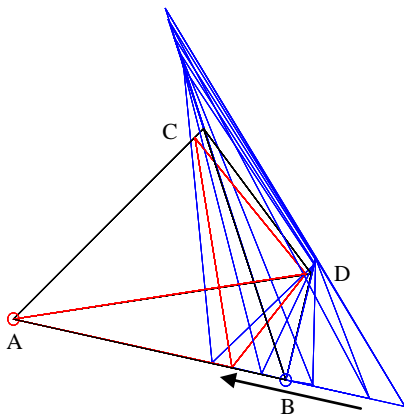


**Figure 4.32:**  $TT_4$  for CS1 and CS2 with an increase in vapour and liquid split ratio.

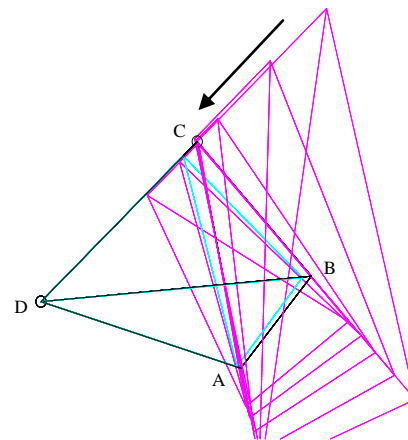


**Figure 4.33:**  $TT_4$  for CS4 and CS6 with an increase in vapour and liquid split ratio.

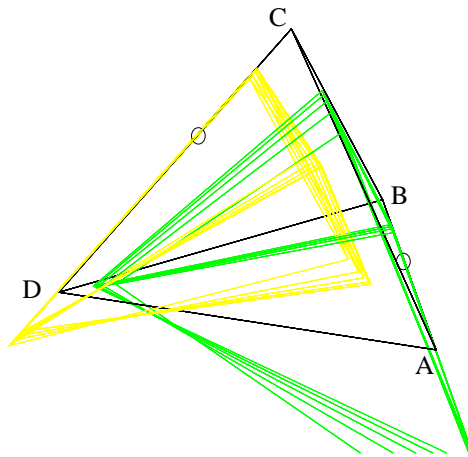


Figure 4.34:  $TT_4$  for CS3 and CS5 with an increase in vapour and liquid split ratio.

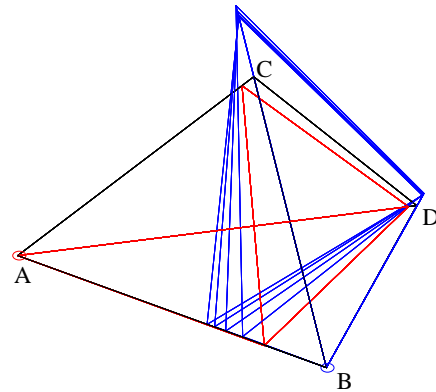


Figure 4.35:  $TT_4$  for CS1 and CS2 with a decrease in vapour and liquid split ratio.

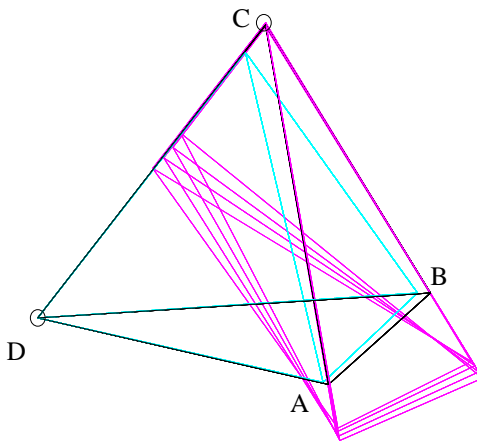


Figure 4.36:  $TT_4$  for CS4 and CS6 with a decrease in vapour and liquid split ratio.

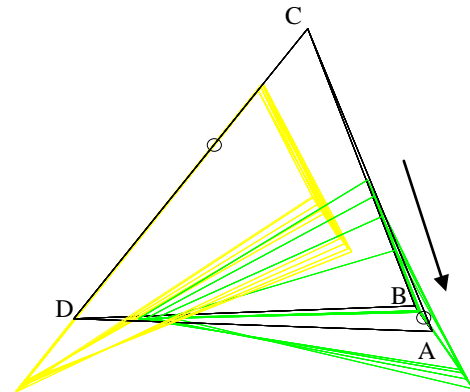


Figure 4.37:  $TT_4$  for CS3 and CS5 with a decrease in vapour and liquid split ratio.

Thus we can conclude that CS3 and CS5 overlap is developed and satisfied from the top right hand side of the liquid and vapour split ratio space and that the intersection of CS1 and CS2 as well as the intersection of CS4 and CS6 is developed and satisfied from the bottom left hand side of the liquid and vapour split ratio space. The development of this feasible line of solutions is based on min reflux ratios of CS2, CS4, CS3 and CS5. The solutions to the development of

these min reflux scenarios will not be discussed in this paper and will be published in papers in the future.

With this information, we can now show the feasible split ratio line for a specific  $R_{\Delta I}$  that will give intersections for all the necessary CSs liquid or vapour profiles and satisfy all matching criteria's. Figure 4.38 shows this feasible line of solutions.

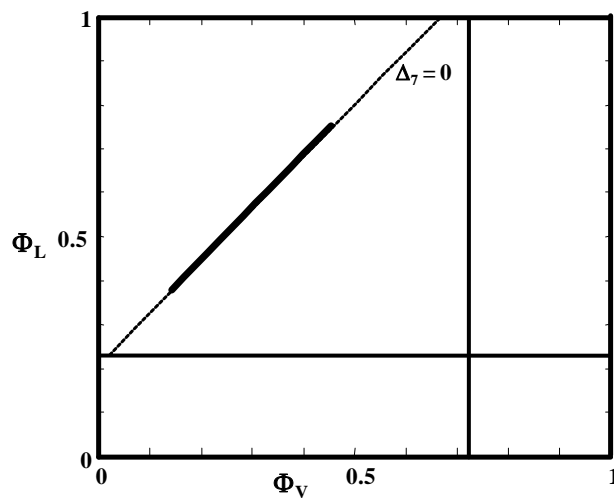


Figure 4.38:  $\Phi_L$ ,  $\Phi_V$  space with feasible operating line shown as the solid line.

*NOTE: We have thus far not discussed the intersection of the  $TT_4$  of CS1 and CS3, CS2 and CS3, CS4 and CS5, and lastly CS5 and CS6, due to the fact that if we operate on the zero net flow line for CS7. All these matching criteria's including the non stressed CSs are automatically met if the adjacent CSs intersect or overlap. I.e. If CS1 and CS2  $TT_4$  overlap when a vapour and liquid split ratio is selected on the operating line, then the  $TT_4$  of CS2 and CS3 will overlap as well as the  $TT_4$  of CS1 and CS3. (Refer to Appendix B)*

### 4.13.2 Overall feasible topology

It has been shown that the line of solutions that allow for a feasible sharp split Kaibel Column does in fact not include all points along CS 7 zero net flow line in the vapour and liquid split ratio space, but has specific boundaries that contain feasible sharp split solutions. If we select a point on the feasible line we achieve a possible design solution. We will now show the feasible column design. Figure 4.39 is the liquid profiles for the Rectifying Section on the L-LI axis, and Figure 4.40 is the  $TT_4$  that corresponds to this rectifying profile. Figure 4.41 is the liquid profiles of CS3 on the L-LI axis, and Figure 4.42 is the  $TT_4$  that matches this profile. The same is performed for the remaining CSs. Figure 4.43 and Figure 4.44 correspond to CS5, Figure 4.45 and Figure 4.46 corresponds to CS2, Figure 4.47 and Figure 4.48 corresponds to CS4 and Figure 4.49 and b correspond to CS6, or the stripping section. Take note that CS7 profile is a residue curve and that its  $TT_4$  is equivalent to the MBT (See Figure 4.23). The combination of all the profiles that create a feasible Kaibel Column is illustrated in Figure 4.51 and by using the profiles as a basis; the probable form of the  $TT_4$ s will be similar to that seen in Figure 4.52.

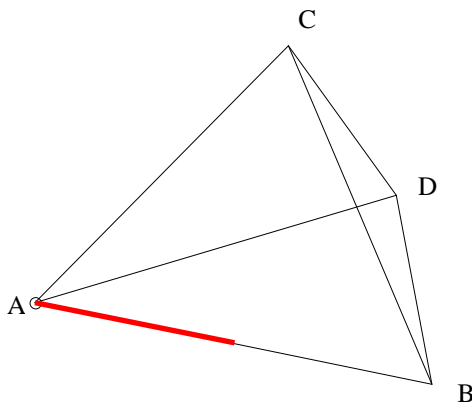


Figure 4.39: Rectifying composition profile.

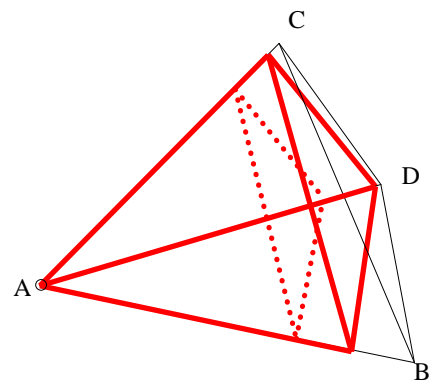


Figure 4.40:  $TT_4$  for Rectifying profile.

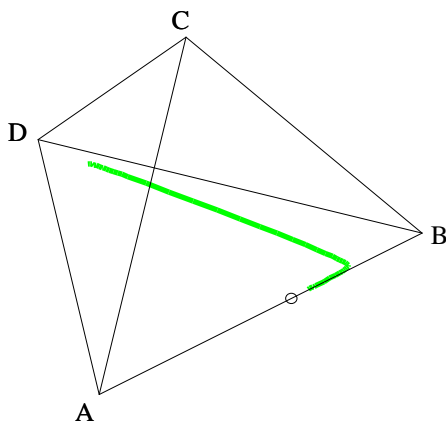


Figure 4.41: Column profile for CS3.

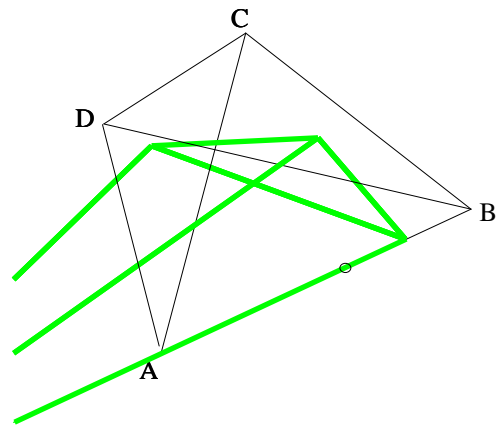


Figure 4.42:  $TT_4$  for CS3

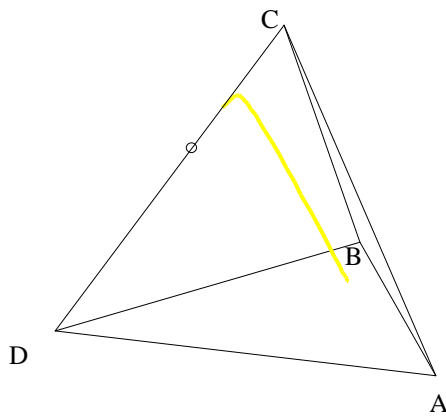


Figure 4.43: Column profile for CS5.

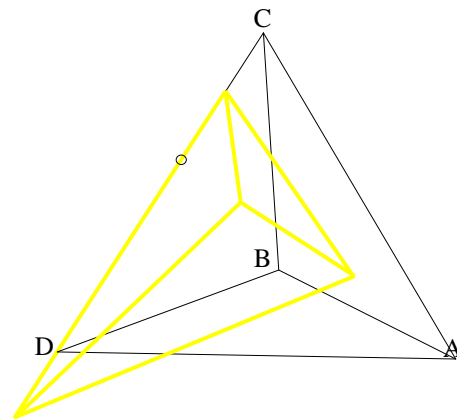


Figure 4.44:  $TT_4$  for CS5.

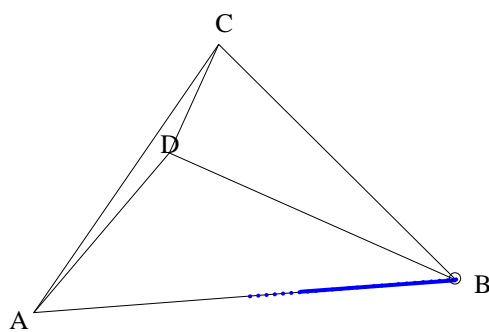


Figure 4.45: Column profile for CS2.

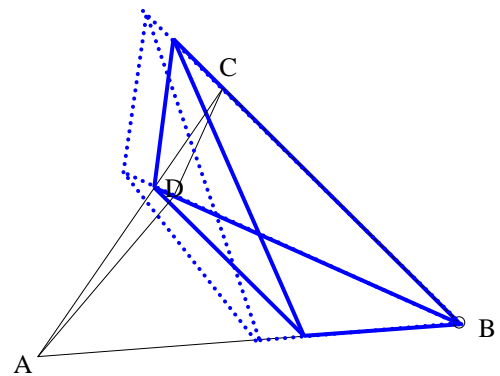


Figure 4.46:  $TT_4$  for CS2.

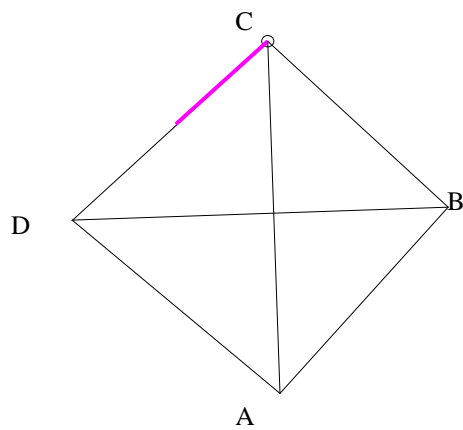


Figure 4.47: Column profile for CS4.

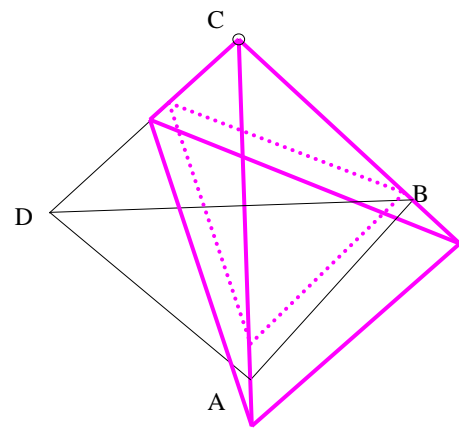


Figure 4.48:  $TT_4$  for CS4

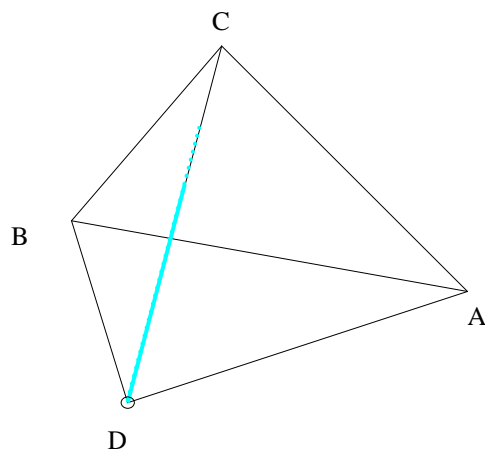


Figure 4.49: Stripping composition profile

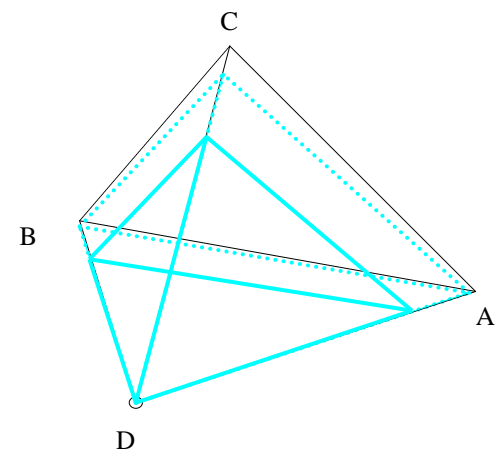


Figure 4.50:  $TT_4$  for Stripping profile

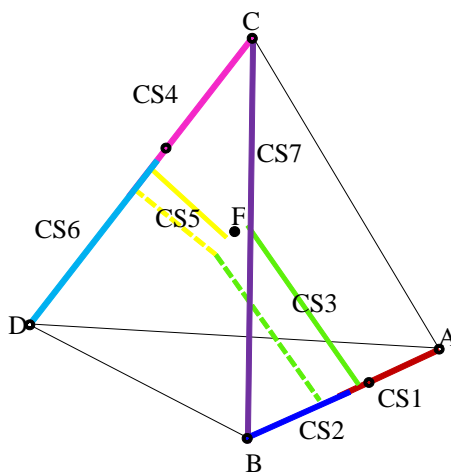


Figure 4.51: Kaibel Column composition profiles.

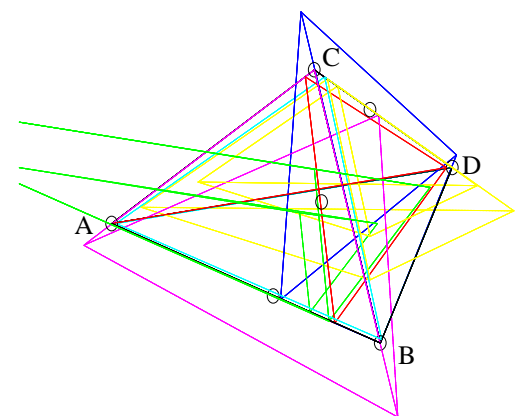


Figure 4.52: All seven  $TT_4$  for Kaibel Column.

#### 4.14 Differences between Single Dividing wall Columns and a Two-Column arrangement

The design procedure started by splitting the Kaibel column into CSs (See Figure 4.5 and Figure 4.6) in order to simplify the system and so we could apply of the CPM technique. We observed that even if a single dividing wall column (DWC) were employed, instead of the arrangement shown in Figure 4.5 (two-column arrangement); exactly the same CS breakdown would result. This means that the applicability of the CPM technique is completely general for this case and the feasible operating line developed in the previous sections is equivalent for the DWC. Figure 4.38 illustrates the feasible operating line for the Kaibel Column for a specific reflux selected in the rectifying section. More specifically, this line is the operating line for the two-column arrangement, because, this arrangement allows for the control of the vapour split ratio.

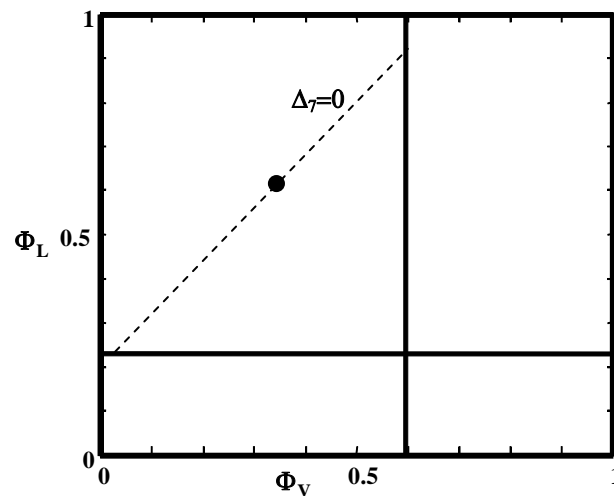


Figure 4.53: Feasible operating point for single divided wall column in  $\Phi_V, \Phi_L$  space.

Thus, it is possible to shift along the operating line and still produce four pure components. The relative amounts of pure products produced have to be consistent for a predefined feed, but the refluxes in individual CSs change accordingly. Even although the configuration of the control strategy employed

and components of the control system selected have to be extremely reliable and operate almost perfectly, it is still possible to control the Kaibel Column (two-column arrangement) on this line.

If we now focus our attention to the DWC, it would now be more apparent that there are several drawbacks from a design point of view for the DWC. We can see that the vapour split ratios cannot be controlled. This means that if a DWC were to be specified as the design arrangement, the system has to be operated at a point on the feasible operating line as illustrated by Figure 4.53. It would be nearly impossible to control all the necessary control variables (Liquid split ratio, zero net flow in CS7 and Reflux ratio in CS1 as an example) in-order to achieve four pure components or steady product flows at a point. Although, we have not taken into consideration the controllability of the system, we can make the obvious conclusion that, no matter what design configuration is selected; controlling the Kaibel Column for sharp split separations would be extraordinarily difficult.

## 4.15 Discussion and Conclusion

In this work, we have successfully modelled the Kaibel column with the aid of CPM techniques. The design procedure involves the simplification of the Kaibel Column by breaking it down into column sections. After breaking the column configuration into sections, the design process requires choosing difference points and reflux ratios for the most important column sections, and by material balance determining the difference points and reflux ratios of the remaining sections. Column profile maps (CPMs) for each of the sections are then produced and superimposed to determine feasible operating profiles.

It has been shown that instead of producing entire CPMs, the procedure can be performed by simply determining the stationary points of the difference point equation. Using these stationary points, transformed tetrahedrons ( $TT_4$ ) can be produced that enables us to track all regions of CPM topology without solving the

difference point equation. We thus demonstrate that the design procedure is graphical but is performed quickly and with little computational effort.

The selection of the reflux ratios and hence the qualitative form of the  $TT_4$ , for a feasible column solution in the column design has led to an extensive analysis of the feasible net flow patterns in the Kaibel Column configuration. We have shown that there are *six* possible flow patterns. These are *1, 2, 3a, 3b, 4 and 5* seen in Figure 4.13 a-f. These net flow patterns for the Kaibel configuration can be shown in the vapour and liquid split ratio space. Regions, of split ratio space, resulting in each of these flow patterns can be found by producing zero net flow lines for the coupled column sections.

Holland et al. (2010) showed that flow pattern 3 for the Petlyuk equivalent is the most efficient due to the lower overall reflux for this flow pattern when compared to the remaining four patterns. It has been shown for the Kaibel Column that although, many flow patterns do exist, only one pattern is feasible. In particular a combination of flow pattern *3a* and *3b*, where the net flow through the section between the two side-draws is zero.

Flow pattern 3 in the Kaibel design is similar to the flow pattern 3 in the Petlyuk configuration and is the most efficient in the Kaibel column for the same reasons given above for the Petlyuk Column. This fact leads to a very practical analytical test of the Kaibel operation and is quite different from the Petlyuk column. For the Petlyuk configuration, if the operating split ratios result in flow patterns other than net flow pattern 3 we can immediately conclude that the column is operating inefficiently (Holland et al., 2010). But, for the Kaibel column, if the operating split ratios result in flow patterns other than net flow pattern 3 the column is not only working inefficiently but isn't operating correctly at all in order to achieve sharp split product specifications.

Although the flow patterns 1, 2, 4 and 5 are not feasible within the feasible *sharp split* Kaibel column, they are extremely important for pseudo non-sharp and non-

sharp split systems. As discussed, the zero net flow line defined from mass balance constraints across CS7 can be represented in the vapour and liquid split ratio space and is shown to be a line of solutions within the space. This is the line of vapour and liquid split ratio combinations that result in feasible sharp split Kaibel configurations.

In addition to net flow, other variables can be represented in split ratio space. The representation of these variables (minimum reflux and co-linearity within the composition space) in split ratio space is a very powerful tool when a selection of feasible vapour and liquid split ratios pairs are selected. This chapter does not deal explicitly with the limiting boundaries and the determination of these limiting boundaries within the vapour and liquid split ratio space but rather, acknowledgment of these bounds is made and shown to exist. The next chapter (Chapter 5) in this series will deal with this topic and will show how to determine these boundaries more efficiently.

Although the topological boundaries, between stationary points, of non-ideal systems have a degree of curvature, the straight lines offer very good estimations to these boundaries. The feasible line of solutions can be generated for these systems with quite a small degree of error.

The feasible line of solutions, demonstrates that a choice of vapour and liquid split ratios, in the Kaibel column, cannot be made arbitrarily if a sharp product is to be achieved. Although we have analysed sharp-split separations in this work, which, entails infinite stages, the feasible region boundaries can be generated for non-sharp-splits.

From a stage number and split ratio perspective it is clear why producing Petlyuk designs, for desired separations, is difficult using iterative solving methods. Without an understanding of the effects of parameters such as reflux ratio and the split ratios it is especially difficult to determine the required number of stages for a separation. For a set number of stages the designer would typically choose

arbitrary split ratios and reflux ratios. These are very unlikely to produce the desired separation and the designer must resort to trial and error operations. It is evident that current design methods are not particularly efficient. The CPM approach on the other hand allows one to not only generate individual solutions, but find all possible solutions for a set of column parameters (reflux ratio and product flow rates). For non-sharp splits, parameters like the total number of required stages, feed stage and side-draw stage are a natural product of the process. These can be determined by tracking variable  $n$  along each composition profile of a column section.

The column profile map methodology for Kaibel design is extremely powerful and efficient. Another aspect that has not been covered in this paper but is discussed in the next chapter of this series is the development of the optimality region. The procedure for generating the optimality region and minimum reflux for the column is similar to the analytical methods employed by Halvorsen (2001). On selecting a reflux ratio and split ratio pair, column solutions can be generated without requiring any iteration. Parameters such as feed stage placement, side-draw stage placement, total required stages, column section stage requirements as well as internal vapour and liquid ratios are an expected outcome of the CPM technique.

In the following chapter, we will demonstrate limiting cases in the vapour and liquid split ratio space along the feasibility line of solutions for the sharp split Kaibel configurations and determine the minimum reflux/optimal region.

## Chapter 5: Optimal operation of the Sharp Split Kaibel Column

*This chapter is an extension of Chapter Four. This work has been prepared in the form of a paper for future publication. This work is as of yet still unpublished.*

---

### **Abstract**

This chapter presents a method for assessing the feasibility of the sharp split Kaibel Column solutions for a quaternary system discussed in Chapter 4. The work details the limiting conditions and variables in the coupled section of the column and uses these variables to limit the solution presented in the previous chapter. It is shown that for set product composition specifications and set reflux ratio in the rectifying section, only a single line within the vapour and liquid split ratio space result in feasible separations. It is also shown that the minimum reflux solution can be found using the methodology. The results are valid for all zeotropic separation systems.

---

## 5.1 CPMs Quaternary Systems

Column Profile Maps (CPM), introduced by Tapp et al. (2004), are generated using the difference point equation (DPE) (see Equation 5.1 below). They are maps of liquid composition trajectories generated for a column section  $k$  ( $CS_k$ ) with a constant net-molar flow and are defined for a single difference point ( $X_{\Delta}$ ) and reflux ratio ( $R_{\Delta}$ ). The DPE for  $CS_k$  is defined as follows:

$$\frac{dX}{dn} = \left(1 + \frac{1}{R_{\Delta k}}\right) (X - Y^*(X)) + \frac{1}{R_{\Delta k}} (X_{\Delta k} - X) \quad (5.1)$$

$$\text{Where: } X_{\Delta k} = \frac{V_k Y_T - L_k X_T}{\Delta_k} \quad (5.2)$$

$$R_{\Delta k} = \frac{L_k}{\Delta_k} \quad (5.3)$$

$$\Delta_k = V_k - L_k \quad (5.4)$$

$X_{\Delta k}$  and  $R_{\Delta k}$  is the difference point and the reflux ratio for  $CS_k$  respectively. A CPM is produced, using the DPE which is solved at various initial conditions, throughout the composition space for selected  $X_{\Delta k}$  and  $R_{\Delta k}$  (where  $n \rightarrow -\infty$  and  $n \rightarrow \infty$ ). The derivation of the Difference Point Equation is shown in Appendix F.

This chapter considers a 4-component feed ( $F$ ) with pure components A (light), B (light intermediate), C (heavy intermediate) and D (heavy) and their respective relative volatilities as [6 4 2 1]. An example of a quaternary CPM is shown in Figure 5.1. It is evident from Figure 5.1; the entire map is not populated with curves, as this will be too confusing to observe graphically.

The quaternary system with constant relative volatilities has boundaries that are straight and thus we can draw straight lines through the nodes (See Figure 5.1).

The boundaries formed from these intersected nodes form regions of qualitatively different topology (See Figure 4.1 and Figure 5.1).

It is important to note that the DPE is defined under constant molar over flow assumptions and is used for distillation modelling. Feed material is assumed to be at saturated liquid or saturated vapour conditions and perfect mixing is assumed over all mixing points.

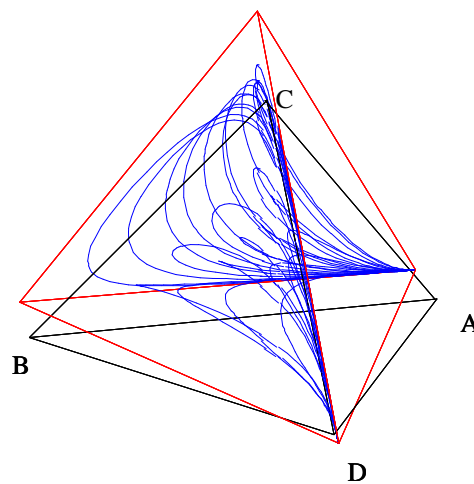


**Figure 5.1: Quaternary Column Profile Map for  $X_{\Delta k} = [0.3, -0.2, -0.3]$  and  $R_{\Delta k} = 9$ .**

**Note: D – Heavy Pure Component, A – Light Pure Component, B– Light Intermediate Pure Component, C – Heavy Intermediate Pure Component.**

The position of these stationary points and boundaries for a particular system are dependent on  $X_{\Delta k}$  and  $R_{\Delta k}$ . For a set  $R_{\Delta k}$ , the stationary points can be ‘shifted’ around the composition space by varying  $X_{\Delta k}$ . Similarly, by setting a constant  $X_{\Delta k}$ , the stationary points can be ‘shifted’ around, on pinch point curves, by varying  $R_{\Delta k}$ . As  $R_{\Delta k}$  tends to infinity, the stationary points tend to the residue curve map stationary points, which are the pure components on the mass balance triangle (MBT). The DPE collapses to the general form of the residue curve equation. The boundaries under these conditions, for the CPM lie on the axes and the CPM becomes topologically equivalent to a residue curve map (RCM).

$\Delta_k$  which is defined as the difference between the vapour and liquid flows in CS  $k$  is a net flow of material within the column section. This net flow can be thought of as a pseudo stream flowing up or down the CS. If  $V_k > L_k$ , then  $\Delta_k > 0$  and therefore a net flow or pseudo stream flowing up is achieved in the CS <sub>$k$</sub> . But if  $V_k < L_k$ , then  $\Delta_k < 0$  and thus a net flow or pseudo stream flowing down is achieved in the CS <sub>$k$</sub> . The value of  $\Delta_k$  is constant within a CS <sub>$k$</sub>  and is thus the same at any point along the length of the CS <sub>$k$</sub> .

The difference point ( $X_{\Delta k}$ ) can be thought of as the pseudo composition vector of  $\Delta_k$ , and being a difference between two compositions is physically valid anywhere in composition space – both inside and outside the MBT. Because  $X_{\Delta k-i}$  is a pseudo composition, the elements must sum to 1 i.e.  $\sum_{i=1}^C X_{\Delta k-i} = 1$ .  $X_{\Delta k-i}$  is the composition of element  $i$  in the pseudo stream  $\Delta_k$  and  $\Delta_k X_{\Delta k-i}$  is the net flow of component  $i$  within CS $k$ . A positive value is a net flow of component  $i$  up and a negative value is a net flow of component  $i$  down the column section. If  $X_{\Delta k-i}$  is negative, the direction of the net flow of component  $i$  is opposite to that of the  $\Delta_k$  and the sum of the remaining components is greater than 1.

The reflux ratio is defined as the ratio of liquid flowing down the CS to the net flow in the CS. Because of its dependence on  $\Delta_k$ ,  $R_{\Delta k}$  can be either positive (when  $\Delta_k > 0$ ) or negative (when  $\Delta_k < 0$ ). CPMs generated for a fixed difference point and positive reflux ratios are qualitatively different from those generated with the same difference point and negative reflux ratio.

The six boundaries (see Figure 5.2) which are defined by four planes which arise from the four surfaces of the quaternary Gibbs tetrahedron, produces fifteen regions where a  $X_{\Delta k}$  placement in each of these regions produce qualitatively different CPM. These fifteen regions correspond to regions of the RCM with differing topology. These six boundaries will be referenced several times in the chapter and are worth labelling. The boundary between the unstable node (Pure A)

and the first light intermediate (Pure B) will be referred to as the light–light intermediate axis or (L–LI).

The boundary between the first light intermediate saddle (Pure B) and the second light intermediate saddle (Pure C) will be referred to as the light intermediate–heavy intermediate axis or (LI–HI axis). The boundary between the second light intermediate saddle (Pure C) and the stable node (Pure D) will be referred to as the heavy intermediate–heavy axis or (HI–H axis). The boundary between the unstable node (Pure A) and the stable node (Pure D) will be referred to as the light–heavy axis or (L–H axis).

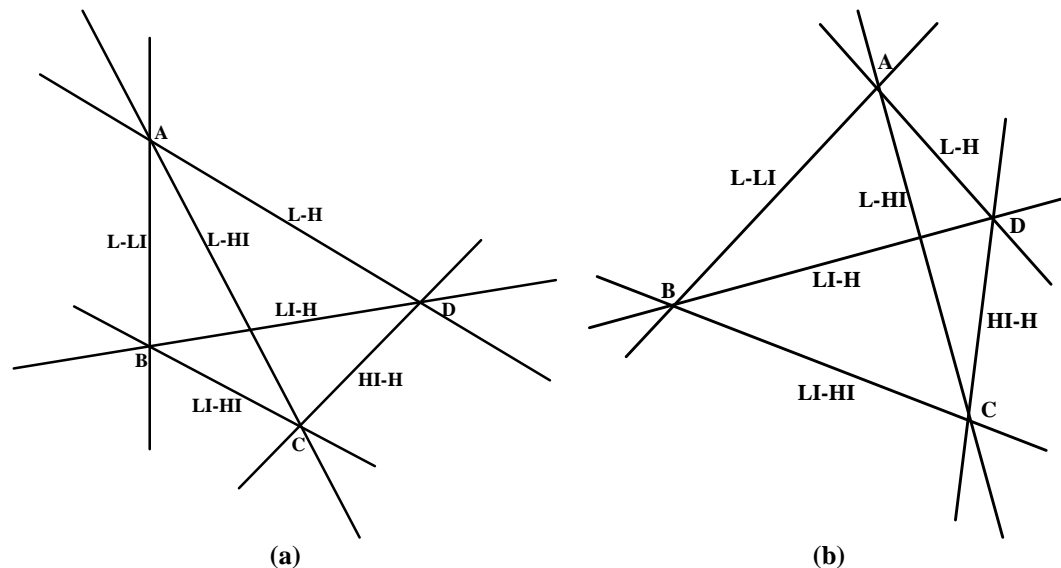


**Figure 5.2:** (a) Quaternary right angled tetrahedron boundary definitions. (b) Quaternary equilateral tetrahedron boundary definitions.

The boundary between the unstable node (Pure A) and the second heavy intermediate saddle node (Pure C) will be referred to as the light–heavy intermediate axis or (L–HI axis). And finally the boundary between the first light intermediate saddle node (Pure B) and the unstable node (Pure D) will be referred to as the light intermediate - heavy axis or (LI–H axis). Figure 5.2 illustrates these

boundary definitions. Figure 5.2 (b) is a transform of Figure 5.2 (a) from a right angle tetrahedron to an equilateral tetrahedron.

## 5.2 Column Section Breakdown

The design process will be initiated by breaking the Kaibel column down into column sections. A schematic representation of the column can be seen in Figure 5.3 below. The CPM technique enables one to apply the column section breakdown approach used by Tapp et al (2004a) to identify individual column sections within the configuration. Tapp et al (2004) defined column sections as lengths of column between points of addition or removal of material and/or energy. Using this definition, we can identify seven column sections in the configuration. The column section breakdown is seen in Figure 5.3 below.

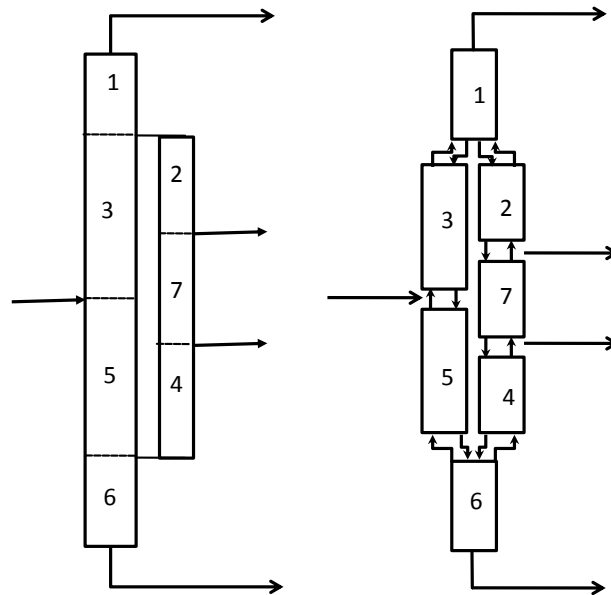


Figure 5.3: Column section breakdown for the Kaibel column.

Column section 1 (CS1) is a standard rectifying section terminated by a total or partial condenser. Column section 6 (CS6) is a standard stripping section terminated by a total or partial reboiler. The group of column sections from 2-7 will be referred to as the “*coupled column sections*”.

### 5.3 Summary of the Sharp Split Kaibel Column solution

In the previous chapter it was shown how the  $\Phi$  space (Vapour split ratio vs. Liquid split ratio space) aids in viewing all sharp split Kaibel solutions. This was achieved by first identifying limiting constraints on the selection and placement of the difference points within the column as well as isolating the net flow through CS 7. It has been shown that the net flow through CS7 has to be zero as an alternate net flow will shift the difference points that obey linear mixing rules within the coupled sections (CS 2, CS 3, CS 4 and CS5) to an infeasible solution. This means the intersecting criteria of the profiles will not be obeyed unless CS 7 net flow is zero.

As a result only one flow pattern is feasible. This is FP 3 which incorporates a dispersion of component A and B upwards in CS 3 and components C and D downwards in CS 5 where CS3 has a net flow of material upwards and downwards in CS 5; a net flow of material downwards in CS 2 is achieved with component A upwards and component B downwards; CS 4 has a net flow upwards with component C upwards and component D downwards. CS 1 is a rectifying section with component A flowing upwards and component B downwards. CS 6 is stripping section with component D downwards and component C upwards. This is illustrated in Figure 5.4 and Table 5.1.

As discussed in Chapter 4 the liquid and vapour split ratios are the independent internal material balance variables chosen for the design process. Our choices of variables such as difference points and reflux ratios are based on our insight and

understanding around these variables when they are altered or adjusted. This does not apply to the split ratio ( $\Phi_V$  and  $\Phi_L$ ) parameters, and we cannot make an intuitive decision on the variables, based on the effects these parameters have on the system. Thus, we will represent variables we do understand in the split ratio space ( $\Phi_L$  vs.  $\Phi_V$ ). The variable representation in the split ratio space will limit and therefore help select liquid and vapour splits that produce a feasible solution.

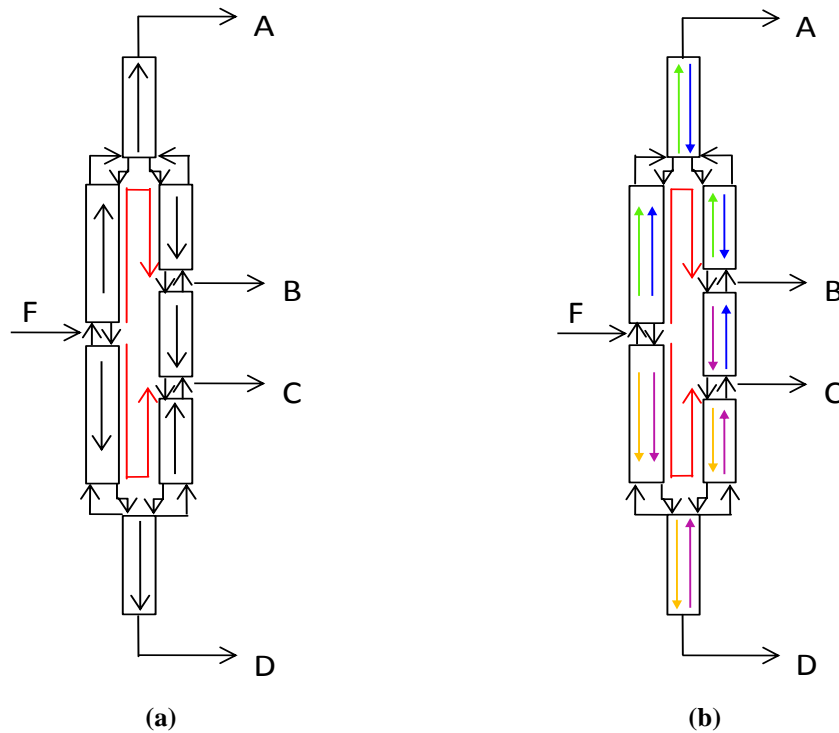


Figure 5.4: Net Flow Pattern 3 with the associated flow direction. (a) Net flow of material through each CS. (b) Net flow of components through each CS.

Table 5.1: Key of components for a general quaternary feed

	Component A
	Component B
	Component C
	Component D
	Net Flow

The various net flow patterns can be controlled or achieved by manipulating the split ratios. The regimes can be visualised, in  $\Phi_V$  vs.  $\Phi_L$  space, by producing lines of zero net flux for the coupled column sections (see Figure 5.5). The dependence of the net flow, for each of the coupled column sections, on the vapour and liquid split ratios from CS1 can be seen in the Equations 4.12 – 4.16. As a consequence, all the equations previously defined are functions of the reflux ratio in CS1. By dividing up the  $\Phi_V$  vs.  $\Phi_L$  space with lines of zero net flow for each of the coupled sections, we can identify regions within the space of different overall net flow pattern. These are labelled 1 to 5 in Figure 5.5.

Each of the regions between the zero net flux lines and the boundaries of the space produce a different net flow pattern in the coupled sections. These are the flow patterns 1 through to 5 for the Kaibel Column. For a detailed description of the split ratio space refer to Chapter 4.

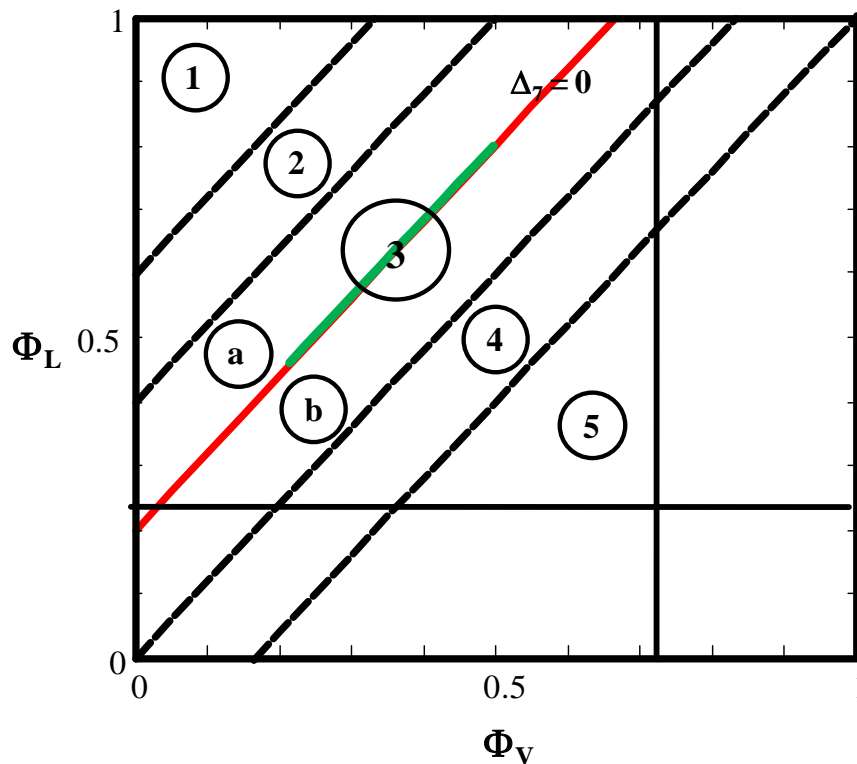


Figure 5.5: Split ratio space with the CS 7 zero net flow as the only feasible sharp split Kaibel solution shown in red.

The reflux ratio of the coupled sections can also be conveniently represented in the  $\Phi_V$  vs.  $\Phi_L$  space. Because of the definitions of the split ratios, lines of constant reflux are linear. The equations for the constant reflux lines for each of the coupled column sections are defined by Equations 4.19 to 4.28. These equations are all functions of  $R_{\Delta 1}$ . From the definition of the split ratios,  $R_{\Delta 7}$ ,  $R_{\Delta 4}$  and  $R_{\Delta 5}$  (Equations 4.20 - 4.25 and 4.27 - 4.28) are dependent on the phase of the side-draws and feed material respectively. A representation of the reflux ratios within the split ratio space is shown in Figure 5.6.

The sign of the reflux is dependent on the sign of the net flow, therefore the regions of the space corresponding to positive and negative net flow, for each of the sections, correspond to positive and negative reflux for those sections as well. In this chapter, the equations that were derived to express the split ratios in terms of the reflux ratio of each CS in will be utilised more extensively to describe limiting operating conditions for the system under optimal operating conditions.

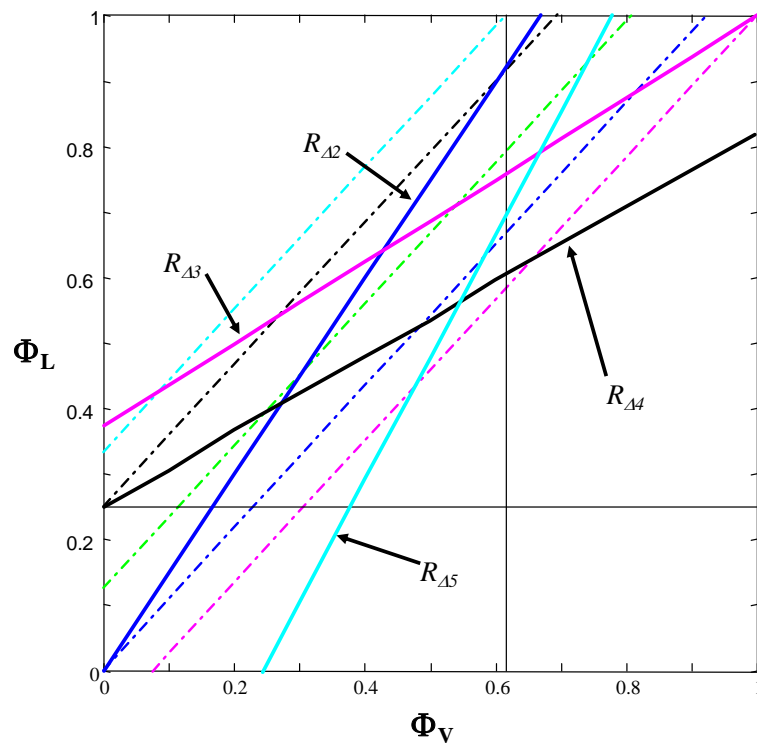


Figure 5.6: Constant reflux lines in the split ratio space for  $R_{\Delta 1} = 12$ .

As discussed, to operate a Kaibel column at sharp split specifications, the column has to be controlled such that the net flow in CS7 is zero. This is extremely powerful because we no longer have to guess values for the split ratios. We have a method to actually calculate probable split ratio combinations and understand their implications, for the design. From a very large range of potential split ratio values (0 to 1 for both liquid and vapour split ratios), we have reduced the possible choices to a single line. This is illustrated in Figure 5.5. The zero net flow of CS7 corresponds to net flow pattern 3. Note that it is not mentioned that the entirety of the  $\Delta_7=0$  line is feasible when attempting a sharp split, but only that it is a closer prospect for a feasible solution.

It was shown in Chapter 4 that the entirety of the red line depicted in Figure 5.5 does not produce feasible Kaibel solutions for the range of split ratios chosen along the line. Instead the green line that coincides with the red line is all the possible feasible solutions for this chosen reflux ratio in CS 1. Depending on the reflux ratio chosen for CS1 ( $R_{\Delta 1}$ ), may depend on how much of the line is completely eliminated from the space entirely. At higher refluxes more of the operating line is visible between the maximum bounds of the original  $\Phi_L$  vs.  $\Phi_V$  region. This result holds with our intuitive understanding of distillation systems, which is that separations are more difficult to achieve at lower reflux when compared to higher refluxes.

## 5.4 Feasible region development

### 5.4.1 Coupled Column Minimum Reflux

#### 5.4.1.1 $R_{min}$ in the CSs adjacent to the side product

As the general Kaibel solution is based on the reflux in CS 1, the coupled sections have limiting refluxes that create boundaries that satisfy the intersecting conditions of adjacent column sections. CS 6's reflux can be determined from an

overall mass balance once the reflux in CS 1 is specified. CS 2 and 4 whose profiles intersect with CS 1 and 6 respectively will be the CSs that are the limiting refluxs that produce sharp split side draw products, as these are the CSs adjacent to the side draw. The limiting reflux for CS 2 and 4 are the minimum refluxes that correspond to the liquid profiles of CS 1 and CS 2 meeting at the split below CS 1 and to the vapour profiles of CS 6 and CS 4 that meet at the split above CS 6 and in either case not overlapping. Due to the fact that all the difference points in all the CSs are predetermined based on the sharp split solution (Refer to Chapter 4) the minimum refluxes are easy to determine.

As the final solution of the Kaibel Column is based on CS 1's reflux, a clear termination point (stationary point) of CS 1's relevant profile on the L-LI boundary is known. The intersecting criteria of CS 1 and CS 2 is based on liquid profile intersections, hence the liquid  $TT_4$  of CS 1 and CS 2 have to intersect (this is indicated by solid lines, where vapour profiles are indicated by dotted lines). CS 2's minimum reflux must produce a profile that terminates at the same point as that of CS 1 on the L-LI boundary. The intersecting planes of CS 2 and CS 1's transformed tetrahedrons ( $TT_4$ ) will coincide at the intersecting point (Illustrated in Figure 5.7 ).

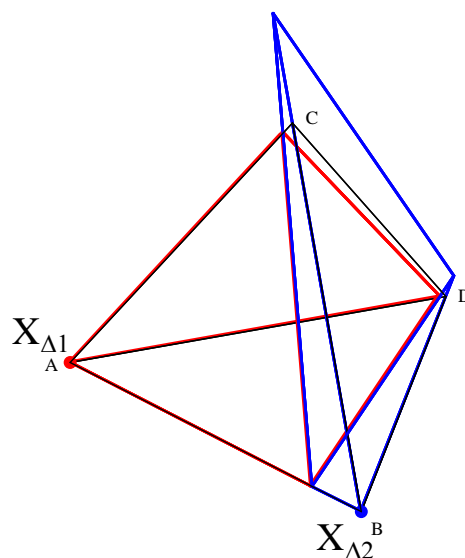


Figure 5.7:  $TT_4$  for CS 1 and CS 2 at  $R_{\Delta 2-\min}$ .

A similar argument to CS 6 and CS 4 is applicable. As CS 6 is a stripping section and its reflux is determined from CS 1 reflux, a clear termination point (stationary point) of CS 6's relevant profile on the H-HI boundary is known. The intersecting criteria of CS 6 and CS 4 is based on vapour profile intersections, hence the vapour  $TT_4$  of CS 6 and CS 4 have to intersect. CS 4's minimum reflux must produce a profile that terminates at the same point as that of CS 6's stationary point on the H-HI boundary. The intersecting planes of CS 6 and CS 4 transformed tetrahedrons ( $TT_4$ ) will coincide at the intersecting point (Illustrated in Figure 5.8).

The minimum reflux in CS1 - CS 2 and CS 4 - CS 6 are the limits of the predefined reflux in CS 1 and hence CS 6 generated in the split ratio space. This means that any reflux achieved or chosen below and above the refluxes of CS 2 and CS 4 respectively would result in an infeasible column solution. As shown in Figure 5.9 constant refluxes lines of the coupled CSs that produce the side draw products can be represented in the split ratio space. Any split ratio combination chosen beyond these constant reflux lines produces an infeasible column. The minimum refluxes of CS 2 and CS 4 are illustrated in the split ratio space in Figure 5.9.

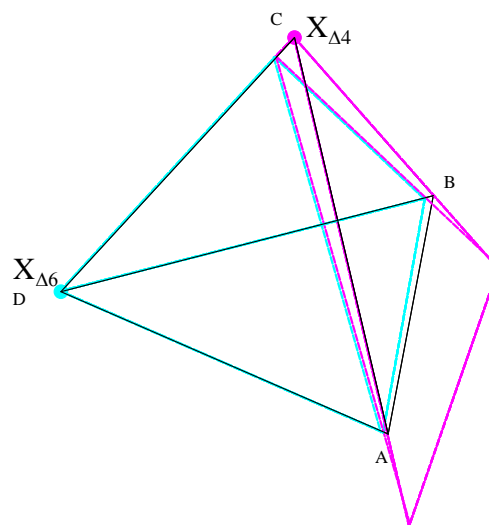
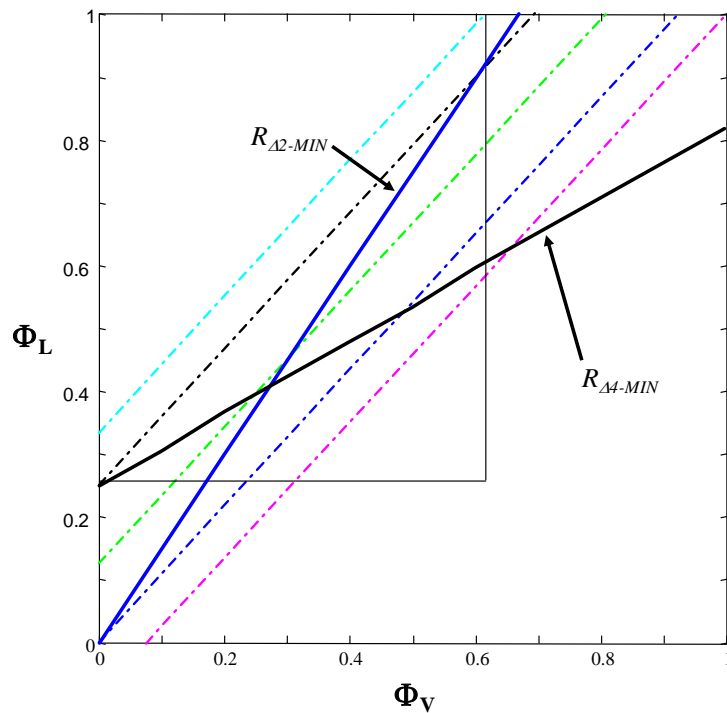


Figure 5.8:  $TT_4$  for CS 6 and CS 4 at  $R_{\Delta 2-\min}$ .

Refluxes below the minimum reflux of CS 2, as  $R_{\Delta 2} < 0$ , because the constant reflux line is above CS 2's net zero line which is in the  $\Delta_2 < 0$  region (Refer to Figure 4.24), exist above the  $R_{\Delta 2-MIN}$  line illustrated in Figure 5.9. This means that no  $\Phi_V$  and  $\Phi_L$  values above the minimum  $R_{\Delta 2}$  line will ever produce an overlap and hence a feasible Kaibel design for our chosen  $R_{\Delta I}$  and products, so we can discard this entire region when choosing our split ratios.

Any split ratio combination chosen below or on this line and more importantly on the zero net flux of CS 7 line will produce feasible profiles for CS 2.



**Figure 5.9: Minimum reflux lines in CS 2 and CS 4.**

In a similar manner, the increasing reflux in CS 4 is above the  $R_{\Delta 4-MIN}$  line as the reflux in CS 4 is positive, as the constant reflux line is above CS 4's net zero line which is in the  $\Delta_4 > 0$  region (Refer to Figure 4.24). Hence, any split ratio combination chosen above or on this line and on the zero net flux of CS 7 line will produce feasible profiles for CS 4. Hence, values of  $\Phi_V$  and  $\Phi_L$  below the minimum  $R_{\Delta 4}$  line can be discarded.

In Figure 5.9, CS 7's zero net flow line that represents feasible solution for the sharp split Kaibel Column solution intersects the minimum reflux line in CS 2. This represents a limit to the feasible solutions on CS 7's zero net flow line discussed in Chapter 4.

#### 5.4.1.2 $R_{min}$ in the CSs adjacent to the feed

We have significantly reduced the range of possible split ratio choices on CS 7's zero net flux line by identifying regions (in  $\Phi_V$  vs.  $\Phi_L$  space) resulting in negative vapour or liquid flows, categorising regions of differing net flow patterns and producing lines of minimum reflux ratio for CS 2 and CS 4 based on two of the required matching criteria (refer to Section 4.7 in Chapter 4). We will now turn our attention to another of the matching criteria; the overlap of  $TT_{4-3}$  and  $TT_{4-5}$ .

It has been shown that due to restrictions of the sharp split solution,  $X_{A2}$  is placed on pure component B and  $X_{A4}$  is placed on pure component C where  $X_{A1}$  and  $X_{A6}$  are limited to the pure components A and pure component D respectively (assuming that the light and heavy products are sharp split). In addition to this, in order to satisfy the sharp split criteria,  $\Delta_7 = 0$ . A basic material balance around the draw off point of the light intermediate product indicates that the net flow of CS 2 is equivalent to the light intermediate draw off. A similar material balance performed around the heavy intermediate draw off shows that the net flow in CS 4 is equivalent to the heavy intermediate product. This implies that if the feed to the column is known and all the recoveries of the products are known, all the net flows the remaining CSs are also known. This means that the positions of  $X_{A3}$  and  $X_{A5}$  are known.

The remaining intersecting criterion that must be satisfied is the intersection of CS 3 and CS 5. As the difference point of CS 1 and CS 2 are limited to the L-LI boundary, CS 3's difference point position is also limited to the L-LI boundary. Similarly, as CS 6 and CS 4 difference points are limited to the H-HI boundary, from mass balance, CS 5 difference point is also limited to the H-HI boundary.

It has been shown that the limiting reflux for the intersection of CS 1 and CS 2 liquid profiles are based on the minimum reflux in CS 2 which is based on the reflux chosen for CS 1. The profiles in CS 1 and CS 2 at  $R_{A2-MIN}$  intersect at a point and any reflux below  $R_{A2-MIN}$  produces profiles in CS 2 that do not intersect with the profile of CS 1. This approach can also be applied to CS 3 and CS 5. In this case though, CS 3 and CS 5 are the CSs adjacent to the feed. As the difference points of the CS 1 and CS 2 are placed at the pure components, the difference point of CS 3 is the composition attained at the top of CS 3 when the CSs adjacent to the feed are at minimum reflux. This argument is also applicable to CS 5 when analysing CS 6 and CS 4. In addition to this, the difference points of CS 3 and CS 5 are limited to the boundaries of the Gibbs triangle on the L-LI and H-HI boundaries. Hence the CPM-E technique described in Chapter 2 which is applicable to sharp and sloppy splits, can be employed to find the last intersecting points (overlap of  $TT_4$ ) of CS 3 and CS 5.

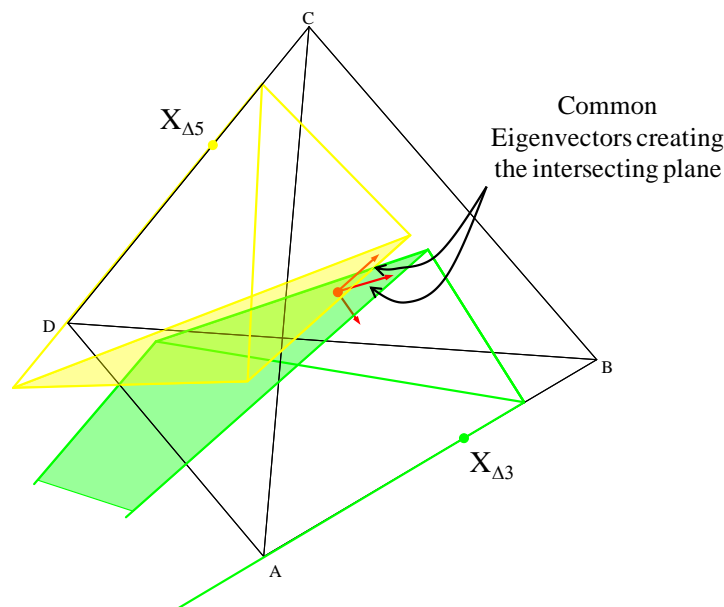


**Figure 5.10:** Common eigenvectors that define the intersecting plane for  $TT_{4.3}$  and  $TT_{4.5}$ .

It has been proven that the product specifications of a conventional column (single feed, two products) limit or define the class of minimum reflux solution achieved

when applying the CPM-E technique. As  $X_{A3}$  and  $X_{A5}$  positions are known, the class of profile/TT<sub>4</sub> intersection under minimum reflux is clear. It can be shown by developing the feasible product specification regions for a quaternary system that define the classes of TT<sub>4</sub> intersection, that the profile intersection of CS 3 and CS 5 occur along the planes of the TT<sub>4-3</sub> and TT<sub>4-5</sub> when achieving minimum reflux of CS 3 and CS 5. The CPM-E technique employs the eigenvectors evaluated at the feed condition to find the plane, line or point where the TT<sub>4</sub> overlap/intersect. Thus, evaluation of the eigenvectors for a quaternary system produces three eigenvectors, where two of the eigenvectors are common and produce the intersecting plane as illustrated in Figure 5.10. An illustration of the profile intersection under minimum reflux conditions for CS 3 and CS 5 is shown in Figure 5.11.

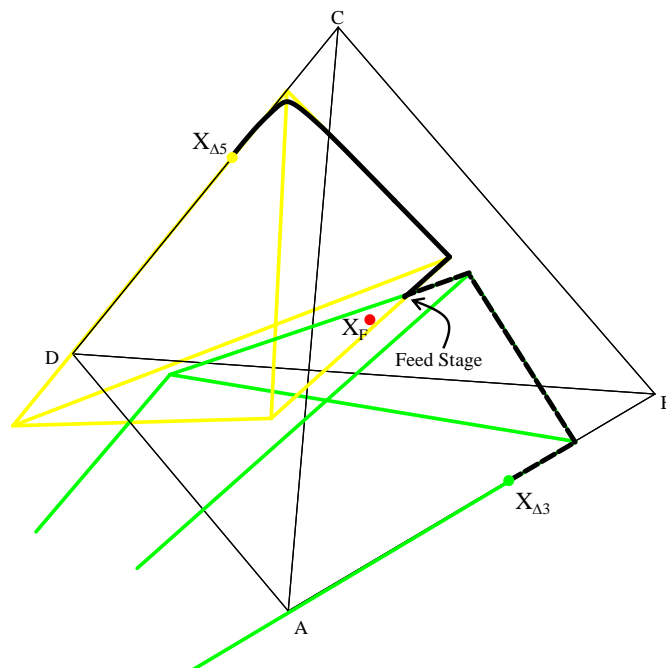


**Figure 5.11: TT<sub>4-3</sub> and TT<sub>4-5</sub> intersection under minimum reflux conditions.**

The minimum reflux in CS 3 and CS 5 are the limits of the predefined reflux in CS 1 generated in the split ratio space. This means that any reflux achieved or chosen below and above the refluxes of CS 5 and CS 3 respectively would result

in an infeasible column solution. As shown in Figure 5.12 constant refluxes lines of the coupled CSs adjacent to the column feed can be represented in the split ratio space. Any split ratio combination chosen beyond these constant reflux lines produces an infeasible column. The minimum refluxes of CS 3 and CS 5 are illustrated in the split ratio space in Figure 5.12.

Refluxes below the minimum reflux of CS 5, as  $R_{\Delta 5} < 0$ , because the constant reflux line is below CS 5's net zero line which is in the  $\Delta_5 < 0$  region (Refer to Figure 4.24), exist below the  $R_{\Delta 5-MIN}$  line illustrated in Figure 5.9. I.e. no  $\Phi_V$  and  $\Phi_L$  values below the minimum  $R_{\Delta 5}$  line will ever produce an overlap and hence a feasible Kaibel design for our chosen  $R_{\Delta I}$  and products, so we can discard this entire region when choosing our split ratios. Any split ratio combination chosen below or on this line and more importantly on the zero net flux of CS 7 line will produce feasible profiles for CS 5.

In a similar manner, the increasing reflux in CS 3 is below the  $R_{\Delta 3-MIN}$  line as the reflux in CS 3 is positive, since the constant reflux line is below CS 4's net zero line which is in the  $\Delta_3 > 0$  region (Refer to Figure 4.24). Hence, any split ratio combination chosen above or on this line and on the zero net flux of CS 7 line will produce feasible profiles for CS 4. Hence, values of  $\Phi_V$  and  $\Phi_L$  below the minimum  $R_{\Delta 3}$  line can be discarded.

In Figure 5.12, CS 7's zero net flow line that represents feasible solution for the sharp split Kaibel Column solution intersects the minimum reflux line in CS 3. This represents another limit to the feasible line of solutions on CS 7's zero net flow line discussed in Chapter 4.

*It is important to note that the minimum reflux solution of CS 3 and CS 5 in this case is only applicable where the zero net flow of CS 7 intersects with the constant reflux lines in the split ratio space. Hence the feasible line, which is limited by the CS 3 in this case is derived for a zero net flow in CS 7.*

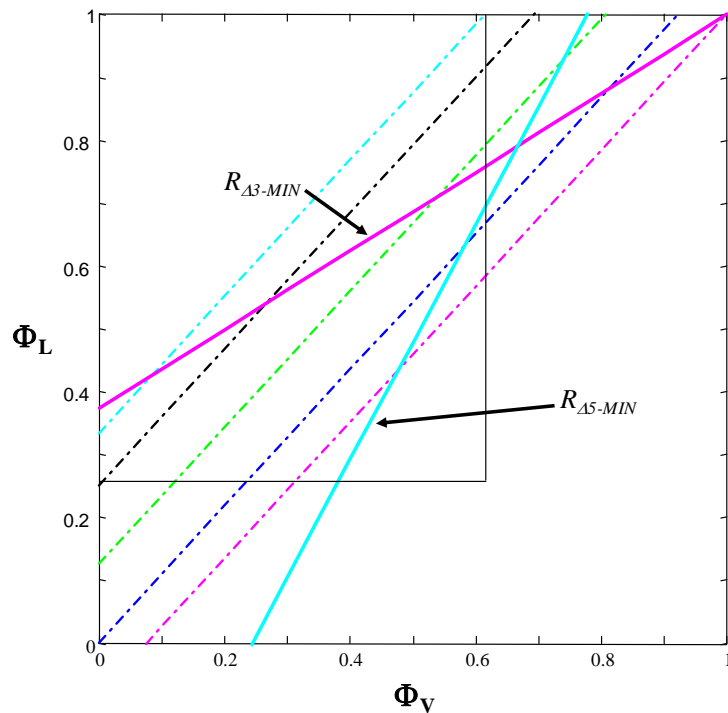


Figure 5.12: Minimum reflux lines in CS 3 and CS 5.

#### 5.4.1.3 Overall Kaibel Column Feasibility

We have considered all the required composition matching criteria and found regions of split ratio space that satisfy them. Figure 5.13 below illustrates examples of the  $R_{\Delta 3-MIN}$  and  $R_{\Delta 5-MIN}$  lines. Superimposed on these lines are the  $R_{\Delta 2-MIN}$  and  $R_{\Delta 4-MIN}$  lines. If we consider all these lines together and the individual  $\Delta_7=0$  line of feasibility for each matching criterion, we can see that there is a reduced region/line that satisfies all matching criteria for our selection of  $R_{\Delta i}$  and products. Any choice of  $\Phi_L$  and  $\Phi_V$  within this region and more importantly on  $\Delta_7=0$  line will result in a feasible Kaibel column design. This is extremely powerful because we no longer have to guess values for the split ratios. We have a method to actually calculate feasible split ratio combinations and understand their implications, for the design. From a very large range of potential split ratio values (0 to 1 for both), we have reduced the possible choices to a very small line. It is

clear that, for this choice of reflux ratio, it is very difficult to arbitrarily choose split ratios that would result in a feasible design.

The feasible line of split ratios is bound on each side by one of the lines generated from the matching criteria. Because these boundaries represent limiting conditions for certain column sections it is useful to explore the conditions along these boundaries further.

Along the  $R_{\Delta 2-MIN}$  line,  $TT_{4-2}$  borders  $TT_1$ . If we disregard the default infinite stage requirement of sharp-split separations, we can immediately conclude that, in this special case, it will take an infinite number of stages for the CS 2 composition profile to reach the rectifying profile because the unstable node pinch point lies on the boundary of  $TT_{4-1}$ . All split ratios chosen along the section  $R_{\Delta 2-MIN}$  line where  $\Delta_7=0$  intersects between point “A” and “B”, in Figure 5.13, will result in an infinite number of required stages for CS 2 and hence an unstable pinch point at the top of CS 2. Similarly, all split ratios chosen between points “A” and “D” along the  $R_{\Delta 4-MIN}$  line where it intersects with  $\Delta_7=0$  will result in an infinite number of required stages for CS 4. This condition results in a stable pinch at the bottom of the CS.

The intersection of the  $R_{\Delta 2-MIN}$  line,  $R_{\Delta 4-MIN}$  line and  $\Delta_7=0$  line (only possible for higher refluxes in CS 1) is more interesting. This specific choice of split ratios is denoted the “balanced main column” (Refer to Chapter 3). This operating point is characterised by minimum feasible vapour flow through CS 2 and CS 4. At these conditions  $TT_{4-2}$  borders  $TT_{4-1}$  and  $TT_{4-4}$  borders  $TT_{4-6}$ . There are two pinching column sections – an unstable node at the top of CS 2 and a stable node at the bottom of CS 4.

Between points “B” and “C” along  $R_{\Delta 3-MIN}$  CS 3 is at minimum reflux conditions along this line where it intersects with  $\Delta_7=0$  line. As for  $R_{\Delta 2-MIN}$  and  $R_{\Delta 4-MIN}$  line, the  $R_{\Delta 3-MIN}$  line results in a single minimum reflux value where  $\Delta_7=0$  line intersects with it, and corresponds to a single values of  $X_{\Delta 3}$ . This minimum reflux

is characterised by a stable node pinch point at the bottom of CS 3 (in the middle of the pre-fractionator).

At the intersection of  $R_{\Delta 3-MIN}$  and the  $R_{\Delta 2-MIN}$  line (point “B”) both CS 2 and CS 3 will pinch (an unstable node at the top of CS 2 and a stable node at the bottom of CS 3). This intersection point is important and will be dealt with later.

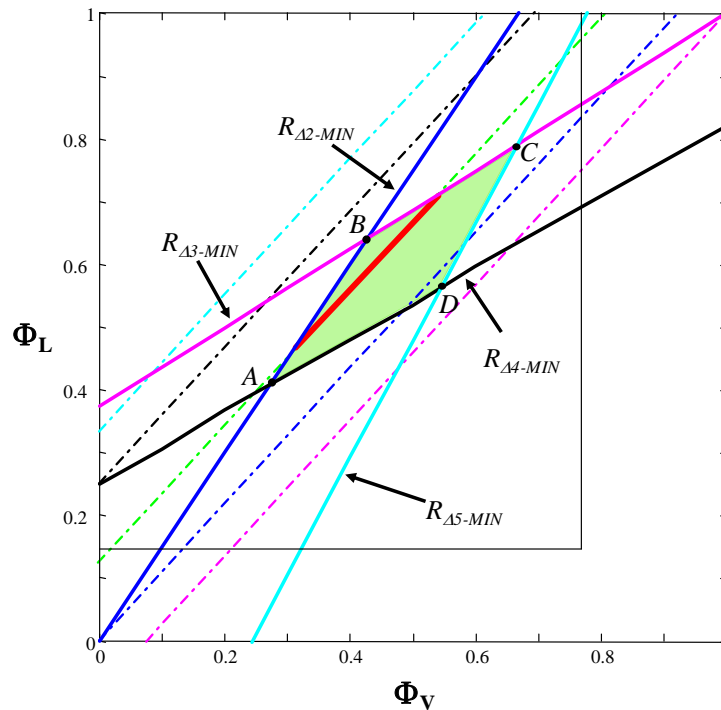


**Figure 5.13: Reduced  $\Delta_7 = 0$  line (red) defined by the region of  $\Phi_L$  and  $\Phi_V$  space resulting in feasible Sharp Split Kaibel solutions.**

Between points “C” and “D” along  $R_{\Delta 5-MIN}$  CS 5 is at minimum reflux along this line. This line is derived from the interaction with CS3 and the feed condition. As a result this line, results in a single minimum reflux value where  $\Delta_7=0$  line intersects with it, and corresponds to a single values of  $X_{\Delta 5}$ . The top of CS 5 will terminate at an unstable pinch point.

At the intersection of  $R_{\Delta 5-MIN}$  and the  $R_{\Delta 4-MIN}$  line (point “D”), CS 4 will pinch in a stable node at the bottom and CS 5 will terminate in an unstable pinch point at the top.

At point “C”,  $R_{\Delta 3-MIN}$  and  $R_{\Delta 5-MIN}$  intersect. This point has no particular significance as the intersection of  $\Delta_7=0$  line (as with the other intersecting instances, this is where the relevance of this point becomes significant) only occurs at infinite CS 1 reflux. For the Petlyuk solution shown in Chapter 3, this point is denoted the “preferred split” and is characterised by minimum feasible vapour flow through the pre-fractionator.

As this point does not occur within the Kaibel Column solution, although the column can have an overall minimum reflux solution by selecting or determining a minimum reflux in CS 1 that produces feasible profile intersecting criteria, the sharp split column cannot have a reflux combination in the pre-fractionator that will result in a minimum vapour flow in these sections when the column is at overall minimum reflux. *This means that the column configuration limits the minimum reflux the overall column can attain.* A non-sharp configuration can achieve both minimum refluxes in either the main column or the pre-fractionator, but because of the available degrees of freedom this is not possible for this column configuration and sharp split solution. If on the other hand a thermally coupled column with two partitions (three coupled columns) were chosen with two vapour and liquid split ratios each, both minimum refluxes can be achieved.

## 5.5 The Effects of varying $R_{\Delta I}$

In Chapter 3 we have discussed the effects of varying the reflux in CS 1 in the Petlyuk column. The effects  $R_{\Delta I}$  has on the constant variable lines in the split ratio space for the Kaibel column are very similar to those for the Petlyuk solution as the configurations are similar and the adjacent CSs are comparable. For the sake

of convenience, we will outline the more common feasible region effects for saturated liquid feed as well as negative flow boundaries upon variation of reflux ratio in CS 1.

### 5.5.1 $R_{\Delta 2}$ and $R_{\Delta 4}$ effects

When  $R_{\Delta I}$  is increased the volume of the transformed tetrahedron for CS 1 inside the MBT increases. The value of  $R_{\Delta 2-MIN}$  required for  $TT_{4-2}$  to border  $TT_{4-1}$  is, therefore, reduced as the planar interaction of  $TT_{4-2}$  and  $TT_{4-1}$  is closer to  $X_{\Delta 2}$ . We find that  $R_{\Delta 4-MIN}$  is similarly reduced because  $R_{\Delta 6}$  is increased the moment  $R_{\Delta I}$  is increased. The net result of the reduction in the values of  $R_{\Delta 2-MIN}$  and  $R_{\Delta 4-MIN}$  is that these lines, in split ratio space, now fan out further from their respective zero net flow lines (infinite reflux lines). See Figure 5.14 below. For our choice of relative volatilities and product points, the  $R_{\Delta 2-MIN}$  line shifts much slower than the  $R_{\Delta 4-MIN}$  line.

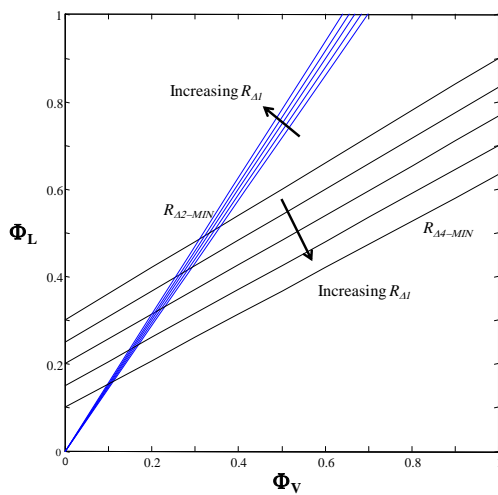


Figure 5.14:  $R_{\Delta 2-MIN}$  and  $R_{\Delta 4-MIN}$  with varying CS 1 reflux.

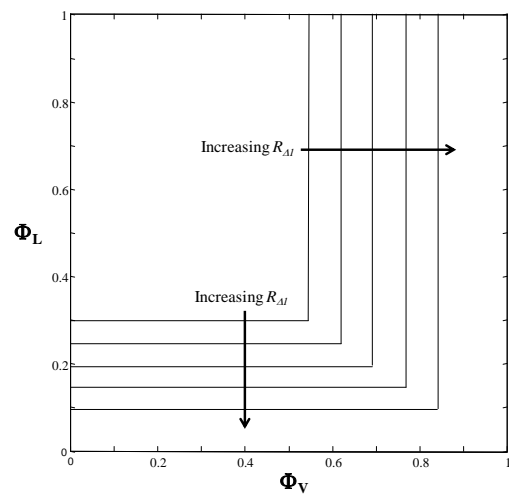


Figure 5.15: Negative flow boundaries with varying CS 1 reflux.

### 5.5.2 Negative Flow Boundaries effects

The vapour negative flow boundary in split ratio space shifts to the right - closer to  $\Phi_V = 1$  for an increased reflux in CS 1. This is as a result of the value of  $\Phi_V$ , in Equation 4.17, must increase as  $R_{\Delta I}$  increases, because the second term in this equation is negative and its magnitude decreases. The value of  $\Phi_L$ , in Equation 4.18, on the other hand, must decrease as the denominator increases. The negative flow boundary, described by Equation 4.18, will shift downwards towards  $\Phi_L = 0$  as  $R_{\Delta I}$  increases. (See Figure 5.15)

### 5.5.3 $R_{\Delta 3}$ and $R_{\Delta 5}$ effects

With increasing  $R_{\Delta I}$  the slope of  $R_{\Delta 5-MIN}$  decreases slightly and its  $\Phi_L$ -intercept shifts downwards. The slope of  $R_{\Delta 3-MIN}$  also decreases, but its  $\Phi_L$ -intercept increases, moving upwards along the  $\Phi_L$  axis. For our choice of products and constant relative volatilities, we again see a marked difference in the rate of change of two boundaries of the same type, in split ratio space. (See Figure 5.16)

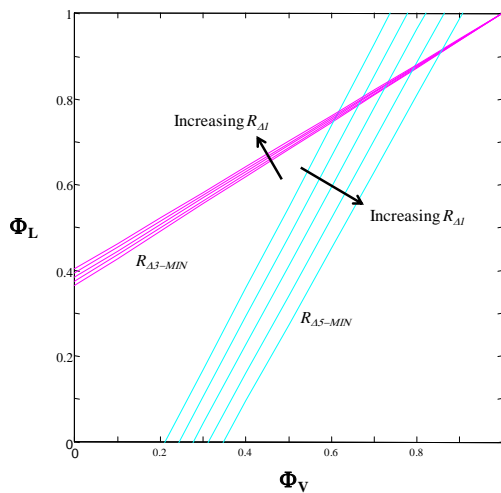


Figure 5.16:  $R_{\Delta-MIN}$  and  $R_{\Delta 4-MIN}$  with varying CS 1 reflux.

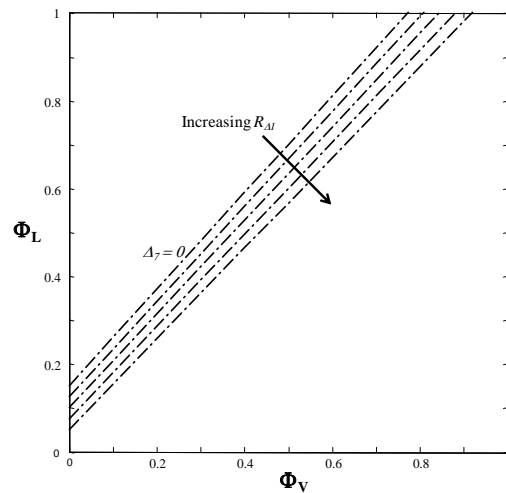


Figure 5.17: CS 7 Zero Net Flow Boundary with varying CS 1 reflux.

### 5.5.4 $\Delta_7 = 0$ effects

CS 7 zero net flow lines shifts towards the origin ( $\Phi_L = 0$ ,  $\Phi_V = 0$  or  $\Phi_L = \Phi_V$ ) line as  $R_{\Delta I}$  is increased. This occurs because the gradient of this straight line, described by Equation 4.16, tends to 1 and the  $\Phi_L$ -intercepts tend to 0 as  $R_{\Delta I} \rightarrow \infty$ . As a consequence the line moves downwards in the split ratio space illustrated by Figure 5.17.

### 5.5.5 Feasible $\Phi_L$ and $\Phi_V$ regions corresponding to $\Delta_7 = 0$

The shifting of the various boundaries in split ratio space combine to increase the overall area of the feasible  $\Phi_L$  and  $\Phi_V$  region as  $R_{\Delta I}$  is increased (see Figure 5.18). This effectively makes the separation easier as a larger range of split ratios result in feasible designs than before. This result holds with our intuitive understanding of distillation, which is that separations are more difficult at low reflux than at high reflux.

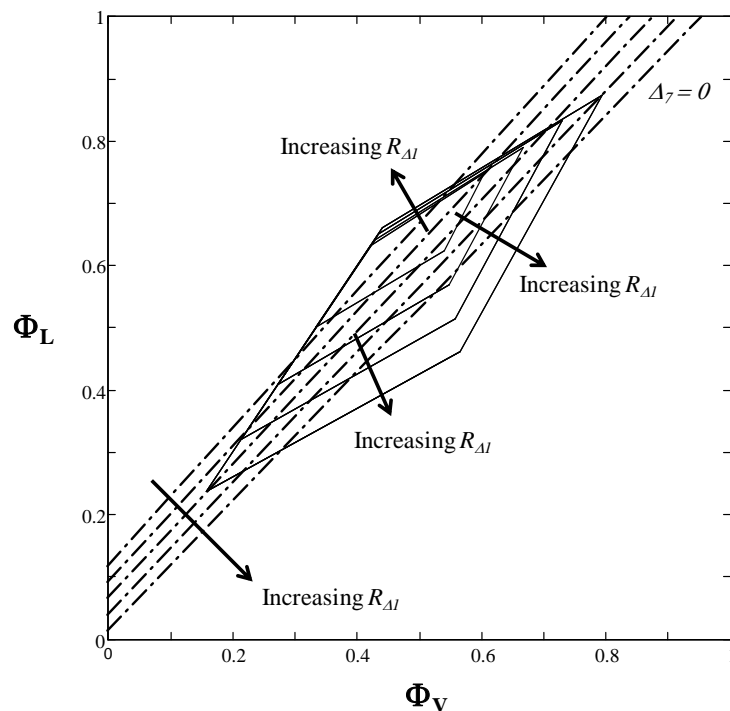


Figure 5.18: CS 7 Zero Net Flow Boundary and feasible region with varying CS 1 reflux.

As the reflux in CS 1 is decreased the feasible line defined by  $\Delta_7 = 0$  moves upwards. As a result the line of feasible solutions decreases. In addition to this the feasible region bound by the minimum reflux in the coupled sections also decreases in area with a decreasing reflux in CS 1. The combined effect causes the feasible line of solution to decrease rapidly with a small change in reflux in the rectifying section (see Figure 5.18).

At minimum overall column reflux the feasible region has zero area. As the feasible solution is only defined on a single line, the minimum reflux will be defined by a point. The region bound by the minimum refluxes of the coupled sections evaluated above expands from this zero area at minimum reflux as  $R_{\Delta I}$  is increased.

## 5.6 Overall Minimum Reflux

Thus far we have derived and shown how the zero net flow in CS 7 which represents the feasible line of solutions derived in Chapter 4 is reduced to a finite region. This was achieved by finding, analysing and implementing limiting criterion in order to satisfy all profile intersecting. The effects of varying the reflux in the rectifying or stripping section how the feasible region is manipulated. It is now our intention to find the overall column minimum reflux.

It has been shown (see Figure 5.18) that the feasible line of solutions shown by the dotted line shifts upwards with a decrease in reflux in CS 1. The line of solutions becomes significantly smaller for a small change in reflux, as the line moves towards the intersection of  $R_{A2-MIN}$  and  $R_{A3-MIN}$  as well the intersection point of  $R_{A2-MIN}$  and  $R_{A3-MIN}$  moves towards the feasible line. Eventually, at a low enough reflux (minimum reflux) the line will become a point, as this is the only visible portion of the feasible line when the limiting minimum reflux criteria is

chosen. This means that where CS 7 zero net flow becomes a tangent to the intersection of CS 2 and Cs 3 at minimum reflux. See Figure 5.19.

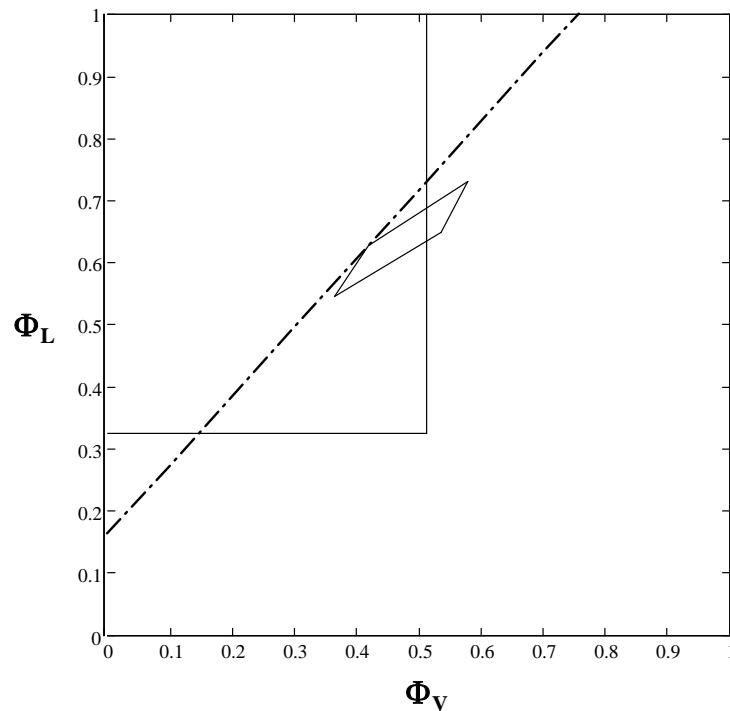


**Figure 5.19: Minimum reflux conditions for the Kaibel Column.**

This is easily envisaged by plotting the split ratio space against the reflux in CS 1 as illustrated in Figure 5.20. The figure illustrates the form of the feasible solution as the reflux in CS 1 is decreased. At higher refluxes the feasible line of solutions is large and as the reflux is decreased the feasible line of solutions decreases until eventually it becomes a single point. The feasible line of solutions, as the reflux in these examples is decreased only intersects the minimum reflux lines of CS's 2 and 3.

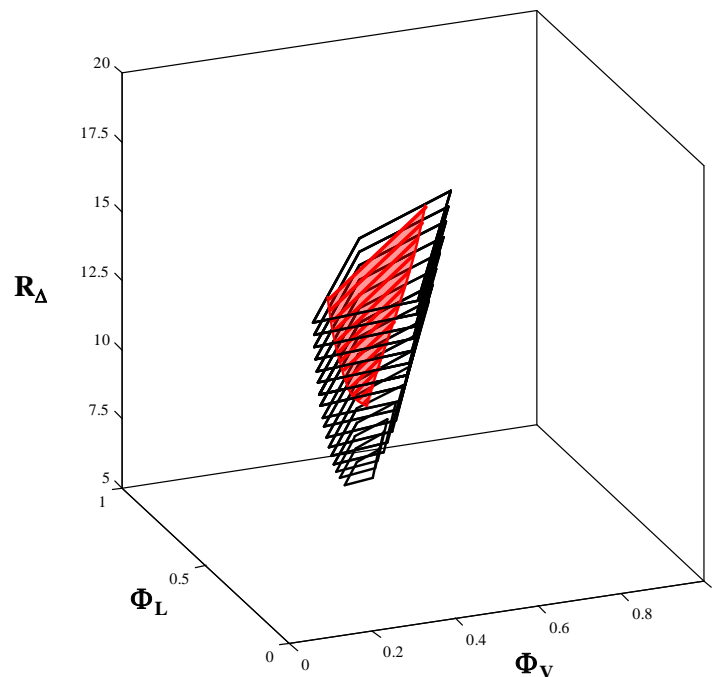


Figure 5.20: Split ratio space as a function of the reflux in CS 1 indicating the solution towards the minimum reflux in CS 1 as well as the overall column.

## 5.7 Discussion and Conclusion

This chapter is an extension of the work in Chapter 4. The identification of the feasible line of solutions for a set reflux chosen in CS 1 was shown in Chapter 4 to have restrictions. These restrictions are explored in chapter.

Variables other than net flow can be represented in split ratio space. In fact, the representation of variables in split ratio space is a very powerful tool for analysing and understanding complex column parameters that have defined vapour/liquid splits. We can very simply produce lines of split ratios corresponding to coupled-column section reflux ratios, lines of constant difference point values and also generate regions corresponding to negative internal flow rates. However, the most powerful result is that by producing minimum reflux ratio lines for CS 2, 3, 4 and 4 we can construct a region/line of split ratios that produce the only feasible

---

Kaibel Column solutions. *These lines contain all feasible split ratios values that allow the design specifications to be met for sharp splits*

Feasible lines in the split ratio space illustrate that the choice of vapour and liquid split ratios, in the Kaibel column, cannot be made arbitrarily. For reflux ratios above the minimum, only a very small region of split ratio space results in feasible designs. The designer would be very fortunate to arbitrarily choose a feasible split ratio pair.

The CPM approach has allowed us to not only generate individual solutions, but find *all possible solutions* for a set of column parameters (reflux ratio and product flow rates). Determining column minimum reflux ratio, for any zeotropic thermodynamics, is one of the most powerful results of the methodology. We can, also determine if a design is infeasible by analysing the boundaries in split ratio space. If the boundaries of the split ratio feasible region occur in the wrong position relative to each other, the designer can immediately infer that the design at the chosen parameters is infeasible. In this case, either the column reflux ratio or product flow rates must be altered in order to make the separation feasible.

At minimum reflux the feasible line is reduced to a single point. As the reflux is increased, the line of the feasible solution increases i.e. more split ratios become feasible for operation. This holds with the intuitive understanding that separation by distillation becomes easier as the reflux ratio is increased.

## **Chapter 6: Design and Analysis of multiple thermally coupled configurations using Column Profile Maps**

*The work in this chapter was done together with Daniel Beneke. This work is as of yet still unpublished but has been prepared in the form of a paper for later publication.*

---

### **Abstract**

This chapter presents a method for assessing the feasibility of multiple thermally coupled units. The Column Profile Map technique has been applied to the design of a variety of quaternary feeds for a column consisting of a main column with various combinations of side rectifiers and strippers, as well as a fully thermally coupled column. The graphical nature of the technique allows one to easily assess feasible designs for systems with less than four components, but may be algebraically extended to higher systems. Iso-reflux plots are presented as a tool to evaluate the minimum operating conditions of a specific column that also shows part of an Attainable Region. The fully thermally coupled arrangement presented here was shown to require the least amount of heat addition for a variety of feeds, but also has by far the lowest efficiencies. Subject to feed compositions, multiple side strippers, in agreement with modern crude refinery practice, have good first law expenditures with efficiencies comparable to other thermally coupled structures.

---

## 6.1 Introduction

The separation of a multi-component mixture via distillation is, although extremely effective, a very energy intensive means of separation. Probably the most widely used application of distillation technology is in petroleum refineries, where a crude oil mixture is separated into gasoline, diesel and kerosene cuts, among others. It has been estimated that the atmospheric distillation unit in a modern refinery consumes energy equivalent to 2% of the crude processed (Bagajewicz and Ji, 2000). The modern atmospheric distillation tower essentially consists of a large main column with several (usually three) thermally coupled side stripping units attached which allows for the removal of all intermediate product cuts.

There have been numerous advances in distillation design, most notably in the area of thermally coupled columns. Fully thermally coupled columns, known as Petlyuk type columns, promise large gains in energy as well as capital expenditures, although it has been suggested that these columns may not be as thermodynamically efficient (Agrawal and Fidkowski, 1998). Other thermally coupled columns such as side rectifying columns have found application in air separation (Petlyuk, 2004) as well as replacing entrainer regeneration columns in extractive azeotropic distillation (Emmrich et al., 2001). Numerous other configurations have been proposed that are thermodynamically equivalent to thermally coupled columns and have the potential for similar degrees of cost saving (Engelien and Skogestad, 2005, Agrawal, 2000b, Agrawal, 2000a, Agrawal and Fidkowski, 1999).

Strangely, with all these advances made in thermally coupled distillation, very little has transpired to crude refineries, with multiple side stripping columns still used in the vast majority of processing plants. Literature contains numerous, rigorous optimization techniques for current crude refinery practice (Bagajewicz, 1998, Bagajewicz and Ji, 2000, Bagajewicz and Soto, 2003, Bagajewicz and Soto, 2000), but almost no investigation into whether the current structure is

fundamentally superior to other options has been found. Even advanced process simulation packages such as Aspen Plus only allows one to model and design traditional refinery columns, i.e. stripping type columns. Only one study in 1995 by (Liebmann and Dhole, 1995) has attempted to address this issue and found that a main column with thermally coupled side rectifiers attached to it, instead of strippers, actually does offer advantages in terms of energy expenditures. Thus, it would be useful to fundamentally understand when a certain thermally coupled structure is superior to another, as this could result in potential savings not only in crude refineries, but also in the applications listed above.

Recently, a novel graphical tool for distillation design and analysis, Column Profile Maps, was proposed by Holland, Tapp and co-workers (Holland et al., 2004a, Tapp et al., 2004). This technique is a generalisation of a set of ordinary differential equations for conventional rectifying and stripping sections pioneered by Doherty and co-workers (Van Dongen and Doherty, 1985). This generalisation has been shown to be applicable to the design of any configuration, not only conventional rectifying and stripping sections. The Column Profile Map technique has subsequently been applied to the design and analysis of complex thermally coupled configurations such as single side rectifying and stripping units (Beneke, 2010), Petlyuk columns (Holland et al., 2010), as well as fully thermally coupled structures for quaternary mixtures such as the Kaibel column (Chapter 1).

Due to its graphical nature, the Column Profile Map design method offers a unique insight into distillation design problems. The special problem of multiple thermally coupled columns presents an interesting design challenge since there is not only an interaction between the main column and the thermally coupled side units to consider, but also between the thermally coupled units themselves. This problem has been approached by other authors using the Underwood equations (Carlberg and Westerberg, 1989), but these methods have the drawback that they are purely algebraic and the designer often lacks insight into the interaction of column sections and the internal flow and separation mechanisms. Thus, in this work we shall investigate whether there is a fundamental difference between

several options of multi-component thermally coupled distillation configurations by utilising the Column Profile Map technique, and therefore determine whether there is a superior structure under certain conditions in terms energy demand and efficiency. To utilise the graphical nature of the method we shall limit the study to quaternary mixtures, and this should lay the foundation for a more advanced study of higher order systems, which are mathematically extendable using this technique. Furthermore, only structures with a main column and thermally coupled side stream units (side rectifying and/or stripping) attached to it will be considered. The aforementioned structures are compared to themselves as well as to the fully thermally coupled Kaibel column and the associated sequence of simple columns.

## **6.2 Background: Column Profile Maps**

As mentioned in the introduction, Column Profile Maps were developed for a generalised column section, enabling it to be used for the design and analysis of almost any conceivable structure, irrespective of the complexity. Thus, this method allows the designer to analyse a specific design before being constrained by pre-conceived structures or other equipment limitations. The generalised column, by definition, is a length of column section between points of material or energy addition or withdrawal (Tapp et al., 2004), as shown in Figure 6.1.

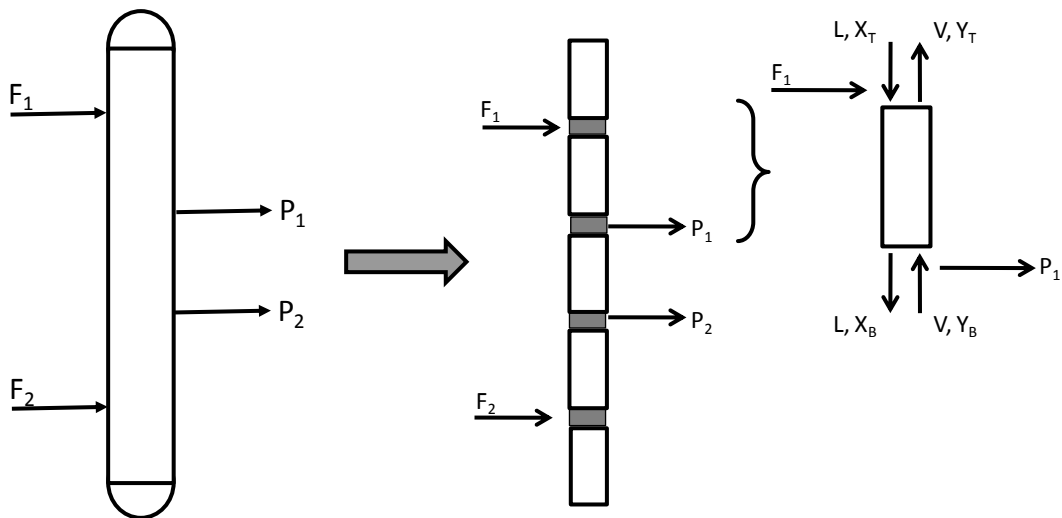


Figure 6.1: An example of a generalised column section

By performing a material balance over the column section followed by a Taylor expansion around stage  $n+1$ , assuming constant molar overflow, yields:

$$\frac{dX}{dn} = \left( \frac{1}{R_{\Delta}} + 1 \right) X - Y^*(X) + \left( \frac{1}{R_{\Delta}} \right) (X_{\Delta} - X) \quad (6.1)$$

$$\text{where } X_{\Delta} = \left( \frac{VY^T - LX^T}{V - L} \right) \text{ and } R_{\Delta} = \frac{L}{V - L} = L / \Delta$$

Equation 6.1 is known as the *Difference Point Equation*, where  $R_{\Delta}$  is a generalised reflux ratio in the column section and  $n$  the number of stages. The parameter  $X_{\Delta}$  is termed the Difference Point which is regarded as a pseudo composition vector, valid anywhere in the composition space. Like regular compositions, the individual elements of the  $X_{\Delta}$  sum to unity. Furthermore, in column sections that are terminated by a reboiler or condenser,  $X_{\Delta}$  is exactly equivalent the composition of the product stream. Negative elements of  $X_{\Delta}$  are perfectly valid and merely imply that the respective component is flowing downward in the column section. This unique property of  $X_{\Delta}$  is not even rare, and may be found in complex

columns with multiple feeds or product streams (Holland et al., 2010). Accordingly, negative reflux ratios indicate that the section is in stripping mode, i.e. there is a net flow of material down the column ( $L > V$ ) and conversely, positive reflux ratios indicate that a column section is in rectifying mode as there is a net flow of material upwards. The vapour composition,  $Y^*(X)$ , can be related to the liquid composition using an appropriate phase equilibrium model. Once the aforementioned parameters have been set a Column Profile Map may be constructed from different initial compositions, as shown in Figure 6.2 for arbitrarily chosen process parameters. The derivation of the Difference Point Equation is shown in Appendix F.

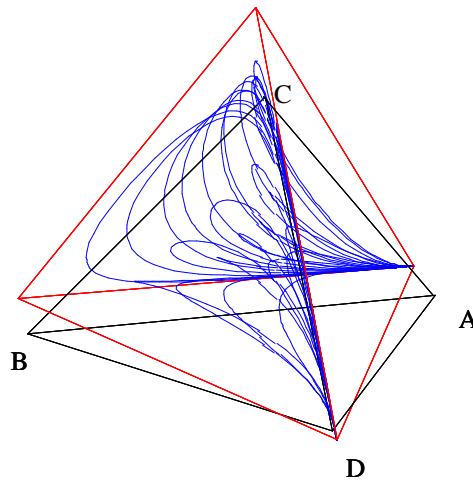


**Figure 6.2:** A quaternary Column Profile Map with  $R_{\Delta} = 9$  and  $X_{\Delta} = [0.2, -0.3, -0.2]$  and relative volatilities of 6, 4 and 2. The “shifted tetrahedron” in red indicates the movement of stationary points at finite reflux from the pure component vertices at infinite reflux.

Figure 6.2 represents possible composition trajectories for a single column section. It should be noted that it is mathematically possible to populate the entire composition space with profiles, even in the negative composition space, but these profiles have not been presented in Figure 6.2 for simplicity. This has been shown to add considerable insight to the synthesis of distillation column sections. For a design to be classified as feasible i.e. a network of column sections constituting a column, composition profiles of adjacent column sections have to intersect one

another. Figure 6.2 also shows that stationary points have been shifted in composition space, and for the special case of constant relative volatilities, these shifted points may be connected by a straight line, constituting a shifted tetrahedron. It is important to note that these shifted stationary points are obtained by algebraically solving the Difference Point Equation, and no integration is required. From a synthesis point of view, these shifted tetrahedrons are especially useful for sharp split problems as one of the sides of these tetrahedrons runs precisely through the product compositions. This unique feature has recently been applied to the design of three component Petlyuk columns (Holland et al., 2010, Holland et al., 2004b) with the aid of shifted triangles.

In the sections that follow we shall apply this property to column synthesis by making use of eigenvector theory. It is thus convenient to introduce properties of the eigenvectors of Column Profile Maps in this section. The eigenvectors may be determined by finding the  $n \times n$  Jacobian matrix of the Difference Point Equation and solving the corresponding eigenvalues and eigenvectors of this matrix. For a range of stationary points we may then generate an eigenvector map for a ternary system, as shown in Figure 6.3. The ternary map in Figure 6.3 essentially represents a plane where the composition of a single component is zero for a quaternary system. Only a ternary map is presented as a quaternary eigenvector map will be too cumbersome to fully visualise as a single point produces a three dimensional eigenvector (three eigenvectors)

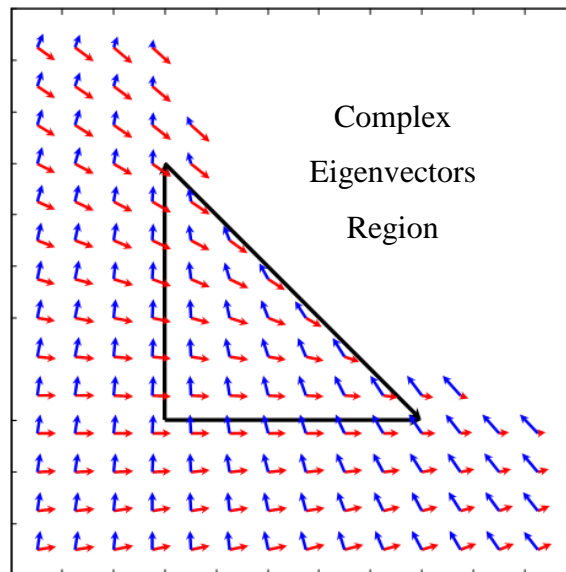


Figure 6.3: A liquid eigenvector map for relative volatilities of 3 and 1.5.

Interestingly, the eigenvectors of the Difference Points Equation are only a function of the thermodynamics of the system and not the reflux ratio nor  $X_d$  placement. Thus, a unique eigenvector map exists for a particular vapour-liquid phase equilibrium model. The eigenvectors characterise the asymptotic direction of the trajectories in the neighbourhood the singularity. The direction of the eigenvectors at a singularity indicates the direction where the remaining singularities may be found. Thus, when a stationary point is located at one of the eigenvector points shown in Figure 6.3, the eigenvectors evaluated at the remaining stationary node will point exactly towards one another. Refer to Appendix G for the mathematical background of eigenvector theory.

## 6.3 Design procedure

### 6.3.1 Initialisation

The first step in synthesising a distillation column using the Column Profile Map technique is identifying a potential structure. We will only consider thermally

coupled columns consisting of one main column with multiple side rectifiers and/or strippers attached to it. Thus, to separate a quaternary mixture, four possible structures may be conceived. These are the Double Side Stripper (DSS), the Double Side Rectifier (DSR), the Hybrid Side Stripper-Rectifier- (HSSR) and the fully thermally coupled Kaibel column. These columns, along with their respective column section breakdowns are depicted in Figure 6.4. Components have been labelled A through D from the lowest to highest boiling components and F denotes the system feed.

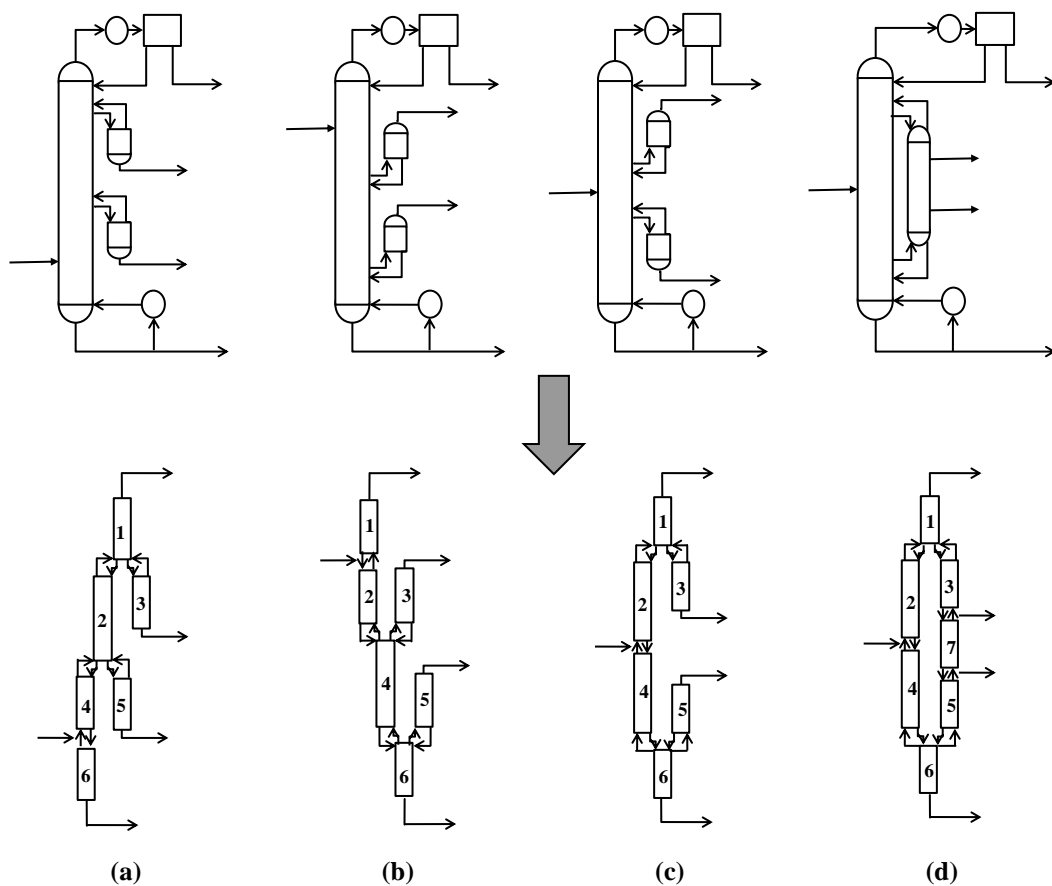


**Figure 6.4:** A column section breakdown of the four possible structures to separate a quaternary mixture with a main column and thermally coupled side stream units: (a) the DSS, (b) the DSR, (c) the HSSR, and (d) the Kaibel column.

For the purpose of consistency, the main column in all structures has been numbered 1, 2, 4 and 6, and the thermally coupled side stream units are column sections 3 and 5. Notice however that the Kaibel column consists of seven column

sections, whereas the other structures only consist of six. The HSSR and the Kaibel column are in fact very similar from a structural point of view, but the addition of a seventh column section to the Kaibel column allows one to remove another set of utilities. In total, the DSS, DSR and HSSR each require four utilities (condensers and reboilers) while the Kaibel column only requires two. Thus, each thermal coupling allows one to eliminate one utility when compared to the conventional simple column sequences, and the fully thermally coupled Kaibel column allows one to eliminate four utilities. In all structures, the vapour and liquid points of entry and exit at the thermally coupled junction are located at the same position.

Notice that the DSS configuration is closely related to crude refinery columns with multiple thermal coupling through side stripping units, although conventional crude refinery columns are slightly more complex containing even more thermally coupled units and liquid pump-arounds. Interestingly, the DSS, DSR and HSSR are analogous to the simple direct, indirect and pre-fractionating split between components B and C, respectively. This will become apparent in subsequent discussions. These structures are the only thermally coupled structures with a single main column that permit feasible flow patterns, as it is a necessary condition for the feed to lie below a side stripping section and above a side rectifying section. The reason for this necessary condition will be elaborated in the following section on net flow patterns.

### 6.3.2 Net flow patterns

Any distillation configuration consists of a network of column sections that are either in rectifying or stripping mode. Rectifying sections are characterised by a net flow of material upwards in the column section, while column sections in stripping mode dictate that flow is directed downwards. Therefore, a column section terminated by a reboiler is *always* in stripping mode, and conversely a section terminated by a condenser is *always* in rectifying mode. This can be proven by mass balance around the reboiler or condenser. However, it is not

immediately obvious what the flow directions of internal column sections are. In fact, for fully thermally coupled columns such as the Kaibel column these internal column sections may even change direction depending on the operation of the column. Holland et al (2010) have shown that there are five potential flow patterns for the Petlyuk column, but only one was shown to be optimal. Similarly, the Kaibel column with a non-sharp product specification has six potential flow patterns but only one is considered optimal. The special case of a sharp product specification, column section 7 in the Kaibel column (Figure 6.4 d) reduces to an infinite reflux section ( $V=L$ ), and therefore has only one viable flow pattern. This implies that there is no net flow of material in this column section.

Somewhat counter-intuitively, the DSR, DSS and HSSR depicted in Figure 6.4 have only one permissible flow pattern regardless of the product specification, since the internal column section flow directions are predetermined by the product producing column sections coupled to them. The net flow directions of each column section in the aforementioned structures are summarised in Figure 6.5.

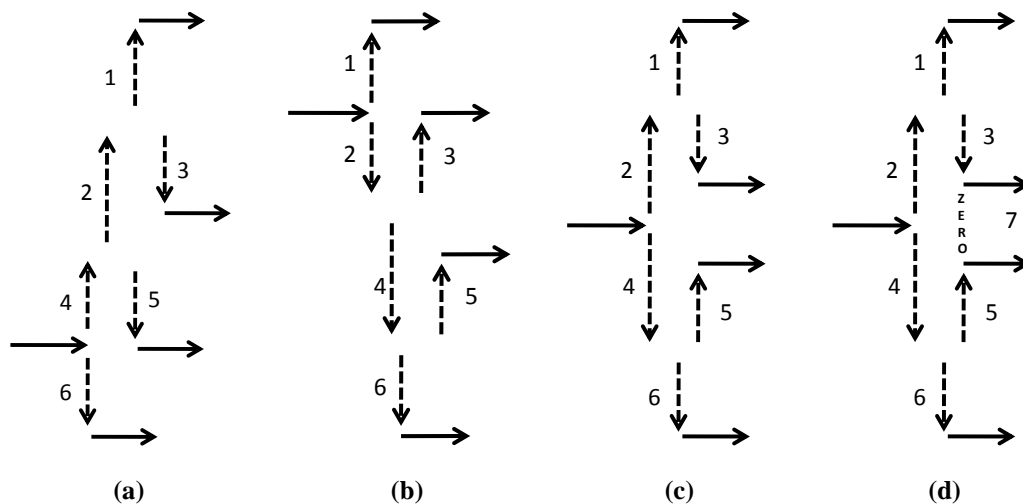


**Figure 6.5:** A summary of the only possible net flow directions in the (a) DSR (b) DSS (c) HSSR and (d) Kaibel column.

Notice that the column sections above and below the column feed stream always flow up and down, respectively. This is effectively a rectifying and stripping column section below and above the feed. Furthermore, notice that all these structures merely break down into a network of equivalent rectifying or stripping sections, or in other words, a network of simple columns. Consider for example Figure 6.5 a. Column section 4 and 6 are considered equivalent rectifying and stripping sections for the feed stream. Similarly, column section 4 can be seen as the feed to the equivalent rectifying and stripping sections consisting of column sections 2 and 5, and so on. As mentioned previously, these four structures are the only ones that permit feasible flow patterns. Placing the stream below a rectifying unit or above a stripping unit would lead to a contradiction of flow patterns, since, somewhere in the column, there would be either two stripping or rectifying sections coupled to each other, essentially a simple column with two reboilers and no condensers, or vice versa.

### 6.3.3 Difference Point placement

The Difference Point,  $X_d$ , can be seen as a pseudo composition that corresponds exactly to the product specification in column sections terminated by a utility. It has been shown in previous work that  $X_d$  in adjacent column sections are linearly related to one another, similarly to distillate, bottoms and feed compositions in simple columns (Holland et al., 2010). The Difference Points in internal column sections also have to abide by the same material balance constraints and are also linearly related to the adjacent column sections, and therefore portray similar behaviour as real bottoms or distillate products. For the DSS, DSR and HSSR structures introduced in the previous section, the relationships between the respective Difference Points are presented in Figure 6.6 for pure component product specifications and an equimolar feed.

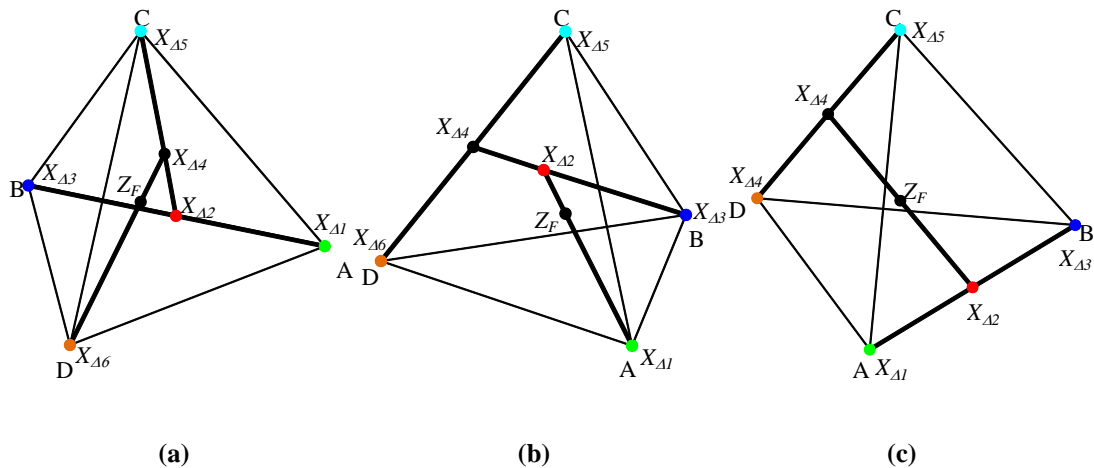


**Figure 6.6: Difference Point placement for (a) the DSS, (b) the DSR, (c) the HSSR, showing the relationship between the respective Difference Points and adjacent column sections.**

Due to the fact that column section 7 of the Kaibel column operates at infinite reflux, its component mass balance properties, i.e. its  $X_{A7}$  placement, is equivalent to the HSSR. A summary of all Difference Points in the respective column sections are given in Table 6.1 for the same specifications for Figure 6.6.

**Table 6.1 A summary of  $X_{A7}$  placement for various structures with sharp splits and an equimolar feed. Shaded cells indicate rectifying sections.**

Column Section	DSS	DSR	HSSR	Kaibel
1	[1,0,0]	[1,0,0]	[1,0,0]	[1,0,0]
2	[0.5, 0.5, 0]	[0, 0.33, 0.33]	[0.5, 0.5, 0]	[0.5, 0.5, 0]
3	[0, 1, 0]	[0, 1, 0]	[0, 1, 0]	[0, 1, 0]
4	[0.33, 0.33, 0.33]	[0, 0, 0.5]	[0, 0, 0.5]	[0, 0, 0.5]
5	[0, 0, 1]	[0, 0, 1]	[0, 0, 1]	[0, 0, 1]
6	[0, 0, 0]	[0, 0, 0]	[0, 0, 0]	[0, 0, 0]
$z_F$	[0.25, 0.25, 0.25]	[0.25, 0.25, 0.25]	[0.25, 0.25, 0.25]	[0.25, 0.25, 0.25]

The shaded cells in Table 6.1 indicates an equivalent rectifying column section, therefore the Difference Points in these column sections may be treated as distillate compositions. In the same manner, the un-shaded cells indicate

equivalent stripping sections which Difference Points are pseudo bottoms compositions.

### 6.3.4 Variable selection

Intuitively, each thermally coupled unit introduces an additional degree of freedom because the designer may specify the amount of liquid or vapour that is directed toward the side unit. This implies that a reflux ratio has to be specified in each thermally coupled side stream unit. However, reflux ratios are unbound parameters and may, theoretically, be specified from zero to negative or positive infinity. Thus, it is convenient to define a split ratio ( $\Phi$ ), which governs the amount of material sent to the side unit. For side stripping and rectifying units this ratio is given in Equations 6.2 and 6.3, respectively.

$$1 - \Phi_L = \frac{L_{SS}}{L_{MC}} \quad (6.2)$$

$$1 - \Phi_V = \frac{V_{SR}}{V_{MC}} \quad (6.3)$$

The subscripts *SS*, *SR* and *MC* indicate a Side Stripper, Side Rectifier and the Main Column, respectively. The parameters  $\Phi_L$  (for liquid splits) and  $\Phi_V$  (for vapour splits) specify the fraction of material being sent from the main column to the adjacent main column section at the split location. The fraction of material directed toward the side unit is thus given by subtracting the respective split ratio from unity. Conveniently, this parameter is bound between zero and one regardless of rectifying or stripping sections, and thus allows for representation in a constrained, positive space. Furthermore, it is more convenient to represent internal variables such as the reflux ratio in the  $\Phi$ -space when searching for feasible designs. This will become apparent in subsequent discussions.

### 6.3.5 Feasibility criteria

#### Eigenvector criteria

A realizable column design has been shown to exist when liquid composition profiles intersect one another (Van Dongen and Doherty, 1985). The constant relative volatility, sharp split design problem is very useful as feasible designs may be found algebraically by solving the pinched Difference Point Equation. In terms of a quaternary separation, the shifted stationary points thus result in a shifted tetrahedron, as depicted in Figure 6.2. A sharp split design may then be rendered feasible if their respective shifted tetrahedrons overlap one another on the same plane and/or the line of the product specifications. In order to illustrate this feasibility criterion, consider the one feed-two product simple column shown in Figure 6.7.

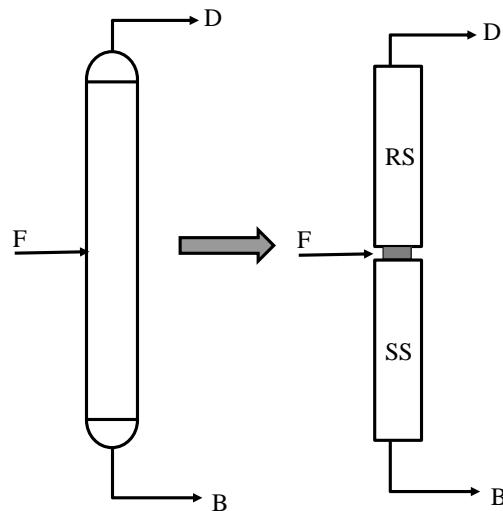


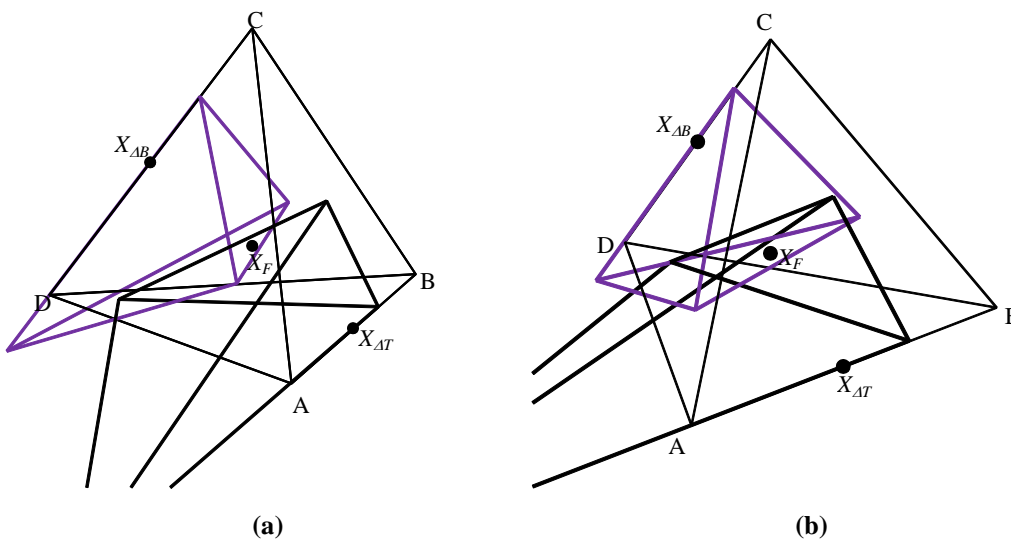
**Figure 6.7:** A simple, one feed two product column with the associated column section breakdown.

The simple column in Figure 6.7 consists of a rectifying (*RS*) and stripping (*SS*) section. The column is fully specified by choosing the product compositions and the reflux ratio, either in the rectifying or stripping section. Once either reflux

ratio has been specified, the other may be determined from an energy balance around the column, but the assumption of constant molar overflow (similar latent heat and heat effects of all components) allows one to determine the remaining reflux ratio by a material balance at the feed stage. The rectifying and stripping section are thus related by Equation 6.4:

$$R_{\Delta S} = \frac{Fq + DR_{\Delta R}}{D - F} \quad (6.4)$$

Where the subscripts  $S$  and  $R$  indicate rectifying and stripping column sections and  $q$  is the vapour quality of the feed. All parameters for both column sections are thus completely specified (as  $X_A$  is equivalent to the product specification in each column section) to construct their associated shifted tetrahedrons. These shifted tetrahedrons are presented in Figure 6.8 a-c, showing a feasible design at minimum reflux, an over-refluxed feasible design and an under-refluxed infeasible design for a quaternary feed.



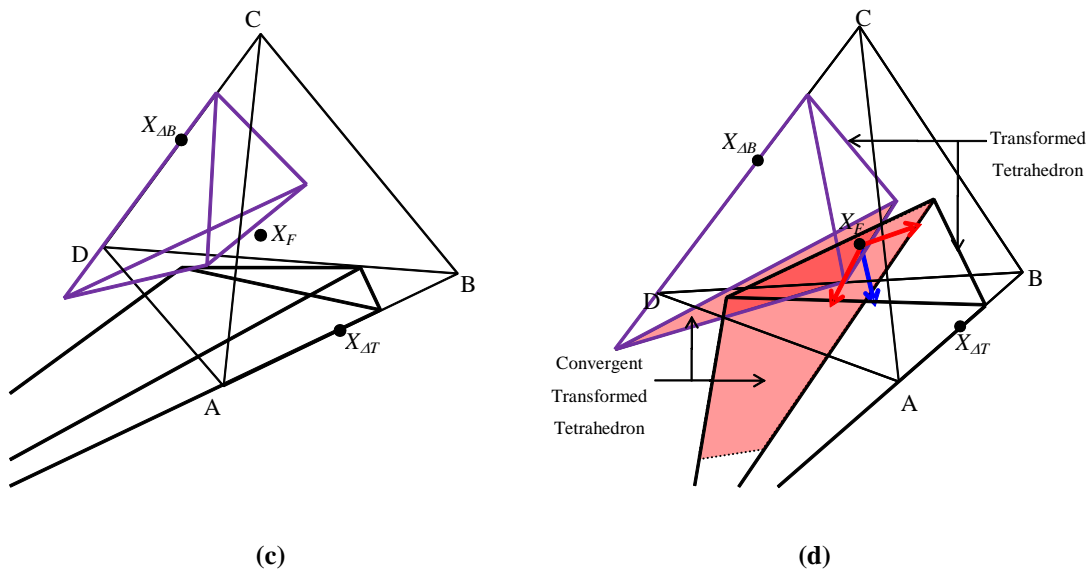


**Figure 6.8:** A design for an equimolar quaternary mixture in a simple column for the AB-CD split at (a) minimum reflux, (b) above minimum reflux, (c) below minimum reflux and (d) planar intersection through eigenvectors evaluated at the feed condition.

Figure 6.8 shows how feasible designs may be graphically discriminated using this simplifying case of the Column Profile Map technique.

The interactions of the transformed tetrahedrons with one another under minimum reflux conditions provides a unique, geometric opportunity for evaluating the feasibility of a certain column (see Figure 6.8 a). In Chapter 1 it is shown that the minimum reflux for ternary systems based on any sharp split would be established when the transformed triangles of the rectifying and stripping section meet along a line through the feed (See Figure 6.9). At specified feed, distillate and bottoms compositions, the exact condition for minimum reflux is thus that the tangent to the saddle pinch profile and the feed pinch point is a straight line through the feed composition. This creates a co-linearity criterion under minimum reflux conditions based on the feed where the saddle node of the rectifying section is collinear with the unstable node of the stripping section and the feed composition. The boundaries between stationary points for constant relative volatility systems are straight lines since the eigenvectors evaluated at the stationary nodes point



minimum reflux conditions. If the feed is a liquid the planes of the liquid transformed tetrahedrons will pass through the feed and vice versa for a vapour feed. Therefore by evaluating the eigenvectors at the feed condition produces the co-planar surface where the saddle pinch and feed pinch lie on the same plane through the feed. The eigenvector evaluation at the feed composition thus produces an opportunity to determine the stationary points along the co-planar surface and therefore the reflux associated to the minimum transformed tetrahedrons.

Finding the stationary points, for any system irrespective of thermodynamic properties, would involve solving the right hand side of the Difference Point Equation when it is equivalent to zero. At a stationary point this implies from a geometrical point of view that the mixing vector,  $\tilde{m} = X_{\Delta} - x$ , becomes co-linear with the separation vector,  $\tilde{s} = x - y(x)$ . In order to determine the pinch point of the transformed tetrahedron on the co-planar surface, simple linear geometrical tools are employed. The commonality of the co-planar surface eigenvectors and the co-linear mixing and separation vectors allows for the determination of the stationary point associated to the minimum reflux transformed tetrahedrons. This feasibility criteria using the eigenvectors are depicted in Figure 6.8 d. Importantly, the solutions obtained using the techniques described above for finding minimum reflux is exactly equivalent to the minimum reflux solutions predicted by the Underwood method.

### Special feed conditions

The solution discussed above is only applicable to feeds that are either pure liquid i.e.  $q=1$ , or pure vapour i.e.  $q=0$ . Since this chapter utilises two-phase feeds with  $0 < q < 1$ , as well as super-heated vapour ( $q < 0$ ) and sub-cooled liquid ( $q > 1$ ) feeds, and not only pure liquid or vapour feeds, a slight modification to the aforementioned minimum reflux solution is required. The solution involves finding the minimum reflux transformed tetrahedrons for both pure liquid and pure vapour feeds first and then determining the transformed tetrahedrons for a different quality of feed. Due to the fact that shifting of the liquid and vapour

transformed tetrahedrons are very similar when changing the reflux, it is remarkable to note that it is only necessary to focus on the liquid or the vapour transformed tetrahedrons to find the solution for a different quality of feed. This can be seen in Figure 6.10.

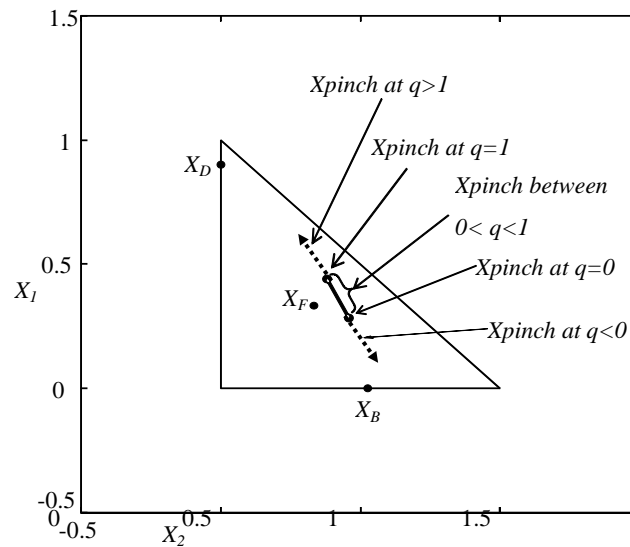


**Figure 6.10: Pinch point locations for various feed qualities**

The solid black line is the location of the rectifying pinch points where the feed has two phases. The dashed lines indicate the pinch location of superheated vapour and sub-cooled liquid on either side of two-phase region. The two phase feed solution will thus involve using the two stationary points at the minimum reflux conditions; one point on the liquid feed solution and the same nature of node on the vapour feed solution will arise. By constructing a straight line through these nodes, sets the relative bound of the two phase feed ( $0 < q < 1$ ). The liquid stationary point solution with a feed quality of 0.5 for example will then lie on the middle point of the line between these nodes. As the difference points are already known, the only variable left to calculate is the relative minimum reflux solution which is now based on the set quality of the feed. If the solution for a super heated vapour feed is required, the same interpolation like procedure can be used. When a super heated vapour is required, then the stationary point is found in the

direction of the vapour transformed tetrahedron on the same straight line and vice versa for a super cooled liquid feed.

The extension to the equivalent higher order systems minimum reflux solution is based on the same principles as the ternary and quaternary systems. As mentioned previously the minimum reflux solution for the ternary system is based on the linear interactions of the eigenvectors, mixing vectors and separation vectors. The quaternary solution is based on the planar interactions of the transformed tetrahedrons for the rectifying and stripping sections and the evaluated eigenvectors at the feed

In the same way as we evaluated the eigenvectors at the feed composition and produced the co-linear and co-planar where the transformed triangles/tetrahedrons met, the eigenvector evaluation at the feed composition for higher order systems produces the co-hyper-planar boundaries where the transformed hyper planes touch. In order to determine higher order system minimum reflux solutions the stationary points must thus interact on hyper planes of the desired number of components as required. In order to determine the pinch point of the transformed hyper planes, the point where the co-linear mixing and separation vector intersects with the co-hyper-planar boundary is one of the minimum reflux stationary points. The exact same solution as mentioned above for different quality of feeds is directly applicable to any higher order systems, but cannot be graphically visualised.

The minimum reflux solution discussed above is called the Column Profile Map-Eigenvector technique (CPM-E). Figure 6.8 d shows the interaction of planes at minimum reflux conditions. The CPM-E technique and hence the eigenvector evaluation at the feed composition depending on the quality of the feed is thus an exact criterion for finding a feasible design and is not limited by the number of components to be considered. This criterion can be extended to non-ideal systems as an approximation, since the eigenvectors at stationary points do not exactly line up with one another along the hyper planes. It is important to note that even

though a wide variety of feed conditions are encountered in our design problems, the generic liquid *and* vapour transformed polygons both always intersect with one another. It is therefore only necessary to evaluate the liquid transformed polygons and profiles (Holland et al., 2010).

### 6.3.6 Thermally coupled column sections

Section 6.3.5 discusses how designs may be classified as feasible for a simple column. The design procedure outlined thus far allows for a unique graphical insight into the design of simple distillation columns. In order to analyse more complex, thermally coupled columns it is therefore useful to retain the general design ideas for simple columns and extrapolate it to more complex systems. A similar approach to the one described in this section has been adopted by other authors using the Underwood equations (Carlberg and Westerberg, 1989), but it is presented here in terms of the our defined variables to show the applicability of the CPM-E technique to the analysis of thermally coupled columns. Fortunately, the definition of  $X_A$  allows one to easily extend this methodology to any structure since it is in fact a pseudo composition. Using the techniques described here, any column may be broken down into a network of simple columns with the same general design procedure described for the simple column. To illustrate this fact, consider a generic thermally coupled side rectifying and stripping unit as shown in Figure 6.1 a and b.

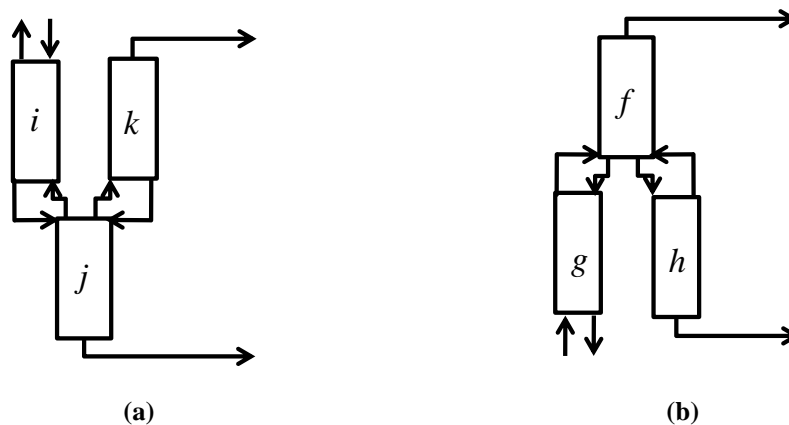


**Figure 6.11: A generic thermally coupled (a) side rectifying and (b) side stripping with the corresponding net flow directions of each column section.**

In the side rectifying arrangement Figure 6.11 a, the vapour from column section  $j$  feeds both column sections  $i$  and  $k$ , while column section  $i$  and  $k$ 's combined liquid streams feed column section  $j$ . The amount of vapour to be distributed between sections  $i$  and  $k$  are governed by the vapour split ratio. Since the vapour split and liquid feed point is assumed to take place at the same location in the column and column sections  $j$  and  $k$  are producing end products, the net material flow from column section  $i$  is effectively the feed to column sections  $j$  and  $k$ . Thus, by adding the directional vapour and liquid in the feed column section,  $i$ , the net feed flow rate may be obtained. In terms of our Column Profile Map parameters this results in:  $F_i = |\Delta_i|$ , since the feed always has to be positive. This is then essentially the pseudo feed to the simple column comprising of rectifying section  $k$  and stripping section  $j$ . Furthermore, the composition of this pseudo feed stream is equivalent to the Difference Point of column section  $i$  ( $X_{\Delta_i}$ ), which may be calculated *a priori* once the product compositions have been set (see section 6.3.2) as shown in Figure 6.6 and Table 6.1. The quality of the pseudo feed is the fraction of liquid in the feed, and can thus be written as:

$$q_i = \frac{L_i}{F_i} = \frac{L_i}{|\Delta_i|} = \frac{L_i}{-\Delta_i} = -R_{\Delta_i} \quad (6.5)$$

In a similar manner, the flow rate, composition and quality of the pseudo feed may be derived for the generic stripping section. The parameters for both configurations are summarised in Table 6.2.

**Table 6.2: Summary of pseudo feed streams to the generic side rectifying and stripping sections**

Structure	Feed flow rate ( $F$ )	Feed composition ( $X_f$ )	Feed quality ( $q$ )
Side Rectifier	$V_i - L_i = \Delta_i$	$X_{\Delta_i}$	$-R_{\Delta_i}$
Side Stripper	$-(V_g - L_g) = -\Delta_g$	$X_{\Delta_g}$	$-R_{\Delta_g}$

Interestingly, the pseudo feed quality is the negative of the generalised reflux ratio in the feed column section. Thus, the feed to a column section with a side rectifier can be seen as pseudo superheated, since  $R_{\Delta_i}$  is always positive, and conversely the feed to a column section with a side stripper can be seen as pseudo sub-cooled since  $R_{\Delta_g}$  is always negative. The key parameters in the column profile map technique thus extend naturally to incorporate thermally coupled columns. Essentially, these definitions aid in breaking down the complex structures to a set of pseudo binary columns which may easily be analysed and interpreted.

### 6.3.7 Stepwise design algorithm

The theory described in the preceding sections can now be put together in a stepwise design algorithm which allows one to evaluate virtually any given structure. This design procedure is summarised as follows:

- **Step 1:** Formulate a configuration to evaluate or design.
- **Step 2:** Set the product specifications for each product producing column section and determine the overall mass balance.
- **Step 3:** Define the appropriate split ratios, choose a reference reflux ratio for one column section (usually one located above/below the feed) and determine the generic mass balances, which specify all internal Difference Points and material flows.
- **Step 4:** Determine the minimum reflux for the “pseudo simple column” using the CPM-E technique with column sections located above and below

the feed, using the Difference Points as bottoms and distillate compositions.

- **Step 4b:** If necessary, specify an over-refluxed factor, i.e. a factor that will account for a non-pinched design.
- **Step 5:** Determine all net material flows and reflux ratios in the respective “pseudo simple column” and use these as the new feed for the new adjacent “pseudo simple column” with the feed conditions outlined in section 6.3.6.
- **Step 6:** Repeat from Step 4 until the entire column has been specified

## 6.4 Finalising the design

### 6.4.1 Iso-reflux analysis

Once a fundamental understanding of the design procedure has been gained, we may easily evaluate our given structures. In order to determine what the operational conditions of a particular structure is, it is at first useful to specify that all column sections operate at minimum reflux. This constraint allows one to search for feasible design using the eigenvector theory discussed above. However, this constraint can be easily relaxed and one can decide to operate a certain set of column sections above minimum reflux once it has been determined. Since our thermally coupled units described above have three internal degrees of freedom (one reflux ratio and two split ratios), it is convenient to represent all column sections in one diagram to obtain an intuitive understanding of the interaction of column sections. This can be done in an iso-reflux plot, shown in Figure 6.12 for the DSS, where  $\Phi_{L1}$  and  $\Phi_{L2}$  indicate the top and bottom liquid split ratios in the DSS as shown in Figure 6.4. This plot is obtained by writing all the reflux ratios in the column sections in terms of the split ratios (see Appendix E). One can then obtain what range of split ratios that will satisfy the minimum reflux condition for each column section.

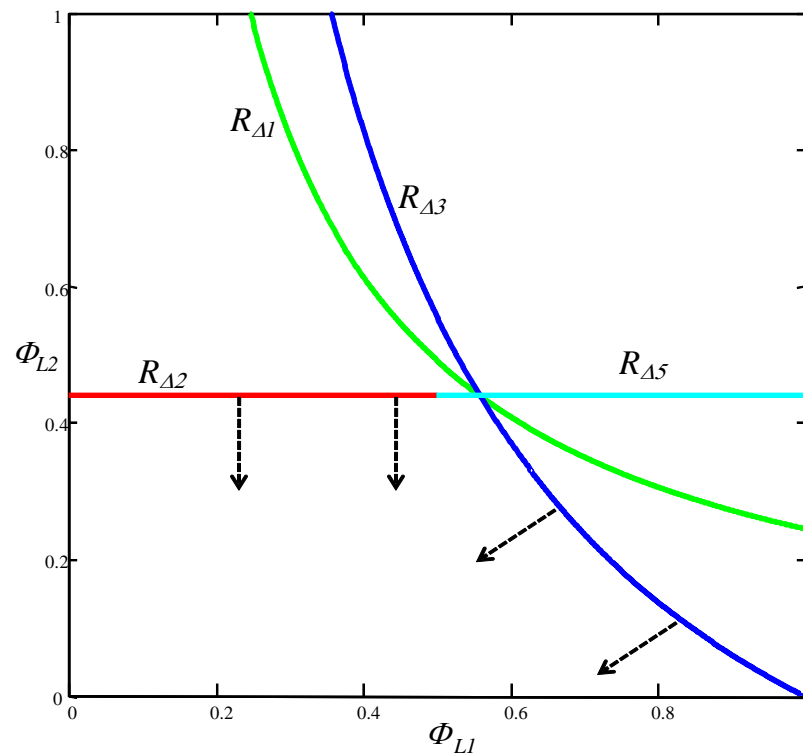


Figure 6.12: An iso-reflux plot for the DSS at minimum reflux.

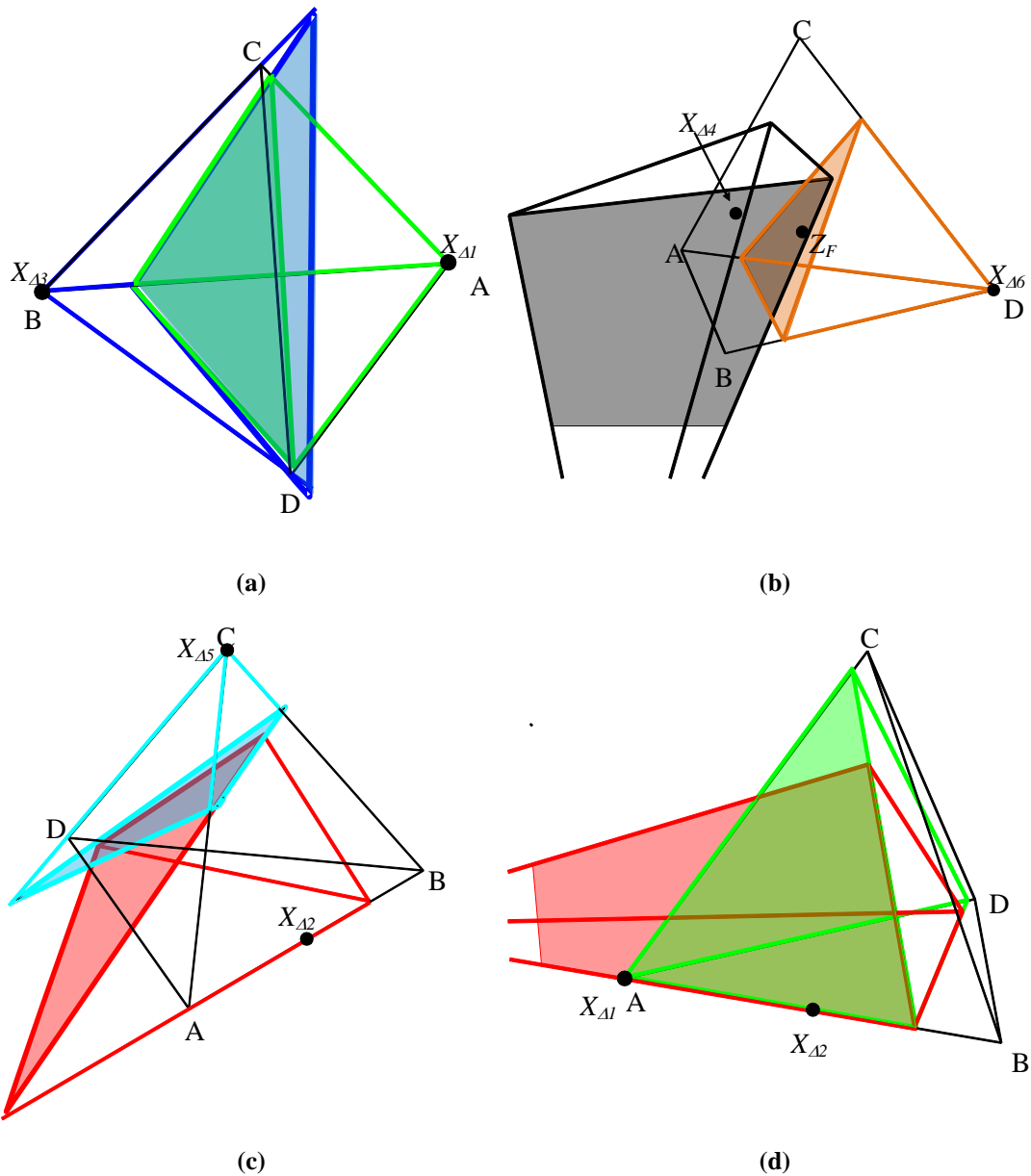
Figure 6.12 shows the range of split ratios that result in specific column sections operating at minimum reflux. The specific reflux ratios at minimum reflux are given in at the end of this section in Table 6.3. From this diagram one is able to quickly realise that there is a certain combination of  $\Phi_{L1}$  and  $\Phi_{L2}$  that results in a specific combination of a column section operating at minimum reflux one adjacent to it. However, there is only a single point where all sections are at minimum reflux with one another. This point occurs where all the iso-reflux lines intersect one another, as every simple pseudo simple column operates at minimum reflux, therefore the entire column operates at minimum reflux. Thus, we have now determined from this relatively simple plot what the reflux ratios in each column section is required to be, and therefore the split ratios too, for the entire column to operate at minimum reflux. Figure 6.12 shows that there is only one selection of  $\Phi_{L1}$  and  $\Phi_{L2}$  that satisfies the minimum reflux criterion, where all iso-reflux lines intersect one another.

Each curve in Figure 6.12 represents the reflux ratio that a particular column section is required to be at. It is important to note that the mass balance has been performed by starting across the feed stage and working upwards. From this mass balance perspective, the reflux of top column sections, i.e. 1 and 3, are dependent on both  $\Phi_{L1}$  and  $\Phi_{L2}$  (blue and green curves), while the refluxes of column sections 2 and 5 are only dependent on  $\Phi_{L1}$  (red and cyan curves). The iso-reflux curves of column sections 1 and 3 are thus curved, while those of column sections 2 and 5 are straight lines that fall exactly on one another. From this figure it may also be inferred that not only is the interaction between the main column and the thermally coupled side units, but also between the side units themselves.

Apart from showing the absolute minimum reflux of all column sections, these iso-reflux lines also depict an Attainable Region. Specifically, this is the Attainable Region when the column sections adjacent to the feed stream are at minimum reflux. All possible combinations of  $\Phi_{L1}$  and  $\Phi_{L2}$  that would lead to a feasible design between minimum reflux and infinite reflux for the other column sections are depicted in the direction of the arrows. Any values of  $\Phi_{L1}$  and  $\Phi_{L2}$  that do not lie in inside this region will lead to design where at least one pair of adjacent column sections are below minimum reflux, and therefore are classified as infeasible designs. It is important to reiterate that the column sections across the feed are still at minimum reflux, and thus this iso-reflux does not depict the entire Attainable Region, but merely a part of it. If this minimum reflux condition were to be relaxed for these column sections, the Attainable region would expand, until an infinite reflux condition is specified whereby the entire  $\Phi$ -space would be attainable.

Notice that there are four iso-reflux lines in Figure 6.12, and not one for each column section, since the minimum reflux condition across the feed stage is completely independent of both split ratios. Interestingly, this Attainable Region shows that there are in fact infeasible designs when one pair of column sections, 1 and 3 in this case, operate at infinite reflux ( $\Phi_{L1} \rightarrow 1$ ), but there are still feasible designs when the other pairs of adjacent column sections, 1 and 2 and 2 and 4

respectively, operate at infinite reflux ( $\Phi_{L1}, \Phi_{L2} \rightarrow 0$ ). The shifted tetrahedrons at minimum reflux are shown in Figure 6.13a-e for each pair of adjacent column sections. The colour of the shifted tetrahedrons corresponds to the colours of the iso-reflux lines in Figure 6.12.



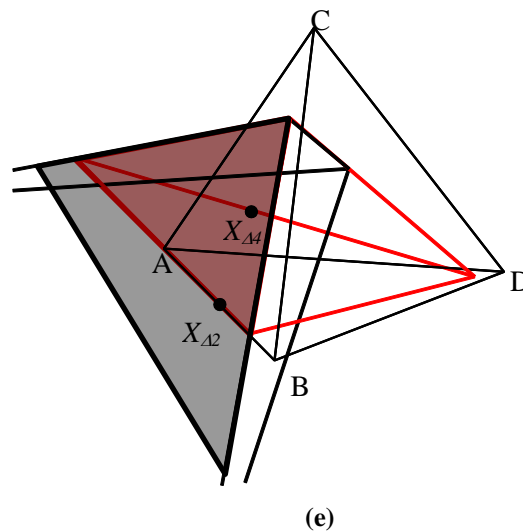


**Figure 6.13: Transformed tetrahedrons at minimum reflux for the DSS. (a) Column sections 1 and 3. (b) Column sections 4 and 6. (c) Column sections 2 and 5. (d) Column sections 1 and 2. (e) Column sections 2 and 4.**

Figure 6.13 a-e shows that, as with the simple columns design, that each pair transformed tetrahedrons of adjacent column sections just touch each other. The column is thus said to be operating at overall minimum reflux. For this particular structure, only liquid composition tetrahedrons have been drawn for the thermally coupled column section, since the liquid profiles line exactly up with one another because of a splitting of liquid phases. The shaded regions in Figure 6.13 a-e show the planes that touch one another at minimum reflux. A “real” column is often said to operate at a factor between 1.05 and 1.50 times the minimum reflux (Seader and Henley, 2006). Thus, using these guidelines, *each* simple column in the entire column has to operate at a factor above minimum for the entire column to operate above minimum reflux and a similar iso-reflux plot can be generated to depict the over-refluxed design. Using the same procedure outlined previously, similar iso-reflux figures for the DSR in its respective  $\Phi$ -space may be constructed along with their shifted tetrahedrons.

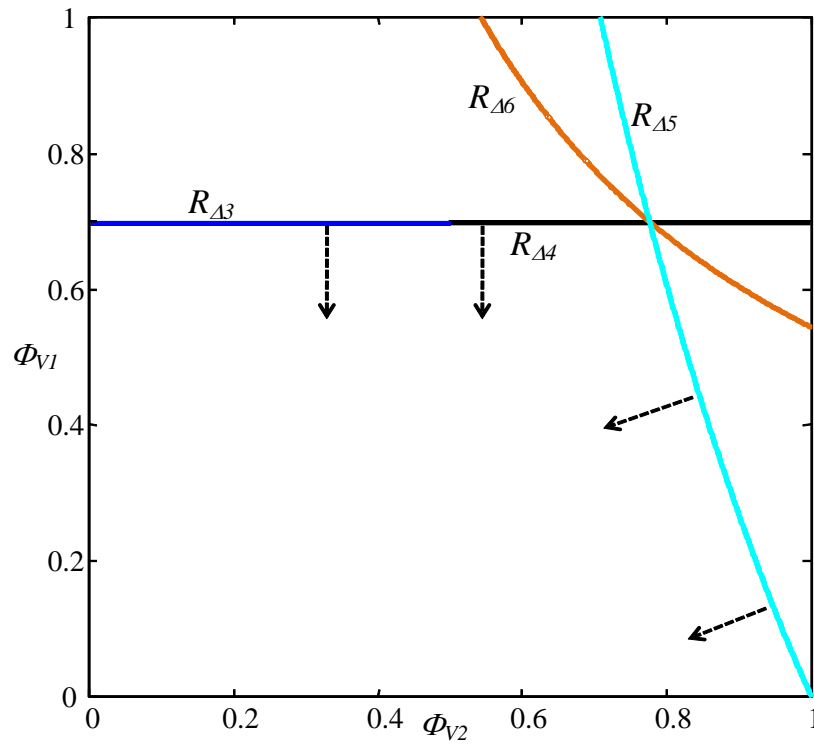
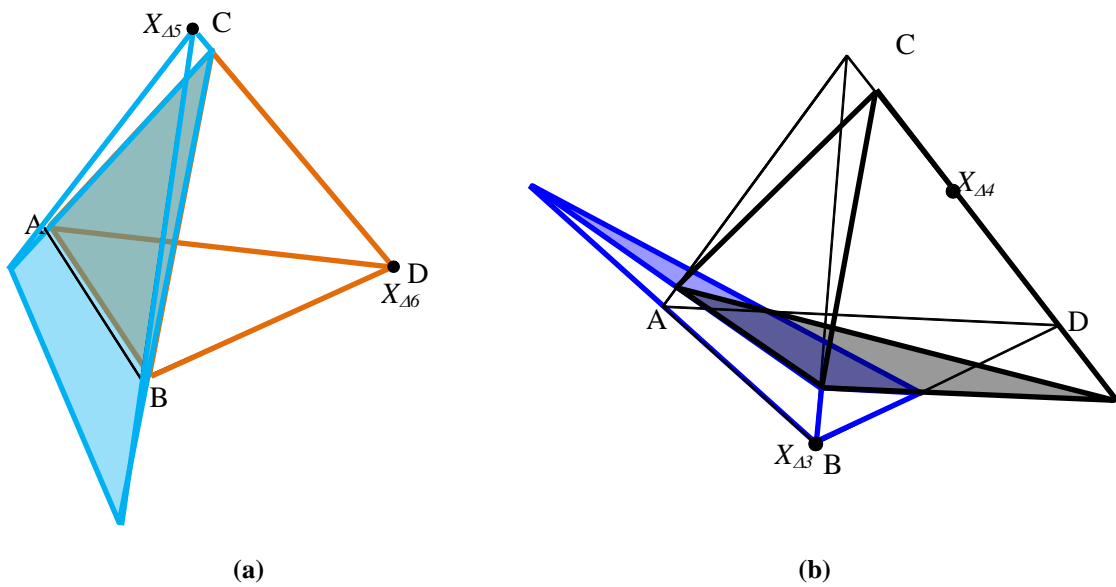
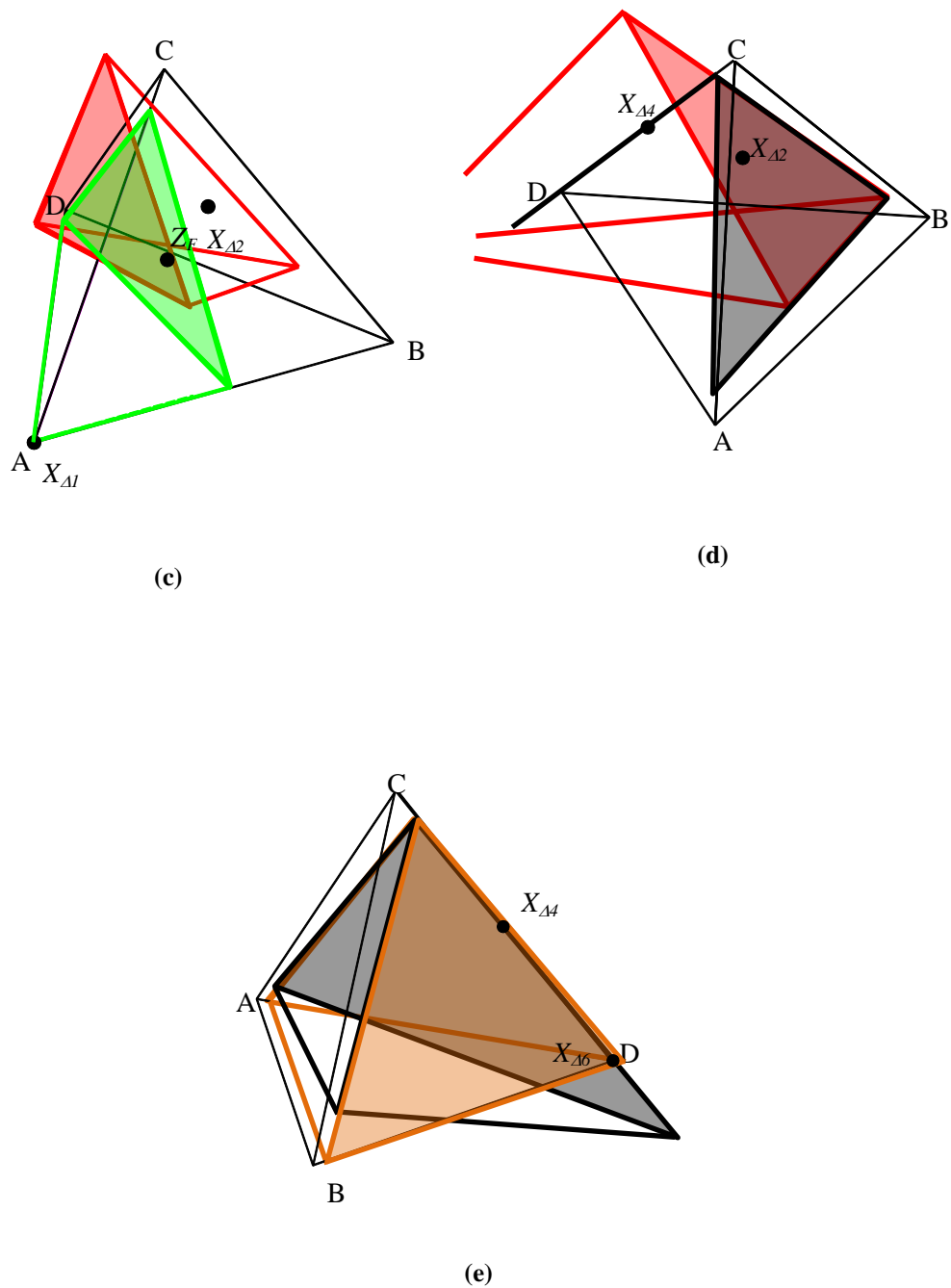


Figure 6.14: An iso-reflux plot for the DSR at minimum reflux.





**Figure 6.15: Transformed tetrahedrons at minimum reflux for the DSR. (a) Column sections 5 and 6. (b) Column sections 3 and 4. (c) Column sections 1 and 2. (d) Column sections 2 and 4. (e) Column sections 4 and 6.**

The DSR operating at minimum reflux may be interpreted in a similar way to DSS structure, but it should be noted that the split ratios are now vapour splits ( $\Phi_V$ ). The mass balance has been performed from the feed stage downwards, and thus

the bottom column sections (4 and 6) are dependent on both split ratios. Again, there is an Attainable region indicated by the direction of the arrows, where over-refluxed feasible designs may be found when the column section 4 and 6 are at minimum reflux. Since there are only vapour split in the DSR, we have chosen to construct shifted vapour tetrahedrons, since these compositions exactly match up with one another at the vapour split stage. Again, the shaded regions indicate where the planes touch each other.

In order to construct iso-reflux plots for the HSSR, it is important to point that the mass balance and minimum reflux calculation have to be initiated across the feed stage. The iso-reflux plots for the HSSR are thus unique because the feed is situated between the two split ratios. Thus, these split ratios are independent of one another at minimum reflux conditions. This is depicted in Figure 6.16, along with the corresponding shifted tetrahedrons in Figure 6.17.

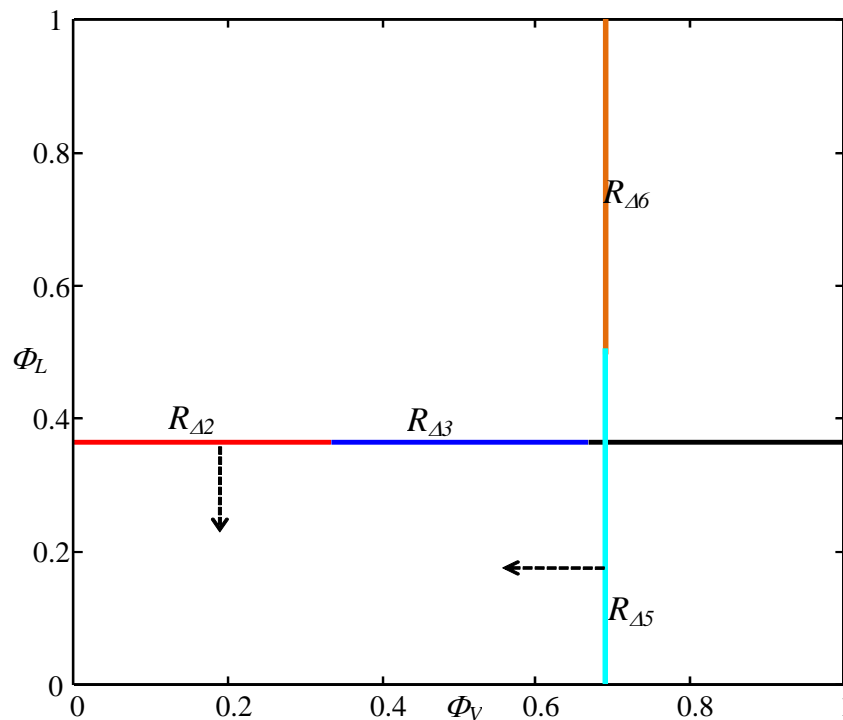
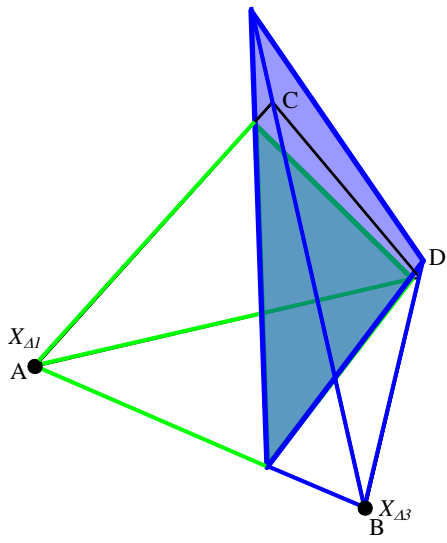
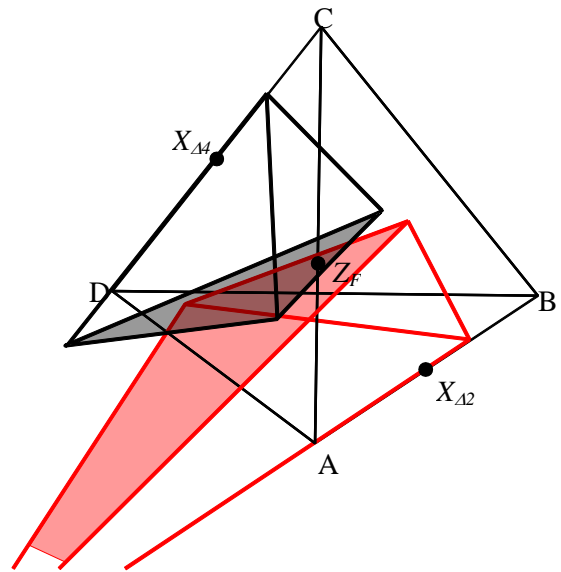


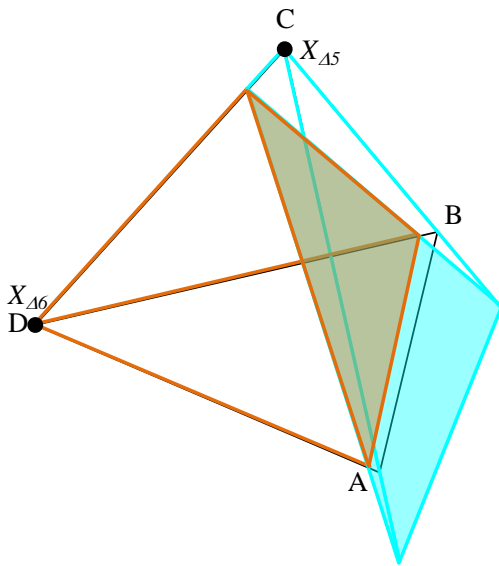
Figure 6.16: An iso-reflux plot for the HSSR and Kaibel column at minimum reflux.



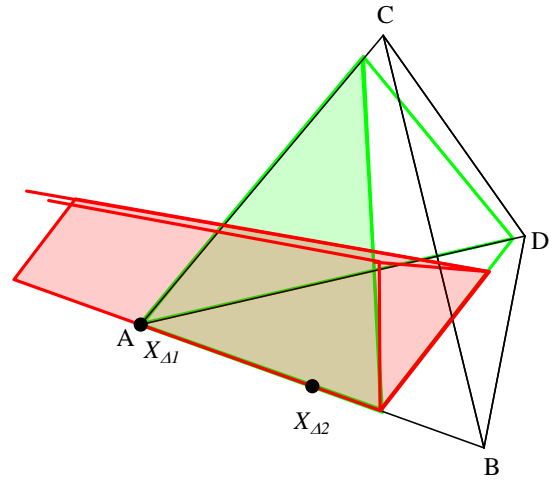
(a)



(b)



(c)



(d)

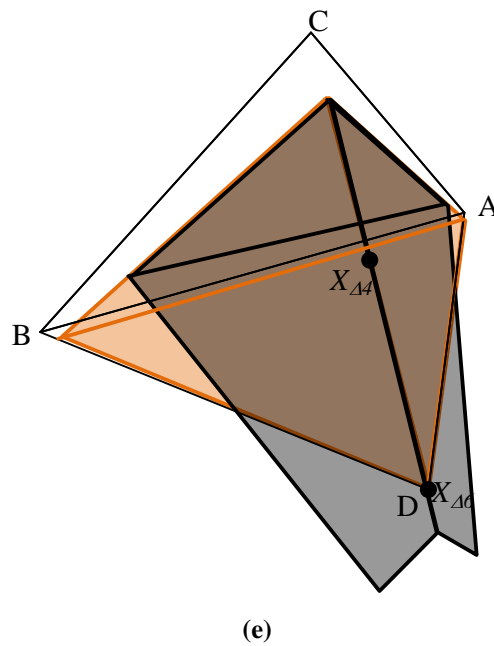


**Figure 6.17:** Transformed tetrahedrons at minimum reflux for the HSSR and Kaibel columns. (a) Column sections 1 and 3. (b) Column sections 2 and 4. (c) Column sections 5 and 6. (d) Column sections 1 and 2. (e) Column sections 4 and 6.

Figure 6.16 shows that the column sections associated to the vapour split, 5 and 6, are only dependent on the vapour split ratio, and conversely, column 1 and 3 are only dependent on the liquid split ratio. Vapour and liquid shifted tetrahedrons have been constructed in Figure 6.17 that represent the appropriate feed condition.

**Table 6.3:** Reflux ratios at minimum reflux for all respective minimum structures

CS	DSS	DSR	HSSR	Kaibel
1	8.77	4.42	6.72	6.72
2	2.44	-2.81	1.22	1.22
3	-3.89	1.33	-4.27	-4.27
4	0.718	-4.88	-3.22	-3.22
5	-2.72	1.22	1.35	1.35
6	-6.16	-10.98	-7.79	-7.79
7	-	-	-	$\infty$

### 6.4.2 Identifying optimal designs

We shall discriminate between good and bad designs based on the minimum energy requirement of a particular structure. As the reboiling column sections are typically the most expensive to operate in terms of utility cost, we will evaluate the vapour flow rates required in each of these column sections. In structures that contain multiple reboiling units, the overall vapour flow rate is merely the sum of all the vapour flows in respective column sections. We shall evaluate all designs based on minimum reflux operation, as this is a fair basis of comparison of the minimum achievable energy expenditure for each structure.

Furthermore, a unique property of multiple side rectifiers and strippers is the fact that they operate at multiple temperature levels. Thus, thermodynamic efficiencies (or second law efficiencies) also have an important role to play when deciding on an optimal structure since one structure may reject heat at a temperature where it is added to another. Once vapour flows have been obtained with our methods we can easily calculate the thermodynamic efficiency of the respective structures using a modified version of the Clausius-Clayperon equation coupled with an energy and exergy balance across the structure (see Appendix D for a detailed derivation). Agrawal and Fidkowski (1998) used this same principle for calculating thermodynamic efficiencies of ternary structures using the Underwood equations. It is easy recognisable that the feed composition of the mixture may influence which structure is superior. In Table 6.4 we consider the effect of the feed composition on which structure is optimal by analysing the minimum vapour flows and the thermodynamic efficiency ( $\eta$ ) for a mixture.

Fifteen different feed compositions have been characterised and evaluated for each structure in Table 6.4. These compositions correspond to various combinations of purity for single components, binary, and ternary mixtures. The structure requiring the minimum vapour flow rate, excluding the Kaibel column, has been shaded grey while the structure with the highest thermodynamic efficiency has been shaded in red. Not considering the Kaibel column for the

moment, the results indicate that the DSS is by far the most prevalent structure in terms of minimum vapour flow rates, highlighted by grey shading.

**Table 6.4: Minimum vapour flows and thermodynamic efficiencies for all respective thermally coupled structures for volatilities of 6, 4, 2 and 1.**

#	Feed Type	$z_f$	DSS		DSR		HSSR		Kaibel	
			$V_{TOT}/F$	$\eta$	$V_{TOT}/F$	$\eta$	$V_{TOT}/F$	$\eta$	$V_{TOT}/F$	$\eta$
-	-	-	$V_{TOT}/F$	$\eta$	$V_{TOT}/F$	$\eta$	$V_{TOT}/F$	$\eta$	$V_{TOT}/F$	$\eta$
1	Equimolar	[0.25, 0.25, 0.25]	2.441	0.451	2.495	0.503	2.516	0.508	1.698	0.120
2	A rich	[0.85, 0.05, 0.05]	2.769	0.196	2.856	0.272	2.857	0.1875	1.506	0.035
3	B rich	[0.05, 0.85, 0.05]	3.700	0.157	3.709	0.130	3.702	0.145	1.927	0.027
4	C rich	[0.05, 0.05, 0.85]	2.864	0.134	2.828	0.160	2.830	0.196	2.713	0.089
5	D rich	[0.05, 0.05, 0.05]	1.142	0.318	1.065	0.461	1.159	0.474	1.023	0.172
6	AB rich	[0.45, 0.45, 0.05]	3.258	0.301	3.286	0.304	3.283	0.283	1.718	0.053
7	AC rich	[0.45, 0.05, 0.45]	2.295	0.298	2.547	0.399	2.553	0.370	1.968	0.104
8	AD rich	[0.45, 0.05, 0.05]	1.617	0.517	1.705	0.732	1.743	0.535	1.007	0.108
9	BC rich	[0.05, 0.45, 0.45]	3.291	0.250	3.297	0.246	3.301	0.285	2.340	0.071
10	BD rich	[0.05, 0.45, 0.05]	2.178	0.426	2.209	0.386	2.183	0.426	1.210	0.083
11	CD rich	[0.05, 0.05, 0.45]	2.030	0.323	1.998	0.399	2.015	0.475	1.892	0.203
12	ABC rich	[0.32, 0.32, 0.32]	3.003	0.333	3.088	0.360	3.091	0.364	2.035	0.083
13	ABD rich	[0.32, 0.32, 0.04]	2.353	0.483	2.392	0.501	2.378	0.469	1.269	0.089
14	ACD rich	[0.32, 0.04, 0.32]	1.833	0.436	1.966	0.605	2.000	0.569	1.600	0.169
15	BCD rich	[0.04, 0.04, 0.04]	2.526	0.377	2.509	0.390	2.535	0.446	1.847	0.115

Out of the fifteen different feed compositions considered there are only four cases where the DSS does not have the minimum vapour flow rate. These four scenarios correspond to a feed rich in C and D, or a combination thereof, where the DSR has the minimum vapour flow rate. This can be attributed to the fact that, since the heaviest boiling components are plentiful, only a small amount of the lighter components have to be vaporised and sent through the column. Thus, the largest savings with the DSS can thus be achieved when the feed is rich in component A, and conversely the largest DSR savings when the feed is rich in components B, C and D, since these are the “condensing components”. Interestingly however, there is not one case where the HSSR is the optimal structure. Closer inspection reveals that the HSSR achieves minimum vapour flow rates where the feed mixture contains large fraction of B and C. Furthermore, the

highest relative vapour flow rates of all structures seem to occur where component A is plentiful, since in all of the structures, all of the A has to be vaporised.

Notably the thermodynamic efficiencies of the Kaibel are very low relative to all other structures, essentially because all the heat is added and rejected at the highest and lowest temperatures, respectively. However, Agrawal and Fidkowski showed that there are potential feed compositions in ternary separations where the fully thermally coupled columns have an advantage in terms of efficiency, but these were found to be very limited. The Kaibel column does however offer vast savings in terms of the overall energy requirement, with as much as a 92% improvement in overall vapour flow over the best thermally coupled structure where the feed is rich in C. Although this may seem like an incredibly high number, it does make sense since the Kaibel column is structurally similar to the HSSR but it essentially does the reboiling of component B for free. The low thermodynamic efficiencies of the Kaibel coupled with its reported control and operability problems make this structure unattractive as a viable separation alternative. Another interesting aspect of Table 6.4 is that the HSSR is generally the most thermodynamically efficient for the widest range of feeds, and conversely, the DSS is the least efficient. Thus, it is obvious that there is a distinct trade-off between first and second law efficiencies when choosing the optimal structure.

In our analyses thus far, we have only addressed a family of thermally coupled columns. However, when considering design alternatives, it is important to compare these complex thermally coupled columns with conventional distillation trains. For the quaternary mixture under consideration, there are in fact five different alternatives, to be precise, the Direct-Direct (DD), Indirect-Indirect (II), Pre-fractionating B/C split (H), Direct-Indirect (DI) and Indirect-Direct (ID) splits. As mentioned previously, the DD, II and H structures are directly related to the DSS, DSR and HSSR structures, respectively. For the same feed characteristics portrayed in Table 6.4, the overall thermodynamic efficiencies and minimum vapour flow rates for the simple structures are given in Table 6.5. The

$TC$  v.  $C$  column in Table 6.5 indicates the ratio of the lowest simple sequence vapour flow rate to the lowest thermally coupled vapour flow rate (in column  $V$ ), along with ratio of the thermodynamically most efficient simple sequence of columns to the thermally coupled structures. All comparisons exclude the fully thermally coupled Kaibel column.

**Table 6.5: Minimum vapour flows and thermodynamic efficiencies for all respective simple column sequences for volatilities of 6, 4, 2 and 1**

#	DD		II		H		DI		ID		TC v. C	
	$V_{Tot}/F$	$\eta$	V	$\eta$								
-												
1	2.910	0.536	3.615	0.423	3.111	0.586	2.880	0.504	3.365	0.430	1.180	1.154
2	2.963	0.212	5.252	0.126	4.203	0.190	2.957	0.210	4.002	0.146	1.068	0.779
3	3.785	0.217	4.986	0.151	3.825	0.218	3.236	0.221	4.936	0.153	0.875	1.408
4	3.342	0.228	3.090	0.230	2.982	0.262	4.141	0.183	3.440	0.204	1.054	1.337
5	1.749	0.321	1.436	0.357	1.632	0.411	1.454	0.335	1.386	0.360	1.301	0.867
6	3.372	0.456	5.121	0.233	4.016	0.344	3.091	0.457	4.471	0.277	0.949	1.503
7	3.006	0.384	4.029	0.266	3.445	0.422	3.405	0.340	3.579	0.254	1.310	1.058
8	2.291	0.350	3.138	0.346	2.826	0.435	2.134	0.356	2.488	0.389	1.320	0.594
9	3.580	0.392	4.057	0.308	3.420	0.461	3.707	0.315	4.207	0.279	1.039	1.618
10	2.688	0.381	3.037	0.404	2.652	0.460	2.170	0.440	2.987	0.410	0.996	1.080
11	2.550	0.447	2.272	0.514	2.312	0.537	2.809	0.426	2.422	0.471	1.137	1.131
12	3.350	0.500	4.451	0.309	3.662	0.496	3.438	0.422	4.131	0.315	1.116	1.374
13	2.751	0.463	3.756	0.372	3.162	0.457	2.390	0.510	3.296	0.437	1.016	1.018
14	2.545	0.478	3.099	0.403	2.800	0.565	2.725	0.462	2.779	0.388	1.388	0.934
15	2.957	0.472	3.121	0.466	2.794	0.586	2.920	0.437	3.221	0.428	1.114	1.314

Noticeably, the last two columns show that the thermally coupled columns are almost always best in terms of first law expenditures (total vapour flow rate), but on the other hand offers substantial improvements on thermodynamic efficiencies. There are however feed mixtures where the best simple sequence requires either a lower or very similar heat demand to thermally coupled structures. Mixtures that are rich in component B and/or C, the intermediate boiling components, are the common denominators for such simple structures. In general, a sequence of simple columns is more efficient. The cases where the simple columns are less

thermally efficient seem to be linked to mixtures with large quantities of components A and D.

## 6.5 Discussion and Conclusions

In this work, a method has been presented to design multiple thermally coupled distillation columns through the use of Column Profile Maps and eigenvector theory. This method allows one to quickly assess the minimum reflux for a simple column for the special case of sharp splits and constant relative volatilities. The key parameters used in the Column Profile Map technique are easily extendable to the design and analysis of complex structures, including multiple thermally coupled units. Under these special conditions, the Column Profile Map technique evaluating the eigenvectors at the feed correspond exactly to the Underwood equations, but have the advantage that graphical conclusions may be drawn using the shifted tetrahedrons.

Furthermore, iso-reflux plots are presented as a quick way of determining the minimum reflux conditions in a multiple thermally coupled column in a constrained split ratio space. The plots not only show the intersection of minimum reflux curves, but also indicate an Attainable Region of all possible operating parameters that result in a feasible design.

Using the aforementioned techniques we have considered four thermally coupled structures. Of these structures, the fully thermally coupled Kaibel column is for the fifteen different feeds considered by far the most prevalent in terms of minimum heat demand, but also has thermodynamic efficiencies which are comparatively very low. Of the “conventional” multiple thermally coupled columns, it is in fact the side stripping column that appears to require the minimum amount of heat for the majority of feeds. This stripping type column is similar to one used in crude refineries and therefore can aid in explain why these type of columns are so widely used. However, there are certain feed scenarios when a multiple side rectifying column may be best, and using the techniques

described in this work, it is a simple task to identify these feeds and design the process accordingly. Interestingly, simple column sequences were also shown to have advantages over their thermally coupled counterparts, especially when the feed is rich in intermediate boiling components. For the majority of the feeds considered, the thermodynamic efficiencies are higher than the best complex column.

---

## Chapter 7: Conclusions and Future Work

### 7.1 Thesis Conclusion

In this work, we have successfully modelled several conventional and complex configurations by utilising the Column Profile Maps (CPMs) techniques. The design, analysis and optimisation for conventional columns as well as thermally coupled configurations is made possible by the derivation of a novel method for calculating minimum reflux called the CPM-E technique.

It has been shown that the eigenvectors evaluated at the given feed condition produces the interaction boundary between the transformed triangle (ternary systems), transformed tetrahedron (quaternary systems) and the all inclusive transformed hyper planes (higher order systems - more than four components) of two Column Sections (CSs) under minimum reflux conditions. The eigenvector evaluation facilitates to locate the linear relationship between the saddle node, feed pinch and feed conditions. This line/plane, called the co-linearity hyper plane (line-ternary; plane-quaternary; hyper surface-five components and more) is the region where two sets of nodes from each CS intersect when minimum reflux conditions are present. As suggested above, the CPM-E technique can be applied to any number of components, where systems that have more than four components are based on an algebraic solution.

The CPM-E technique is accurate for any zeotropic system and becomes a very good approximation of minimum vapour requirements for highly complicated azeotropic systems such as the Acetone-Benzene-Chloroform system. The lack of precision for these systems when the CPM-E technique is utilised, is owed to the non-linearity of the distillation boundary.

An important finding through the employment of the CPM-E techniques is the exploration of the feasible region which consists of three distinct (ternary system)

solutions that arise from the different transformed hyper surface interactions. These regions are found through the employment of different combinations of the feed evaluated eigenvectors. Hence three regions within composition space are found that limits the product specification for these sets of common eigenvectors. The CPM-E technique is shown to be exactly equivalent to the minimum vapour requirements as predicted by the Underwood methods. A basic simulation prepared in ASPEN Plus, initialised from the solutions of the CPM-E system for a real, ternary, ideal system (Dodecane-Tridecane-Tetradecane) indicates that the CPM-E technique is a very accurate and precise method for determining minimum reflux solutions.

The design techniques when CPMs are applied were successfully applied to several configurations. Most importantly, besides demonstrating the value of the methods to complex columns we have extended the ideas of CPMs and incorporated the CPM-E techniques to all the complex configurations. The incorporation of the CPM-E techniques have aided in both developing the feasible regions within split ratio parameter space as well as also facilitated to find the overall minimum reflux of each complex and simple configuration.

Five complex configurations have been investigated to demonstrate the CPM as well as CPM-E techniques. Each configuration design and analysis is discussed below.

### 7.1.1 Petlyuk Column

We have successfully modelled the Petlyuk column using CPM techniques. As the technique requires, the column is broken down into column sections and a CPM is produced for each of these sections using the difference point equation. These CPMs can then be superimposed and feasible operating profiles found. It has been shown that there are *five* possible net flow patterns. These are flow patterns 1 to 5. The net flow pattern within the column is determined by the choice of vapour and liquid split ratios.

We can very simply produce lines of split ratios corresponding to coupled-column section reflux ratios, lines of constant difference point values and also generate regions corresponding to negative internal flow rates. The most powerful result is that by producing Phi Eigenvector Boundaries (PEB) as well as minimum reflux ratio lines for CS 2 and 4 we can construct a region of split ratios that result in feasible Petlyuk column designs. These boundaries (PEB 1 and 2 and minimum refluxes for CS 2 and 4) are constructed from the eigenvector evaluation at the appropriate points as specified by the CPM-E technique.

The feasible region, of split ratio solutions, is exactly equivalent to the optimality region defined by Halvorsen and Skogestad (2001). From a stage number and split ratio perspective it is clear why producing Petlyuk designs, for desired separations, is difficult using iterative solving methods. The CPM approach on the other hand has allowed us to not only generate individual solutions, but to find *all possible solutions* for a set of column parameters (reflux ratio and product flow rates) without any such disadvantages. Parameters such as the total number of required stages, feed stage and side-draw stage are a natural product of the process. These can be determined by tracking variable  $n$  along each composition profile of a column section.

Determining column minimum reflux ratio, for any zeotropic thermodynamics, is one of the most powerful results of the methodology. We can determine this value directly by analysing the position of the feed point relative to the boundaries of  $TT_3 1$  and  $TT_3 6$  through the application of the CPM-E technique.

### 7.1.2 Kaibel Column

We have extended the ideas from the ternary Petlyuk system and successfully developed a general solution for the Kaibel column. The CPM techniques have been applied to the Kaibel Column design and are implemented in the same manner as for the Petlyuk Column design. We have shown that there are *six* possible flow patterns for the Kaibel configuration. These are *1, 2, 3a, 3b, 4 and 5*. The net flow patterns for the Kaibel configuration is a result of the feasible

combinations of the net flux of material through adjacent CSs and can be shown in the vapour and liquid split ratio space. Regions, of split ratio space, resulting in each of these flow patterns can be found by producing zero net flow lines for the coupled column sections.

It has been shown for the Kaibel Column that although, many flow patterns do exist, only one pattern is feasible under *sharp split* conditions. In particular a combination of flow pattern *3a* and *3b*, where the net flow through the section between the two side-draws is zero.

As discussed, the zero net flow line defined from mass balance constraints across CS7 can be represented in the vapour and liquid split ratio space and is shown to be a line of solutions within the space. This is the line of vapour and liquid split ratio combinations that result in feasible sharp split Kaibel configurations.

The feasible line of solutions, demonstrates that a choice of vapour and liquid split ratios, in the Kaibel column, cannot be made arbitrarily if a sharp product is to be achieved. Although we have analysed sharp-split separations in this work, which, entails infinite stages, the feasible region boundaries can be generated for non-sharp-splits.

Although the defined line of solutions is shown, the entirety of the zero net flux line of CS 7 in the split ratio space does not produce feasible profile intersections. We show through the use of the CPM-E techniques that we can construct a region of split ratios that result in feasible Kaibel column design. The region is developed in a similar manner to the Petlyuk solution, where the main difference is knowing exactly where all the difference points are located from a given feed and sharp split product specification. The feasible region is determined from an initially chosen reflux in CS 1 or CS 6. As a result the column may not operate under over all minimum reflux. We can determine this value directly by analysing the position of the feed point relative to the boundaries of the rectifying and stripping section similarly to that of the Petlyuk solution.

### 7.1.3 Side Unit Configurations

A method has been presented to design multiple thermally coupled distillation columns through the use of Column Profile Maps and eigenvector theory. This method allows one to quickly assess the minimum reflux for a simple column for the special case of sharp splits and constant relative volatilities. Iso-reflux plots are presented as a quick way of determining the minimum reflux conditions in a multiple thermally coupled column in a constrained liquid and vapour split ratio space. The plots show the intersection of minimum reflux and indicate an Attainable Region of all possible operating parameters that result in a feasible design. The region produced is defined for CSs adjacent to the feed of the configuration which are always at minimum reflux with the remaining CSs above minimum.

Using the aforementioned techniques we have considered four thermally coupled structures. These configurations are the Double Side Stripper (DSS), Double Side Rectifier (DSR) and the Hybrid Side Stripper and Rectifier (HSSR) as well as the Kaibel Column. The minimum vapour flow results and thermodynamic efficiencies of these configurations are compared to the solutions derived for the Kaibel Column configuration in Chapter 5. In addition to this, the configurations are also compared to the simple column configuration equivalent for each thermally coupled configuration. Interestingly, simple column sequences show to have advantages over their thermally coupled counterparts, especially when the feed is rich in intermediate boiling components. For the majority of the feeds considered, the thermodynamic efficiencies are higher than the best complex column.

## 7.2 Future work

The CPM techniques have allowed us to define any system or configuration at minimum reflux. As discussed, the CPM-E can be applied to any zeotropic system and the results of these types of systems are limited to sharp and sloppy splits. This is due to the linear behaviour, for a defined CS, of the profiles along the TTs and hence the defined eigenvector evaluation provides this linear interaction boundary. Previously mentioned arguments define minimum reflux solutions for four and higher number components that portray the same conditions. The restriction of the CPM-E to sloppy splits allows us to evaluate very good approximations to non-sharp product specifications. As the specification moves further away from the Gibbs boundary, the CPM-E technique becomes more inaccurate. Investigations into non-sharp minimum reflux solution have started and a brief summary is given below.

In order to compensate for non-sharp product specifications, some compensation should be made for the curvature of the topology as the product specification shifts away from sharp splits. As discussed by Levy et al. (1985), the minimum reflux solution is found once a profile from either CS terminates on the other. With non-sharp split the termination point is no longer on a linear solution but on a curved profile. But, as we have already shown, the tangency condition of the termination point of the profile and the feed composition still exists and is true regardless of the thermodynamic nature of the system. With this said, exploitation of this feature at minimum reflux is pertinent to all non sharp solutions.

The eigenvector evaluation at any feed condition is the “constant” criteria for sharp and sloppy splits, which does not pertain to the final solution of non sharp splits. But, the feasible product region which is derived from the eigenvector evaluation at the feed condition is directly applicable to any kind of split and is also an indication of the feed pinch intersection of the interacting sections (stripping terminates on rectifying or vice versa).

The eigenvalue evaluation, for any reflux and a difference point chosen inside the mass balance triangle, reveals an interesting fact; the overall complex region remains constant. This is not an unpredictable result, as the eigenvector map is only dependant on thermodynamics and does not transform with internal material adjustments. This boundary as it turns out, has shown to be the “constant” criterion for both sharp and non-sharp splits.

This is based on the fact that any transformed triangle with its difference point selected within the mass balance triangle produces a tangent to the complex boundary. More specifically, the light-heavy boundary becomes a tangent to the complex region. This phenomenon is illustrated in Figure 7.1. This means that the complex boundary (red boundary in Figure 7.1) can be used to illustrate the reflux change for a set difference point. This concept is better illustrated in Figure 7.2. With this it is possible to select a point along the complex boundary and determine the reflux based on a difference point.

This will aid in our search for a minimum reflux, as the node location at the feed pinch is a tangent on the other profile through the feed as well as the above mentioned tangency on the complex boundary.

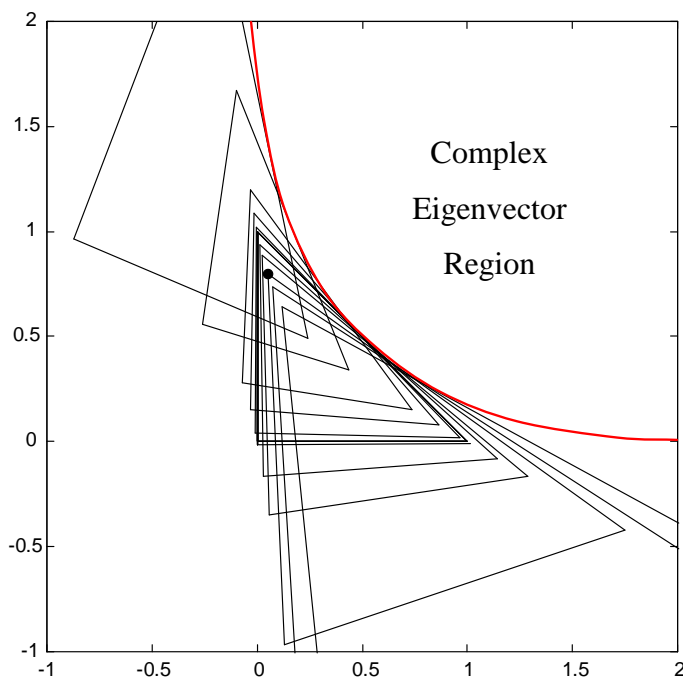


**Figure 7.1: Transformed triangles for a range of refluxes which depicts the tangency of the light-heavy boundary on the focus region boundary.**

The non-sharp split minimum reflux derivation would create an opportunity for the evaluation of azeotropic systems. This is owed to the fact that the solution would be based on regions of considerable curvature. As most azeotropic systems portray this characteristic, there is an exciting prospect for developing the theory for the most complex azeotropic systems. Due to the fact that the minimum reflux ideas of conventional columns can easily be extended to complex columns, the minimum reflux solutions for non sharp split product specifications and hence azeotropic systems can be used, not only to design and analyse minimum reflux conditions but over refluxed systems as well.

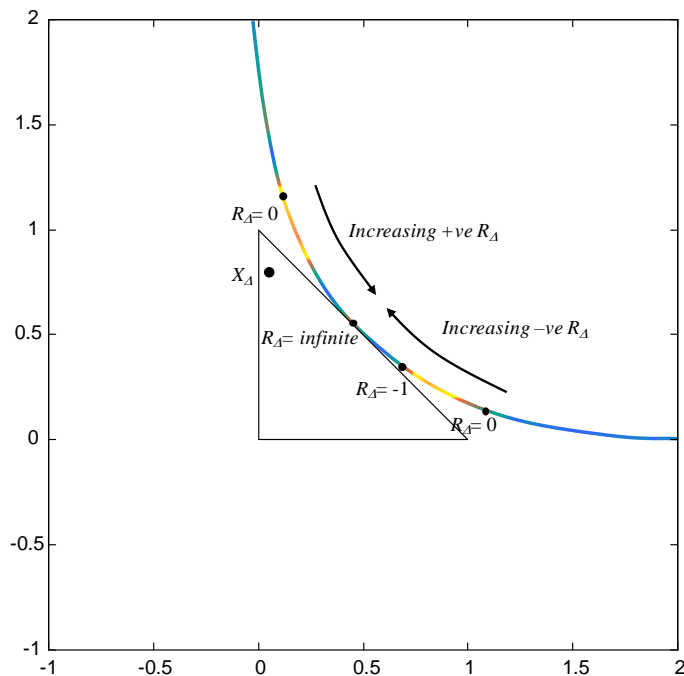


**Figure 7.2: Reflux value representation on the Complex Boundary.**

The CPM-E techniques have been used in this work to demonstrate the extension to higher order systems. This has opened new doors to numerical solutions as systems with more than four components cannot be visualised. The necessary rules and tests have been presented that allows one to solve these problems.

In this work we have focussed mainly on single liquid and vapour splits in the thermally coupled sections. Future work should also address topics such as double

---

dividing walls or the equivalent thermally coupled 3-column configurations. The ideas should begin with a quaternary system and then be extended to a pentenary system. The biggest drawback to the double dividing wall would be visualising the design variables as there are many more degrees of freedom that need to be tracked simultaneously. I.e. As there are two dividing walls, there would be 2 defined pairs of split ratios for liquid and vapour.

---

## Publications and Presentations

### Posters and Presentations:

1. *Experimental validation of Column Profile Maps using a Petlyuk Column under total reflux conditions for the acetone-methanol-ethanol system.*  
Ronald Abbas, Shehzaad Kauchali, Diane Hildebrandt, David Glasser.  
Presented at the SAIChE Annual Postgraduate Conference, 2007, Pretoria, South Africa.
2. *Column Profile Maps for a Dividing Wall Column using a Non-Ideal System.*  
Ronald Abbas, Shehzaad Kauchali, Diane Hildebrandt, David Glasser.  
Presentation and poster presented at 5<sup>th</sup> International Conference ICSST' 2007. Beijing, China.
3. *Sharp-Split Kaibel Column Design by Utilising Column Profile Map Techniques.* , Ronald Abbas, Simon T. Holland, Diane Hildebrandt and David Glasser. Presented at the AIChE Annual Meeting, 2008, Philadelphia, PA, USA.
4. *Computer-Aided graphical tools for synthesizing complex columns.* Daniel A. Beneke, Ronald Abbas, Michaela Vrey, Simon Holland, Brendon Hausberger, Diane Hildebrandt and David Glasser. Presented at the Foundations of Computer Aided Process Design (FOCAPD) conference, 2009, Breckenridge, CO, USA.
5. *Novel minimum reflux calculation using Eigenvector maps.* Ronald Abbas, Simon T. Holland and Ivar Halvorsen. Poster presented at the DA 2010 Conference Journal. 2010, Eindhoven, Netherlands.

6. *Design and Analysis of multiple thermally coupled configurations using Column Profile Maps*. Daniel A. Beneke, Ronald Abbas, Diane Hildebrandt and David Glasser. Accepted for presentation at AIChE Spring Meeting, 2011, Chicago, IL, USA.
7. *Minimum Reflux Calculation for Non-sharp Splits in Multi-component Distillation Systems using Column Profile Maps*. Ronald Abbas, Chan Yee Ma and Diane Hildebrandt. Accepted for presentation at AIChE Spring Meeting, 2011, Chicago, IL, USA.

**Publications and peer reviewed conference proceedings:**

1. *Computer-Aided graphical tools for synthesizing complex columns*. Daniel A. Beneke, Ronald Abbas, Michaela Vrey, Simon Holland, Brendon Hausberger, Diane Hildebrandt and David Glasser. Published in the FOCAPD 2009 conference journal, 2009.
2. *Complex Column Design by Application of Column Profile Map Techniques: Sharp-Split Petlyuk Column Design*. Simon T. Holland, Ronald Abbas, Diane Hildebrandt and David Glasser. Published in *Industrial and Engineering Chemistry Research*,. 2010, Volume 49, Issue 1, Pages 327-349.
3. *Column Profile Maps as a tool for synthesizing complex column configurations*. Diane Hildebrandt, Daniel A. Beneke, Ronald Abbas, Michaela Vrey, Simon Holland, and David Glasser. Published in *Computers and Chemical Engineering*. 2010, Volume 34, Issue 9, Pages 1487-1496.
4. *Novel minimum reflux calculation using Eigenvector maps*. Ronald Abbas, Simon T. Holland and Ivar Halvorsen. Published in the DA 2010 Conference Journal. 2010.

5. *Novel minimum reflux determination using Column Profile Maps*. Ronald Abbas, Mark Peters, Simon T. Holland and Ivar Halvorsen. Submitted to Industrial and Engineering Chemistry Research. Currently in review, 2010.
  
6. *Complex Column Design by Application of Column Profile Map Techniques: Sharp-Split Kaibel Column Design*. Ronald Abbas, Simon T. Holland and David Glasser. Submitted to Industrial and Engineering Chemistry Research. Currently in review, 2010.

---

## References

Abdul Mutalib, M. I. and Smith, R. (1998a), Operation and Control of Dividing Wall Distillation Columns Part1: Degrees of Freedom and Dynamic Simulation, *Trans IChemE*, 76, Part A, pp 308-318.

Abdul Mutalib, M. I. and Smith, R. (1998b), Operation and Control of Dividing Wall Distillation Columns Part2: Simulation and Pilot Plant Studies Using Temperature Control, *Trans IChemE*, 76, Part B, pp 319-334.

Agrawal, R. & Fidkowski, Z.T. (1998), Are thermally coupled distillation columns always thermodynamically more efficient for ternary distillations? *Ind Eng Chem Res*, 37, pp 3444-3454.

Agrawal, R. & Fidkowski, Z.T. (1998), More Operable Arrangements of Fully Thermally Coupled Distillation Columns, *AIChE. J.*, 44(11), pp 2565-2568.

Agrawal, R. & Fidkowski, Z.T. (1999), New thermally coupled schemes for ternary distillation. *AIChE J*, 45, pp 485-496.

Agrawal, R. (2000a), Multieffect distillation for thermally coupled configurations. *AIChE. J*, 46, pp 2211-2224.

Agrawal, R. (2000b), Thermally coupled distillation with reduced number of intercolumn vapor transfers. *AIChE. J*, 46, pp 2198-2210.

Amminudin, K. A.; Smith, R.; Thong, D. Y. C. & Towler, G. P. (2001), Design and Optimization of Fully Thermally Coupled Distillation Columns, Part 1: Preliminary Design and Optimization Methodology, *Trans IChemE*, 76, Part A, pp701-715,

- Annakou, O. & Mizsey, P. (1996), Rigorous Comparative Study of Energy-Integrated Distillation Schemes, *Ind. Eng. Chem. Res.*, 35 (6), pp 1877-1885
- Barrtfeld, M and Aguirre, P.A. (2003), Optimal Synthesis of Multicomponent Zeotropic Distillation Processes. 2. Pre-processing Phase and Rigorous Optimization of Efficient Sequences *Ind. Eng. Chem. Res.*, 42 ,pp 3441-3457.
- Bausa, J.; Watzdorf, R. V. & Marquardt, W. (1998), Shortcut methods for non-ideal multicomponent distillation: 1. simple columns. *AIChE. J.*, 44, p 2181.
- Bagajewcz, M. & Ji, S. (2000), Rigorous Procedure for the Design of Conventional Atmospheric Crude Fractionation Units. Part I: Targeting. *Ind Eng Chem Res.*, 40, pp 617-626.
- Bagajewcz, M. & Soto, J. (2000), Rigorous Procedure for the Design of Conventional Atmospheric Crude Fractionation Units. Part II: Heat Exchanger Network. *Ind Eng Chem Res.*, 40, pp 627-634.
- Bagajewcz, M. & Soto, J. (2003), Rigorous Procedure for the Design of Conventional Atmospheric Crude Fractionation Units. Part III: Trade-off between Complexity and Energy Savings. *Ind Eng Chem Res.*, 42, pp 1196-1203.
- Bagajewcz, M. (1998), On the design flexibility of atmospheric crude fractionation units. *Chemical Engineering Communications*, 166, pp 111 - 136.
- Bharwada, J. ( 1982), *Winter Meeting AIChE*, Orlando, FL.
- Brown, G. G., & Holcomb, D. E. (1940), Vapor-liquid phase equilibrium in hydrocarbon systems. *Petrol. Eng*, 11, 23.
- Caballero, J. A. & Grossmann, I. E. (2004), Design of distillation sequences: From conventional to fully thermally coupled distillation systems. *Comp. Chem. Eng.*, 28, pp2307-2329.

Cahn, R. P.; Di Micelli, E. & Di Micelli, A. G. (1962), Separation of Multicomponent Mixture in Single Tower – U.S. Patent 3,058,893.

Carlberg, N.A. & Westerberg, A.W. (1989a), Temperature-Heat Diagrams for Complex Columns. 3. Underwood's Method for the Petlyuk Configuration. *Ind. Eng. Chem. Res.* Vol. 28, pp 1386-1397.

Carlberg, N.A. and Westerberg, A.W. (1989b), Temperature-Heat Diagrams for Complex. Columns. 2. Underwood's Method for Side-strippers and Enrichers. *Ind. Eng. Chem. Res.* Vol. 28, p 1379-1386.

Doherty, M. F. & Perkins, J. D. (1977), Properties of Liquid-Vapour Composition Surfaces at Azeotropic Points., [\*Chem. Eng. Sci.\*, 32, pp 1112-1114](#) .

Doherty, M. F. & Perkins, J. D. (1978a), On the Dynamics of Distillation processes - 1. The simple distillation of multicomponent non-reacting, homogenous liquid mixtures. *Chem. Eng. Sci.*, 33, p281.

Doherty, M. F. & Perkins, J. D. (1978b), On the Dynamics of Distillation processes - 2.The simple distillation of model solutions. *Chem. Eng. Sci.*, 33, p569.

Doherty, M. F. & Perkins, J. D. (1979a), On the Dynamics of Distillation processes – 3. The topological structure of ternary Residue Curve Maps. *Chem. Eng. Sci.*, 34, p1401.

Doherty, M. F. & Perkins, J. D. (1979b), The Behaviour of Multicomponent Azeotropic Distillation Processes. *Inst. Chem. Eng. Symp. Ser.* 56,4, P 2121.

Doukas, N. & Luyben W. L. (1978), Economics of Alternative Distillation Configurations for Separation of Ternary Mixtures. *Ind. Eng. Chem. Process Des. Dev.*, 17, p 273.

- Doherty, M. F., & Malone, M. F. (2001). *Conceptual Design of Distillation System*. New York: McGraw-Hill, Inc.
- Dünnebier, G., & Pantelides, C. (1999), Optimal design of thermally coupled distillation columns. *Ind. Eng. Chem. Res.*, 38, 162.
- Eldridge, R. B., Seibert, A. F., Robinson, S. (2005, April), *Hybrid separations/distillation technology: Research opportunities for energy and emissions reduction*. Report prepared for the Industrial Technologies Program, U.S. Department of Energy, Energy Efficiency and Renewable Energy.
- Emmrich, G., Gehrke, H & Ranke, U. (2001), The Progressive Extractive Distillation Arrangement for the Morphylane Extractive Distillation Process. *Chemie Ingenieur Technik*, 73, 715.
- Engelien, H. K. & Skogestad, S. (2005), Minimum energy diagrams for multieffect distillation arrangements. *AIChE. J.*, 51, pp 1714-1725.
- Fidkowski, Z. & Krolikowski, L. (1986), Thermally Coupled System of Distillation Columns: Optimization Procedure. *AIChE. J.*, 32 (No. 4).
- Fidkowski, Z. T. & Krolikowski, L. (1987), Minimum Energy Requirements of Thermally Coupled Distillation Systems. *AIChE. J.*, 33, p 643.
- Fidkowski, Z. T. & Krolikowski, L. (1987), Minimum Energy Requirements of Thermally Coupled Distillation Systems. *AIChE. J.*, 33, p 643.
- Fidkowski, Z. T & Krolikowski, L. (1990), Energy requirements of nonconventional distillation systems. *AIChE. J.*, 36, p 1275.

- Fidkowski, Z. T.; Doherty, M. F. & Malone, M. F. (1991), Nonideal Multicomponent Distillation: Use of Bifurcation Theory for Design. *AIChE. J.*, 37, p 1761.
- Fidkowski, Z. T.; Doherty, M. F. & Malone, M. F. (1993), Feasibility of Separations for Distillation of Nonideal Ternary Mixtures. *AIChE. J.*, 39, p 1303.
- Fien, G. A. F. & Liu, Y. A. (1994), Heuristic Synthesis and Shortcut Design of Separation Processes Using Residue Curve Maps: A Review. *Ind. Eng. Chem. Res.*, 33, pp 2505-2522.
- Finn, A. J. (1996), Rapid Assessment of Thermally Coupled Side-Columns. *Gas Sep. Purif.*, 10(3), p 169.
- Fonyo, Z.; Szabo, J. & Foldes, P. (1974), Study of Thermally Coupled Distillation Columns, *Acta. Chim.*, 82, p 235.
- Franklin, N. L.; Forsyth, J. S. (1953), The interpretation of Minimum Reflux Conditions in Multi-Component Distillation. *Trans. Inst. Chem. Eng.*, 31 (reprinted in the Jubilee Supplement of *Trans. Inst. Chem. Eng.* 1997, 75).
- Frey, R. M.; Doherty, M. F.; Douglas, J.M. and Malone, M.F. (1984) Controlling Thermally Linked Distillation Columns. *Ind. Eng. Chem. Process. Des. Dev.*, 23, 483-490
- Furter, W. F. & Tassios, D. P. (1972), Extractive and Azeotropic Distillation. *Adv. Chem. Ser.* No. 115, pp 35-45.
- Glinos, K., & Malone, F. (1988), Optimality regions for complex column arrangements for ideal distillation. *Chem. Eng. Res. Des. Dev.*, 66, p 229.
- Halvorsen, I. and Skogestad, S. (1997), Optimizing Control of Petlyuk Distillation: Understanding the Steady-State Behavior, *Comp. Chem. Eng.*, 21, pp 249-254.

Halvorsen, I. and Skogestad, S. (1999), Optimal Operation of Petlyuk Distillation: Steady-State Behavior, *J. Proc. Contr.*, 9, p407-424.

Halvorsen, I. J. Minimum Energy Requirements in Complex Distillation Arrangements. Dr. Ing. Thesis, Norwegian University of Science and Technology (NTNU), Trondheim, Norway, 2001.

Halvorsen, I. J.; Skogestad, S. (2003), Minimum energy consumption in multicomponent distillation, 1. Vmin diagram for a two-product column. *Ind. Eng. Chem. Res.*, 42, pp 596-604.

Halvorsen, I. J.; Skogestad, S. (2003), Minimum Energy Consumption in Multicomponent Distillation. 2. Three-Product Petlyuk Arrangements. *Ind. Eng. Chem. Res.*, 42, 605-615.

Halvorsen, I. J.; Skogestad, S. (2003), Minimum Energy Consumption in Multicomponent Distillation. 3. More than Three Products and Generalized Petlyuk Arrangements. *Ind. Eng. Chem. Res.*, 42, 616-629.

Hausen, H. (1952), Berechnung der Rektifikation mit Hilfe kalorischer Mengeneinheiten. *Z. VDI-Beih. Verfahrenstechnik*, 1, 17.

Hendry, J. E.; Rudd, D. F. & Seader, J. D. (1973), Synthesis in the Design of Chemical Processes. *AIChE. J.*, 19, 1.

Hernández, S.; Segovia-Hernández, J. G. & Rico-Ramírez, V. (2006) Thermodynamically Equivalent distillation schemes to the Petlyuk column for ternary mixtures. *Energy* ., 31, pp 2176–2183

Hernández, S., & Jiménez, A. (1999a). Controllability analysis of thermally coupled distillation systems. *Ind. Eng. Chem. Res.*, 38, p 3957.

Hewitt, G., Quarini, J. and Morrell, M., More Efficient Distillation, *The Chemical Engineer*, pp. 16-19, 21 Oct, 1999.

Holland, S. T., Tapp, M., Hildebrandt, D. & Glasser, D. (2004a). Column profile maps. 2. Singular points and phase diagram behaviour in ideal and nonideal systems. *Ind. Eng. Chem. Res.*, 43, pp 3590-3603.

Holland, S. T., Tapp, M., Hildebrandt, D.; Glasser, D. & Hausberger, B. (2004b). Novel separation system design using "moving triangles". *Comp. Chem. Eng.*, 29, pp 181-189.

Holland, S. T.; Abbas, R.; Hildebrandt, D. & Glasser, D. (2010), Complex Column Design by Application of Column Profile Map Techniques: Sharp-Split Petlyuk Column Design. *Ind. Eng. Chem. Res.*, 49, pp 327-349.

Holland, S. T. PhD (Eng) Thesis. Column Profile Maps: A Tool for the Design and Analysis of Complex Distillation Systems. University of the Witwatersrand, Johannesburg, South Africa, 2006.

Jiménez, A.; Hernández, S.; Montoy, F. A. & Zavala-García, M. (2001), Analysis of control properties of conventional and nonconventional distillation sequences. *Ind. Eng. Chem. Res.*, 40, p 3757.

Julka, V. & Doherty, M. F. (1990), Geometric Behaviour and Minimum Flows for Nonideal Multicomponent Distillation. *Chem. Eng. Sci.*, 45, p 1801.

Kaibel, B.; Jansen, H.; Rietfort, T.; Zich, E. & Olujic, Z. (2007), Unfixed wall: the key to a breakthrough in dividing wall column technology, in: H. Kister, M. Pritchard (Eds.), Proceedings of the Topical Distillation Conference, *AIChE. J.*, Washington DC, 2007, pp. 29-41.

Kaibel, G. (1987), Distillation Columns with vertical Partitions. *Chem. Eng. Technol.* 10, pp 92-98.

Kaibel, G. (1988), Distillation Column Arrangement with Low Energy Consumption, *ICHEME Symposium Series*, no. 109, pp 43-59

Kaibel, G. Innovation Award 1995: Split Wall for the Environment. Web page <http://www.basf-ag.basf.de/basf/html/e/entwick/innov/trenn95.htm>

King, C. J. (1980), Separation Processes. *Chemical Engineering Series*; McGraw-Hill: New York.

Knapp, J. P. & Doherty, M. F. (1990), Thermal integration of homogeneous azeotropic distillation sequences. *AIChE. J.*, 36, p 969

Koehler, J.; Aguirre, P. & Blass, E. (1991). Minimum reflux calculations for non-ideal mixtures using the reversible distillation model. *Chem. Eng. Sci.*, 46, p 3007.

Koehler, J.; Poellmann, P. & Blass, E. (1995), A Review on Minimum Energy Calculations for Ideal and Nonideal Distillations *Ind. Eng. Chem. Res.*, 34, pp 1003-1020

Kolbe, B. and Wenzel, S. (2002), Novel Distillation Concepts Using One-Shell Columns. *International Conference on Distillation and Absorption, Baden-Baden, Germany*. September 30 – October 2.

Liebmann, K. & Dhole, V. R. (1995), Integrated crude distillation design. *Computers & Chemical Engineering*, 19, pp 119-124.

Linhoff, B. Ph.D. Dissertation, University of Leeds. U.K., 1979.

Lestak, F.; Egenes, D. J. & Reay, D. (1999), Efficiency at Low Cost. *AIChE Spring Meeting*, Houston, Texas; Paper 3c.

- Levy, G. S.; Van Dongen, D. B. & Doherty, M. F. (1985), Design and Synthesis of Homogeneous Azeotropic Distillations. 2. Minimum Reflux Calculations for Nonideal and Azeotropic Columns. *Ind. Eng. Chem. Fund.*, 24, p 463-474.
- Lewis, W. K.; Matheson, G. L. (1932), Studies in Distillation. *Ind. Eng. Chem.*, 24 (5), pp 494–498.
- Lucia, A., Amale, A., & Taylor, R. (2006), Energy efficient hybrid separation processes. *Ind. Eng. Chem. Res.*, 45, p 8319.
- Lucia, A.; Amale, A. & Taylor, R. (2008), Distillation pinch Points and More. *Computers and Chemical Engineering*, 32, pp 1342–1364.
- Malinen, I.; Tanskanen, J. (2009), Thermally coupled side-column configurations enabling distillation boundary crossing. 1. An overview and a Solving Procedure. *Ind. Eng. Chem. Res.*, 48, 6387–6404.
- Ognisty, T. P. (1995), Analyze Distillation Columns With Thermodynamics. *Chem. Eng. Prog.* pp 40-46.
- Parkinson, Gerald "Dividing-Wall Columns Find Greater Appeal". *Chemical Engineering Progress*. 28 May, 2009.
- Parkinson, G. "Chementator". *Chemical Engineering Progress*. July, 21 and 22, 1998.
- Petlyuk, F. B.; Platonov, V. M. & Slavinskii, D. M. (1965), Thermodynamically Optimal Method of Separating Multicomponent Mixtures, *Int. Chem. Eng.*, 5 (3), p 555.
- Petlyuk, F., B. (2004), Distillation theory and its application to optimal design of separation unit, Cambridge, Cambridge University Press.

Pham, H. N.; Ryan, P. J. & Doherty, M. F. (1989), Design and Minimum Reflux for Heterogeneous Azeotropic Distillation Columns. *AIChE. J.*, 35, p 1585.

Poellmann, P.; Glanz, S. B. & Blass, E. (1994). Calculating minimum reflux of non-ideal multicomponent distillation using eigenvalue theory. *Comp. Chem. Eng.*, 18, S49.

Poellmann, P.; Bauer, M. H. & Blass, E. (1996), Investigation of Vapour- Liquid Equilibrium of Non-Ideal Multicomponent Systems,” *Gas. Sep. Purif.* 10, 225.

Rudd, H. (1992), Thermal Coupling for Energy Efficiency. *The Chemical Engineer.*, S14.

Safrit, B. T., & Westerberg A. W. (1997), Algorithm for Generating the Distillation Regions for Azeotropic Multicomponent Mixtures. *Ind. Eng. Chem. Res.*, 36, p 1827.

Schultz, M. A.; Stewart, D. G.; Harris, J. M.; Rosenblum, S. P.; Shakur, M. S. and O’Brian, D. E. Reduce Costs with Dividing Wall Columns. *Chemical Engineering Progress*. May (2002).

Seader, J. D. & Henley, E. J. (2006). *Separation process principles*, Hoboken, N.J., Wiley.

Segovia-Hernández, J. G., Hernández, S., & Jiménez, A. (2002), Control behaviour of thermally coupled distillation sequences. *Transactions of IChemE*, 80 (Part A), p 783.

Segovia-Hernández, J.G.; Hernández, S. & Jiménez, J. (2005), Analysis of dynamic properties of alternative sequences to the Petlyuk column. *Comp. Chem. Eng.*, pp 1389–1399

Shinskey, F. G. (1977), *Distillation Control for Productivity and Energy Conservation*. McGraw Hill: New York.

- Shiras, R. N.; Hansson, D. N. & Gibson, C. H. (1950), Calculation of Minimum Reflux in Distillation Columns. *Ind. Eng. Chem.*, 42 (No. 18), pp 871-876.
- Spadoni, G. and Stramigioli, C. (1983), Optimum Design of Thermally Coupled Distillation System, *3rd Int. Cong. Comp. Chem. Eng, Paris*, p27-44.
- Stichlmair, J. Distillation and Rectification. (1988) *Ullmann's Encyclopedia of Industrial Chemistry*; VCH: Weinheim, Germany, Vol. B3, p 94.
- Stupin, W. J. and Lockhart, F. J. (1972), Thermally Coupled distillation - A Case History, *Chem. Eng. Prog.*, 68(10), p71.
- Tapp, M.; Holland, S. T.; Hildebrandt, D. & Glasser, D. (2004a), Column Profile Maps. 1. Derivation and Interpretation. *Ind. Eng. Chem. Res.*, 43 (2), 364.
- Tedder, D. W. and Rudd, D. F. (1978), Parametric Studies in Industrial Distillation: Part 1. Design Comparisons, *AIChE. J.*, 24, p 303.
- Triantafyllou, C. and Smith, R. (1992), The Design and Optimization of Fully Thermally Coupled Distillation Columns, *Trans. Inst Chem. Eng.*, 70, p 118.
- Underwood, A. J. V. (1945), Fractional Distillation of Ternary Mixtures-Part I. *J. Znst. Pet.*, 31, pp 111-118.
- Underwood, A. J. V. (1946a) Fractional Distillation of Ternary Mixtures-Part II. *J. Znst. Pet.*, 32, pp 598-613.
- Underwood, A. J. V. (1946b), Fractional Distillation of Multicomponent Mixtures-Calculation of Minimum Reflux Ratio. *J. Znst. Pet.*, 32, pp 614-626.
- Underwood, A. J. V. (1948) Fractional Distillation of Multicomponent Mixtures. *Chem. Eng. Prog.*, 44 (8), p 603.

Urdaneta, R. Y.; Bausa, J. & Marquardt, W. (2004), Minimum energy demand and split feasibility for a class of reactive distillation columns. In A. Barbosa-Povoa & H. Matos (Eds.), *In ESCAPE-14*, p. 517. Elsevier B.V.

Vogelpohl, A. (1974), Die naueherungsweise Berechnung der Rektifikation von Gemischen mit binaren Azeotropen. *Chem. Ing. Tech.*, 46, p 195.

Van Dongen, D. B. (1983), Distillation of Azeotropic Mixtures: The Application of Simple Distillation Theory to Design of Continuous Processes. Ph.D. Dissertation, University of Massachusetts, Amherst.

Van Dongen, D. B.; Doherty, M. F. (1984), On the Dynamics of Distillation Processes-V. The Topology of the Boiling Temperature Surface and its Relation to Azeotropic Distillation. *Chem. Eng. Sci.*, 39, pp 883-892.

Van Dongen, D. B.; Doherty, M. F. (1985), Design and Synthesis of Homogeneous Azeotropic Distillation. **1.** Problem Formulation for a Single Column. *Znd. Eng. Chem. Fundam.*, 24, pp 454-463.

Wachter, J. A.; Ko, T. K. T.; Andres, R. P. Minimum Reflux Behaviour of Complex Distillation Columns. *AIChE J.* **1988**, 34 (No. 7), 1164-84.

Westerberg, A. W. (1985), The Synthesis of Distillation Based Separation Systems, *Comp. Chem. Eng.* 9(5), p 421.

Westerberg, A. W. and Wahnschafft, O. (1996), Synthesis of Distillation Based Separation Systems, *Advances Chem. Eng. J. L. Anderson, ed.*, 23, pp 63-170.

Wenzel, S. & Röhm, H. (2003), Auslegung thermisch und stofflich gekoppelter destillationskolonnen mittels gesamtkostenoptimierung. *Chemie Ingenieur Technik*, 75, pp 534-540.

Wolff, E. A., & Skogestad, S. (1995), Operation of integrated three product (Petlyuk) distillation columns. *Industrial and Engineering Chemistry Research*, 34, p 2094.

Wright, R. O. Fractionation Apparatus. U.S. Patent 2471134, (1949).

Kim, Y. H. (2005), Structural design of fully thermally coupled distillation columns using a semi-rigorous model. *Comp. Chem. Eng.*, 29, pp 1555-1559.

Yeomans, H., & Grossmann, I. E. (2000), Optimal design of complex distillation columns using rigorous tray-by-tray disjunctive programming models. *Ind. Eng. Che. Res.*, 39, p 4326.

## Appendix A

### *Proof of overlap of vapour $TT_3$ s if liquid $TT_3$ s overlap.*

*Hypothesis:* If two liquid  $TT_3$ s overlap, the corresponding vapour  $TT_3$ s will overlap also.

Consider two  $TT_3$ s ( $TT_3$  A and  $TT_3$  B) of a configuration with sharp product specifications that are required to achieve composition matching by overlapping close to an axis. The composition profiles of the corresponding sections run along the boundaries of these  $TT_3$ s. The extreme condition at which this composition matching can be satisfied is when stationary points of the two  $TT_3$ s coincide. i.e.  $X_{PA} = X_{PB}$ . The composition of vapour  $TT_3$  A in equilibrium with  $X_{PA}$  is  $Y_{PA}^*$ . This composition is a stationary point of vapour  $TT_3$  A. However, the equilibrium composition of  $X_{PB}$  is  $Y_{PB}^* = Y_{PA}^*$  since  $X_{PA} = X_{PB}$ . This composition is also a stationary point of vapour  $TT_3$  B. Hence, we can conclude that if the liquid  $TT_3$ s touch at nodes the vapour  $TT_3$ s will also touch at nodes.

We can extend this argument to include, not only, situations where the liquid  $TT_3$ s touch but where they produce a small overlap. If  $X_{PA} = X_{PB}$  and is then shifted, by changing parameters, such that light component value (for arguments sake) is increased and this shifting increases the liquid  $TT_3$  overlap,  $Y_{PA}^*$  must also shift in a direction that increases its light component value and will therefore increase the vapour  $TT_3$  overlap. Hence if liquid  $TT_3$ s (for sharp split) overlap, the corresponding vapour  $TT_3$ s will do likewise.

## Appendix B

### *Proof of Coinciding Pinch Points for CS 1, 2 and 3 at Sharp-Split Conditions.*

*Hypothesis:* If two stationary points of coupled CS system 1, 2 or 3 coincide at a point, a stationary point of the third section must also coincide at this point.

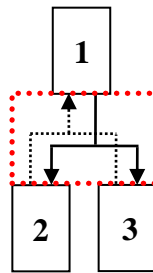


**Figure BB 1: Mixing point of CSs 1, 2 and 3**

Material balance over streams from CSs 1, 2 and 3:

$$\Delta X_{\Delta 1} = \Delta X_{\Delta 2} + \Delta X_{\Delta 3}$$

$$V_1 Y_{P1} - L_1 X_{P1} = V_2 Y_{P2} - L_2 X_{P2} + \Delta X_{\Delta 3}$$

If liquid pinch points from sections 1 and 2 overlap i.e.  $X_{P2} = X_{P1}$

Material Balance becomes :

$$V_1 Y_{P1} - L_1 X_{P1} = V_2 Y_{P2} - L_2 X_{P1} + \Delta X_{\Delta 3}$$

But at pinch point  $Y_i = Y_i^*(X_i)$ , (passing streams are in equilibrium), therefore :

$$Y_{P1} = Y_{P2} = Y_{P1}^*(X_{P1})$$

$$V_1 Y_{P1}^* - V_2 Y_{P1}^* - (L_1 X_{P1} - L_2 X_{P1}) = \Delta X_{\Delta 3}$$

But  $L_3 = L_1 - L_2$  and  $V_3 = V_1 - V_2$

$$V_3 Y_{P1}^* - L_3 X_{P1} = \Delta X_{\Delta 3}$$

Pinch  $X_{P1}$  and equilibrium  $Y_{P1}^*$  satisfy section 3 material balance. The only passing streams in the CPM 3 that satisfy both material balance and equilibrium are the pinch points, so  $X_{P3} = X_{P1}$  and  $Y_{P3}^* = Y_{P1}^*$ .

## Appendix C

***Proof of TT 1, 2 and 3 overlap for all  $\Phi_V$  and  $\Phi_L$  resulting in a negative value of  $R_{\Delta 2}$  where  $|R_{\Delta 2}| > |R_{\Delta 2MIN}|$  at Sharp-Split Conditions.***

*Hypothesis:* At  $R_{\Delta 2MIN}$  boundaries  $B_1$ ,  $C_2$  and  $B_3$  are collinear. Any values of  $\Phi_V$  and  $\Phi_L$  chosen such that  $R_{\Delta 2} < 0$  and  $|R_{\Delta 2}| > |R_{\Delta 2MIN}|$  will result in an overlap of TT 1, 2 and 3.

At  $R_{\Delta 2MIN}$ , boundaries  $B_1$ ,  $C_2$  and  $B_3$  are collinear. This is therefore a feasible solution of the CS 1-2-3 system. In order to determine whether or not TTs 1, 2 and 3 overlap for  $|R_{\Delta 2}| > |R_{\Delta 2MIN}|$ , we must determine the rate and direction of movement of the nodes of the respective TTs as  $\Phi_V$  and  $\Phi_L$  are varied. The positions of the nodes of a TT are dependent on  $X_{\Delta}$  and  $R_{\Delta}$ . Arbitrarily varying  $\Phi_V$  and  $\Phi_L$  results in dramatically different values of  $R_{\Delta 2}$ ,  $R_{\Delta 3}$  and  $X_{\Delta 3}$ , and consequently, dramatically different positions of the stationary points. We need to negate the effect of variation of  $X_{\Delta 3}$  on the positions of the CS 3 stationary points so that we need only compare one variable type (i.e. reflux ratio of CS 2 and 3) and determine its effect on the rate of stationary point movement. If  $\Phi_V$  and  $\Phi_L$  are varied along lines of constant  $X_{\Delta 3-i}$ , the rate of change of  $R_{\Delta 2}$  and  $R_{\Delta 3}$  can be compared. Once the rate of change of  $R_{\Delta k}$  is known for each section, the rate of movement of the stationary points can be determined.

Below is the expression for  $\Phi_V$  and  $\Phi_L$  resulting in constant  $X_{\Delta 3-i}$  (Equation 3.20).

$$\Phi_L = \frac{(R_{\Delta 1} + 1)}{R_{\Delta 1}} \Phi_V + \frac{1}{R_{\Delta 1}} \left( \frac{X_{\Delta 3-i} - X_{\Delta 1-i}}{X_{\Delta 2-i} - X_{\Delta 3-i}} \right) \quad (3.20)$$

We will vary  $\Phi_V$  and  $\Phi_L$  along these lines and determine the rate of change of  $R_{\Delta 2}$  and  $R_{\Delta 3}$ . Examples of these lines are seen in the Figure F.1 below.

The reflux ratio for CS 3 is given by Equation 6.15 below:

$$R_{\Delta 3} = \frac{(1 - \Phi_L)R_{\Delta 1}}{(1 - \Phi_V)(R_{\Delta 1} + 1) - (1 - \Phi_L)R_{\Delta 1}} \quad (3.15)$$

Combining Equation 15 and Equation 3.20 to eliminate  $\Phi_L$  and differentiating with respect to  $\Phi_V$  we obtain:

$$\begin{aligned} \frac{dR_{\Delta 3}}{d\Phi_V} &= \frac{-R_{\Delta 1} - 1}{(1 - \Phi_V)(R_{\Delta 1} + 1) - \left(1 - \frac{(R_{\Delta 1} + 1)\Phi_V}{R_{\Delta 1}} - \frac{X_{\Delta 3-i} - X_{\Delta 1-i}}{R_{\Delta 1}(X_{\Delta 2-i} - X_{\Delta 3-i})}\right)R_{\Delta 1}} \\ &= \frac{-(R_{\Delta 1} + 1)}{\left(1 + \frac{X_{\Delta 3-i} - X_{\Delta 1-i}}{X_{\Delta 2-i} - X_{\Delta 3-i}}\right)} \end{aligned}$$

For sharp product splits the light component  $X_{\Delta 1-i} \approx 1$  and  $X_{\Delta 2-i} \approx 0$

$$\frac{dR_{\Delta 3}}{d\Phi_V} = \frac{-(R_{\Delta 1} + 1)}{\left(\frac{1}{X_{\Delta 3-i}}\right)} = -X_{\Delta 3-i}(R_{\Delta 1} + 1) \quad (C1)$$

The reflux ratio for CS 2 is given by equation below:

$$R_{\Delta 2} = \frac{\Phi_L R_{\Delta 1}}{\Phi_V (R_{\Delta 1} + 1) - \Phi_L R_{\Delta 1}} \quad (3.14)$$

Combining Equation 3.14 and Equation 3.20 to eliminate  $\Phi_L$  and differentiating with respect to  $\Phi_V$  we obtain:

$$\begin{aligned} \frac{dR_{\Delta 2}}{d\Phi_V} &= \frac{R_{\Delta 1} + 1}{\Phi_V (R_{\Delta 1} + 1) - \left(\frac{(R_{\Delta 1} + 1)\Phi_V}{R_{\Delta 1}} + \frac{X_{\Delta 3-i} - X_{\Delta 1-i}}{R_{\Delta 1}(X_{\Delta 2-i} - X_{\Delta 3-i})}\right)R_{\Delta 1}} \\ &= \frac{R_{\Delta 1} + 1}{\left(\frac{X_{\Delta 1-i} - X_{\Delta 3-i}}{X_{\Delta 2-i} - X_{\Delta 3-i}}\right)} \end{aligned}$$

For sharp product splits the light component  $X_{\Delta 1-i} \approx 1$  and  $X_{\Delta 2-i} \approx 0$

$$\frac{dR_{\Delta 2}}{d\Phi_V} = \frac{R_{\Delta 1} + 1}{\left(1 - \frac{1}{X_{\Delta 3-i}}\right)} = \frac{-X_{\Delta 3-i}(R_{\Delta 1} + 1)}{(1 - X_{\Delta 3-i})} \quad (C2)$$

From Equations C.1 and C.2, we see that both  $R_{\Delta 2}$  and  $R_{\Delta 3}$  decrease with increasing  $\Phi_V$  along lines of constant  $X_{\Delta 3-i}$ . The rate of change of  $R_{\Delta 2}$ , with respect to  $\Phi_V$ , is equal to the rate of change of  $R_{\Delta 3}$  divided by  $(1-X_{\Delta 3-i})$ . In split ratio regions 1, 2 and 3:  $0 < (1-X_{\Delta 3-i}) < 1$  for all  $\Phi_V$  and  $\Phi_L$ . This means that the magnitude, of the rate of change of  $R_{\Delta 2}$ , is greater than that of  $R_{\Delta 3}$  along lines of constant  $X_{\Delta 3-i}$ .  $R_{\Delta 3}$ , which is positive in region 3, becomes smaller as  $\Phi_V$  is increased. Boundary  $B_3$  consequently, shifts towards the light component.  $R_{\Delta 2}$ , which is negative, becomes more negative i.e. the magnitude of the negative  $R_{\Delta 2}$  increases. Boundary  $C_2$  also shifts towards the light component. However, due to the more rapid rate of change of  $R_{\Delta 2}$  than  $R_{\Delta 3}$ , we can conclude that boundary  $C_2$  will move towards the light component faster than boundary  $B_3$  hence the two  $TT_3$ s will maintain overlap. In split ratio region 4, the  $TT_3$ s overlap by default. Both  $TT_2$  and  $TT_3$  operate at positive reflux ratio.  $TT_3 2$  will look similar to Figure 3.34 and  $TT_3 3$  will look similar to  $TT_2$  in Figure 3.32 (except that the  $TT_3 3$  saddle point and stable node will have higher light component values). Because the  $TT_2$  unstable node is above  $x_1 = 1$  and the  $TT_3 3$  unstable node is below  $x_1 = 1$ , for all  $R_{\Delta} > 0$ , overlap is guaranteed. The same is true for split ratio region 5. Although in this region  $CS_3$  operates at negative reflux, the qualitative form of the  $TT_3 3$  always allows overlap with  $TT_3 2$ . We can say therefore that  $TT_3 2$  will overlap  $TT_3 3$  for all values of  $R_{\Delta 2} > R_{\Delta 2 MIN}$  as we can choose any constant  $X_{\Delta 3-i}$  line along which to vary  $\Phi_V$ .

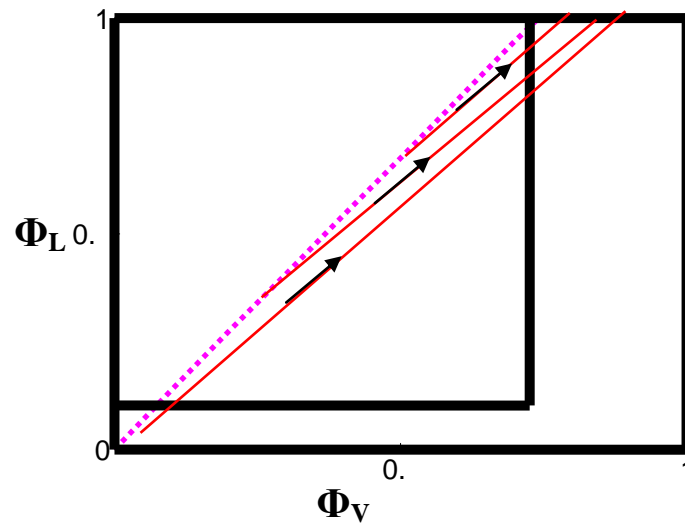


Figure CC.1: Lines of Constant  $X_A$  derived for values of  $X_{A3}$  between 0 and 1

## Appendix D

*Derivation of the thermodynamic efficiencies for various thermally coupled configurations.*

An Energy Balance for a general column, assuming equivalent latent heat of components:

$$\sum Q_R = \sum Q_C, \Rightarrow H_{vap} \sum V_R = H_{vap} \sum V_C \quad (D1)$$

Exergy balance for a general column, assuming  $\Delta H_{Mix} = 0$ :

$$W_{lost} = T_o \Delta S_{irr} = T_o (F \Delta S_{MIX,F} + \sum Q_R / T_R - \sum Q_C / T_C),$$

where  $\Delta S_{MIX,F} = -R \sum z_{Fi} \ln(z_{Fi})$  (D2)

$Q_R$  and  $Q_C$  are determined from Equation D1.

In order to eliminate the temperature variables in favour of constant relative volatilities we substitute the Modified Clausius-Clayperon equation (D3) into equation D2 for each volatility pair.

$$\ln(\alpha_{i,j}) = \frac{-H_{vap}}{R} \left( \frac{1}{T_i} - \frac{1}{T_j} \right) \quad (D3)$$

The definition for thermodynamic efficiency definition reduces to:

$$\eta = \frac{\Delta S_{MIX,F}}{\Delta S_{MIX,F} + \Delta S_{irr}} \quad (D4)$$

Substituting  $\alpha$  for T and solving, we obtain:

$$\text{Double Side Stripper: } \eta = \frac{-F \sum z_{Fi} \ln(z_{Fi})}{(V_3 + V_5 + V_6) \ln(\alpha_1) - V_3 \ln(\alpha_2) + V_5 \ln(\alpha_3)} \quad (\text{D5})$$

$$\text{Double Side Rectifier: } \eta = \frac{-F \sum z_{Fi} \ln(z_{Fi})}{V_1 \ln(\alpha_3) + V_3 \ln(\alpha_1) + V_5 \ln(\alpha_2)} \quad (\text{D6})$$

$$\text{Hybrid Rectifier/Stripper: } \eta = \frac{-F \sum z_{Fi} \ln(z_{Fi})}{V_1 \ln(\alpha_1) + V_5 \ln(\alpha_3) - (V_1 + V_5 - V_6) \ln(\alpha_2)} \quad (\text{D7})$$

$$\text{Kaibel: } \eta = \frac{-F \sum z_{Fi} \ln(z_{Fi})}{V_1 \ln(\alpha_1)} \quad (\text{D8})$$

## Appendix E

*Reflux Ratio equations in terms of defining Column Section for the various configurations*

### Double Side Stripper

$$R_{\Delta 1} = -\frac{R_{\Delta 6}B + Fq}{\Phi_{L2}\Phi_{L1}D} \Rightarrow \Phi_{L2} = -\frac{R_{\Delta 6}B + Fq}{\Phi_{L1}R_{\Delta 1}D} \quad (\text{E1})$$

$$R_{\Delta 2} = \frac{R_{\Delta 6}B + Fq}{\Phi_{L2}(F - B - S_2)} \Rightarrow \Phi_{L2} = \frac{R_{\Delta 6}B + Fq}{R_{\Delta 2}(F - B - S_2)} \quad (\text{E2})$$

$$R_{\Delta 3} = \frac{(1 - \Phi_{L1})(R_{\Delta 6}B + Fq)}{\Phi_{L2}\Phi_{L1}S_1} \Rightarrow \Phi_{L2} = \frac{(1 - \Phi_{L1})(R_{\Delta 6}B + Fq)}{R_{\Delta 3}\Phi_{L1}S_1} \quad (\text{E3})$$

$$R_{\Delta 4} = \frac{R_{\Delta 6}B + Fq}{B - F} \Rightarrow \text{Not a function of the split ratio} \quad (\text{E4})$$

$$R_{\Delta 5} = \frac{(1 - \Phi_{L2})(R_{\Delta 6}B + Fq)}{\Phi_{L2}S_2} \Rightarrow \Phi_{L2} = \frac{R_{\Delta 6}B + Fq}{R_{\Delta 5}B + Fq + R_{\Delta 5}S_2} \quad (\text{E5})$$

### Double Side Rectifier

$$R_{\Delta 2} = \frac{R_{\Delta 1}D + Fq}{D - F} \Rightarrow \text{Not a function of the split ratio} \quad (\text{E6})$$

$$R_{\Delta 3} = \frac{\frac{(1 - \Phi_{V1})(D(1 + R_{\Delta 1}) - F(1 - q))}{\Phi_{V1}} - S_1}{S_1} \Rightarrow \Phi_{V1} = \frac{D(1 + R_{\Delta 1}) - F(1 - q)}{D(1 + R_{\Delta 1}) - F(1 - q) + S_1(1 + R_{\Delta 3})} \quad (\text{E7})$$

$$R_{\Delta 5} = \frac{\frac{(1-\Phi_{V2})(D(1+R_{\Delta 1})-F(1-q))}{\Phi_{V1}\Phi_{V2}} - S_2}{S_2} \Rightarrow \Phi_{V1} = \frac{(1-\Phi_{V2})D(1+R_{\Delta 1}) + (1+\Phi_{V2})F(1-q)}{\Phi_{V2}(1+R_{\Delta 5})S_2} \quad (\text{E8})$$

$$R_{\Delta 6} = \frac{\frac{D(1+R_{\Delta 1})-F(1-q)}{\Phi_{V1}\Phi_{V2}} + B}{B} \Rightarrow \Phi_{V1} = -\frac{D(1+R_{\Delta 1})-F(1-q)}{\Phi_{V2}(1+R_{\Delta 1})B} \quad (\text{E9})$$

### Hybrid Side Stripper and Rectifier

$$R_{\Delta 2} = \frac{\Phi_L R_{\Delta 1} D}{D(1+R_{\Delta 1}) - (1-\Phi_L)R_{\Delta 1}D + S_1 - \Phi_L R_{\Delta 1}D} \Rightarrow \Phi_L = \frac{R_{\Delta 2}(D+S_1)}{R_{\Delta 1}D} \quad (\text{E10})$$

$$R_{\Delta 3} = \frac{(\Phi_L - 1)R_{\Delta 1}D}{S_1} \Rightarrow \Phi_L = \frac{R_{\Delta 1}D + R_{\Delta 3}S_1}{R_{\Delta 1}D} \quad (\text{E11})$$

$$R_{\Delta 4} = \frac{\Phi_L R_{\Delta 1}D + Fq}{D+S_1-F} \Rightarrow \Phi_L = \frac{(D+S_1-F)R_{\Delta 4} - Fq}{R_{\Delta 1}D} \quad (\text{E12})$$

$$R_{\Delta 5} = \frac{\frac{(1-\Phi_L)(D+S_1 - \Phi_L R_{\Delta 1}A - F(1-q))}{\Phi_V} - S_2}{S_2} \Rightarrow \Phi_L = \frac{-(D+S_1-F(1-q))(1+\Phi_V) + \Phi_V S_2(1+R_{\Delta 5})}{(1-\Phi_V)R_{\Delta 5}D} \quad (\text{E13})$$

$$R_{\Delta 6} = \frac{\frac{D+S_1-F(1-q) + \Phi_L R_{\Delta 1}D}{\Phi_V} + B}{B} \Rightarrow \Phi_L = -\frac{D+S_1-F(1-q) + \Phi_V(1+R_{\Delta 6})B}{R_{\Delta 1}D} \quad (\text{E14})$$

## Appendix F

### *Derivation of the Difference Point Equation*

The generalised column section (CS) is defined as a length of column between points of addition or removal of mass or energy. The stages in a column section can be numbered from the bottom up (Figure FF. 1) or from the top down (Figure FF. 2).

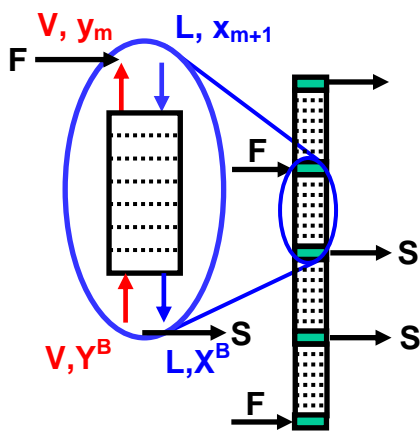


Figure FF. 1: Column section numbered from the bottom up

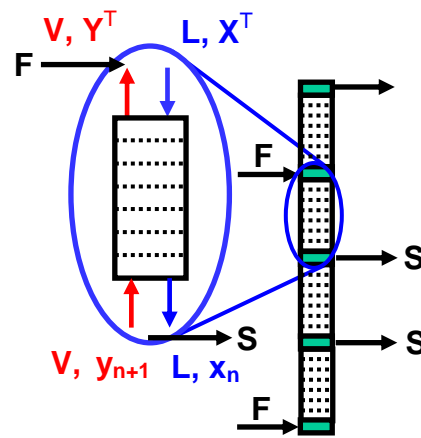


Figure FF. 2: Column section numbered from the top down

The compositional change from one stage to another can be determined by material balance. The difference equation describing this compositional change with stage number  $m$  (in Figure FF. 1) is seen in (F1) below.

Van Dongen and Doherty (1985), approximated the rectifying and stripping difference equations with differential equations. This can be done for the generalised column section, as well, using an analogous derivation, as follows.

The material balance over the generalised column section in Figure FF. 1 is:

$$Lx_{i,m+1} = Vy_{i,m} + LX_i^B - VY_i^B \quad (\text{F1})$$

$$\text{Letting } X_{\Delta i} = \frac{VY_i^B - LX_i^B}{\Delta} \quad (\text{F2})$$

and

$$\Delta = V-L \text{ where } \Delta \neq 0 \quad (\text{F3})$$

Substituting (F2) and (F3) into (F1) yields :

$$x_{i,m+1} = \frac{V}{L} y_{i,m} - \frac{\Delta}{L} X_{\Delta i} \quad (\text{F4})$$

Now letting  $R_{\Delta} = \frac{L}{\Delta}$  we obtain

$$x_{i,m+1} = \left( \frac{R_{\Delta} + 1}{R_{\Delta}} \right) y_{i,m} - \left( \frac{1}{R_{\Delta}} \right) X_{\Delta i} \quad (\text{F5})$$

We can expand  $x_{i,m+1}$  around  $m$  using a Taylor Series

$$x_{i,m+1} = x_{i,m} + \frac{dx_i}{dh} \Big|_{h=m} (\Delta h) + \frac{1}{2} \frac{d^2 x_i}{dh^2} \Big|_{h=m} (\Delta h)^2 + \dots \quad (\text{F6})$$

Where  $\Delta h = (m+1) - m = 1$ .

Substituting (F6) into (F5) we obtain,

$$x_i + \frac{dx_i}{dh} + \frac{1}{2} \frac{d^2 x_i}{dh^2} + \dots = \left( \frac{R_{\Delta} + 1}{R_{\Delta}} \right) y_i - \left( \frac{1}{R_{\Delta}} \right) X_{\Delta i} \quad (\text{F7})$$

If we assume that only the first derivative is significant we can approximate (F7) by,

$$x_i + \frac{dx_i}{dh} = \left( \frac{R_d + 1}{R_d} \right) y_i - \left( \frac{1}{R_d} \right) X_{di} \quad (\text{F8})$$

Rearranging we obtain,

$$\begin{aligned} \frac{dx_i}{dh} &= -x_i + \left( \frac{R_d + 1}{R_d} \right) y_i - \left( \frac{1}{R_d} \right) X_{di} \\ &= -\left( \frac{R_d + 1}{R_d} \right) x_i + \left( \frac{1}{R_d} \right) x_i + \left( \frac{R_d + 1}{R_d} \right) y_i - \left( \frac{1}{R_d} \right) X_{di} \\ &= \left( \frac{R_d + 1}{R_d} \right) (y_i - x_i) + \left( \frac{1}{R_d} \right) (x_i - X_{di}) \end{aligned} \quad (\text{F9})$$

This ordinary differential equation (F9) is called the difference point equation (DPE) and can be solved with arbitrary boundary conditions;  $x_i(h=1) = X_i^B$ . It approximates the composition profile from the bottom of a column section upwards and becomes increasingly accurate as  $h \rightarrow \infty$ . At stationary/pinch points, where  $\frac{dx_i}{dh} = 0$ , the difference point equation (F9) and the difference equation (F1) are exactly equivalent. The difference point equation (F9) approximation to the difference equation (F1) is more accurate for difficult separations where the separation vector  $s$  is small (i.e.  $s_i = x_i - y_i$  is small). It is exactly equivalent to (F1) if solved using Euler integration with unit step size.

To obtain the composition profile from the top of a column section downwards we simply have to reverse the direction of integration. The ODE describing this compositional change down the column section is seen in (F10) below.

$$\frac{dx_i}{dn} = \left( \frac{R_d + 1}{R_d} \right) (x_i - y_i) + \left( \frac{1}{R_d} \right) (X_{di} - x_i) \quad (\text{F10})$$

---

$$\text{Where } X_{\Delta i} = \frac{VY_i^B - LX_i^B}{\Delta} = \frac{VY_i^T - LX_i^T}{\Delta} \quad (\text{F11})$$

In this case increasing values of  $n$  denote stages further down from the stage at which the boundary/initial value is chosen. In general the form of the difference point equation seen in (F10) will be used and the stage count will be performed down a column section.

## Appendix G

### *Mathematical Background*

#### G.1. Eigenvalues and eigenvectors

Liapounov's first theorem states that the nature of a singular point  $X_S$  of equation (G1) is topologically similar to the singular point of the linearised equations:

$$\frac{du}{dn} = J(X_S)u$$

$$u_i = x - X_S \quad i = 1 \dots c-1$$

$$J(X_S) = \left[ \begin{array}{ccc} \vdots & & \\ \dots & \left( \frac{\partial f_i}{\partial x_j} \right)_{p,x=const} & \dots \\ \vdots & & \end{array} \right]_{x=X_S} = \text{Jacobian matrix}$$

$$f_i = \frac{R_\Delta + 1}{R_\Delta} (x_i - y_i(x)) + \frac{1}{R_\Delta} (X_{\Delta_i} - x_i) \quad (\text{G1})$$

By assuming that the  $n \times n$  matrix  $J(X_S) = [a_{ij}]$  is constant, that is, its entries do not depend on  $n$ , we are left with an eigenvalue problem, where the eigenvalue characterizes the kind of singularity that occurs and the pair of eigenvectors determine the asymptotic direction of the trajectories in the neighbourhood of the singularity. In order for a singular point to be investigated, it is necessary to set up the characteristic equation

$$\begin{vmatrix} a_{11} - \lambda & a_{12} \\ a_{21} & a_{22} - \lambda \end{vmatrix} = 0$$

and find its roots  $\lambda_1$  and  $\lambda_2$ . (The characteristic equation shown is for a ternary system).

Each pair of eigenvectors represents the axis of a new coordinate system which separate different behaviour of the phase diagram around the singularity and the singularity being the origin. Linear independent eigenvectors separate the space into four regions, while collinear eigenvectors divide the space into two regions, as illustrated in Figure GG. 1a and Figure GG. 1b.

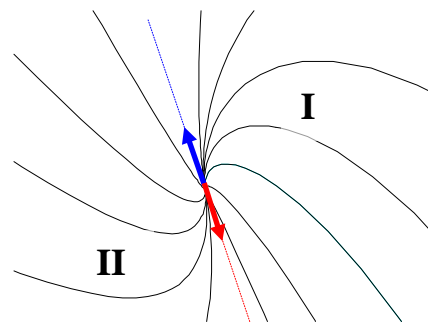
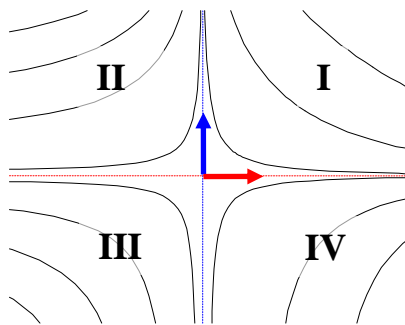


**Figure GG. 1a: Example of a saddle node with two linear independent eigenvectors that divide the space into four regions.**

**Figure GG. 2b: Example of a stable node with two collinear eigenvectors that divide the space in two regions.**

Complex eigenvectors are a result of complex roots of the characteristic equation. The space consists of one region as there is no determinable asymptotic direction in the real space. I.e. a characteristic node for complex eigenvectors would be a stable focus, see Figure GG. 1c.

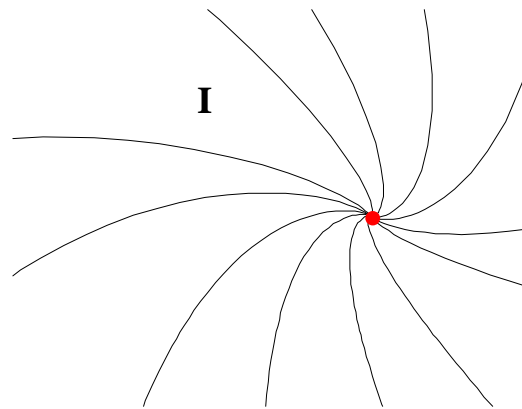


**Figure GG. 3c: Example of a stable focus with complex eigenvectors that results in a space that consists of one region.**

To characterize the kind of singularities in space it is necessary to look at the eigenvalues. The kind of singularity that can occur in a system is determined by the dimension of the characteristic equation. The eigenvalues for ternary systems are described by the sign of  $\lambda_1$  and  $\lambda_2$ . (Quaternary systems are described by the signs of  $\lambda_1\lambda_2$  and  $\lambda_3$ .) Hence for ternary systems there exists a limited combination of eigenvalues and therefore cases of singularities that can occur in the system.

## G.2 Eigenvalue and eigenvector maps

As the eigenvectors are a function of the thermodynamics only ( $v = f(y_i(x))$ ), there exists a unique eigenvector map for each system modelled by a particular set of thermodynamic data. The eigenvector map can be obtained by plotting the eigenvectors over a range of  $x$ .

In analogy to the eigenvector map there exists an eigenvalue map. As the eigenvalues are a function of  $\lambda = f(y_i(x), R_\Delta)$  eigenvalue maps can be plotted for every  $R_\Delta$  for each system.

### Cases of singularities occurring in a ternary system

Provided that  $\det J(X_s) \neq 0$  the singularities are elementary and the following cases for a ternary system are possible:

1. The roots  $\lambda_1, \lambda_2$  are distinct and real  $\rightarrow$  two linear independent eigenvectors:
  - $\lambda_1 < 0, \lambda_2 < 0$ . The singular point is asymptotically stable (stable node);
  - $\lambda_1 > 0, \lambda_2 > 0$ . The singular point is asymptotically unstable (unstable node);
  - $\lambda_1 < 0, \lambda_2 > 0$ . The singular point is asymptotically unstable (saddle point);
2. The roots of the characteristic equation are complex:  $\lambda_1 = p + iq, \lambda_2 = p - iq \rightarrow$  eigenvectors are complex:
  - $p < 0, q \neq 0$ . The singular point is asymptotically stable (stable focus);
  - $p > 0, q \neq 0$ . The singular point is asymptotically unstable (unstable focus);
  - $p = 0, q \neq 0$ . The singular point is asymptotically stable (midpoint);
3. The roots of the characteristic equation are not distinct  $\rightarrow$  eigenvectors are collinear:
  - $\lambda_1 = \lambda_2 < 0$ . The singular point is an asymptotically stable node;
  - $\lambda_1 = \lambda_2 > 0$ . The singular point is an asymptotically unstable node;

The case  $\det J(X_s) = 0$  results in non-elementary singularities of the following kind:

1. The roots of the characteristic equation has at most one zero eigenvalue  $\rightarrow$  two linear independent eigenvectors:
  - $\lambda_1 = 0, \lambda_2 < 0$ . The singular point is an asymptotically stable half node-saddle (Doherty);
  - $\lambda_1 = 0, \lambda_2 > 0$ . The singular point is an asymptotically unstable half node-saddle (Doherty);

To be able to exploit the knowledge of the eigenvectors and eigenvalues we have to look at specific systems.

## Appendix H

*Extended abstract within the conference proceedings for the FOCAPD 2008 conference held in Breckenridge, Colorado*

### Column Profile Maps and its Applications to Distillation Synthesis

Daniel A. Beneke, Ronald Abbas, Diane Hildebrandt\* and David Glasser

*Centre of Material and Process Synthesis (COMPS), University of the Witwatersrand, Johannesburg, South Africa*

#### Abstract

There has recently been a renewed interest in the design of distillation processes due to the development of Column Profile Maps (CPMs). Using CPMs one is able to change topology within the composition space and hence many separations that have been thought of as difficult or unviable, can now be achieved. The CPM technique has also been proven to be extremely useful as a design tool as any column configuration, irrespective of complexity, can be modelled and graphically understood. This paper aims to summarize the most important and interesting results and applications obtained using the CPM technique. It shows how CPMs may be used to synthesize complex columns like a Petlyuk or Kaibel column, as well as showing how new sharp split separations can be devised.

Keywords: Column Profile Maps, Distillation design, Sharp splits

#### Introduction

In modern chemical industries, the task of separation is a very energy consuming process, where distillation is the process most widely used for fluid separations. Distillation columns are used for about 95% of liquid separations and the energy usage from this process accounts for around 3% of the world energy consumption, as estimated by Hewitt et al. (1999).

Graphical methods for designing distillation schemes have been popular over the years. Residue Curve Maps (RCMs) are often used as a graphical method for designing multi component distillation systems. RCMs are basically a range of trajectories that track the liquid compositions of the chemical species over time in a simple distillation operation. RCMs can tell one much about the feasibility of separation and the nature of singular points, such as azeotropes and pure component vertices.

However, the RCM technique has its limitations in that it only gives information at infinite reflux, quite an impractical condition for the design engineer. Recently, in a series of papers by Tapp et al. (2004) and Holland et al. (2004 a, b) a new theory was explored in distillation: Column Profile Maps (CPMs). CPMs were derived from an adaptation of ODEs proposed by Van Dongen and

Doherty (1985), which take into account the net molar flows and reflux ratios in a column section. CPMs were shown to display the same topological behaviour as RCMs, as well as being an extremely useful tool in distillation design by allowing the designer to set reflux ratios and net molar flows to suit the specifications of the separation.

#### Column Profile Maps

A CPM describes the behaviour of a multi-component system by setting appropriate parameters such as the net molar flow and the reflux ratio. The first step in constructing a CPM, is to define a Column Section, which according to the definition of Tapp et al. (2004) is “a length of column between points of addition or removal of material and/or energy”. A steady state material balance over a Column Section accompanied with a Taylor expansion yields:

$$\frac{dX}{dn} = \left( \frac{1}{R_{\Delta}} + 1 \right) (X - Y(X)) + \left( \frac{1}{R_{\Delta}} \right) (X_{\Delta} - X) \quad (1)$$

$$\text{Where } X_{\Delta} = \left( \frac{VY^T - LX^T}{V - L} \right) \text{ and } R_{\Delta} = \frac{L}{V - L} = L / \Delta$$

Equation (1) is known as the Difference Point Equation (DPE).  $X_{\Delta}$  can be thought of as a pseudo composition vector and is valid anywhere in the composition space, even in the space outside the Mass Balance Triangle (MBT). It is however subject to the constraint that the sum of the components of  $X_{\Delta}$  be 1.  $X_{\Delta}$  need only be a real composition in columns sections that are terminated by a condenser or reboiler. Notice that the DPE is not bound by physically relevant initial conditions, thus one is able to perform the integration outside of the composition space. Furthermore, notice that the DPE reduces to the Residue Curve Equation at infinite reflux. Thus, for an arbitrary choice of  $X_{\Delta}$  and  $R_{\Delta}$  one can now begin to construct a CPM for an ideal system<sup>1</sup>, as in Figure HH.1.

---

<sup>1</sup> In this paper, an ideal system refers to the assumption of constant relative volatilities. Unless it is otherwise stated,  $\alpha_1=3$ ,  $\alpha_2=1$ , and  $\alpha_3=1.5$ , which means that  $x_1$  is the low boiler,  $x_3$  is the intermediate boiler and  $x_2$  is the high boiler.

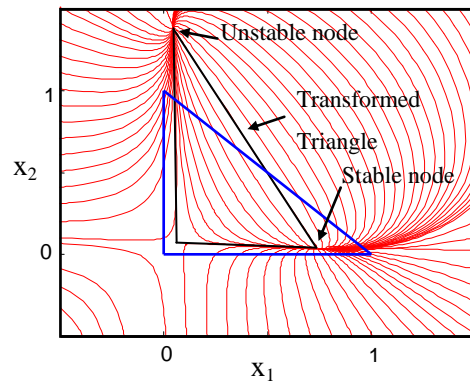


**Figure HH.1.** CPM for  $X_A = [0.3, -0.2]$  and  $R_A = 9$

Notice in Figure HH.1 how stationary points (nodes) have been shifted in the composition space, resulting in completely different profiles within the blue Mass Balance Triangle (MBT). These stationary points can be determined by algebraically solving the  $DPE=0$ . If we connect these shifted nodes with straight lines we can see a Transformed Triangle (TT) being formed. In theory, one can now move these nodes in composition space by simply fixing the aforementioned parameters. This could lead to many new and exciting designs that have been previously thought to be unviable.

## Results

### Petlyuk design

Using the CPM design methodology, one is able to break down any column configuration into simpler Column Sections, and from there design the entire column according to the separation specifications. The famed Petlyuk Column, which offers significant savings in energy, can also be broken down into Column Sections (CS) as shown in Figure HH.2. For simplicity, we shall look at

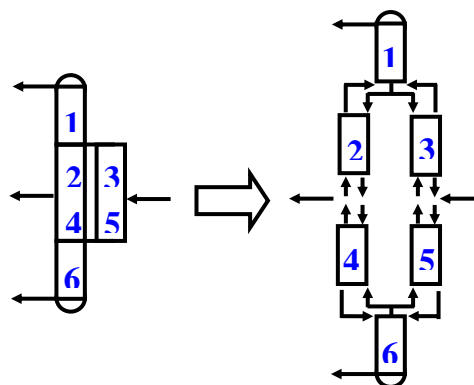


**Figure HH.2.** Column section breakdown for the Petlyuk column

the case where the Petlyuk operates at overall infinite reflux, but with CS 2-5 operating at a finite reflux, i.e. a column that draws infinitesimal product flows, but does not necessarily operate with  $L=V$  in sections 2, 3, 4 and 5. For this example, we shall set an intermediate product specification of 90% and achieving this specification will be the primary concern when deciding on a  $X_{\Delta}$ . CS 1-6 will simply operate on Residue Curves.

It can be shown mathematically that the constraints placed on this system leads to:

CS 2 and 4 have identical TTs

CS 3 and 5 have identical TTs

CS 2 and 4 and CS 3 and 5 operate on the same Difference Point, with equal magnitude but opposite signs for  $R_{\Delta}$ .

The criterion for feasible column profiles is that the liquid profiles intersect twice. If one then superimposes the 2 CPMS for the coupled sections, for an appropriate selection of  $X_{\Delta}$  and  $R_{\Delta}$ , it can be seen that the feasible region intersects with the product specification. Hence a feasible design has been found, as shown in Figure HH.3.

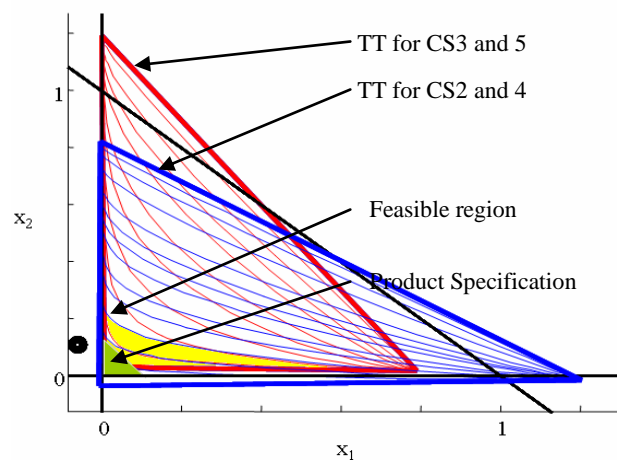


**Figure HH.3. Superimposed transformed triangles for coupled column system**

### Modelling Sharp Splits with CPMs

Invariably, the aim of any separation process is to achieve essentially pure products. Thus the sharp split constraint presents an interesting and relevant case study.

Tapp et al (2004) have shown that there are 7 regions of  $X_{\Delta}$  placement which result in unique Pinch Point curves (see Figure HH.4). The boundaries of these regions correspond to the extended

axes of the MBT. In terms of CPMs, a sharp split effectively means that  $X_{\Delta}$  is placed on the boundary of these regions. A sharp split thus displays Pinch Point Curve behaviour of 2 regions.

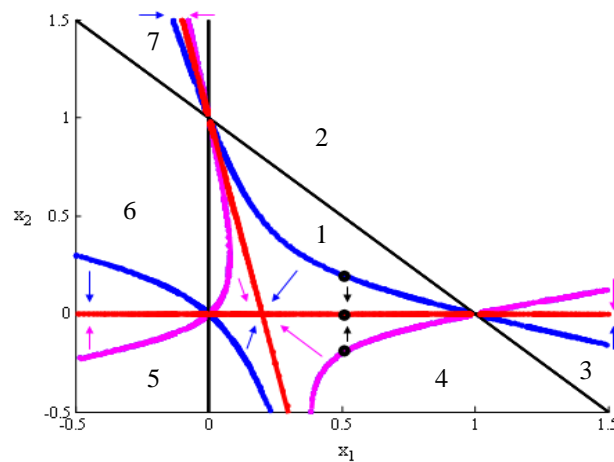


**Figure HH.4. Pinch Point Curve Behaviour for different placement of  $X_{\Delta}$ .**

It is interesting to note that the nodes for sharp splits are shifted in composition space in a different manner to non-sharp splits. Pinch point curves for sharp splits are linear, and appear to intersect at a point. In fact, the curves don't intersect, but merely meet at a point. The point at which this occurs is termed the "bumping point", because at this point nodes "bump" each other from their positions. For example, a saddle could be bumped from its position and be replaced by a stable node and thereby altering the topology within the MBT drastically. This result is very useful, as one could now theoretically place a node almost anywhere in composition space to suit the separation by simply choosing  $R_{\Delta}$  and  $X_{\Delta}$  appropriately.

An immediate application of this is fixing  $X_{\Delta}$  to the intermediate boiler vertex. By making use of the "node bumping" phenomenon, it is now possible to fix a stable node or an unstable node to the intermediate boiling vertex, as shown in Figure HH.5. This result suggests that the intermediate boiler can be completely removed in a single stripping section, and hence making the removal of the intermediate boiler significantly easier. Similarly, there are certain choices for  $R_{\Delta}$  and  $X_{\Delta}$  which can fix a saddle to the high or low boiler vertex, and hence making separation much more difficult for these components.

It is of special interest to determine when and how a certain node can be fixed in composition space.

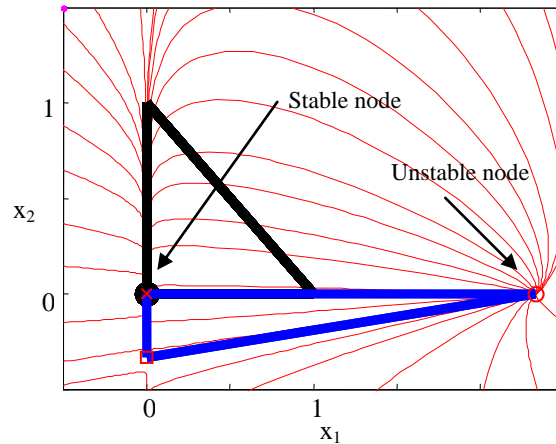


Figure HH.5. A stable node fixed on the intermediate boiler

For the special case where  $X_{\Delta}$  is placed on one of the 3 pure component vertices, a node is also fixed to the same vertex. So by knowing the position of a stationary point and  $X_{\Delta}$ , we can trace the nature of the node by varying  $R_{\Delta}$ . For example, Figure HH.6 shows which values of  $R_{\Delta}$  correspond to a specific node on the intermediate boiler vertex. The nature of the nodes are defined by the eigenvalues of the Jacobian when the DPE=0.

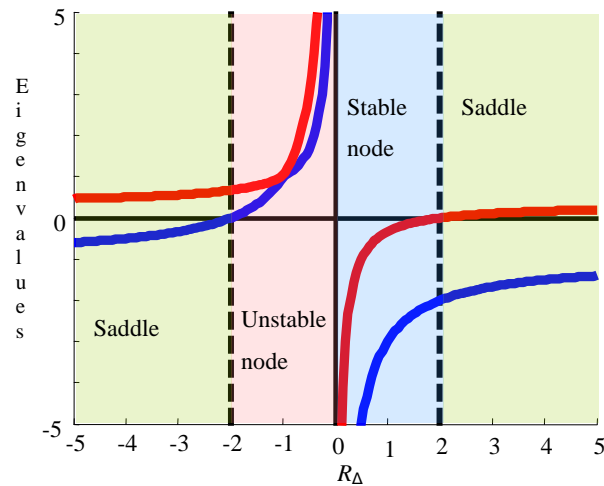


Figure HH.6. Operating regions for  $X_{\Delta}=[0;0;1]$

### Sharp split Kaibel column design

This work considers the implementation of a Kaibel column, (i.e. a fully-thermally coupled column with an adiabatic wall dividing the column into two equal halves for the production of four product streams). The Kaibel Column allows for a feed mixture of four or more components from which it produces a distillate, bottoms and two product side streams. Compared to the

conventional 3 column direct split sequence, the Kaibel column can be built in a single shell, making it an attractive alternative in terms of capital cost savings along with its counterpart; the Petlyuk Column. Further, the reduction in the number of reboilers and condensers' required leads to improved operating costs.

In this section of work we demonstrate the use of CPMs for the comprehensive analysis and design of Kaibel columns by applying the CPM technique for a system at sharp-split conditions. From the results of the topological analysis, it is shown that, for set product composition specifications, when using an ideal system (constant relative volatilities), there is only one set of feasible operating parameters.

The Kaibel Column Section breakdown is similar to the Petlyuk in Figure HH.1, but with an additional CS between CS 2 and 4, as two products are removed between these CSs. It can be shown that for the Kaibel column, CS 2 and 4's  $X_{\Delta}$ 's are placed on the intermediates pure components. A mass balance shows that the net flow through the connecting CS of the side draws is zero. As a result, this mass balance can only be satisfied completely if the difference point for component 2 (B) in this same CS ( $X_{\Delta 7, 2}$ ) is infinitely big. Due to the fact that this CS has a net zero flow, does not mean that the profile produced will be a residue curve, but by substituting zero net flow into the DPE the differential becomes an infinite reflux expression.

Figure HH.7 is the only correct CS mass balance layout in the quaternary system mass balance space. As can be seen from Figure HH.7 only one solution is possible as this is the only feasible mass balance that exists.

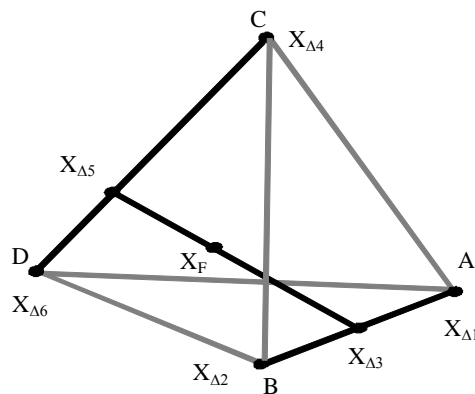


**Figure HH.7. Mass balance lines between intersecting CSs**

We can represent the results on a phi space diagram as shown by Figure HH.8. The single zero net flow line for CS 7 of the Kaibel arrangement is the only operating line that will produce feasible results for a double shell-single reboiler system (Red line). If we shift over to a Kaibel Dividing Wall Column (DWC) we operate at a single point (black dot in Figure HH.8), as one cannot throttle the vapour split at the bottom of the column. This shows that there is no movement

allowed to change the system by changing the liquid and vapour splits. As can be seen from Figure HH.8, the Petlyuk feasible region in the Phi space is much larger and thus much more operable than the single operating line for the Kaibel.

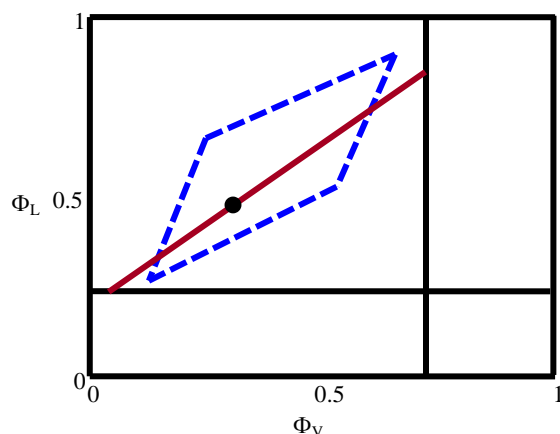


**Figure HH.8. Phi space diagram for the Petlyuk and Kaibel Column**

### Conclusion

In this paper it has been shown that CPMs have tremendous potential in designing and understanding simple and complex distillation systems. Nodes can almost be placed at will in composition space to suit the requirements of the separation, so much so that it is possible to place stable or unstable nodes on the intermediate boiler's vertex. The CPM technique offers a better understanding of the interaction between parameters due to its graphical nature. Furthermore, it has been shown that CPMs are extremely useful in designing complex distillation systems such as the Petlyuk or Kaibel column, and hence more efficient and creative designs can be thought of.

### Acknowledgements

The authors would like to give special thanks to Drs. Simon Holland and Michaela Very who laid the foundation on CPMs, and who without this work would not be where it is today.

### References

- Hewitt G, Quarini J, Morell M. More efficient distillation. *Chem Eng.* 1999;Oct. 21
- Holland, S.T., Tapp, M.; Hildebrandt, D. and Glasser, D, Column Profile Maps. 2. Singular Points and Phase Diagram Behavior in Ideal and Nonideal Systems, *Ind. Eng. Chem. Res.*,43(14), p3590-3603, (2004 a).
- Holland, S.T., Tapp, M.; Hildebrandt, D. and Glasser, D. and Hausberger, B., Novel Separation System Design Using "Moving Triangles", *Comp. and Chem. Eng.*,29, p181-189, (2004 b).
- Tapp, M., Holland, S.T.; Hildebrandt, D., and Glasser, D., Column Profile Maps. 1. Derivation and Interpretation, *Ind. Eng. Chem. Res.*,43(2), p364-374, (2004).
- Van Dongen, D. B.; Doherty, M. F. Design and Synthesis of Homogeneous Azeotropic Distillations. 1. Problem Formulation for a Single Column. *Ind. Eng. Chem. Fundam.*, 24, p.454, 1985.

# Appendix I

*Extended abstract within the IChemE Symposium series for the Distillation and Adsorption 2010 conference held in Eindhoven, Netherlands.*

## Novel Minimum Reflux Calculation using Eigenvector Maps

Ronald Abbas<sup>1</sup>, Simon Holland<sup>2</sup> and Ivar Halvorsen<sup>3</sup>

<sup>1</sup>Centre of Material and Process Synthesis, School of Chemical and Metallurgical Engineering, University of the Witwatersrand, Private bag 3, WITS 2050, Johannesburg, South Africa.  
[Ronald.Abbas@students.wits.ac.za](mailto:Ronald.Abbas@students.wits.ac.za)

<sup>2</sup>Centre of Material and Process Synthesis, School of Chemical and Metallurgical Engineering, University of the Witwatersrand, Private bag 3, WITS 2050, Johannesburg, South Africa.  
[Simon.Holland@wits.ac.za](mailto:Simon.Holland@wits.ac.za)

<sup>3</sup>SINTEF ICT, Applied Cybernetics, N-7465 Trondheim, Norway. [Ivar.J.Halvorsen@sintef.no](mailto:Ivar.J.Halvorsen@sintef.no)

### Abstract

Column Profile Map Eigenvectors (CPM-E) technique is introduced to determine the minimum energy demand for multicomponent feed in two-product distillation processes. The technique is a short cut, geometrical, non-iterative method and can be used to predict how the minimum reflux solution is related to the feed-component distribution for all possible operating conditions. The new method makes use of Column Profile Maps and the concept of "moving triangles" and develops co-linearity criteria based on the eigenvectors of the Jacobian of the separation vector evaluated at the feed composition. The CPM-E technique is a powerful tool that can be applied to complex column arrangements, such as Petlyuk or Kaibel Columns. The CPM-E approach is non-exclusive and can therefore be applied to any type of split, sharp or non-sharp, irrespective of the number of components. It will be shown that the CPM-E technique can be used to determine minimum reflux solutions quickly and effectively. From this, it is shown that three limiting product composition regions under minimum reflux conditions are present. The links between the CPM-E technique and the determination of minimum energy demand using Underwood's methods are explored.

Keywords: Eigenvectors, graphical, non-iterative, minimum reflux, co-linearity

## 1. Introduction

The continuous increasing cost of energy has made it necessary for industry to reduce its energy consumption. In addition to this, the effort to prevent climate change has caused stringent environmental regulations that have generated the need to adopt new and efficient unit operations. Intensive investigations have been undertaken to develop new and more useful models to operate distillation units as optimally as possible. Koehler et al.<sup>1</sup> give a review of methods for determining minimum energy requirements for conventional columns as well as complex column configurations up to 1995. They show that many of the minimum energy demand techniques are related to the methods of Underwood. Many works done by Doherty and co-workers<sup>2-4</sup> have proposed several techniques that produce accurate minimum reflux solutions for ideal as well as highly non-ideal azeotropic systems. The drawback of these techniques is the selection of the initial reboiler duty which indicated uncertainty whether the selected duty will produce a minimum reflux solution. The approaches adopted by Doherty and co-workers rely heavily on pinch points as well as on the interaction of vectors between the pinch points of both the rectifying and stripping sections. The focus of this manuscript is to demonstrate a novel method, called Column Profile Maps Eigenvector (CPM-E) technique, to determine the minimum energy demand in any conventional column and to show the link between CPM-E and Underwood based method such as  $V_{\min}$  diagrams<sup>5</sup>.

## 2. Background

### 2.1 Column Profile Maps

Column Profile Maps, introduced by Tapp et al.<sup>6</sup>, is produced from the Difference Point Equation (Equation 1). These Maps are composition trajectories generated for column sections (CS) for a pre-defined difference point ( $X_{\square}$ ) and reflux ratio ( $R_{\square}$ ).  $\square$  is better described as the net flow of material and is a pseudo stream flowing up or down in a column section.

$$\frac{dX}{dn} = \left(1 + \frac{1}{R_{\Delta}}\right) (X - Y^*(X)) + \frac{1}{R_{\Delta}} (X_{\Delta} - X)$$

where:  $X_{\Delta} = \frac{VY_T - LX_T}{\Delta}$ ;  $R_{\Delta} = \frac{L}{\Delta}$ ;  $\Delta = V - L$  (1)

If the vapour flow were larger than the liquid flow in a column section,  $\Delta$  would be positive as we know it to be in a rectifying section (RS) and the direct opposite applies to the stripping section. A material balance indicates that the distillate product flow is equivalent to the positive net flow in the rectifying section. Similarly, the bottoms product flow is equal to the negative net flow in the stripping section. The difference point ( $X_{\Delta}$ ) is the pseudo composition vector of the net flow, and is physically valid anywhere in composition space. It can be shown from mass balance that the difference point for a conventional column is equivalent to the product specifications of the column. The reflux ratio is defined as the ratio of liquid flowing down the column section to the

net flow in the column section. Because of its dependence on  $\Delta$ ,  $R_{\Delta}$  can either be positive or negative. This means flow up in a rectifying section and down in a stripping section tells us that we can only have reflux ratios that are positive in the rectifying section and negative in the stripping section. Any other direction other than specified would result in an infeasible profile intersection.

### **2.2 Eigenvector Maps**

The eigenvectors characterize the asymptotic direction of the trajectories in the neighbourhood of the singularity. Holland et al.<sup>7</sup> introduced Eigenvalue and Eigenvector Maps and illustrated the usefulness of these maps for manipulating phase diagrams and therefore column profiles. The maps predict movement of the singularities based on the value of the design parameters of the difference point selected in the composition space and the reflux ratio. An eigenvector map can be obtained by plotting the eigenvectors over a range of  $x$  values.

### **3. Conditions for Minimum Reflux, transformed triangles and co linearity rule.**

The boundary value method introduced by Levy et al.<sup>2</sup>, is implemented by identifying co-linear lines drawn from the saddle node of the rectifying section through the feed and the unstable node through the feed for sharp, direct splits. By plotting the liquid profiles for each section, showing that one of the profiles ends on the other and then illustrating co-linearity of the pinched lines, minimum reflux is established. The fact that column profile maps are similar to the stage by stage methods used by Doherty and co-workers indicates that the condition for minimum reflux for either method must be the same. Tapp et al.<sup>5</sup> showed that the Column Profile Maps at finite reflux are simply transforms of the residue curve maps. The transform shifts the fixed points of the system in the space, maintaining (in constant relative volatility systems) the shape of the boundaries initially defined by the MBT. This has resulted in the phenomenon being referred to as “Transformed Triangles” (TT). The description of co-linearity lines (CLL) at minimum reflux conditions indicates that it will be easier to track the saddle pinch and feed pinch which supplement co-linearity by using TTs of the rectifying and stripping sections. Thus it is more convenient to solve for the stationary points that define the nodes and rather plot the straight lines between these nodes.

In Figure II.1a and b, the reflux ratio is greater than the minimum; the profiles cross and continue further on. Figure II.1b describes a column that is subject to less energy input for the same product specifications as it is closer to the minimum reflux condition, since the overlap of the profiles is not as great as it is in the previous Figure (Figure II.1a). Therefore, the desired structure that represents minimum reflux is shown in Figure II.1c where the stripping profile ends or terminates on the rectifying profile. The point on the rectifying profile and stripping profile where they

intersect is the feed stage. The feed it seems is the last possible ‘point’ for the TTs to intersect. Any reflux selected above the minimum will result in an overlap of TTs and any reflux selected below the minimum will result in no overlap of the TTs and therefore no feasible intersection of profiles will occur. At specified feed conditions, distillate and bottoms compositions, the exact condition for minimum reflux is that the tangent to the saddle pinch profile at the feed pinch point is a straight line through  $X_F$ . This is true regardless of whether the mixture is ideal, non-ideal, or azeotropic<sup>2</sup>.

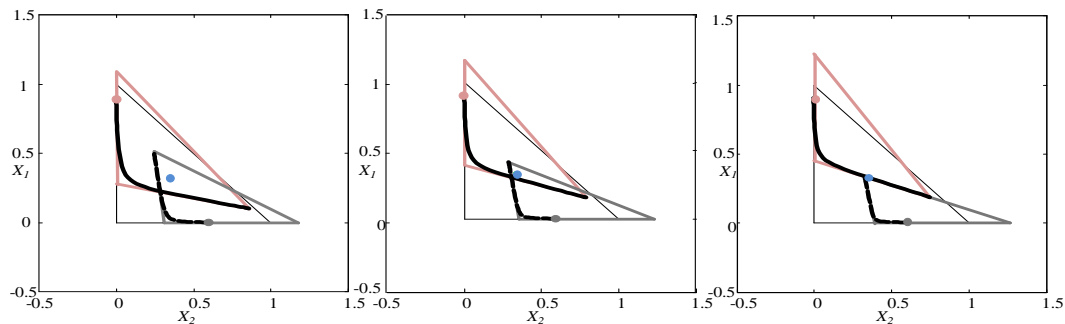


**Figure II.1(a). Crossing Profiles with corresponding overlapping TTs.**

**Figure II.1(b). Smaller reflux, but still over refluxed system.**

**Figure II.1(c). System at minimum reflux conditions.**

#### 4. CPM-E technique derivation

##### 4.1 Eigenvector application and CPM-E technique

Holland et al.<sup>7</sup> demonstrated that the eigenvectors at the singularities, of constant-relative-volatility systems, always point along the direction of the TT boundaries. Because the boundaries are straight in these systems, the eigenvectors at each singularity point directly at the other singularities. Any point chosen along one of these boundaries will have eigenvectors that point directly at the same singularities, which define it. It is evident at this point that the eigenvectors evaluated on the minimum reflux TT have to be co-linear with the CLL. We can now predetermine the CLL where the minimum reflux TTs touch. Because the CLL passes through the feed composition, evaluation of the eigenvector at the feed composition show all possible CLL based on a specified feed condition. Finding these lines implies that we are a step closer to finding the stationary points where the profiles/TTs of the minimum reflux coincides. Once we find at least one stationary point associated to a profile/TT at minimum reflux conditions, finding and quantifying the minimum reflux solution would be possible.

To find the stationary points, non-specific for a thermodynamically ideal ternary system, would involve solving the right hand side of the Difference Point Equation (Equation 1) for the liquid composition when it is equivalent to zero. Taking a closer look at the terms in the Difference Point Equation, we identify two vectors. The first vector, called the separation vector is the difference between the liquid composition and the vapour composition in equilibrium with the liquid

composition i.e.  $\tilde{s} = (X - Y^*(X))$ . The second vector is called the mixing vector and is the difference between the difference point and the liquid composition i.e.  $\tilde{m} = (X_{\square} - X)$ . At the stationary point this implies from a geometrical point of view that the mixing vector is co-linear with the separation vector. This is illustrated in Figure II.2. The main aim is thus, to find a stationary point along the CLL. In order to determine the point, simple straight line geometrical tools are employed. The straight CLL aids with this as it passes through the stationary node. The only other line that passes through the liquid stationary point is the mixing and separation vectors co-linear line. Two unknown points arise from these points. They are the liquid pinch point and the equilibrium vapour pinch point illustrated in Figure II.2. Due to the fact that the vapour composition is only a function of the constant relative volatility and liquid composition, the only unknown is the liquid composition at the stationary point. In other words, the solution to the pinch point is found by equating the gradients of the mixing vector and separation vector, and then solving for the elements of the liquid composition simultaneously with the straight line equation of the CLL. This composition would be the stationary point solution on the CLL which is one of the stationary points on the minimum reflux TT solution (Figure II.2). If the transformed triangle can be found algebraically by simply specifying the  $R_{\Delta}$  and  $X_{\Delta}$ , then the reverse must also be true. By knowing the fixed points of a Column Profile Map or its associated TT we must be able to determine  $R_{\Delta}$  and  $X_{\Delta}$ . There is no need to determine the difference point as it has already been specified through the product specification. Therefore the only unknown is the reflux ratio. This very powerful result of the calculated reflux is the minimum reflux solution for a given feed. This result was found without iterations or tedious steps and is based on simple mathematics. The results of the minimum reflux are illustrated in Figure II.2.

#### **4.2 Additional CPM-E solutions**

In addition to the eigenvector we have focussed on that has produced a base of solutions along our CLL, there is another eigenvector with a larger slope that we have not yet considered, but is of immense importance and produces a different set of solutions along it. We will name the co-linearity line of smaller (absolute) gradient; derived from the red eigenvector, Co-Linearity Line 1 (CLL1) and the line of larger (absolute) gradient; derived from the blue eigenvector, Co-Linearity Line 2 (CLL2).

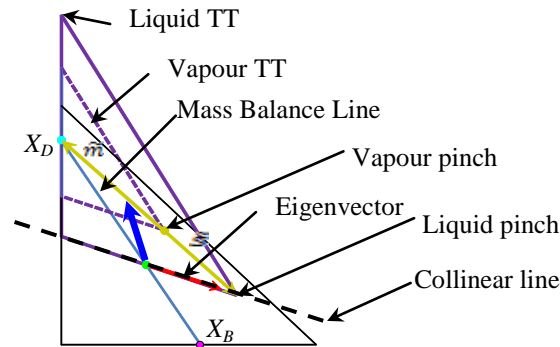


**Figure II.2. CLL stationary point with mixing and separation vector passing through the node of the transformed triangle for the minimum reflux solution**

Additional solutions exist, other than along CLL1, which governs minimum reflux for different purities of either the distillate or bottoms product. The selection of  $X_D$  will affect the TT for each specified minimum reflux but will not affect the interaction properties of the TTs under minimum reflux conditions. Therefore, for each and every product selection, there is a specified TT that is related to a minimum reflux solution because of its association to the specified difference point placement. CLL1 and CLL2 are distinct solutions, but they can be used together under certain composition selections to produce additional solutions other than those already discussed. It is important to note that minimum reflux solutions derived from CLL1 produce TTs that interact along CLL1 (See Figure II.3). Therefore, minimum reflux solutions derived from CLL2 approach along CLL2 where the distillate product has lower concentrations of light key components (See Figure II.4). Increasing the impurity of the high boiler that reports to the top and solving for the minimum reflux at select points, shows a point where the solutions based on CLL1 'swap-over' to CLL2.

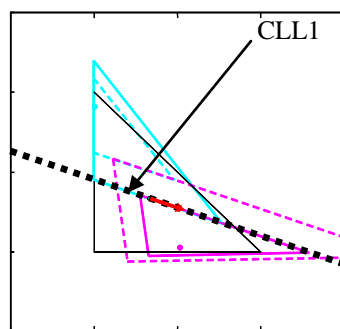


**Figure II.3. Minimum reflux solution along CLL1**

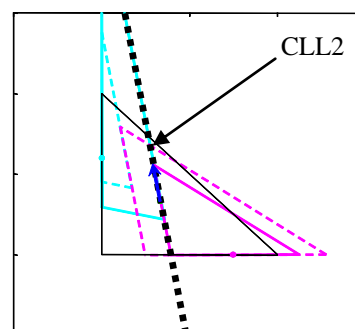


**Figure II.4. Minimum reflux solution along CLL2**

The point where the swap-over takes place is where both eigenvectors that produce CLL1 and CLL2 are employed. This phenomenon is feed specific and is non selective to regions in the real space and is called the preferred split. This means that the feed composition at this special minimum reflux solution has become a stationary point for both the rectifying section and stripping section and therefore the preferred split will exhibit a pinch region on both sides of the feed stage and not individually as we have previously seen when either CLL1 or CLL2 are common. Selecting product compositions on the 'swap-over' point from CLL1 to CLL2 or vice versa and calculating the minimum reflux at the point for either common CLL produces the preferred split. This of course is only true if the split is sharp. If the feed is assumed to be a saturated liquid, finding the preferred split is as simple as determining the vapour composition in equilibrium with the feed composition and then extending a straight line through both points. The intersection of the line with the light intermediate axis is the preferred split. This line exhibits interesting results when product compositions are selected along it and the CPM-E technique is applied to them. Both CLLs remain common and therefore the feed composition remains a stationary point where the rectifying section's TT and stripping section's TT meet. Holland et al.<sup>8</sup> have described this phenomenon as "double-feed-pinches". The "double-feed-pinch" point is phase dependent. Vapour feed columns will exhibit a vapour profile "double-feed-pinch" point - although it should be noted that both phases in both cases will pinch.

## **5. Minimum Reflux regions**

### ***5.1 Regions developed from CPM-E technique***

The sign of the reflux in each column section is of great importance and will limit our choices of difference points in the MBT. Considering that a common CLL for a set of minimum reflux solutions remain the same, and as a result the contact boundaries of the liquid TTs and therefore the vapour TTs of the associated solutions remain the same as well, selecting difference points outside the vapour TT, but within the MBT will result in oppositely signed refluxes in the column sections.

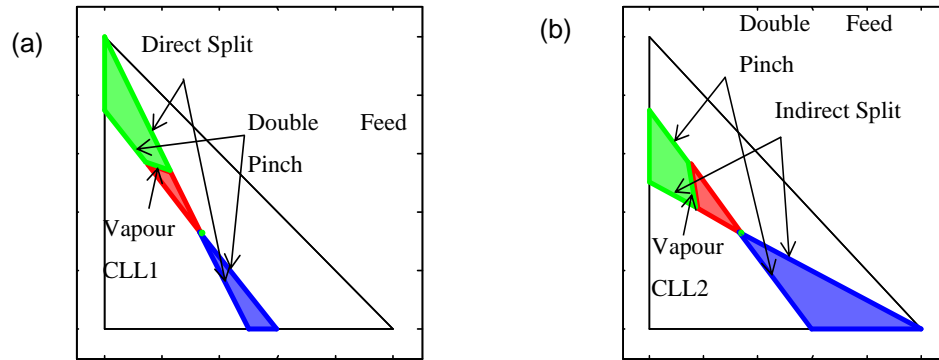


**Figure II.5. (a) Feasible and infeasible regions associated to common CLL1. (b) Feasible and infeasible regions associated to common CLL2.**

This sets a limit for each CLL employed or feed composition selected. The vapour boundary that is associated with the coincident CLL is the last lines of possible  $X_D$  selection points. Three distinct boundaries, besides the obvious MBT, will limit our search for feasible minimum reflux solutions. They include: the double-feed-pinch, the bow-tie region and the vapour CLL depending on which column section is chosen to analyse. This means, that if a CLL is chosen to find a reflux solution based on the product selection i.e. high light key purity in distillate uses CLL1 and high heavy key in bottoms uses CLL2, then only the region that applies to the utilised CLL will produce feasible solutions and any region outside this one will not produce anything useful. By superimposing the three boundaries (double-feed-pinch, bow tie region and vapour CLL), three defining feasible regions arise (See Figure II.5a-b). The interaction of the CLLs with the feed and each other is a significant aspect with regards to the number of components. Thus, if there were for example four components, more than three feasible regions would exist.

### 5.2 Region development associated to the $V_{min}$ diagrams

Comparing the combination of Figure II.5a-b and Figure II.6, it is quite easy to see that parts of regions from each CLL solution are omitted from Figure II.6. The exact minimum reflux solutions are associated to sharp split separations either in the distillate product or bottoms product, and depend purely on the CLL used. Thus the region of feasibility used in order to determine the minimum reflux solution. This means that if for instance CLL1 were to be used, not the entire green region characterised in Figure II.5a produces exact minimum reflux solutions by utilising CPM-E. Only the sharp split in the distillate composition i.e. light-intermediate axis that coincides with the feasible region produces exact solutions. The remaining region is merely an approximation. The bottoms compositions undergo similar behaviour when CLL2 is utilised. The sharp split i.e. heavy-intermediate axis coinciding with the blue region in Figure II.5b represents true minimum. Although CLL1 distillate region illustrated in Figure II.5a is reduced to a line does not mean that the blue region associated to the bottoms composition when CLL1 is used is reduced

to the sharp split criterion. Due to the fact that the stripping section profile terminates on the rectifying section profile or equivalently the TT of the stripping section means that the impurity is based on any component pertaining to the material balance can be selected within the feasible region. The opposite argument is true for CLL2s feasible region. In this way we reduce the regions depicted in Figure II.5a-b to the sloppy-split minimum reflux regions shown in Figure II.6. The combined exact minimum reflux solution regions are illustrated in Figure II.6. Figure II.7 is the  $V_{\min}$  diagram that is associated to the exact minimum reflux regions produced in Figure 6. There is of course a way to find these regions based on either method, but for now, we will just mention that the eigenvectors used in the CPM-E method have a relationship to the common Underwood roots used in the  $V_{\min}$  diagram<sup>5</sup>. The comparison of the Rmin calculated by utilising the CPM-E technique produces exactly the same results as compared to the result of the Underwood equations. Table 1 shows the comparison between the Underwood<sup>9</sup> method, the boundary value method (BVM) introduced by Levy et al.<sup>2</sup> and the CPM-E technique.

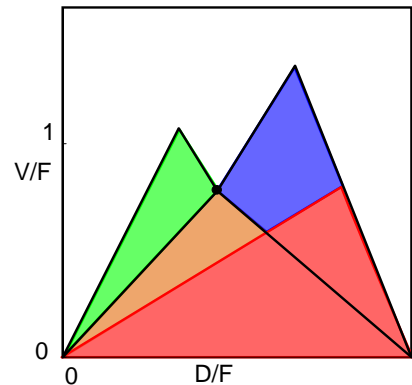
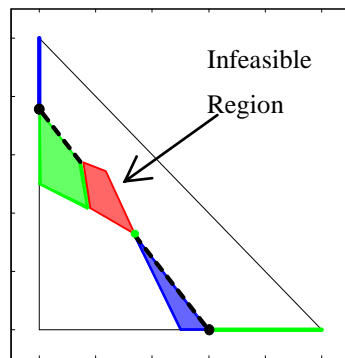


**Figure II.6. Minimum reflux regions associated to Underwood roots. Equimolar feed**  
**Figure II.7. Vmin diagram associated to Underwood roots. Equimolar feed.**

**Table II.1. Table 1. Comparison of different methods to CPM-E technique**

Relative volatilities		Feed composition		Product compositions		Reflux ratio		
$\alpha_{12}$	$\alpha_{13}$	$X_{F1}$	$X_{F2}$	$X_{D1}$	$X_{B1}$	Underwood	BVM	CPM-E
1.25	1.5	0.3	0.3	0.95	0.01	9.08	9.1	9.08
2.37	12.67	0.3	0.3	0.999	0.001	1.52	1.54	1.52

## 6. Conclusion

We have illustrated a general method for calculating minimum reflux ratios, for ternary and higher order systems, through the use of Column Profile Maps and eigenvector maps, named the CPM-E technique. The method applies to ideal, non-ideal, and azeotropic distillations, becoming identical

with Underwood's method for ideal mixtures. The technique makes use of eigenvectors evaluated at the feed composition in order to find a linear relationship between the saddle node and feed conditions. This line is called the co-linearity line (CLL). Three distinct solutions exist for the CPM-E technique. A solution that arises when each of the individual CLLs are common and a special solution when both CLLs are common. The simplicity of the method originates from uncomplicated mathematics combined with graphical interpretation. This is not only true for conventional columns, but for any thermally coupled systems.

### Nomenclature

$X$ : Liquid phase composition	$\Delta$ : Net flow defined as $\Delta = V - L$ [mol/s]	Subscripts :
$Y^{\#}(X)$ : Equil <sup>m</sup> vapour composition	$X^T$ : Liquid composition top of CS	F: Feed Composition
$R_{\Delta}$ : Reflux ratio of column section	$Y^T$ : Vapour composition top of CS	D: Distillate product composition
$L$ : CS internal liq flow rate [mol/s]	$N$ is the stage number equivalent	B: Bottoms product composition
$V$ : CS internal vap flow rate [mol/s]	$X_{\Delta}$ is the Difference point of a CS	CS Is Column Section

### References

1. J. Koehler et.al., *Ind. Eng. Chem. Res.*, 34(1995) 1003-1020
2. G. S. Levy et.al., *Ind. Eng. Chem. Fund.*, 24(1985) 463.
3. H. N. Pham et.al., *AIChE J.*, 35(1989), 1585.
4. Z. T. Fidkowski et.al., *AIChE J.*, 37(1991), 1761.
5. I. J. Halvorsen and S. Skogestad., *Ind. Eng. Chem. Res.*, 42(2003), 616-629.
6. M. Tapp et.al., *Ind. Eng. Chem. Res.*, 43 (2)(2004), 364.
7. S. T. Holland et.al., *Ind. Eng. Chem. Res.*, 43(14)(2004), 3590-3603.
8. S. T. Holland et.al., *Ind. Eng. Chem. Res.*, 49(2010), 327-349.
9. A. J. V. Underwood., *J. Inst. Petroleum.*, 32 (1996), 619-626